

Preliminary Design of Composite Overwrapped Pressure Vessels for a Suborbital Pressure Fed Liquid Rocket

*Thesis submitted to the faculty of North Carolina State University
in partial fulfillment of the requirements for the degree of*

*Master of Science
In
Mechanical Engineering*

John Slugg

November 13, 2020

Contents

| | |
|--|-----------|
| Pretext | 4 |
| Acknowledgments | 4 |
| Executive Summary | 5 |
| Abstract | 5 |
| Acronym Definitions | 6 |
| 1 Introduction | 7 |
| 1.1 Background | 7 |
| 1.2 COPV History | 8 |
| 1.3 Design Context | 9 |
| 1.3.1 Mission Statement / LRL Overview | 9 |
| 1.3.2 Rocket Design Overview | 9 |
| 2 System Specifications | 11 |
| 2.1 Constraints | 11 |
| 2.1.1 Tanks shall operate as designed at MEOP | 11 |
| 2.1.2 Tanks shall meet or deceed mass budget | 11 |
| 2.1.3 Tanks shall accommodate adequate propellant flow rate | 13 |
| 2.1.4 Tanks shall possess factor of safety based on probability of failure analysis with probability of survival ≥ 0.999 | 13 |
| 2.1.5 Propellant COPV's shall possess capacity sufficient for a karman line shot | 15 |
| 2.2 Functional Specifications | 15 |
| 2.2.1 Tanks shall withstand loading of parachute deployment | 15 |
| 2.2.2 Tanks liners must be compatible with stored compounds | 18 |
| 2.2.3 Tanks shall maintain pressure at MEOP | 24 |
| 2.2.4 Tanks shall function under in-flight loading conditions | 25 |
| 2.3 Objective Specifications | 26 |
| 2.3.1 Composite components should meet standards for fiber volume fraction | 26 |
| 2.4 COPV Specifications - Tabular | 27 |
| 3 Trade Studies | 28 |
| 3.1 Propellant Tank Configurations | 28 |
| 3.1.1 Common bulkhead design | 28 |
| 3.1.2 Common bulkhead advantages | 29 |

| | | |
|----------|--|-----------|
| 3.1.3 | Common bulkhead disadvantages | 30 |
| 3.1.4 | Common bulkhead systems integration impact | 30 |
| 3.1.5 | individual propellant tanks | 31 |
| 3.1.6 | Individual tank advantages | 31 |
| 3.1.7 | Individual tank disadvantages | 32 |
| 3.1.8 | Individual tank systems integration impact | 33 |
| 3.1.9 | propellant tank configuration selection | 33 |
| 3.2 | Tank Head Geometry | 34 |
| 3.2.1 | Hemispherical | 34 |
| 3.2.2 | Semi-Elliptical | 35 |
| 3.2.3 | Torispherical | 35 |
| 3.2.4 | Tank head design selection | 36 |
| 3.3 | Material Options | 38 |
| 3.3.1 | Liner option evaluations | 38 |
| 3.3.2 | Oxidizer COPV liner option evaluation | 38 |
| 3.3.3 | Oxidizer COPV liner material selection | 41 |
| 3.3.4 | Fuel COPV liner option evaluation | 42 |
| 3.3.5 | Fuel COPV liner material selection | 42 |
| 3.3.6 | Pressurant COPV liner option evaluation | 42 |
| 3.3.7 | Pressurant COPV liner material selection | 43 |
| 3.3.8 | Overwrap option evaluation | 43 |
| 3.3.9 | Overwrap material selection | 52 |
| 3.4 | Slosh Mitigation | 53 |
| 3.4.1 | Existing slosh mitigation system designs | 53 |
| 3.4.2 | Slosh mitigation system selection | 66 |
| 4 | COPV Design | 67 |
| 4.1 | Design Selection | 67 |
| 4.2 | Stack Configuration | 67 |
| 4.3 | Baffle Design | 69 |
| 4.4 | Liner Design | 77 |
| 4.5 | Overwrap Design | 78 |
| 4.6 | Parametric Model | 80 |
| 4.7 | Analysis and Revision | 81 |
| 4.7.1 | Loading Validation | 81 |
| 4.7.2 | Flow Analysis | 89 |
| 4.8 | Conclusion | 92 |
| 4.8.1 | Final Designs | 92 |
| 4.8.2 | Future work | 95 |
| 4.8.3 | Closing summary | 96 |
| 5 | References | 96 |

| | | |
|----------|---|------------|
| 6 | Appendices | 101 |
| 6.1 | Code | 101 |
| 6.1.1 | Propellant COPV Analysis Script - MATLAB | 101 |
| 6.1.2 | Pressurant COPV Analysis Script - MATLAB | 120 |
| 6.1.3 | Probability of Failure Analysis Script - MATLAB | 139 |
| 6.1.4 | Slosh Mitigation Baffle Analysis Script- MATLAB | 141 |
| 6.1.5 | Stacking Center of Mass Script- MATLAB | 146 |
| 6.1.6 | Failure Criteria Comparison- MATLAB | 149 |
| 6.2 | Appendix B | 154 |
| 6.2.1 | Drawings | 154 |
| 6.2.2 | Fiber data sheet | 182 |
| 6.2.3 | Link to project file downloads | 183 |
| 6.2.4 | Parametric model update sequence | 183 |

Pretext

Acknowledgments

Dr. Landon Grace, Project Advisor

Dr. Kara Peters, Department Chair

My time at North Carolina State University has been difficult, both academically and personally. I have experienced trials and tribulations, but have grown because of them and persevered despite them. I have learned a great deal about mechanics, dynamics, materials, mathematics, and rocketry. However, possibly more importantly I have learned about the things in life I truly value, how to make the best of what is available. I have come to find that life is neither about the destination nor the journey, but those who accompany you throughout; So I would like to say thank you to the following people who have contributed greatly to this chapter of my life.

Thank you to:

Dr. Landon Grace for advising this project and teaching me composite mechanics

Dr. Kara Peters for advisement throughout my time at NCSU

Dr. Afsaneh Rabiei for encouraging me to follow my own path

Alexander Allen for the friendship and help you have given along the way

Renzo Benavides for introducing me to Liquid Rocketry Lab and being a friend

Liquid Rocketry Lab Structures Team for being a fabulous group of coworkers

Dr. David Gill for inspiring me to pursue graduate study and to marvel at engineering

Prof. Nicole Larson for feeding my love of composite materials and believing in me

Dr. Philip Bradford for insight into textile considerations for composite materials

All Liquid Rocketry Lab team members for being an incredible group of coworkers

My parents who have given me tremendous support in all my pursuits in life

Executive Summary

The objective of this paper is to detail the preliminary design of composite overwrapped pressure vessels for use on the Liquid Rocketry Lab pilot launch vehicle. These pressure vessels will be designed to act as propellant and pressurant vessels for use aboard the spacecraft. The pressure vessels will act to contain the rockets fuel, oxidizer, and pressurant which will be fed through the powerpack to generate sufficient flight thrust. All components are designed to be manufactured using resources available to Liquid Rocketry Lab. The outcome of this project are analytically validated designs along with all necessary information to advance the designs.

Pressure vessel liners will be manufactured by a to be determined source and composite overwrapping to be completed by Blue Force Technologies, a Durham based composite manufacturer. Filament winding decisions will be based upon Blue Force Technologies processing capabilities. Before manufacturing all pressure vessels should pass review by a professional engineer. Should the pressure vessels fail review by a professional engineer, the design should be improved until it receives approval at which point manufacturing can commence.

This paper will cover all requirement research, design space definition, design selection, design justification, modeling, and validation. Completion of this project work evaluated with sufficient merit to earn a completed grade acts to fulfill North Carolina State University requirements for completion of MAE 586 acting as partial fulfillment of the requirements for the degree of Master of Science in Mechanical Engineering.

Abstract

With the recent boom in the space industry, composites and their usage in launch vehicles has increased. For rockets utilizing pressurized systems, composite overwrapped pressure vessels have become commonplace within the industry thanks to their ability to maintain low mass while containing high pressures. Despite their ubiquity within industry there is not much literature on the design process as many of these applications are proprietary. This paper discusses the design process utilized in the creation of preliminary designs of propellant and pressurant COPVs for a suborbital liquid propellant rocket. First, specifications are defined to contextualize the problem by creating a set of application specific requirements. Next, trade studies are used to explore the solution space and answer the big design questions based upon the information available. Then, preliminary designs are created parametrically and analyzed to examine their validity on a basic level. Finally, suggestions are made for continuation of the design process with the objective of manufacturing these COPVs to integrate with the rest of the flight hardware being developed for the launch vehicle.

Abbreviation Definitions

| | | |
|----------------|-------|---|
| AGL | | Above ground level |
| Al | | Aluminum |
| AMSL | | Above mean sea level |
| CAD | | Computer aided design |
| CAE | | Computer aided engineering |
| CBPV | | Common bulkhead pressure vessel |
| CFD | | Computational fluid dynamics |
| COPV | | Composite overwrapped pressure vessel |
| CP | | Commercially pure |
| CTE | | Coefficient of thermal expansion |
| EDS | | Earth departure stage |
| FEA | | Finite element analysis |
| FoS | | Factor of safety |
| GNC | | Guidance and Navigation Control |
| GUI | | Graphical user interface |
| HTP | | High test peroxide |
| LBB | | Leak before burst |
| LRL | | Liquid Rocketry Lab |
| MEOP | | Maximum expected operating pressure |
| NASA | | National Aeronautics and Space Administration |
| PV | | Pressure Vessel |
| RMS | | Root mean squared |
| RP-1 | | MIL-R-25576 Rocket propellant grade kerosene |
| SCC | | Stress corrosion cracking |
| SS | | Stainless Steel |
| T _g | | Glass transition temperature |

Introduction

1.1 Background

Composite overwrapped pressure vessels (COPV)s are in essence pressure vessels which consist of a liner surrounded by a wound composite. A diagram of a simple COPV is shown in figure 1.1. COPVs have become wide used across many industries including, but certainly not limited to: food and beverage, protective equipment manufacturing, aerospace, automotive, and defense. With the recent boom in space applications COPVs been increasingly employed in rockets thanks to their lightweight construction.

As shown in figure 1.1 COPVs have several components including, the overwrap, the liner, as well as polar bosses. The tank head is the closure at either end and the cylinder is the right cylindrical section between the two heads. Depending on the application COPVs may also have other internal features such as piping or baffles which complete a specific task.

COPVs are commonly manufactured through the use of filament winding, a process which uses a collection tows (bundles of individual fibers) and a thermosetting resin system to wrap a mandrel in a fiber reinforced polymer composite. Filament winding is desirable thanks to its capability to deposit continuous fiber at at specific angles as well as its applicability for use with simplistic asymmetric parts. The mandrel for which a COPVs overwrap is wound about is most often a sacrificial liner which becomes part of the COPVs structure.

The liner is usually made from metal, plastic, or composite materials. Because the intention of a COPV is to reduce mass that would traditionally be consumed by a full metal PV, COPVs are commonly designed so that the liner (which is often made from a material with lower specific strength than the overwrap) bares minimal load. This allows the textile composite overwrap which perform best under tension to act as the primary load baring feature.

Polar bosses act as orifices on either end of the vessel which allow for flow in or out of the COPV. Polar bosses typically have threaded or welded joints to piping from or to which flow is directed; However for some applications, more complex mating mechanisms such as expansion fittings must be used. These bosses may contain multiple orifices rather than a single axisymmetric orifice as is shown in figure 1.1 should the application require it.

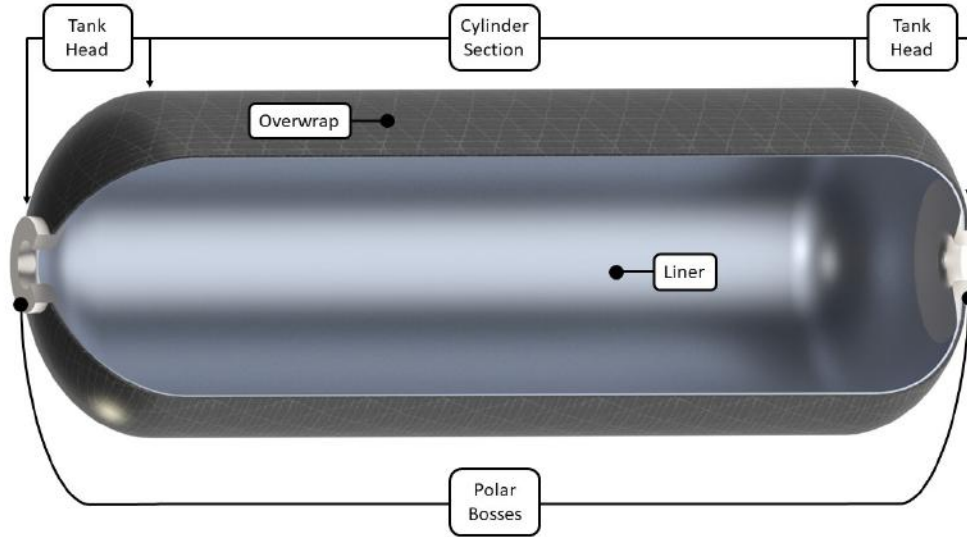


Figure 1.1: Basic COPV diagram with labeled components

1.2 COPV History

NASA engineers began pioneering COPV development in the 1960's with the goal of improving PV mass efficiency [1]. In the early 1970's Pat B. McLaughlan was working on "the NASA Firefighter's Breathing System Program", a project with the objective of "improving respiratory protection for municipal firefighters" [2]. This project began the development and adoption of COPV's for the commercial market [2]. The result of the program was declassification of COPV's which NASA had previously developed for aeronautic applications. COPV's offered the potential for a lightweight alternative to traditional all steel or aluminum type 1 PVs while maintaining adherence to Department of Transportation standards [2, 3].

COPV design started with type 2 PVs which consisted of glass fibers wound around a steel or aluminum liner and eventually developed into type 3 PVs which are characterized by "advanced fibers" wound around a metal liner [2, 3]. The first advanced fibers to be made into a commercial type 3 COPV were Kevlar[®], eventually followed by the use of carbon fiber [2]. All the while COPV technology continued to improve at NASA as they became integrated into launch vehicles such as the Space Shuttle Orbiter; However "stress rupture failure" became an evident concern as a precise understanding of composite fiber loading continued to elude NASA engineers [2].

As COPV research advanced, engineers developed a greater understanding of composites and composite overwraps which has led to common use of lighter, lower safety factor COPVs within the aerospace industry [2]. Nowadays liner options have expanded from steel and aluminum to a wide variety of metals and polymeric materials for type 4 PVs [2, 3]. Recently type 5 or composite liner COPVs have become commercially available as a result of a U.S. Air Force Research project in collaboration with University of Texas and were first utilized on the student built satellite FASTRAC 1 [4].

1.3 Design Context

1.3.1 Mission Statement / LRL Overview

Liquid Rocketry Lab is a student run research organization at North Carolina State University. The LRL Pilot project mission objective is to launch a liquid bipropellant rocket 100km to the Kármán Line. The launch will follow a simplistic trajectory as the only objective is to go as high as possible and to do so with safety held as the primary consideration. LRL is currently on track to become the first student organization to build a liquid propellant rocket to reach space, a secondary objective of the project.

Upon completion of launch vehicle manufacturing and testing, vehicle launch will occur at Spaceport America adjacent the White Sands Missile Range near Las Cruces, New Mexico. After completion of the pilot project, LRL intends to shift its focus towards becoming a fully funded propulsion research center to act as a home for engineering excellence and as a hub for aerospace within North Carolina's research triangle.

NOTE: PROPELLANTS ARE NOT, AND NEVER WILL BE STORED NOR HANDLED ON OR IN CLOSE PROXIMITY TO NORTH CAROLINA STATE UNIVERSITY CAMPUS BY LIQUID ROCKETRY LAB OR ITS AFFILIATES

1.3.2 Rocket Design Overview

Avionics: Avionic systems within the launch vehicle consist of ground control, automated systems monitoring, actuating GNC hardware, and all other electro-mechanical systems. Many of these avionic systems integrate intimately with other systems such as plumbing, recovery, and GNC.

Software: Software is used to control all avionic systems. Software on the flight vehicle will, control automated systems, give vital value feedback for launch operations, assess flight dynamics, and issue control authority for corrective maneuvers. It is being written in a unique human readable language for real time human monitoring as a redundancy to automated monitoring.

Plumbing: Plumbing within the launch vehicle are responsible for filling and conveying fluids within the flight system. Plumbing allows for propellants and pressurants to be loaded into the rocket and then conveys these fluids from the COPVs in which they are stored to the engine for combustion. Plumbing also supports the function of cleaning and fluid systems maintenance. The plumbing system moderates pressure drop / pressure level maintenance within the launch vehicle.

Recovery: The recovery system is responsible for getting the rocket back to ground safely. This includes drag devices such as parachutes, ballutes, associated deployment mechanisms, along with descent regime modeling. Recovery has loading implications for other subsystems and may have to work intimately with GNC and Avionics on projects such as recovery guidance and tracking of any separating components.

Airframe: The airframe is comprised of the systems which provides support and act as the skin for much of the rocket. For the sake of this paper, 'airframe' also accounts for the nosecone / payload fairing. The airframe acts as a mounting point for all other systems and will likely be broken into multiple sections rather than a single continuous frame.

GNC: Guidance Navigation and Control is the system responsible for maintaining trajectory of the rocket. It combines control surfaces, avionics, and software to apply moments about the rockets center of pressure while in flight. The GNC system will be one of the most robust systems within the launch vehicle providing ultimate control regardless of the situation. GNC is particularly responsive to mass changes in other systems and requires the consideration of dynamic changes throughout flight.

Engine: The engine/powerpack assembly are the parts of the rocket that provide thrust for flight. The current design has a regeneratively cooled combustion chamber with a truncated ideal contour nozzle. The engine aims to provide approximately 3000 lbf of thrust. Combustion occurs with an intended chamber pressure of 500 psi and a testing atmospheric exit pressure of 14.7 psi. The engine currently plans for a combined propellant mass flow rate of 5.34 kg/s mixed at a ratio of 7:1 (HTP:RP-1).

System Specifications

2.1 Constraints

2.1.1 Tanks shall operate as designed at MEOP

MEOP or maximum expected operating pressure is a main determining factor of required strength for a PV for most applications. For a COPV it, in concert with other loading defines the amount of overwrap required. MEOP is determined by the engines required flow rate, the required pressure drop throughout the propulsion system, and for the pressurant tank the engines required burn time. For compressible fluids such as the pressurant, gas volume also contributes to determination of MEOP as a larger vessel would require lower pressure to hold the same volume of gas.

Propellant COPVs shall be designed to a MEOP of 1000 psi

The MEOP requirement stated by William Hitchcock, LRL Vice President of Propulsion, and confirmed by LRL President of Engineering Alexander Allen is 1000 psi. This pressure will allow for proper propellant flow rate and injection pressure at the engine.

Pressurant COPV shall be designed to a MEOP of 6000 psi

The MEOP requirement stated by Alexander Allen and confirmed by William Hitchcock for the pressurant tank is 6000 psi. This pressure will allow a sufficiently small tank while providing enough pressurant to maintain 1000 psi in the propellant tanks throughout the entirety of the burn cycle. Because the pressurant will be a compressible fluid, both pressure and volume are flexible parameters.

2.1.2 Tanks shall meet or exceed mass budget

The Tsiolkovsky Rocket Equation also known as the Ideal Rocket Equation describes an idealized situation in which a change in a rocket's velocity, and subsequently it's achievable altitude is dictated by the rockets exhaust velocity and its mass ratio [5]. A rockets mass ratio is defined as the rockets mass when full of propellant, here-forth referred to as 'full mass' divided by the rockets mass when empty here-forth referred to as 'dry mass' [5]. Because this relationship exists, the mass of each system within the rocket is critical to the rockets ability to achieve its mission objective.

This need for strict control over mass along with limitations on engine thrust is what has led to the concept of a mass budget. In essence the cap on the mass budget

for the rocket as a whole is the maximum allowable dry mass of the rocket such that when full, the mass ratio is great enough to allow for sufficient velocity throughout the rockets flight to meet its objective. Just as a financial budget is distributed to an organizations departments to meet the individual needs of each department, a mass budget is distributed to a rockets subsystems to meet the individual needs of each subsystem. For this application an initial mass budget for the rocket as a whole has been sorted by auditing the needs of each subsystem with an applied buffer factor. The cap for which the sum of subsystem masses must deceed has been set by using an analytical program to predict rocket height based upon thrust and weight.

To give an initial estimate of tank weight contribution, minimum tank weight was estimated using the COPV analytical scripts in code appendices 6.1.1 and 6.1.2. The scripts assume aluminum liners with hemispherical tank heads and a carbon fiber reinforced epoxy overwrap. The liner was set to a thickness of 0.10". This estimate was then multiplied by 1.5 and rounded to the nearest 5 lb. This buffer factor has been added to account for tank bosses, fittings, internal plumbing, and any additional wrapping that may be required. This value was confirmed as a valid estimate for subsystem budget by LRL President of Engineering Alexander Allen who compiled the entire mass budget.

Mass of propellant tanks shall not exceed 260 lbm

Using the COPV analytical Matlab script in code appendix 6.1.1 the initial expected weight for the propellant tanks is 167.35 lb for a common bulkhead design and 174.21 lb for an individual tank design. To give a buffer, the higher of the two values was multiplied by 1.5 and rounded to the nearest 5 lb giving 260 lbm. Note that this value does not include any internal features such as baffling or plumbing.

Mass of pressurant tank shall not exceed 140 lbm

Using the COPV analytical Matlab scripts in code appendices 6.1.1 and 6.1.2 a minimum expected weight for the propellant tanks is 91.14 lb. This value was multiplied by 1.5 and rounded to the nearest 5 lb giving 140 lbm. Note that this value does not include any internal features such as baffling or plumbing.

2.1.3 Tanks shall accommodate adequate propellant flow rate

Mass flow rate is a standard unit of measure for propellant flow. As previously stated the engine requires a combined mass flow rate (\dot{m} of 5.34 kg/s to maintain combustion stability. This is the current working estimate which has been solved for by LRL President of Engineering Alexander Allen. With a mix ratio of 7:1 (HTP:RP-1) this gives mass flow rates $\dot{m}_{HTP} = 4.67$ kg/s and $\dot{m}_{RP-1} = 0.67$ kg/s. To ensure that these needs are met, the tanks must have appropriately sized outlet ports and a sufficiently non-flow-restrictive set of interior features.

Oxidizer tank shall accommodate $\dot{m}_{HTP} = 4.67$ kg/s

Fuel tank shall accommodate $\dot{m}_{RP-1} = 0.67$ kg/s

2.1.4 Tanks shall possess factor of safety based on probability of failure analysis with probability of survival ≥ 0.999

As explained in a 2007 article by Grimes-Ledesma et al. [6], the Phoenix Model is a probabilistic model based on a Weibull distribution that assesses probability of failure as a function of stress and time. The fundamental equation for the Phoenix Model is shown below [6]:

$$P(t, \sigma) = 1 - e^{(-((\frac{t}{t_{c,ref}})(\frac{\sigma_{op}}{\sigma_{burst}})^{\rho})^{\beta})} \quad (2.1)$$

Phoenix Model:

t = time, $t_{c,ref}$ = reference time (end time), σ_{op} = stress at MEOP, σ_{burst} = expected rupture stress, ρ = power law exponent, β = Weibull shape parameter for lifetime

This fundamental Phoenix Model equation as described in [7], is best used to evaluate probability of failure for steady state conditions. For complex loading histories such as the one that will be exhibited during flight, the “conditional reliability equation” can be used. However, this requires that stresses are known for the entire loading history, which is incredibly difficult to model without experimental launch data. In lieu of a conditional reliability equation, Engelbrecht-Wiggans et al. explain that a lifetime distribution for failure probability can be modeled using a “cumulative distribution function for time to failure” [8]. The cumulative distribution function is described by the equation below [8]:

The cumulative distribution function is likely the best model for a high vibration situation as is expected during flight. However when examining this model a new problem arises; Though the article offers parameter value suggestions such as “For carbon fiber composites ... β is typically less than 0.3, and for T1000 carbon/epoxy tows can be as low as 0.07” [8], these parameter values must be determined experimentally and are unique to each composite material type [9]. Because of current limitations, this

$$F_{1979, \bar{\sigma}}(t) = 1 - e^{-\left(\frac{\bar{\sigma}}{\sigma_{ref}}\right)^r + \left(\frac{\bar{\sigma}}{\sigma_{ref}}\right)^\rho \frac{t}{t_{ref}})^{\beta}} \quad (2.2)$$

Cumulative distribution function for time to failure:

t = time, t_{ref} = time scaling parameter, σ_{ref} = stress scaling parameter, $\bar{\sigma}$ = average stress over lifetime, r = parameter reflecting the sensitivity of the material to instantaneous load, ρ = power law exponent, β = Weibull shape parameter for lifetime

model cannot be used. However given the opportunity to acquire accurate parameter values, use of a cumulative distribution model would be suggested.

Due to these issues with more detailed models, a simpler model is suggested in a 2003 article by Chang et al [10]. Chang et al. propose the use of the Lifetime Model “two-parameter Weibull distribution equation” shown below [10]:

$$P(t) = e^{-\left(\frac{t}{\beta}\right)^\alpha} \quad (2.3)$$

Probability of failure for a specified design life time interval:

t = time, α = Weibull shape factor, β = Weibull shape parameter for lifetime

Note that both the Phoenix Model and the cumulative distribution function both have a ‘1-’ in front of the $e^{(\dots)}$ term. This is because these equations are modeling *probability of survival* rather than probability of failure. In the report by Chang et al. it is suggested that probability of survival must be greater than 0.999 or 99.9% [10]. This means that $1-P(t)$ must be ≥ 0.999 . In the article Chang et al. provides α values as well as equations to obtain β values based upon the composite material type chosen for the overwrap. The table below containing this information has been recreated from the report [10]:

Table 2.1: Lifetime Model Weibull parameter values for given composite types

| Composite System | Shape Parameter | Scale Parameters |
|------------------|-----------------|--|
| Glass/epoxy | $\alpha = 1.00$ | $\beta = (1.4 \times 10^{13})10^{(-0.158(\%ULT))}$ |
| Kevlar/epoxy | $\alpha = 0.93$ | $\beta = (2.0 \times 10^{18})10^{(-0.198(\%ULT))}$ |
| Graphite/epoxy | $\alpha = 0.20$ | $\beta = (1.4 \times 10^{51})10^{(-0.515(\%ULT))}$ |

“%ULT is the applied stress level as a percentage of the ultimate burst strength (e.g., for applied stress level of 50% ultimate burst strength, %ULT = 50).” [10]

Using the code shown in Code Appendix entry 6.1.3, probability of success was calculated using the assumption of a carbon fiber over wrap. MEOP was held constant based on the contextual assumptions that propellant COPVs are pressurized to 1000 psi and pressurant COPVs are pressurized to 6000 psi. Expected burst strength was incrementally increased until a probability of success equal to 0.999 was achieved. For both propellant and pressurant COPVs this analysis resulted in a factor of safety (FoS) of 1.426. This means that to meet this requirement, the COPVs must be manufactured

with a maximum service pressure of MEOP*FoS or **1426 psi** for the propellant COPVs and **8550 psi** for the pressurant COPV.

2.1.5 Propellant COPV’s shall possess capacity sufficient for a karman line shot

This specification outlines the entire purpose of the propellant COPVs; Holding enough propellant to carry the rocket to space. The basis of this specification is the concept known as "The Tyranny of the Rocket Equation" [11]. Pettit explains that The Tyranny of the Rocket Equation is based on Tsiolkovsky’s ideal rocket equation (explained in [5]) along with the idea that once a destination is set and a propellant system with a specific energy capability is selected, one simply has to work with the energy they have to get them to the destination. In other words, once the destination and the propellant system are selected "the rocket mass fraction is now dictated by the rocket equation" [11]. This means that with increasing weight, additional propellant is required; However additional propellant adds to the weight of the rocket.

Through use of this concept a preliminary balance has been struck between dry and wet mass to hit a rocket mass fraction capable of the mission objective. Because this estimate has been made solely using estimates given by LRL sub-teams about their likely sub-system masses, the propellant mass and in kind propellant volume is likely to change with evolution in design. Because of this propellant capacity viewed as volume for the sake of COPV design will have to be a variable parameter within the design which can be changed to update the design in the future. For the sake of calculations performed in this paper the current estimate for propellant requirements generated by LRL President of Engineering Alexander Allen are as follows:

| | |
|--------------------|------------|
| HTP mass: | 733.04 lbm |
| HTP volume: | 410.49 L |
| RP-1 mass: | 104.72 lbm |
| RP-1 volume: | 32.99 L |

2.2 Functional Specifications

2.2.1 Tanks shall withstand loading of parachute deployment

Because the COPV must be designed not only as tanks for propellants and pressurants but also as structural components for the rocket, the highest tensile loads the tanks are likely to face during flight aside from pressurization are during parachute deployment. Each COPV must bare the tensile load of any remaining internal pressure, plus the loads imparted by the recovery system equal to the rockets negative acceleration multiplied by the mass below the cross section of the tank being examined. Depending on the vehicles velocity at system deployment, drag brake size, energy dissipation mechanisms within the recovery system, and the mass of rocket components to impart load on the tanks, the stresses within the tanks will be non-trivial. This consideration is especially

important when considering integration of the tanks with airframe sections and design of the interface between them.

Tank shall withstand an additional axial tensile load of 3195 lbf

As currently modeled, the recovery system regime consists of an initial ballute deployment close to 35km AMSL , followed by a drogue chute deployment at 5km AGL, followed by the main chute deployment at 1.5km AGL before touchdown [12, 13]. Figure 2.1 shows various metrics important to determining specifics of the recovery system.

A ballute is an aerodynamic braking device that uses a combination of features borrowed from balloons and parachutes [14]. Ballutes are useful for "extremely high flow velocities"[14], and because the falling rocket is expected to be traveling at just over mach 3.8 at the time of ballute deployment, high deployment velocity is what makes ballutes desirable for the application[12].

"Drogue parachutes are used to slow and stabilize the [rocket] during descent and establish proper conditions for main parachute deployment to follow" [15]. Drogue chutes are commonly used in rocket recovery, fighter jet arrestment, and other parachute braking systems. Incorporation of a drogue chute helps ensure main chute deployment stability and acts as a countermeasure for tangling of the main chute's riser lines upon deployment.

The main chute's objective is to decelerate to touchdown velocity ensuring a minimally damaging landing for the launch vehicle. Parachute design is highly varied based on the application, however common contextually applicable parachute designs under consideration are cruciform and ringsail chutes. The exact geometry of these chute is currently undetermined aside from the minimum allowable drag area. Parachutes have historically been the most common method of recovery for re-entry vehicles. It was not until recently that companies such as SpaceX and Blue Origin have begun using powered landings; However even these companies continue to use parachutes to recover payload fairings and crew capsules.

The preliminary recovery simulation script written by Jeffrey-Wilensky [12, 13] produced the acceleration profile for descent seen in figure 2.2. The maximum expected acceleration seen by the system with a magnitude of $-52.21 \frac{m}{s^2}$ occurs when the ballute enters a higher density atmospheric layer at approximately 140 seconds after apogee. Assuming the RP-1 tank is positioned above the HTP tank, and that the pressurant tank is contained within the airframe, the RP-1 tank will undergo the highest tensile stress of all the tanks because it has the most mass positioned below it.

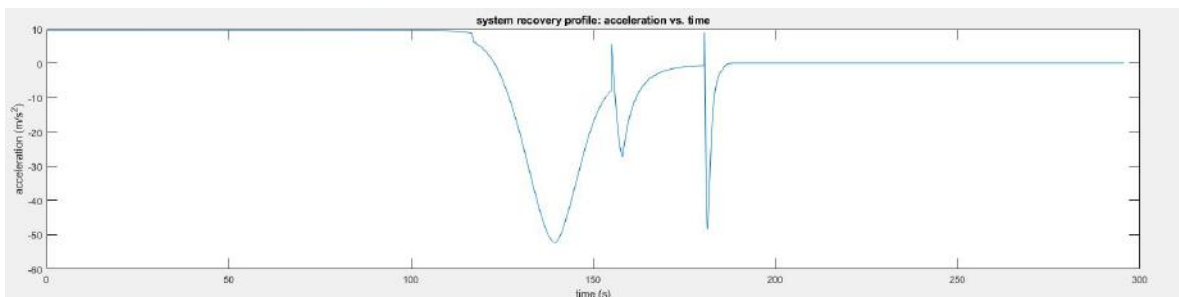


Figure 2.2: System descent profile (acceleration as a function of time) [12]

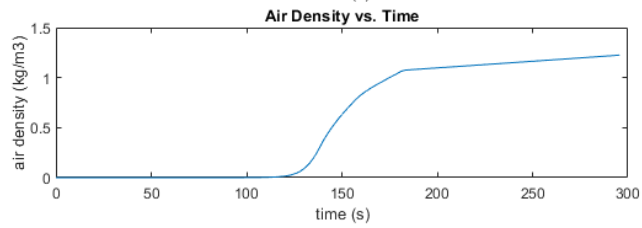
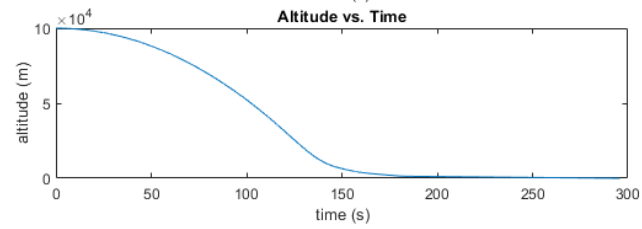
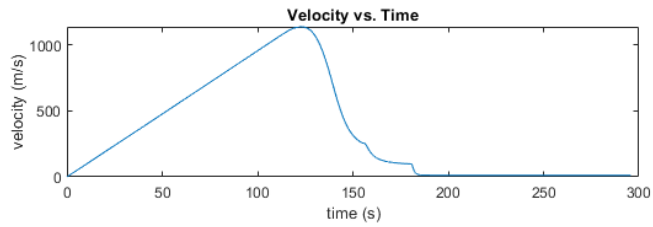
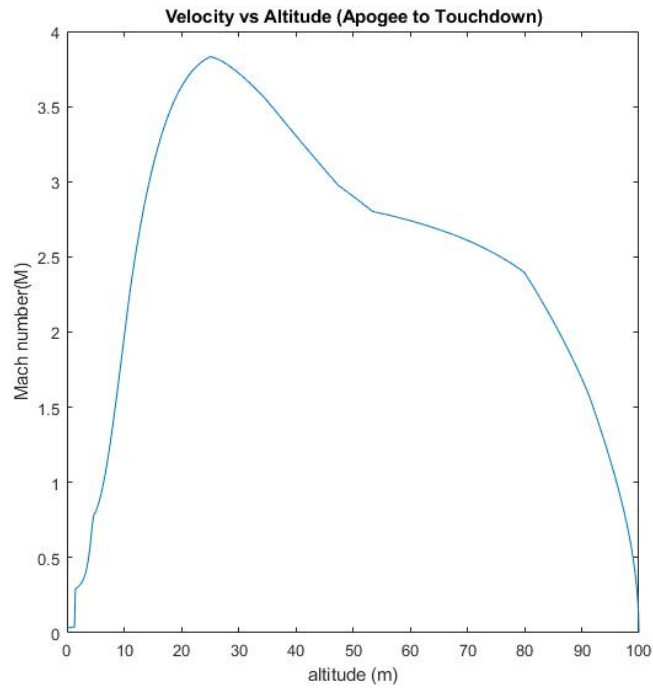


Figure 2.1: descent profile characteristics [12]

Using the Matlab COPV analysis scripts in code appendices 6.1.1 and 6.1.2 as a basis, a composite shell thickness of 0.16 inches and an 8 inch outer radius is assumed. Additionally assuming the rocket has 600 lb of dry weight below the top of the fuel tank. Additionally it is assumed that whatever mechanism is used to integrate the COPVs to the airframe joins the tanks after the curvature of the tank head leaving only the cylindrical midsection of the tanks bearing weight on deployment.

With these assumptions the composite overwrap is found to have a cross sectional area of 7.96in^2 . Using the weight assumption as along with the given acceleration, a force of 3194.358 lbf is calculated. Using the definition of stress ($\sigma = \frac{P}{A}$; P = applied force, A = cross sectional area) we obtain a stress value of $401.57 \frac{\text{lbf}}{\text{in}^2}$. Given that the tanks have been rated to MEOP = 1000 psi, provided the tanks have been depressurized below 600 psi, they should be rated to withstand the imparted load.

2.2.2 Tanks liners must be compatible with stored compounds

A lack of compatibility between a COPV liner and the chemical it is storing creates potential for unpredictable catastrophic failure. The primary failure mode of concern for pressure vessels with regard to material incompatibility is stress corrosion cracking. SCC is a phenomena in which a part under tensile stress within a corrosive environment forms localized defect zones which lead to fracture [16]. SCC is of particular interest in metals as chemical concentration variance along grain boundaries leads to corrosive susceptibility [16]; However SCC can also occur in polymeric materials along with polymer degradation.

Liner material must be class A or B for all contents

Note: Class A and B are defined using the following criteria on the A,B,C,D, ^{1,2} Cole-Parmer scale[17]

A - Suitable

B - Good, minor effect, slight corrosion or discoloration

C - Fair, moderate effect, not recommended for continuous use

D - **Do not use** - severe effect

¹ - Satisfactory up to 72°F

² - Satisfactory up to 120°F

*Note: COVPs with advanced fibers and metal liners are classified as **type 3** COPVs. COPVs with advanced fibers and polymeric liners are classified as **type 4** COPVs.*

Oxidizer tank liner material selection

To examine useful materials for an HTP COPV liner, a high level material compatibility review was conducted. According two web resources, [17, 18] the following list of materials exhibit material compatibility of type A or B as required by specification:

- ABS plastic
- Aluminum
- Stainless Steel
- Ceramic Al203
- Ceramic magnet
- CPVC
- Hastelloy-C[®]
- NORYL[®]
- Polycarbonate
- PTFE (Teflon[®])
- PVC
- Viton[®]

These materials can then be separated into the following classifications:

Metals

- Aluminum
- Stainless Steel
- Hastelloy-C[®]

Ceramics

- Ceramic Al203
- Ceramic magnet

Polymers

- ABS plastic
- CPVC
- NORYL[®]
- Polycarbonate
- PTFE (Teflon[®])
- PVC
- Viton[®]

For the application, ceramics can be dismissed due to their low fracture toughness and low specific tensile strength. This leaves metals and polymers as possible liner materials.

Material candidates for oxidizer type 3 COPV liner

Because the metals outlined in the high level review have significant variance among a given material category, a deeper examination is required. Hastelloy-C[®] can be removed from the list as it is prohibitively expensive, difficult to work with, hard to procure in the desired quantities or geometries, and the high operating temperatures at which it exhibits its greatest corrosion resistant benefits would not be utilized in this application.

In a presentation by Parabilis Space Technologies the chemical resistance of different alloys of aluminum and stainless steel to HTP was considered [19]. Parabilis used a numerical class system for describing material compatibility, but for the sake of uniformity the ratings will be translated into the alphabetical scale previously defined. Table 2.2 gives the material and corresponding class of each metal variety that falls into class A or B.

Because 355 and B356 are casting alloys and the wall thickness of a liner would be too small compared to the liners other dimensions to cast, these alloys can be disregarded. 1xxx series Al is regarded as commercially pure aluminum. 1060, 1160, and 1260 aluminum all fall under this CP designation and 1060 is the most abundant CP Al alloy. CP aluminums are low in mechanical properties compared to their alloyed counterparts, and are typically more expensive. Because of this, 1160 and 1260 will be eliminated from candidacy.

Table 2.2: HTP compatible metal liner materials

(a) Compatible aluminum alloys

| Aluminum | |
|----------|----------------|
| Alloy | Class |
| B356 | A ² |
| 1060 | A ² |
| 1160 | A ² |
| 1260 | A ² |
| 5254 | A ² |
| 5652 | A ² |
| 7072 | A ² |
| 355 | B |
| 6061 | B |

(b) Compatible stainless steel alloys

| Stainless Steel | |
|-----------------|-------|
| Alloy | Class |
| 304 | B |
| 316 | B |
| 347 | B |

Similarly, 5652 aluminum is more difficult to get a hold of than 5254, so 5652 will be removed from this material review in favor of 5254 Al. To maintain uniformity all material entries were retrieved from the same database. This database, Knovel, did not have information on 7072 Al [20]. Because of this as well as the difficulty in procurement 7072 Al has also been eliminated.

Table 2.3 shows truncated and edited versions from tables appearing in Knovel to convey information relevant to this application [20]. The table section of aluminum processability considerations in table 2.3 has been curated to reflect manufacturing processes likely to occur in liner manufacturing. Though not all of these processes will necessarily be used, it is nearly certain that welding, machining, and cold working will be used to some degree in the manufacturing of any liner. Because of this, materials with an "unacceptable" or "borderline" processability rating can be eliminated from candidacy on the grounds that a liner would likely not be able to be made from the material. Due to a lack of stainless steel information from Knovel, it will be assumed that all stainless steels rank sufficiently high in required processability considerations. Using this process of elimination, viable material candidates for type 3 liners for use with HTP are:

- 5254 Al (H34,H36,H38,H112)
- 6061 Al (T1,T4,T451,T51,T6,T651)
- 304L SS
- 316 SS
- 347 SS

Table 2.3: Type 3 COPV liner material comparison

| Aluminum Alloys | | | | | | | | | | | | | | |
|-----------------|---------|----------|-----------|-----------|------------|-----|---------|----------|-------------|-----------------|-------|-----------------|-------|-------|
| Alloy | UNS no. | temper | UTS (ksi) | TYS (ksi) | % δ | BHN | G (ksi) | Se (ksi) | E (103 ksi) | ρ (lb/in3) | s.g. | CTE (10-6 °F-1) | ν | μ |
| 1060 | A91060 | O | 10 | 4 | 43 | 19 | 7 | 3 | 10 | 0.098 | 2.705 | 13.1 | 0.33 | 0.4 |
| 1060 | A91060 | H12 | 12 | 11 | 16 | 23 | 8 | 4 | 10 | 0.098 | 2.705 | 13.1 | 0.33 | 0.3 |
| 1060 | A91060 | H14 | 14 | 13 | 12 | 26 | 9 | 5 | 10 | 0.098 | 2.705 | 13.1 | 0.33 | 0.3 |
| 1060 | A91060 | H16 | 16 | 15 | 8 | 30 | 10 | 6.5 | 10 | 0.098 | 2.705 | 13.1 | 0.33 | 0.3 |
| 1060 | A91060 | H18 | 19 | 18 | 6 | 35 | 11 | 6.5 | 10 | 0.098 | 2.705 | 13.1 | 0.33 | 0.3 |
| 5254 | A95254 | O | 33 | 13 | 22 | 60 | 19 | 17 | 10.2 | 0.096 | 2.66 | 13.3 | 0.33 | 0.4 |
| 5254 | A95254 | H32 | 40 | 29 | 13 | 73 | 23 | 18 | 10.2 | 0.096 | 2.66 | 13.3 | 0.33 | 0.3 |
| 5254 | A95254 | H34 | 43 | 32 | 12 | 78 | 25 | 19 | 10.2 | 0.096 | 2.66 | 13.3 | 0.33 | 0.3 |
| 5254 | A95254 | H36 | 46 | 35 | 11 | 82 | 27 | 20 | 10.2 | 0.096 | 2.66 | 13.3 | 0.33 | 0.3 |
| 5254 | A95254 | H38 | 50 | 39 | 10 | 88 | 29 | 21 | 10.2 | 0.096 | 2.66 | 13.3 | 0.33 | 0.3 |
| 5254 | A95254 | H112 | 34 | 13 | | 62 | 20 | 17 | 10.2 | 0.096 | 2.66 | 13.3 | 0.33 | 0.3 |
| 6061 | A96061 | O | 18 | 8 | 25 | 30 | 12 | 6 | 10 | 0.098 | 2.7 | 13.1 | 0.33 | 0.3 |
| 6061 | A96061 | T1 | 22 | 13 | 20 | 40 | 14 | 7 | 10 | - | - | - | - | - |
| 6061 | A96061 | T4, T451 | 35 | 21 | 22 | 65 | 24 | 14 | 10 | 0.098 | 2.7 | 13.1 | 0.33 | 0.3 |
| 6061 | A96061 | T51 | 42 | 35 | 11 | 80 | 25 | 14 | 10 | - | - | - | - | - |
| 6061 | A96061 | T6, T651 | 45 | 40 | 12 | 95 | 30 | 14 | 10 | 0.098 | 2.7 | 13.1 | 0.33 | 0.3 |

| Alloy | UNS no. | temper | corrosion resistance | cold workability | machinability | weldability | resistance and spot weldability | extrudability |
|-------|---------|----------|----------------------|------------------|---------------|-------------|---------------------------------|---------------|
| 1060 | A91060 | O | Excellent | Excellent | Unacceptable | Excellent | Very Good | Excellent |
| 1060 | A91060 | H12 | Excellent | Excellent | Unacceptable | Excellent | Excellent | Excellent |
| 1060 | A91060 | H14 | Excellent | Excellent | Borderline | Excellent | Excellent | Excellent |
| 1060 | A91060 | H16 | Excellent | Very Good | Borderline | Excellent | Excellent | Excellent |
| 1060 | A91060 | H18 | Excellent | Very Good | Borderline | Excellent | Excellent | Excellent |
| 5254 | A95254 | O | Excellent | Excellent | Borderline | Excellent | Very Good | Very Good |
| 5254 | A95254 | H32 | Excellent | Very Good | Borderline | Excellent | Excellent | Very Good |
| 5254 | A95254 | H34 | Excellent | Very Good | Fair | Excellent | Excellent | Very Good |
| 5254 | A95254 | H36 | Excellent | Fair | Fair | Excellent | Excellent | Very Good |
| 5254 | A95254 | H38 | Excellent | Fair | Fair | Excellent | Excellent | Very Good |
| 5254 | A95254 | H112 | Excellent | Very Good | Fair | Excellent | Excellent | Very Good |
| 6061 | A96061 | O | Very Good | Excellent | Borderline | Excellent | Very Good | Very Good |
| 6061 | A96061 | T1 | Very Good | Very Good | Fair | Excellent | Excellent | Very Good |
| 6061 | A96061 | T4, T451 | Very Good | Very Good | Fair | Excellent | Excellent | Very Good |
| 6061 | A96061 | T51 | Fair | Very Good | Fair | Excellent | Excellent | Very Good |
| 6061 | A96061 | T6, T651 | Very Good | Very Good | Fair | Excellent | Excellent | Excellent |

| Stainless Steel Alloys | | | | | | | | |
|------------------------|-----------------|---------|-----------------|-------------------|-----------|-----------|-------------------------|-----|
| material name | ρ (lb/in3) | G (ksi) | CTE (10-6 °F-1) | E (ksi) | UTS (psi) | YTS (psi) | elongation at break (%) | BHN |
| 304L Stainless Steel | 0.28902 | | 10.4 | 27992.3 - 29007.5 | 81801.3 | 30457.9 | 58 | |
| 316 Stainless Steel | 0.28902 | | 9.72 | 27992.3 | 89923.4 | 60190.7 | 45 | 190 |
| 347 Stainless Steel | 0.28902 | 11167.9 | 10.4 | 28282.4 | 100076 | 65267 | 40 | 212 |

Material candidates for oxidizer type 4 COPV liner

Acceptable liner materials for Type 4 COPVs must be considered as well. Mechanical properties for tank manufacturing is a primary concern and eliminator of chemically compatible materials. Viton[®] can be eliminated due to its low elastic modulus and high elasticity (it is a rubbery material). While it may be a useful material for O-rings which may show promise should expansion joints be needed, it is not suitable for a rigid tank liner. The remaining polymeric materials are have a Tg much higher than Viton[®] and are rigid at room temperature.

To select viable materials the manufacturing processes used to make the liners must be taken into consideration along a given the materials properties. Given the geometry of a pressure vessel, the methods for producing a type 4 COPV liner include rotomolding, blow molding, and welding [21]. rotomolding and blow molding offer a seamless liner and allow easy integration of a metallic boss to connect to the rest of the propellant feed system. Welding by virtue of the process creates seams where the welds have been made which may act as source or imperfections.

Due to the expensive tooling required for rotomolding and blow molding this an unrealistic option for one off specialty parts. Therefore welding is the most realistic manufacturing technique for the project scope. To ensure a decent level of cylindricity throughout the length of the liner it would be optimal to use an extruded pipe section as the cylindrical section of the liner. PVC is commonly produced in large diameter pipe for ducting and can be easily thermoformed and welded. Additionally, PVC is a class A material within the previously defined scale [17]. These traits make PVC the best liner material option for a type 4 oxidizer COPV within the constraints of this project.

Fuel tank liner material selection

The fuel to be used in the launch vehicle, RP-1, is a highly refined kerosene which has been designed to increase combustion efficiency and reduce production of soot compared with jet fuel or less refined kerosene [22, 23]. Additionally, like HTP, RP-1 has the benefit that it is liquid at room temperature eliminating the need for cryogenic storage considerations. Because RP-1 is simply a highly refined kerosene, and literature specific to RP-1 material compatibility is sparse and primarily related to elastomers, material compatibility with kerosene in general will be examined rather RP-1. According to the chemical compatibility database offered by Davis Instruments, a subsidiary of Cole-Parmer [24], the following materials exhibit compatibility of type A or B as required by specification:

- Acetal (Delrin[®])
- Aluminum
- Stainless Steel
- Brass
- Bronze
- Carbon graphite
- Carbon steel
- Carpenter 20
- Cast iron
- Nitrile
- Ceramic Al₂O₃
- Ceramic magnet
- ChemRaz (FFKM)
- Kalrez[®]
- Kel-F[®]
- Neoprene
- Polypropylene
- Polyurethane

- PPS (Ryton[®])
- PVC
- Titanium
- PTFE
- PVDF (Kynar[®])
- Viton[®]

These materials can then be separated into the following classifications:

Metals

- Aluminum
- Stainless Steel
- Brass
- Bronze
- Carbon steel
- Carpenter 20
- Cast iron
- Titanium

Ceramics

- Ceramic Al203
- Ceramic magnet

Polymers

- Acetal (Delrin[®])
- Nitrile
- ChemRaz[®] (FFKM)
- Kalrez[®]
- Kel-F[®]
- Neoprene
- Polypropylene
- Polyurethane
- PPS (Ryton[®])
- PTFE
- PVC
- PVDF (Kynar[®])
- Viton[®]

Similar to the oxidizer liner materials, ceramics can be dismissed due to their low fracture toughness and low specific tensile strength. This leaves metals and polymers as possible liner materials.

Material candidates for fuel type 3 COPV liner

Metals which exhibit low specific strength or an inability to be formed into thin walled structures such as cast iron or bronze can be disregarded for this application. Additionally carpenter 20, brass, and titanium can be dismissed due to their high cost in comparison to other viable options. Carbon steel can be eliminated due to its susceptibility to oxidize without surface treatment which could cause contamination of the stored propellant or destructive interference with other parts of the plumbing or engine. Similarly to the HTP liner, this leaves aluminum and stainless steel alloys as the most viable candidates for the application.

Kerosene is generally considered a non-corrosive material with low volatility [25] meaning that Kerosene should be compatible with the majority of alloys for both Al and SS; However in the interest of thoroughness the following alloys are confirmed to

be safe for use with kerosene, and material design inquiry outside of the below listed materials require specific research to ensure compatibility. All material options with an asterisk(*) have been tested with JP8, a kerosene base jet propellant, but not pure kerosene.

Table 2.4: RP-1 compatible metal liner materials

(a) Compatible aluminum alloys

| Aluminum | | |
|----------|-------|--------|
| Alloy | Class | Source |
| 5052 | A* | [26] |
| 7075 | A* | [26] |
| 6061 | A* | [26] |

(b) Compatible stainless steel alloys

| Stainless Steel | | |
|-----------------|-------|--------|
| Alloy | Class | Source |
| 304 | A | [24] |
| 316 | A | [24] |
| 347 | A* | [26] |

Material candidates for fuel type 4 COPV liner

As with the HTP tank liner, elastomeric materials should be dismissed from consideration including nitrile, ChemRaz[®], neoprene, and Kalrez[®]. Additionally due to limitations on roto and blow molding capabilities as previously expressed, only extrudable, thermoformable, and weldable materials which come in pipe sections will be considered. This leaves PPS and PVC as viable options for type 4 fuel COPV liners.

Pressurant tank liner material candidates

The pressurant for the rocket is currently planned to be nitrogen (N₂), a fairly inert gas. Because these N₂ is non-reactive with most structural materials, liner selection for the pressurant tank will be highly dependent on cost and manufacturability rather than chemical compatibility. Therefore, it will be noted that at operating temperature all previously considered structural materials are compatible with nitrogen. Before a final design decision is made the material candidates most likely for use should be checked for compatibility with N₂ at expected operating temperatures.

2.2.3 Tanks shall maintain pressure at MEOP

According to the previously cited report by Chang et al. “leak testing should be performed after proof-pressure test[ing]. During the leak check the pressure should be maintained at MEOP for 30 minutes minimum” [10]. For the purposes of LRL testing should occur over a period of time equal to the time the launch vehicle is expected to be pressurized on the pad plus the expected flight time or 30 minutes, whichever is longer.

A faulty gauge could result in the disqualification of a tank that actually should pass inspection. Because of this all gauges used to test must be checked against standards to ensure their reliability. Additionally gauges with a tolerance of value insignificant to functional performance must be used. tanks should also be over pressurized with relation to the required limit for flight, ideally to failure. However, as testing to failure is likely not within the LRL budget, a pressurization of $1.1 \cdot MEOP$ should ensure tank viability in the event of slight over-pressurization.

2.2.4 Tanks shall function under in-flight loading conditions

Flight dynamics provide a wide array of loading conditions which must be considered for system design. A 2016 report by Newlands et al. at Aspire Space gives an overview of these forces and provides equations for modeling [27]. In the report they discuss inertial loads, axial loads, and gust loads. Newlands et al. opt to avoid discussion of slosh loads in the article.

Newlands et al. explain that inertial loads are caused by mass resisting acceleration [27]. These inertial loads are governed by Newtons third law $F = ma$. This can be applied locally to a particular mass component of the rocket using the formulation $F = m_{local} \cdot a_{global}$ where $a_{global} = \Sigma F / \Sigma m$ [27]. If applied off axis, these local inertial loads can cause bending of the rocket resulting in bending loads on the tanks. Bending loads are also possible with side loads such as uneven lift on different surfaces of the rocket.

Because the COPVs are pressurized during their functional state causing them to be relatively rigid entities, primary loading concerns for the COPVs are in the axial direction rather than side loading. That is to say inertial loads caused by mass above an entity in the thrust direction are the biggest concern. These loads will show up in the COPVs as compression caused by the acceleration of the rocket and the mass above the integral section of the COPV being examined. Inertial loads will change in magnitude throughout the flight as propellant is consumed. Once a dynamic model has been created for the rockets flight it will be important to determine the maximum inertial load on the COPVs.

Other axial loads include drag, thrust, and internal pressure. Newlands et al. state that these forces can be summed using equation 2.4 where T is thrust, S is loaded area, and ΔP is the difference in pressure inside and outside of a pressurized entity [27]. The report notes that continuous loads such as skin drag and mass should be treated as an integral.

$$A(z) = -T + D_{nose} + D_{fuselage} + D_{base} + S\Delta P + a_z \sum_{z=0}^z \quad (2.4)$$

COPVs shall exhibit a safety factor of 1.426 for in flight loads

The report gives a suggested safety factor of 1.5. It seems to be a safe assumption that the 1.426 safety factor as determined by probability of failure analysis earlier on can be applied to this case as well. Newlands et al. suggestion of 1.5 came from its common use in civil engineering and implied that it was pulled out of thin air to some degree. [27]. After a dynamic model is created and more of the rocket is modeled, the COPVs should be simulated to meet this requirement.

2.3 Objective Specifications

2.3.1 Composite components should meet standards for fiber volume fraction

Fiber volume fraction of a composite (V_f) describes the volumetric proportion of fiber to the composite as a whole. Fiber volume fraction is an important metric of the composites viability because the composites properties are a direct result of the composition of its constituents. Fiber reinforced composites are developed such that the matrix distributes loading to the fibers. If there is a low fiber volume fraction that means there is less reinforcement to distribute load to placing more load on each fiber and generally creating a weaker composite. Because fibers are generally circular in cross section they have a maximum packing density below 100%.

For hexagonally packed fibers the maximum packing density is 0.9068 [28]. However, because fibers are not completely uniform this value is virtually unattainable which is actually a good thing. Because fibers must have matrix surrounding them to distribute the load, if fibers were perfectly packed there would be stress concentrations along the points of contact between the fibers. Additionally perfect packing would inhibit proper fiber wet-out which would increase void content within the composite.

In terms of fiber volume fraction the objective is to achieve as high as possible while promoting full wet-out. Filament winding processes typical draw tows (bundles of aligned fibers) through a resin bath before they are wound around a mandrel. As they leave the resin bath, tows often pass through dies or combs to remove large amounts of excess resin. The tension within the winding tow offers compaction for the fibers beneath which causes excess resin to seep out to the surface where it is then scraped off. This is the process used by Blue Force Technologies.

Another less common form of filament winding that is used for higher tolerance parts uses prepreg or fibers pre-impregnated with resin. Because the prepreg tows (towpreg) have a high fiber volume fraction and near full wetout, use of this process prevents excess resin in the part. However use of towpreg often requires use of an autoclave making it an unlikely candidate for this project.

Overwrap shall possess a fiber volume fraction $\geq 60\%$

On June 29th 2020, LRL structures engineers made a visit to Blue Force Technologies to discuss their manufacturing capabilities. It was determined during the visit that Blue Force Technologies offers filament winding capability sufficient to wrap the tanks for this project. The tour guide Isaac Aspey explained that they have previously wrapped COPVs for other spacecraft such as the Virgin Galactic Spacecraft.

Isaac, who has extensive experience working with the filament winder at Blue Force stated that their system can repeatably produce parts with a fiber volume fractions of 60%-65%. Given the application, a volume fraction of less than 60% would simply be wasted weight on the rocket. Checking with the COPV analysis Matlab scripts in the code appendix, use of a fiber volume fraction of 60% seems to work well. It offers a wide safety zone for variance allowing volume fraction to go as low as 48% without the need for additional lamina.

2.4 COPV Specifications - Tabular

| Req. | Req. Type | Specification | Limits | Units |
|-----------------------|------------|---|---|----------------|
| MEOP | Constraint | Tanks shall operate as designed at MEOP | Propellant = 1000 Pressurant = 6000 | psi |
| Mass | Constraint | Tanks shall meet or exceed mass budget | Propellant = 260 Pressurant = 140 | lbm |
| Mass Flow Rate | Constraint | Tanks shall accommodate adequate propellant flow rate | $\dot{m}_{HTP} = 4.67$ $\dot{m}_{RP-1} = 0.67$ | $\frac{kg}{s}$ |
| FoS | Constraint | Tanks shall possess factor of safety based on probability of failure analysis with probability of survival ≥ 0.999 | 1.426 x MEOP | psi |
| Volume | Constraint | Propellant COPV's shall possess capacity sufficient for a karman line shot | HTP = 410.49 RP-1 = 32.99 | L |
| Volume | Constraint | Pressurant COPV shall possess capacity sufficient for a karman line shot | Vol. = 63.00 @ 6000 psi | L |
| Load | Functional | Tanks shall withstand loading of parachute deployment | Tensile load = 3195 | lbf |
| Material | Functional | Tanks internal features must be compatible with stored compounds | A or B | Class |
| Pressure loss | Functional | Tanks shall maintain pressure at MEOP | $P_0 - P_F \leq$ <i>gauge tolerance</i> | psi |
| Dynamic loads | Functional | Tanks shall function under in-flight loading conditions | 1.426 x Max Load | psi |
| Fiber Volume fraction | Objective | Composite components should meet standards for fiber volume fraction | $V_f \geq 55$ | % |

Table 2.5: Quantified Specifications

Trade Studies

3.1 Propellant Tank Configurations

Tank configuration is one of the largest design decisions for the propellant COPV system. With implications on weight, manufacturability, plumbing integration, material selection, and overall system geometry, the decision of tank configuration will impact all future decisions made in the design process. The objective of this trade study is to determine the best propellant tank configuration for the suborbital pressure fed rocket specified. The two configurations which will be examined are a common bulkhead design and individual propellant tanks. This trade study will consider advantages and disadvantages of common bulkhead and individual tank systems. Through literature review and systematic decision making this trade study will result in a selected configuration for the rockets propellant tanks with full justification.

3.1.1 Common bulkhead design

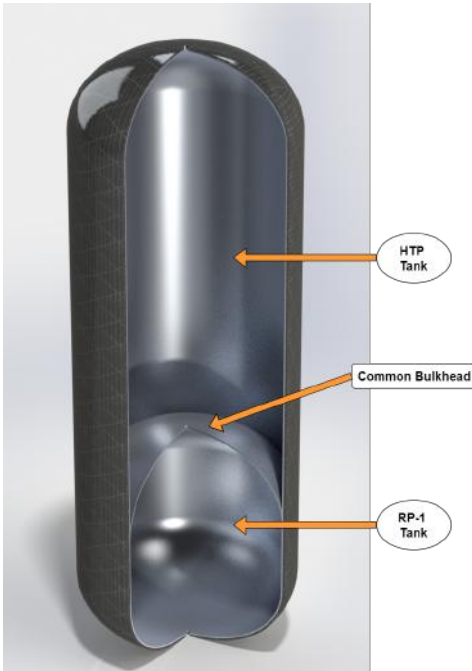


Figure 3.1: Common bulkhead propellant COPV

As shown in figure 3.1, a common bulkhead propellant tank design uses a single diaphragm, or bulkhead which separates the fuel and oxidizer. Common bulkhead tank designs are often an appealing option for upper stage or payload propellant storage. The elimination of two end caps in favor of one bulkhead offers substantial material savings in addition to reducing the height when compared with two individual tanks. Notable launch vehicles that employ common bulkhead propellant tanks in their first stage include: Falcon9 [29], Vulcan Centaur [30], and New Glenn [31].

This weight reduction and effective shortening make the common bulkhead design so appealing for upper stages or payloads because these stages are often more stout. This stout geometry is commonly due to more balanced propellant ratios, thinner atmosphere providing less drag. For satellites or other deep payload shots, the ability to use gravity gradient stabilization or an otherwise weakened gravitational force and a lack of dynamic pressure

allow for geometries which would conventionally be considered unstable. However the for the application of a single stage suborbital pressure fed system, weight reduction and stack shortening can be utilized for mass efficiency and to abide by aerodynamic geometric constraints.

Because the intention of a common bulkhead is to reduce weight, the bulkhead must be designed with mass efficiency. This mass efficiency may result in thin sections which would likely rely on the pressure differential between the HTP and the RP-1 tanks remaining relatively small. This low pressure differential would allow the separated tanks pressure to maintain a quasi-equilibrium stress state across the bulkhead. Despite this, the shared bulkhead must be designed to encounter a pressure differential of considerable magnitude to maintain safety in the event of a pressure regulation mishap.

An additional consideration is that the bulkhead must be made of a material such that it is chemically comparable with both HTP and RP-1. This requires that the liner be made from a material that is not only effective as a liner but is also effective as a standalone structural material. Additionally the tank material but be process-able such that it can be welded or crimped with the other tank half to ensure that it remains pressure tight.

3.1.2 Common bulkhead advantages

lightweight: As previously mentioned the common bulkhead design offers substantial weight savings over individual tanks by eliminating two tank heads and replacing them with a single bulkhead. In a study performed by Dr. Steven S. Pietrobon, earth departure stage (EDS) masses excluding engine mass were compared [32]. This comparison found that the best fit line for dry EDS mass (m_s) as a function of propellant mass (m_p) for all tank designs, both common bulkhead and individual, was given by equation 3.1 [32].

$$m_s = 0.19m_p^{0.848} \quad (3.1)$$

For comparison, dry EDS mass as a function of propellant mass for only common bulkhead design EDSs was given by equation 3.2 [32].

$$m_s = 0.1583m_p^{0.848} \quad (3.2)$$

Though these are models based on a wide range of historical stages, the trend illustrates the potential weight savings of a common bulkhead design. Using this model, based on current propellant mass estimates for the launch vehicle, a common bulkhead design would be approximately 16.7% lighter.

Shorter stack capabilities: Use of a common bulkhead offers capability for a shorter stack. This creates greater flexibility for design optimization between aerodynamic and weight considerations. This is not to say that a shorter stack is necessarily beneficial, only that the flexibility that allows for a shorter stack should it aid with dynamic considerations has the opportunity to be beneficial. By the definition of volume, capability for a shorter stack is also capability for a stack of the same height with a smaller external radius. A smaller radius means less cross sectional and surface area. It is this reduction in drag area which is most likely to be beneficial.

Less interfaces: Use of common bulkhead propellant tanks requires two fewer interfaces for integration. Where use of individual tanks would require an airframe section between the two tanks, use of a common bulkhead would eliminate this allowing for a continuous tank section with which only needs integration at the top and bottom of the tank.

3.1.3 Common bulkhead disadvantages

Non-disassemblable: A notable disadvantage of the common bulkhead design from an interchangeability perspective is that if one of the two tanks has an irreparable issue, both tanks must be discarded. This poses a financial liability to Liquid Rocketry Lab. As a prototype launch vehicle, it is not unlikely that something will go wrong. Though a common bulkhead tank may save cost during winding, the common tank system as a whole would certainly cost more than either individual tank. Additionally, inter-tank internal plumbing would have to be affixed permanently during liner construction to ensure no leakage between HTP and RP-1 tanks creating another non-disassemblable architecture.

Complex liner design: The complex design of the liner would require additional seams and additional components which would act as opportunities for defects. This also creates a more challenging problem for plumbing integration. Internal piping between tanks would have to be welded into the system during liner construction to ensure a proper seal at the bulkhead. This may create problems for tank maintenance. Another complexity that exists in this design is the necessity for relative pressure equalization across the bulkhead. This requirement would be easy to plan for from an avionics and propulsion perspective, but would have potential for catastrophic failure should the feed system malfunction.

Probability for catastrophic failure: In the unlikely event that the bulkhead were to leak, burst, or fracture, the HTP and RP-1 would combine creating the opportunity for a near perfect stoichiometric mix between fuel and oxidizer. Should this event arise, if there were to be a spark or fire, there is potential for a maximum energy explosion to occur. This is the worst case scenario. Although LRL has countermeasures in place to keep all personnel safe in the event of a maximum energy explosion, a failure of this type would destroy all launch vehicle hardware rendering it useless for future launch attempts.

3.1.4 Common bulkhead systems integration impact

Airframe Integration: As previously noted, use of a common bulkhead design would eliminate the need for an airframe section which would exist between two individual tanks. This would eliminate the development of another component which could act as an opportunity for a defect or design flaw. The same interface design could be used on both ends of the common bulkhead tank requiring the design of only one interface type.

Plumbing Integration: If plumbing must be routed through the tank, this would require a series of complex internal features. This challenge would become increasingly complex when the tanks strain during pressurization and the required nuances to account for that deformation. Things such as expansion joints would become more complex as leakage between the two propellant sections could cause catastrophic failure.

3.1.5 individual propellant tanks

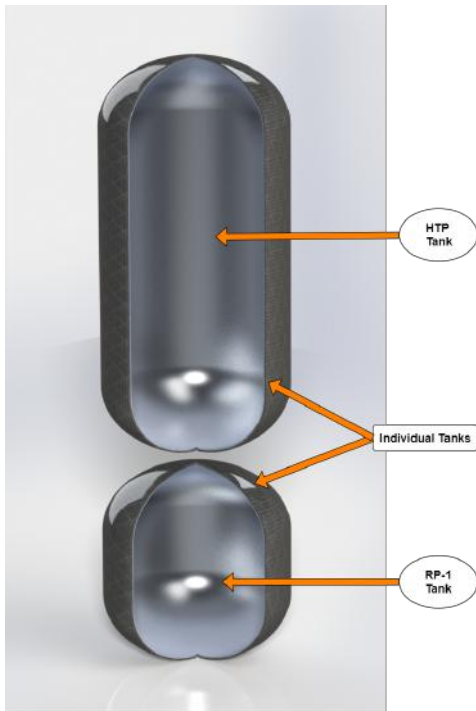


Figure 3.2: Individual tank propellant COPVs

As shown in figure 3.2, an individual propellant tank design has completely separate fuel and oxidizer tanks. Due to its simplicity individual propellant tanks are commonly used by amateur and professional liquid rocket manufacturers alike. Notable systems that have used individual propellant tanks in their first stages include: Saturn V [33], Atlas V [30], and SLS [34]. Because of the relative simplicity most early liquid propellant rockets used individual bulkhead designs including the very first liquid propellant rocket created by Robert Goddard in 1926 [35]. Additionally, individual tanks are almost exclusively used in hypergolic systems due to the danger presented by close proximity of the constituents.

The use of individual propellant tanks naturally makes the stack taller as the height of an additional two tank heads must be accounted for. This adjustment in height is neither a positive nor a negative but must be taken into consideration when choosing as it is likely to have an effect on the systems aerodynamics. By using two completely separate tanks rather than a common bulkhead design, the

stack becomes more modular. Modularity in prototype systems is often enticing as it allows for adaptations and iterations to be performed selectively as it is by nature designed for disassembly.

3.1.6 Individual tank advantages

Disassembly: An individual propellant tank design allows for disassembly to a greater degree than a common bulkhead design. Not only can the two parts of the tanks be separated and worked on separately, but the plumbing required for each of the two tanks would also be easier to disassemble as it would not necessarily be trapped within the tank. Ease of disassembly provides benefits for transportation, cleaning, repair, inspection, and testing.

Ease of manufacturing: Manufacturing of individual propellant tanks would be simpler because each tank could be manufactured as its own unit. With the need for internal systems such as slosh mitigation mechanisms and diffusers, tanks can be created one at a time. Additionally, poor manufacturing of one will not effect the performance or viability of the other. Though the stack could potentially be shorter with a common bulkhead design, a common bulkhead tank would be taller than either one of the individual tanks on their own. This has the potential to pose an issue with manufacturing should the common bulkhead tank be longer than is manufacturable on the filament winder LRL has access to.

Ease of design: Designing individual tanks would be simpler from the standpoint of validation. Setting up both FEA and CFD analysis on individual tanks is less complicated than with a common bulkhead design. With individual tanks there is no need to test for the event of pressure imbalance between the tanks. Use of individual tanks also eliminates the need for bulkhead design, and the same tank heads can be used on both propellant tanks.

3.1.7 Individual tank disadvantages

Heavier: As noted in the common bulkhead advantages, a set of individual tanks would be approximately 16.7% heavier than a common bulkhead design based upon the model presented by Pietrobon [32]. Additionally use of the COPV analysis Matlab scripts given in code appendices 6.1.1 and 6.1.2 gives a weight discrepancy estimate of 6.86 lb between the two designs. This estimate does not take into consideration the bosses for plumbing connection at the ends of the COPVs or other internal features such as diffusers or slosh mitigation mechanisms leading to a variance of only about 4%.

However, individual tanks require two more bosses than a common bulkhead design, an additional airframe section, additional plumbing length, and additional fasteners. Because of these considerations the analysis tool fails to account for, the estimate of 4% which only considers the liner and overwrap weight contains significant error giving a much smaller discrepancy than is accurate. Because of this, the assumption of 16.7% given by the Pietrobon model will be used for judgment of this consideration.

Additional interfacing: In contrast to the common bulkhead design, use of two tanks will require an additional airframe section between them. This airframe section would have to be sufficiently rigid yet allow for tank expansion. This airframe section would likely be a relatively complex assembly potentially requiring the bonding of metal with fiber reinforced polymer composites. This presents opportunity for defects which could effect the function of the system. Of course either design has its own challenges and potential for introduction of error, however the requirement for this interface is a notable consideration.

Taller stacking capability: Individual tanks would require an additional two tank heads along with an additional airframe section while maintaining the same internal volume. Therefore the minimum stack height for a given radius is necessarily taller for

individual tanks than with a common bulkhead tank. This is not to say that a taller stack is necessarily detrimental, only that the lack of flexibility may prevent a shorter stack or a thinner rocket should it be needed to aid with dynamic considerations.

3.1.8 Individual tank systems integration impact

Airframe integration: As previously noted, use of individual tanks would require the addition of an airframe section. This would require an additional two interfaces for integration - each of the two tanks connecting to the airframe section. Addition of this airframe section would require consideration to its weight contribution. It would also require consideration for access to the plumbing between the two tanks. Integration at the top and bottom of the tank section with the airframe would be the same as with a common bulkhead design.

Plumbing integration: Use of individual tanks would make planning for integration with the plumbing system much simpler. There would be less complicated compression joint design required. Internal plumbing would be simplified and expansion joints could be accessed easily for inspection or maintenance.

3.1.9 propellant tank configuration selection

Despite the notable benefits of a common bulkhead design, *an individual tank design will be utilized* in this design for this paper. Because the launch vehicle will be a prototype system, the need for access, disassembly, modularity, and frequent inspection make an individual tank system optimal. Use of individual tanks will simplify both design and manufacturing of the system. Additionally the complexity around the bulkhead of a common bulkhead tank, its increased probability for catastrophic failure, as well as its added complexity for manufacturing would lend unacceptable levels of uncertainty to the system.

3.2 Tank Head Geometry

A COPV can be split into a number of sections for the purpose of discussion. These sections include the liner, overwrap, head, cylinder, and polar boss as labeled in figure 1.1. The objective of the tank head is to enclose the ends while distributing the stress from the pressure into the material. Because PVs have many different applications, tank heads are selected to best suit the specifications of a particular use. This section is a discussion of various common tank head types and their applicability to the LRL launch vehicle.

There are many different varieties of tank heads for all different uses. The following three head designs discussed are some of the most commonly used designs, all of which have their own advantages and disadvantages. The options have been narrowed to the following three designs over others due to their applicability to the use case along with their commercial availability.

Tank head geometry has most notable implications for tank weight, tank height, and cost. Taller heads examined in this discussion require less material but result in a taller stack. Conversely, shorter heads discussed allow for a shorter stack but require a thicker head. This problem of determining weight becomes more difficult when considering stresses within an anisotropic composite. Head geometry also has implications for polar boss design as the boss must form an airtight seal with the head.

Integration impact: Selection of hemispherical tank heads will effect the design of connecting airframe sections, overall stack height, as well as the design of and stress distribution around the polar boss(es). For tanks with through piping, the tank head will affect the length of the internal piping. Additionally, required laminate architecture will effected due to the differences in stress distribution across different head types.

3.2.1 Hemispherical

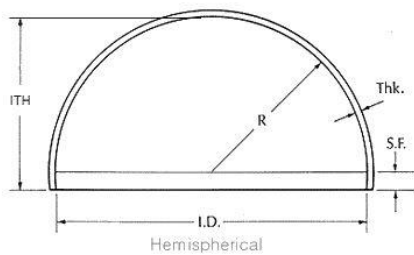


Figure 3.3: Hemispherical tank head design [36]

A hemispherical tank head is one that sweeps 180 degrees with a single radius in the meridional direction and a full 360 degrees in the equatorial direction to form an enclosed cap. The radius of the hemisphere is equal to the radius of the pressure vessels cylinder section allowing for a smooth transition between the two sections of the tank. due to its fully radiused cross section the hemispherical design offers the most uniform stress distribution [37, 38]. Due to the large amount of deformation required to form the hemispherical geometry, manufacturing of hemispherical heads can be difficult.

The difficulty of making hemispherical heads often makes them more expensive to purchase [38] and sometimes requires a welded assembly rather than being formed from a single sheet [37]. However when they are made from a single sheet of material, required deformation for shaping results in hemispherical heads being thinnest tank heads [37].

Despite being the thinnest they are able to withstand the same amount of pressure as other designs due to their previously mentioned ability to evenly distribute stress [38].

As shown in figure 3.3, hemispherical tank heads usually have a small region of right cylinder at the base of the hemisphere. In this region the head transitions to match the thickness of the tanks cylinder section. This prevents a mismatch in diameters from occurring where the head meets the cylinder. Additionally, because most tank heads are welded to their cylinders, this region acts as a spacer between the head and the cylinder distancing the heat effected zone from the geometric transition.

3.2.2 Semi-Elliptical

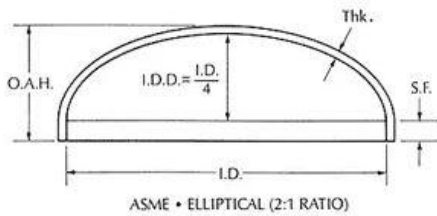


Figure 3.4: ASME Code Semi-Elliptical tank head design [39]

Semi-elliptical or elliptical tanks have a non-circular curve that sweeps 180 degrees in the meridional direction and a full 360 degrees in the equatorial direction to form an enclosed cap. Traditionally semi-elliptical heads are defined by their diameter and the ratio between their major and minor radii with 2:1 elliptical being the most common design (Arc height = 1/4 tank diameter) [37]. As the curve approaches the heads edges it tightens to become tangent to the cylinder.

As with the the hemispherical head, the semi-elliptical head has a right cylindrical section at the base of the curve to allow for a transition region between the tanks head and cylinder. Moore and Tomlinson note that semi-elliptical heads are commonly produced using “three radii that approximate an ellipse - large in the crown, smallest at the outside diameter, with an intermediate radius in the middle” [37]. This manufacturing method defers to code requiring a minimum likeness of the combination of these radii to a true ellipse [37].

Because stress is less uniformly distributed across a semi-elliptical head than with a hemispherical head, it requires thicker material to withstand the same amount of stress. However because the overall depth of a semi-elliptical head is less than a hemispherical head, it is easier to manufacture from a single piece of material. This makes the semi-elliptical design cheaper to manufacture compared to a hemispherical head.

3.2.3 Torispherical

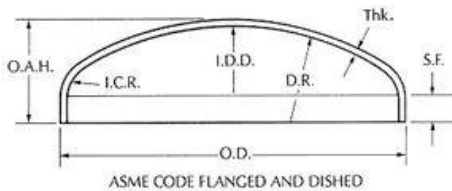


Figure 3.5: ASME Code flanged and dished tank head design [40]

Often referred to as the flanged and dished design in the United States, torispherical tank heads are similar to semi-elliptical tank heads in the sense that they are formed using a series of radii. Typically the radius used to form the crown is larger than its semi-elliptical counterpart, and the radius acting as the transition to the cylinder (known as the knuckle radius) is tighter than a semi-elliptical [37]; However as shown in Thattil et al. [41] the crown radius can be relatively small or the knuckle

radius can be relatively large compared with a semi-elliptical. As the crown and knuckle radii converge to a common value, the head geometry converges to hemispherical.

The combination of a large crown radius and a tight knuckle radius results in a shorter tank head which is usually the reason a Torispherical design would be selected [37], but the tight knuckle radius results in higher concentrations of stress [37, 38]. To combat the effects of stress concentration thicker material is required for the tank head [37]. Due to practical manufacturing considerations the rounded section of the tank head is made from a material of uniform thickness which results in additional material across a large radius crown [37].

Because less deformation is required to form a shallow head, this makes manufacturing from a single sheet relatively simple. Because the torispherical design only requires two radii, tooling for this design is cheaper and easier to make. This combination of manufacturing considerations mean that torispherical heads for low pressure applications are often cheaper than their previously mentioned counterparts [41] but become uneconomical at higher pressures [38].

3.2.4 Tank head design selection

A 2015 article by Lawate et al. compares Hemispherical, Ellipsoidal, and Torispherical heads. One of the first remarks made about the a hemispherical design is that “it is the strongest shape; capable of resisting about twice the pressure of a torispherical head of the same thickness” [38]. However Lawate et al. also note that the hemispherical design is also the most expensive [38].

A 2017 study by Thattil and Pany analyzes the stress in both hemispherical and torispherical tank heads under pressure. Contrary to the claim by Lawate et al. the two designs investigate by Thattil et al. did not have remarkably different values, and in some modes of stress for certain locations across the tank head the torispherical design actually had lower stress [41]. It is important to note that the torispherical head studied by Thattil et al. are much closer to hemispherical than the torispherical head studied by Lawate et al.. Lawate et al. does not give an exact knuckle radius meaning that their findings cannot be directly compared to Thattil et al.. However, the head height to cylinder radius ratio for Lawate is 48:120 where the same ratio for Thattil et al. is 105:120 which gives some insight on how close each design is to hemispherical.

The semi-elliptical head used in the Lawate et al. study also has a head height to cylinder radius ratio of 48:120. Interestingly Lawate et al. found that max von mises stress was approximately 30% lower in the torispherical tank compared to the semi-elliptical tank [38]. From these findings Lawate et al. concluded that use of a torispherical design is preferable to a semi-elliptical design when selecting a low tank head geometry [38]. However, to reiterate, the torispherical head used by Lawate et al. use large radii which is fairly uncommon when considering a torispherical design.

In a study performed by Brundrett [42], the three tank head designs were considered for conventional all metal pressure vessels. This study was used as the basis for discussion by pressure vessel engineers Moore and Tomlinson [37]. It was found that for a given pressure, a 2:1 semi-elliptical design was able to use a safe operating thickness 55% thinner than a torispherical design indicating potentially substantial weight savings with a semi-elliptical as compared with a torispherical. That said, in Brundrett’s study, the

more common configuration of a large crown radius a small knuckle radius was used for the torispherical tank. [37, 42].

The stark contrast in findings by Brundrett and Lawate expose the degree to which changes in knuckle and crown radii affect resulting stress. In a Chemical Engineering Magazine article, the author, a professional engineer with 15 years experience working with ASME code pressure vessels stated that “the decision of whether to specify and use a torispherical head versus an ellipsoidal head is mainly an issue of head clearance” [43]. With two conflicting studies and a professional statement largely dismissive of the findings for both studies it is safe to say that should a shorter stack be required, selection of either a torispherical or a semi-elliptical head type would require further investigation.

The one thing that all sources agree upon is that a hemispherical design is the best at distributing stress. Lawate et al. found that the hemispherical head studied exhibited on approximately 60% less maximum stress than the torispherical head and 72% lower maximum stress than the semi-elliptical head [38]. Additionally the Lawate et al. “observed [maximum deformations] in elliptical and torispherical heads ... 9.26 times (826.83% more) and 9 times (801.96% more) respectively as compared to deformation in [the] hemispherical head” [38]. The studies performed by Brundrett and Thatti et al. (albeit to differing degrees) also found that a hemispherical design outperforms the other designs both in required thickness and maximum Von Mises stresses.

Outcome: Due to its remarkable performance along with its lack of confounding findings, a *hemispherical tank head design will be utilized* for all three pressure vessels in this study. Should future considerations require a shorter stack, a deeper comparison between and modeled analysis of semi-elliptical and torispherical tanks should be performed. It should also be noted that because the composite is bearing the majority of the load, not the liner, use of a hemispherical head requires no special considerations while filament winding. Because stresses will be distributed evenly, no additional material should required at any particular region of the tank head. However fiber orientation will be a concern with all head designs because the fiber orientation will change with respect to its original global axis as it moves from the cylinder to the head.

3.3 Material Options

3.3.1 Liner option evaluations

In the liner material compatibility specification, liner materials were narrowed to compatible options. This trade study will evaluate the advantages and disadvantages of each option with respect to the application.

3.3.2 Oxidizer COPV liner option evaluation

The below options have been selected as suitable materials for their HTP compatibility and practicality for COPV liner manufacturing. They have been split into categories based on their generalized materials. The following discussion assesses the validity of each material individually for the given use case. After discussion the options will be compared and a recommendation will be made for oxidizer tank liner material. For all metal gauge thicknesses discussed the American Standard Gauge system will be used; Otherwise nominal thickness in inches will be used.

| Aluminum | Stainless | Polymers |
|--|---|--|
| <ul style="list-style-type: none">• 5254 | <ul style="list-style-type: none">• 304 | <ul style="list-style-type: none">• PVC |
| <ul style="list-style-type: none">• 6061 | <ul style="list-style-type: none">• 316 | <ul style="list-style-type: none">• CPVC |
| | <ul style="list-style-type: none">• 347 | |

Oxidizer COPV liner discussion

Based upon the specification that all materials must have class A or B compatibility with the stored material, all of the selection options are viable. The discussion then leads to evaluation of material processability, integration considerations, and material property concerns.

Aluminum: Given that 5254 aluminum is relatively uncommon and is difficult to find in thin sheet stock, 6061 is the best candidate for an aluminum liner. Aluminum sheet stock is sold in thicknesses designated both by gauge and by nominal thickness. Because the liners primary purpose is to act as a chemical barrier and as a mandrel for winding rather than as a structural component, thin material is sufficient. Cylinders can be formed by rolling sheet metal, and tank heads are commercially available in aluminum in thicknesses of 18 ga. and thicker. Aluminum sheet is available from Alro Steel to be used for an oxidizer cylinder in thicknesses of 18 ga. and thicker. Due to required length of the oxidizer cylinder, there will likely be both longitudinal and hoop weld seams if standard sheet metal is used. Another potential option would be to purchase a roll of sheet aluminum which could be used to manufacture a cylinder with only one weld seam along its length.

Processability: The primary processing concern for thin aluminum is its ability to be welded. Punch through is a common issue for non-backed aluminum welds, so welding must be completed by a trained professional or with an automated system. Despite this difficulty aluminum is otherwise highly processable both in terms of sheet metal forming and machining. Any precision cutting that needs to be done on aluminum should probably be accomplished by means of a water jet as similar issues as seen with welding arise when plasma cutting thin aluminum.

Integration considerations: According to LRL Vice President of Propulsion William Hitchcock, stainless steel tubing will be the primary plumbing within the flight vehicle. Should aluminum be selected as the liner material, dissimilar metals will have to meet at some point within the system. Though this is certainly possible, the decision about where this joint will occur is critical as stainless steel and aluminum act substantially different under load. The other consideration for integration is the material selected for slosh mitigation mechanisms. These mechanisms will be made from the same material as the slosh mitigation system will act as a skeleton for the thin walled liner.

Material properties: The following table shows typical mechanical properties for 6061-T6 aluminum [44]. None of the mechanical properties are particularly concerning, but one important strength that aluminum offers is in its density. With a density of 0.0975 lb/in^3 aluminum offers high specific strength, unmatched by stainless steel. Aluminum offers the benefit of potentially substantial weight savings compared to stainless steel. Using the COPV analysis script shown in appendix 6.1.1, it is estimated that an aluminum oxidizer liner made from 18 ga. material would weigh just 33.07 lb.

| Property | Value | Unit |
|------------------------|--------|------------------|
| Density | 0.0975 | lb/in^3 |
| Tensile Yield Strength | 40000 | psi |
| Elongation at Break | 12 | % |
| Modulus of Elasticity | 10000 | ksi |
| Poisson's Ratio | 0.33 | 1 |
| Fatigue Strength | 14000 | psi |

6061-T6 aluminum mechanical properties. For full properties see <http://asm.matweb.com/search/SpecificMaterial.asp?bassnum=MA6061T6>[44].

Stainless steel: Of the stainless steels that meet the criteria for compatibility, 304 and 316 are the most common varieties. Of these two alloys 304 is typically cheaper but 316 has slightly better properties. However, because the liner is designed as a non-structural component, the cost effectiveness of 304 outweighs the mechanical benefits of 316. Because of this, 304 will be the primary stainless steel investigated. Stainless steel tank heads are commercially available in thicknesses of 18 ga. and thicker. The same can be said for stainless steel sheet metal which is available from Alro steel.

Processability: for the needs of the application stainless steel is highly processable. It is easily weldable and does not face punch through issues to near the extent seen from sheet aluminum. Because of this in addition to water jetting precision sheet metal cutting for stainless steels can be done using a plasma jet cutter. Additionally stainless can be sheet metal formed and machined.

Integration considerations: Because most of the plumbing to be done within the flight vehicle is currently planed to use stainless steel, joints between the liner and the plumbing can be welded rather than threaded. Although there will likely be threaded sections to allow for disassembly, the ability to weld plumbing directly to the liner gives more flexibility as to where threaded sections can go.

Material properties: The following table shows typical mechanical properties for 304 stainless steel [45]. The only property that raises concern is the materials density. With a density of 0.289 lb/in^3 stainless steel is close to three times as heavy as aluminum per unit volume. Traditionally stainless steel is used in rockets which use cryogenic propellants because austenitic stainless steels (such as 300 series) possess a face centered cubic unit cell structure. This cell structure prevents the material from having a ductile to brittle transition temperature meaning that the material exhibits relatively consistent elastic properties at low temperatures. However, because the propellant system used in the launch vehicle is non-cryogenic, this is not a benefit.

Though the elongation at break stainless exhibits is substantially higher than aluminum, the liner will not undergo considerable strain due to the high modulus of the overwrap. This means that excessive elongation at break does not act as a benefit either. Using the COPV analysis script in appendix 6.1.1, it is estimated that an stainless steel oxidizer liner made from 18 ga. material would weigh 98.02 lb.

| Property | Value | Unit |
|------------------------|-------|------------------|
| Density | 0.289 | lb/in^3 |
| Tensile Yield Strength | 31200 | psi |
| Elongation at Break | 70 | % |
| Modulus of Elasticity | 10000 | ksi |
| Poisson's Ratio | 0.29 | 1 |

304 stainless steel mechanical properties. For full properties see <http://asm.matweb.com/search/SpecificMaterial.asp?bassnum=MQ304A> [45].

Polymer: PVC and CPVC are the two liner materials compatible with HTP which also possess the mechanical properties to act as a mandrel for filament winding. They also offer processability which make them applicable to act as liners for the launch vehicle. PVC and CPVC are very similar materials, however it is more common to find thin walled extrusions of PVC which would most likely act as the cylinder for the liner. Because of this PVC will be the primary polymer considered. Thin walled extrusions of the diameter likely to be required (6 inches plus) commonly have a wall thickness of 0.176 inches.

Processability: PVC is a highly processable material and could easily be welded with other PVC to create an air tight liner. Additionally, PVC is thermoformable meaning that if not commercially available a PVC tank head could be formed with relative ease. PVC is also machinable, which means because of its relative thickness, precision cutting can be done using a CNC milling machine. Precision cutting can also be completed with the use of a water jet.

Integration considerations: Integration is likely the largest downside for a PVC liner. Because the primary plumbing within the rocket will be made from stainless steel, integrating the liner with the plumbing would be a challenging task. Because PVC is so soft in comparison to stainless steel, threading in the PVC would easily strip. Also the PVC may deform under pressure. Additionally, though possible by work arounds such as external manufacturing, implementing a slosh mitigation system within the tank may prove difficult with a PVC liner.

Material properties: The following table shows typical mechanical properties for rigid PVC [46]. As can be seen, mechanical properties for PVC are substantially lower than both stainless steel and aluminum. Both modulus and tensile strength raise some concern as their values are very low. In fact the thin walled extrusions of PVC are intended for air ducts, not to be pressurized. These low properties may be sufficient provided a high modulus, high strength overwrap; However they do raise some alarms.

What makes PVC a desirable candidate is its low density. With less than half the density of aluminum and less dense than stainless by nearly a factor of six, PVC is undoubtedly the lightest material in consideration. Using the COPV analysis tool shown in appendix 6.1.1, it is estimated that a PVC oxidizer liner made from 0.176 inch thick material would weigh 76.87 lb.

| Property | Value | Unit |
|------------------------|--------|-----------|
| Density | 0.0488 | lb/in^3 |
| Tensile Yield Strength | 5802 | psi |
| Elongation at Break | 40 | % |
| Modulus of Elasticity | 435 | ksi |
| Poisson's Ratio | 0.4 | 1 |

Rigid PVC mechanical properties. For full properties see <https://polymerdatabase.com/Commercial%20Polymers/PVC.html> [46].

3.3.3 Oxidizer COPV liner material selection

Due to its low density, high processability, low cost, and decent mechanical properties, aluminum is the best candidate for use as an oxidizer liner. Therefore *a 6061 aluminum oxidizer COPV liner will be utilized* in the design for this paper. Although welding of thin aluminum is difficult, it has been widely demonstrated as possible and can be done consistently with the use of an automated welding process.

3.3.4 Fuel COPV liner option evaluation

The below options have been selected as suitable materials for their RP-1 compatibility and practicality for COPV liner manufacturing. They have been split into categories based on their generalized materials. The following discussion assesses the viability of each material individually for the given use case. After discussion the options will be compared and a recommendation will be made for fuel tank material selection.

| Aluminum | Stainless | Polymers |
|--|---|---|
| <ul style="list-style-type: none">• 5052 | <ul style="list-style-type: none">• 304 | <ul style="list-style-type: none">• PPS |
| <ul style="list-style-type: none">• 6061 | <ul style="list-style-type: none">• 316 | <ul style="list-style-type: none">• PVC |
| <ul style="list-style-type: none">• 7075 | <ul style="list-style-type: none">• 347 | |

Fuel COPV liner discussion

As can be seen, the above list of materials for the fuel liner closely resembles that of the oxidizer liner material options. For aluminum 6061 is the most common of the alloys listed and is sufficient in mechanical properties for the application. For this reason 6061 will be the aluminum of choice for fuel COPV liner consideration. The stainless steel options are identical to those discussed in the oxidizer discussion for that reason 304 will be the stainless steel of choice for fuel COPV liner consideration. Similarly the of the polymers, PPS is more costly, less available, and offers little mechanical variance when compared with PVC. Because of this PVC will be the polymer of choice for fuel COPV liner consideration.

3.3.5 Fuel COPV liner material selection

Because the fuel tank will be subjected to the same manufacturing methods and similar loading as the oxidizer tank, the same conclusion can be drawn without re-evaluation. Due to its low density, relatively high processability, low cost, and decent mechanical properties, aluminum is the best candidate for use as an fuel liner. Therefore ***a 6061 aluminum fuel COPV liner will be utilized*** in the design for this paper. Although welding of thin aluminum is difficult, it has been widely demonstrated as possible and can be done consistently with the use of an automated welding process.

3.3.6 Pressurant COPV liner option evaluation

As noted previously in specifications the pressurant for the rocket will be nitrogen, a fairly inert gas. Because N₂ is non-reactive with most structural materials, liner selection for the pressurant tank will be highly dependent on cost and manufacturability rather than chemical compatibility. Therefore, it will be noted that at operating temperature all previously considered structural materials are compatible with nitrogen.

3.3.7 Pressurant COPV liner material selection

Because both the HTP and RP-1 COPV liners will be made from aluminum it will likely be most cost efficient to tool only for aluminum tanks. Additionally because the composite overwrap are acting as the primary structure of the COPV, the pressurant tank can be designed in such that it exhibits the same amount of strain as the propellant COPVs. Since the lowest properties for aluminum with relation to the other materials was elongation at break, planning for similar strain conditions alleviates concern over that property. All other concerns are consistent in practicality and are thus consistent in resolution to the propellant tanks. Therefore *a 6061 aluminum fuel COPV liner will be utilized* in the design for this paper.

3.3.8 Overwrap option evaluation

COPVs typically utilize polymer reinforced glass, aramid, or carbon fibers. The matrix material when considering fiber type will be assumed as epoxy due to its compatibility with all three fibers. Figure 3.6 shows a table listing typical values of material properties for composites utilizing each fiber type [47].

| Property | E-Glass/Epoxy | | Kevlar 49/Epoxy | | Carbon/Epoxy | |
|--|----------------|--------------------|-----------------|---------------------|-----------------------------|----------------------------------|
| | Unidirectional | Fabric (M10E/37B3) | Unidirectional | Fabric (K120/M10.2) | Unidirectional (AS4/3501-6) | Woven Fabric (AGP370-5H/3501-6S) |
| Fiber volume ratio, V_f | 0.55 | 0.50 | 0.60 | — | 0.63 | 0.62 |
| Density, ρ , g/cm ³ (lb/in ³) | 1.97 (0.071) | 1.90 (0.068) | 1.38 (0.050) | — | 1.60 (0.058) | 1.60 (0.058) |
| Longitudinal modulus, E_1 , GPa (Msi) | 41 (6.00) | 24.5 (3.55) | 80 (11.6) | 29 (4.2) | 147 (21.3) | 77 (11.2) |
| Transverse in-plane modulus, E_2 , GPa (Msi) | 10.4 (1.50) | 23.8 (3.45) | 5.5 (0.80) | 29 (4.2) | 10.3 (1.50) | 75 (10.9) |
| Transverse out-of-plane modulus, E_3 , GPa (Msi) | 10.4 (1.50) | 11.6 (1.68) | 5.5 (0.80) | — | 10.3 (1.50) | 13.8 (2.0) |
| In-plane shear modulus, G_{12} , GPa (Msi) | 4.3 (0.62) | 4.7 (0.68) | 2.2 (0.31) | 18 (2.6) | 7.0 (1.00) | 6.5 (0.94) |
| Out-of-plane shear modulus, G_{23} , GPa (Msi) | 3.5 (0.50) | 3.6 (0.52) | 1.8 (0.26) | — | 3.7 (0.54) | 4.1 (0.59) |
| Out-of-plane shear modulus, G_{13} , GPa (Msi) | 4.3 (0.62) | 2.6 (0.38) | 2.2 (0.31) | — | 7.0 (1.00) | 5.1 (0.74) |
| Major in-plane Poisson's ratio, ν_{12} | 0.28 | 0.11 | 0.34 | 0.05 | 0.27 | 0.06 |
| Out-of-plane Poisson's ratio, ν_{23} | 0.50 | 0.20 | 0.40 | — | 0.54 | 0.37 |
| Out-of-plane Poisson's ratio, ν_{13} | 0.28 | 0.15 | 0.34 | 0.05 | 0.27 | 0.50 |
| Longitudinal tensile strength, F_{1t} , MPa (ksi) | 1140 (165) | 433 (62.8) | 1400 (205) | 369 (53.5) | 2280 (330) | 963 (140) |
| Transverse tensile strength, F_{2t} , MPa (ksi) | 39 (5.7) | 386 (55.9) | 30 (4.2) | 369 (53.5) | 57 (8.3) | 856 (124) |
| Out-of-plane tensile strength, F_{3t} , MPa (ksi) | 39 (5.7) | 27 (3.9) | 30 (4.2) | — | 57 (8.3) | 60 (8.7) |
| Longitudinal compressive strength, F_{1c} , MPa (ksi) | 620 (90) | 377 (54.6) | 335 (49) | 129 (18.7) | 1725 (250) | 900 (130) |
| Transverse compressive strength, F_{2c} , MPa (ksi) | 128 (18.6) | 335 (48.6) | 158 (22.9) | 129 (18.7) | 228 (33) | 900 (130) |
| Out-of-plane compressive strength, F_{3c} , MPa (ksi) | 128 (18.6) | 237 (34.4) | 158 (22.9) | — | 228 (33) | 813 (118) |
| In-plane shear strength, F_6 , MPa (ksi) | 89 (12.9) | 84 (12.2) | 49 (7.1) | 113 (16.4) | 76 (11.0) | 71 (10.3) |
| Out-of-plane shear strength, F_4 , MPa (ksi) | — | 44 (6.3) | — | 33 (4.8) | — | 65 (9.5) |
| Out-of-plane shear strength, F_5 , MPa (ksi) | — | 41 (5.9) | 37 (5.4) | 33 (4.8) | — | 75 (10.8) |
| Longitudinal thermal expansion coefficient, α_1 , 10 ⁻⁶ /°C (10 ⁻⁶ /°F) | 7.0 (3.9) | — | -2.0 (-1.1) | — | -0.9 (-0.5) | 3.4 (1.9) |
| Transverse thermal expansion coefficient, α_2 , 10 ⁻⁶ /°C (10 ⁻⁶ /°F) | 26 (14.4) | — | 60 (33) | — | 27 (15) | 3.7 (2.1) |
| Out-of-plane thermal expansion coefficient, α_3 , 10 ⁻⁶ /°C (10 ⁻⁶ /°F) | 26 (14.4) | — | 60 (33) | — | 27 (15) | 52 (29) |
| Longitudinal moisture expansion coefficient, β_1 | 0 | — | 0 | — | 0.01 | 0.05 |
| Transverse moisture expansion coefficient, β_2 | 0.2 | — | 0.3 | — | 0.20 | 0.05 |
| Out-of-plane moisture expansion coefficient, β_3 | 0.2 | — | 0.3 | — | 0.20 | 0.27 |

Figure 3.6: Typical properties of varying fiber reinforced epoxy composites [47]

Properties and implications

Because the overwrap will be produced using filament winding, only unidirectional fiber properties will be considered. Note that each of the properties discussed is only applicable to an individual oriented lamina of fiber, not for the overwrap laminate as a whole. The following properties will be discussed for each of the fibers and their performance will be ranked in levels -1,0, and 1 indicating worst to best in that order. Should values be matching for two options which out-perform the third option, they will be assigned a level of 1 and the worse option will be assigned a level of -1. Should values be matching for two options which under-perform the third option, they will be assigned a level of -1 and the better option will be assigned a level of 1. Should all three options match in value they will be assigned a level of 0. All discussed properties have been taken from figure 3.6 taken from "Engineering mechanics of composite materials" a composite mechanics textbook authored by Isaac M. Daniel and Ori Ishai [47].

Fiber volume ratio, V_f : Fiber volume ratio, more commonly referred to as fiber volume fraction is the volumetric proportion of fiber reinforcement in a composite in relation to the volume of the composite as a whole. Because properties are dictated the by rule of mixtures equations discussed throughout this section, fiber volume fraction largely dictates the discussed properties. Capacity for high fiber volume fraction is as much if not more a function of processing than it is a function of fiber type, however because some fibers are more apt. to wet out than others it is also a material consideration.

| | E-Glass/Epoxy | Kevlar 49/Epoxy | Carbon/Epoxy |
|-------|----------------------|------------------------|---------------------|
| V_f | 0.55 | 0.60 | 0.63 |
| level | -1 | 0 | 1 |

Density, ρ : For rocketry as with every other aerospace applications, a lighter system is superior. This means that use of materials with lower densities is optimal.

| | E-Glass/Epoxy | Kevlar 49/Epoxy | Carbon/Epoxy |
|--------|--------------------------------|--------------------------------|--------------------------------|
| ρ | 0.071 <i>lb/in³</i> | 0.050 <i>lb/in³</i> | 0.058 <i>lb/in³</i> |
| level | -1 | 1 | 0 |

Tensile moduli: Tensile modulus can be described as a materials resistance to strain under an applied tensile load. More specifically it is given by the Young's equation $E = \frac{\sigma}{\epsilon}$. For the application of COPVs, a high tensile modulus means that while pressurized, the tanks will see less deformation. This reduction in deformation allows for easier integration with other components as less expansion must be accounted for; Therefore, for this case higher modulus materials are preferable.

Longitudinal modulus, E_1 : Longitudinal modulus describes the modulus in the fiber direction. This is the primary direction of reinforcement in the composite. In this direction modulus is given by the fiber dominated rule of mixtures equation $E_1 = E_{1f} * V_f + (1 - V_f) * E_m$ where E_{1f} describes the fiber modulus in the longitudinal

direction and E_m describes the modulus of the matrix. Note that this rule of mixtures equation is a representation using an isostrain condition which assumes equal strain in both the fiber and the matrix. Because the longitudinal modulus is fiber dominated and the reinforcement has a higher elastic modulus than the matrix, E_1 has higher values than E_2 and E_3 which are matrix dominated properties.

| | E-Glass/Epoxy | Kevlar 49/Epoxy | Carbon/Epoxy |
|-------|----------------------|------------------------|---------------------|
| E_1 | 6.00 Msi | 11.6 Msi | 21.3 Msi |
| level | -1 | 0 | 1 |

Transverse in-plane modulus, E_2 : Transverse in-plane modulus describes the tensile modulus in the direction perpendicular to the fiber orientation in the laminar plane. The transverse direction uses the matrix dominated rule of mixtures equation $E_2 = [\frac{V_f}{E_f} + \frac{(1-V_f)}{E_m}]^{-1}$. Note that this representation assumes an isostress condition which assumes stress is equal in both the fibers and the surrounding matrix.

| | E-Glass/Epoxy | Kevlar 49/Epoxy | Carbon/Epoxy |
|-------|----------------------|------------------------|---------------------|
| E_2 | 1.50 Msi | 0.80 Msi | 1.50 Msi |
| level | 1 | -1 | 1 |

Transverse out-of-plane modulus, E_3 : Transverse out-of-plane modulus describes the tensile modulus in the direction perpendicular to the laminar plane. This orientation can be difficult to conceptualize, however if one imagines a rectangular prism laminate structure of unidirectional fiber with a square cross section as viewed from the end of the fiber axis, it can be reasoned that pulling in either the vertical or horizontal direction should produce identical results. This explains why the E_2 and E_3 moduli are identical. It also explains why the same rule of mixtures equation is used for both transverse directions for unidirectional reinforcement but not woven reinforcement.

| | E-Glass/Epoxy | Kevlar 49/Epoxy | Carbon/Epoxy |
|-------|----------------------|------------------------|---------------------|
| E_2 | 1.50 Msi | 0.80 Msi | 1.50 Msi |
| level | 1 | -1 | 1 |

Shear moduli: Shear modulus is the shear analog to tensile modulus. It describes a materials resistance to shear strain for a given shear stress. It can be intuitively thought of as “rigidity” and is given by the shear analog of Young’s equation $G = \frac{\tau}{\gamma}$. For the application of COPVs where the majority of fibers are being loaded in directions off axis to a given fibers local longitudinal direction, shear modulus becomes an important parameter to consider. In this application resistance to shear or a high shear modulus is beneficial, as shear leads to changes in fiber direction resulting in mechanical properties different than anticipated. Figure 3.7 gives a visualization of shear orientations.

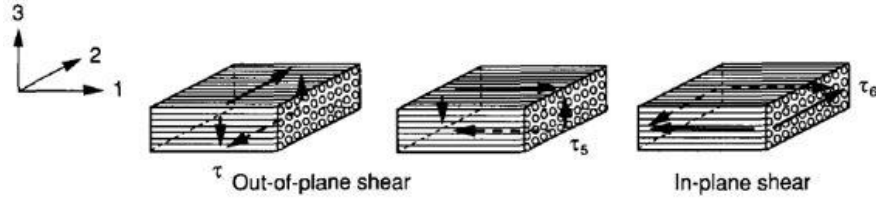


Figure 3.7: Visual depictions of shear within a composite laminate structure [47]

In-plane shear modulus, G_{12} : The in-plane shear modulus dictates resilience to shear strain of the material in the lamina plane. As pressure causes a COPV to deform, the fibers comprising the overwrap face shear loading. The primary shear loading is in-plane as the fibers are loaded relatively uniformly in the out-of-plane directions. Stiff resistance to this strain offered by a high shear modulus is important to prevent deformation similar to tensile modulus. Because of this, a high tensile modulus is preferable for this application. In this instance the in-plane shear modulus is a matrix dominated response meaning that it uses the inverse rule of mixtures equation $G_{12} = \frac{G_{12f}G_m}{V_fG_m + (1-V_f)G_{12f}}$, however “this approach tends to underestimate the in-plane shear modulus” [47]. For a more accurate model the Halpin-Tsai semiempirical relation of $G_{12} = G_m \left(\frac{1+\xi\eta V_f}{1-\eta V_f} \right)$ where ξ is an empirical parameter (typically 1) and $\eta = \frac{G_{12f}-G_m}{G_{12f}+\xi G_m}$ can be used [47].

| | E-Glass/Epoxy | Kevlar 49/Epoxy | Carbon/Epoxy |
|----------|----------------------|------------------------|---------------------|
| G_{12} | 0.62 Msi | 0.31 Msi | 1.00 Msi |
| level | 0 | -1 | 1 |

Out-of-plane shear plane modulus, G_{23} : As previously noted out-of plane shear modulus is less of a concern for the application. However rigidity of the system is still preferable to flexibility, so a high out-of-plane shear modulus will be denoted as preferable. Of the three shear orientations, shear in the 23 direction is least likely to occur. Calculation of the 23 shear modulus requires use of poisons ratio and strain bulk modulus of the composite.

| | E-Glass/Epoxy | Kevlar 49/Epoxy | Carbon/Epoxy |
|----------|----------------------|------------------------|---------------------|
| G_{23} | 0.50 Msi | 0.26 Msi | 0.54 Msi |
| level | 0 | -1 | 1 |

Out-of-plane shear plane modulus, G_{13} : Out of plane shear in the 13 direction is unlikely to show itself in this application; However if it does, it will be in the form of interlaminar shear. Due to the geometry of the laminate G_{13} is calculated by the same means as G_{12} . Once again a higher modulus is preferable for the application.

| | E-Glass/Epoxy | Kevlar 49/Epoxy | Carbon/Epoxy |
|----------|----------------------|------------------------|---------------------|
| G_{13} | 0.62 Msi | 0.31 Msi | 1.00 Msi |
| level | 0 | -1 | 1 |

Poisson ratios: Poisson ratio is the amount a material changes in one direction in relation to another direction while under strain. Poisson ratio can have large affects related to stresses and strains within the laminate. A high Poisson ratio correlates with large relative change in one direction in relation to another. If a laminate is symmetric, this renders the “B matrix” or the coupling stiffness matrix equal to zero [47]. If a laminate is balanced this renders the “D matrix” or the bending stiffness matrix equal to zero [47].

Within a laminate, these stiffness components are derived from the idea that a mismatch in lamina stiffness (a function of Poisson ratio) will result in a mismatch in laminar deformation. If the laminate is asymmetric, then the mismatch will occur across the laminates mid-plane causing bending or warp. If the laminate is unbalanced it can result in torsion and interlaminar stresses due to torsion [47].

Because stress within a pressure vessel is roughly double in the hoop direction than in the longitudinal direction, fibers will be laid accordingly. Because of this the individual fiber properties will be biased in one direction resulting in an unbalanced overwrap. However, there is the option to produce a symmetric laminate. This means that the overwrap will likely have a zeroed B matrix but a non-zero D matrix. Because of this unbalance, a low Poisson ratio is preferred for the application to ensure as little unbalanced strain as possible when loaded.

Major in-plane Poisson’s ratio, ν_{12} : Major in-plane Poisson’s ratio has the effect of introducing internal stresses within an unbalanced composite under load. It also contributes to overall deformation as previously described. Poisson’s ratio in the 12 direction follows the fiber dominated isostrain rule of mixtures represented by $\nu_{12} = V_f\nu_{12f} + V_m\nu_m$. A more accurate representation of ν_{12} can be obtained through the use of the self consistent field model. The expression for this is $\nu_{12} = V_f\nu_{12f} + V_m\nu_m + \frac{(\nu_m - \nu_{12f})(K_m - K_f)G_m V_f - V_f^2}{K_f K_m + G_m(V_f K_f + V_m K_m)}$ where K_m is the bulk modulus of the matrix and K_f is the bulk modulus of the fiber [47]. However for most instances the isostrain assumption is sufficient.

| | E-Glass/Epoxy | Kevlar 49/Epoxy | Carbon/Epoxy |
|------------|----------------------|------------------------|---------------------|
| ν_{12} | 0.28 | 0.34 | 0.27 |
| level | 0 | -1 | 1 |

Out-of-plane Poisson’s ratio, ν_{23} : Out-of-plane Poisson’s ratio in the 23 direction will cause the individual fibers to shrink (along with the thickness of the overwrap) as the tank is pressurized. This will have a similar but likely less pronounced effect than in the 13 direction as the fiber will be laid such that the maximum strain will occur in the fiber direction. The basic formulation for ν_{12} requires knowledge of laminate bulk modulus K_2 and is represented as $\nu_{12} = 1 - \frac{E_2}{2K_2} - 2\nu_{12}^2 \frac{E_2}{E_1}$ [47].

| | E-Glass/Epoxy | Kevlar 49/Epoxy | Carbon/Epoxy |
|------------|----------------------|------------------------|---------------------|
| ν_{23} | 0.50 | 0.40 | 0.54 |
| level | 0 | 1 | -1 |

Out-of-plane Poisson's ratio, ν_{13} : Due to symmetry the out-of-plane Poisson ratio for the 13 direction is equal to the major in-plane Poisson ratio and is calculated using the same formulation. ν_{12} like ν_{23} will effect the overwrap thickness under load. Because the 1 direction is the primary loading direction for the fibers it is possible that ν_{13} will have a more pronounced effect on loaded laminate thickness than ν_{23} .

| | E-Glass/Epoxy | Kevlar 49/Epoxy | Carbon/Epoxy |
|------------|----------------------|------------------------|---------------------|
| ν_{13} | 0.28 | 0.34 | 0.27 |
| level | 0 | -1 | 1 |

Tensile strength: Tensile strength along with density will be of great importance when determining the weight of the vessels. A higher strength fiber allows for use of less material resulting in a lighter COPV. Because the reinforcement fibers will primarily be loaded in tension, tensile strength is of high concern for this application. Therefore, higher tensile strengths are highly desirable for use in COPVs. Tensile strength is defined by the composites stress at failure for uniaxial loading in the considered direction. lamina tensile strengths can be determined experimentally, or estimated from the constituent materials bulk properties.

Longitudinal tensile strength, F_{1t} : Longitudinal tensile strength is the most important strength to consider as fiber will be laid such the stress will be highest in the fiber direction. Longitudinal tensile strength defined by the composites stress at failure when uniaxially loaded in the fiber direction. F_{1t} is a contributing factor to a number of different failure criteria which estimate the failure strength of the laminate. the most common of these criteria are max stress, max strain, Tsai-Hill and Tsai-Wu. The discrepancy in strength for longitudinal and transverse loading is caused by the vast difference in strength between the fibers and their matrix.

| | E-Glass/Epoxy | Kevlar 49/Epoxy | Carbon/Epoxy |
|----------|----------------------|------------------------|---------------------|
| F_{t1} | 165 ksi | 205 ksi | 330 ksi |
| level | -1 | 0 | 1 |

Transverse tensile strength, F_{2t} : Transverse tensile strength in the 2 direction is the second most important tensile strength. Failure of COPVs can occur due to splitting of fibers in the transverse direction, and because the strength in the transverse direction is so much lower than in the longitudinal direction, this failure mode must be taken into consideration when designing fiber orientation. The strength is significantly lower in the transverse direction because it is a matrix dominated response where fibers act as stress concentrators. As with longitudinal, transverse tensile strength is given by stress at failure of a uniaxially loaded lamina. This property helps estimate laminate failure strength with a number of different failure criteria.

| | E-Glass/Epoxy | Kevlar 49/Epoxy | Carbon/Epoxy |
|----------|----------------------|------------------------|---------------------|
| F_{t2} | 5.7 ksi | 4.2 ksi | 8.3 ksi |
| level | 0 | -1 | 1 |

Out-of-plane tensile strength, F_{3t} : COPVs should not be under out-of-plane tensile loading. Because of this all levels have been set to zero as this property should not be contributing to judgment of fiber selection. Should this assumption prove to be incorrect, out-of-plane transverse tensile strength is equal to transverse tensile strength due to symmetry. Because all levels have been set to zero and with properties being symmetric the resulting rating should be equal regardless of whether or not this property is considered.

| | E-Glass/Epoxy | Kevlar 49/Epoxy | Carbon/Epoxy |
|----------|----------------------|------------------------|---------------------|
| F_{t3} | 5.7 ksi | 4.2 ksi | 8.3 ksi |
| level | 0 | 0 | 0 |

Compressive Strength Though the primary loading of COPVs will be in tension, provided that the tanks are to be structural components in the stack they will have to bare the weight of all that is stacked above them while on the pad before pressurization. They will also face compressive inertial loads during flight and have to bare their own weight while resting on tooling in the shop or in transit which will put the sections of laminate above the tanks neutral plane in compression. Another instance in which compression may occur is in the event of external impact. In all cases is is optimal for the compressive strength of the composite to be high.

Longitudinal Compressive strength, F_{1c} Longitudinal compressive strength can be utilized to support the weight of the rocket on the pad and handling compressive inertial loads by orienting fibers along the length of the pressure vessel. Longitudinal compressive strength is a buckling response, and for high volume fractions can be approximated as $F_{1c} = \frac{G_m}{1-V_f}$ which is a shear driven failure [47]. Laminate failure response is estimated using failure criteria which rely on this property.

| | E-Glass/Epoxy | Kevlar 49/Epoxy | Carbon/Epoxy |
|----------|----------------------|------------------------|---------------------|
| F_{c1} | 90 ksi | 49 ksi | 205 ksi |
| level | 0 | -1 | 1 |

Transverse Compressive strength, F_{2c} Transverse compressive strength is a likely compressive mode to occur while on the pad and in flight as most fibers will be off axis from the longitudinal direction. This orientation will contribute both transverse compressive and shear loads. Transverse compressive failure is less predicable and is caused by a number of failure modes, but it too can be approximated from bulk constituent properties [47]. As with all other strengths the failure criterion used to validate the composite rely on this property.

| | E-Glass/Epoxy | Kevlar 49/Epoxy | Carbon/Epoxy |
|----------|----------------------|------------------------|---------------------|
| F_{c2} | 18.6 ksi | 22.9 ksi | 33 ksi |
| level | -1 | 0 | 1 |

Out-of-plane Compressive strength, F_{3c} Due to symmetry, out-of-plane compressive strength is the same as transverse compressive strength, however it is less likely to occur under normal conditions. The instance where out-of-plane compressive strength is likely to occur is with accidental impact loading. Impact damage is a common disqualifier for composite parts, so out of plane compressive strength is important in the sense that higher strength fibers can take more load. However, ductility is also important for impact damage because a ductile material is better equip to dissipate energy. Therefore resilience to impact damage cannot be judged solely by out-of-plane compressive strength.

| | E-Glass/Epoxy | Kevlar 49/Epoxy | Carbon/Epoxy |
|----------|----------------------|------------------------|---------------------|
| F_{c3} | 18.6 ksi | 22.9 ksi | 33 ksi |
| level | -1 | 0 | 1 |

In-plane shear strength, F_6 : In plane shear strength is an important property to consider because as previously stated, the majority of fibers will not be directly in the loading direction. Multi-directional loading will present itself not only as stresses in principle directions but also as shear. Though ideally the laminate will be designed to minimize shear, regardless of what is done, shear will exist. This is because fiber cannot be wrapped fully in the longitudinal direction due to the polar bosses. Lamina shear strength is approximated using bulk constituent properties or can be tested empirically [47]. As with other strengths, shear strength for the laminate factors into failure analysis. The same four which were previously mentioned work for shear strength as well. As with other strengths the highest strength possible is desired from the material for this application.

| | E-Glass/Epoxy | Kevlar 49/Epoxy | Carbon/Epoxy |
|-------|----------------------|------------------------|---------------------|
| F_6 | 12.9 ksi | 7.1 ksi | 11.0 ksi |
| level | 1 | -1 | 0 |

Coefficients of thermal expansion, CTE: Coefficients of thermal expansion describe the amount of change in a materials size due to a change in temperature. In this case CTE describes change in length of either the longitudinal or transverse fiber direction. CTE will potentially affect both integration of the COPVs and internal stresses of the composite. Larger CTEs correlate to larger change in length per degree resulting in higher internal stresses and more complications with integration. Introduction of thermal stresses is both a use and manufacturing consideration. Because epoxy cures in an exothermic reaction and often requires heating of the part, raised temperatures at cure can introduce residual thermal stresses. When in use, expansion or contraction of a material can introduce stresses within the composite, especially when mated with a dissimilar material. Because of this the lowest magnitude CTE possible is optimal for this application.

Longitudinal thermal expansion coefficient, α_1 : Longitudinal CTE describes the amount a composite grows or shrinks in the fiber direction. Because of fibers high longitudinal moduli, longitudinal CTE is usually relatively low in magnitude compared to transverse CTE. Longitudinal CTE is given by the equation $\alpha_1 = \frac{E_{f1}\alpha_f V_f + E_m\alpha_m(1-V_f)}{E_{f1}V_f + E_m(1-V_f)}$ [47].

| | E-Glass/Epoxy | Kevlar 49/Epoxy | Carbon/Epoxy |
|------------|-----------------------------|------------------------------|------------------------------|
| α_1 | 3.9 ($10^{-6}/^{\circ}F$) | -1.1 ($10^{-6}/^{\circ}F$) | -0.5 ($10^{-6}/^{\circ}F$) |
| level | -1 | 0 | 1 |

Transverse thermal expansion coefficient, α_2 : As previously noted transverse CTE is typically higher in fiber reinforced composites because the fiber modulus is substantially lower in the transverse direction. This provides potential for significant internal stress during cure. Because epoxy is a thermosetting matrix it heats during its cure cycle. The polymer solidifies at temperature, and when it cools it grows or shrinks depending on the materials CTE. This growing or shrinking while locked into the geometry creates stress within the material. Luckily because CTE is positive in the longitudinal direction this acts as negative pre-load making the net stress within the composite less than it would be otherwise when placed under tension. Despite this benefit to the CTE, minimization is still optimal as it makes integration less complicated. Transverse CTE is given by the equation $\alpha_2 = \alpha_{2f}V_f(1 + \nu_{12f}\frac{\alpha_{1f}}{\alpha_{2f}}) + \alpha_m V_m(1 + \nu_m) - (\nu_{12f}V_f + \nu_m V_m)\alpha_1$ where $V_m = (1 - V_f)$ [47].

| | E-Glass/Epoxy | Kevlar 49/Epoxy | Carbon/Epoxy |
|------------|------------------------------|----------------------------|----------------------------|
| α_2 | 14.4 ($10^{-6}/^{\circ}F$) | 33 ($10^{-6}/^{\circ}F$) | 15 ($10^{-6}/^{\circ}F$) |
| level | 1 | -1 | 0 |

Out-of-plane thermal expansion coefficient, α_3 : Out-of-plane CTE has the same values as transverse CTE due to symmetry. α_3 has the same effect as α_2 for the same reasons and is calculated using the same equation.

| | E-Glass/Epoxy | Kevlar 49/Epoxy | Carbon/Epoxy |
|------------|------------------------------|----------------------------|----------------------------|
| α_3 | 14.4 ($10^{-6}/^{\circ}F$) | 33 ($10^{-6}/^{\circ}F$) | 15 ($10^{-6}/^{\circ}F$) |
| level | 1 | -1 | 0 |

Coefficients of moisture expansion, CME: “Micromechanical relations for the coefficients of moisture expansion are entirely analogous [to coefficients of thermal expansion]” [47]. “CME is defined by the ratio of the length variation to the mass variation percent due to moisture evaporation or absorption” [48]. CME is an important consideration for determining proper storage conditions for the rocket. Ideally the rocket would soak at and be launched under similar atmospheric conditions to when it was manufactured. Because CME is completely analogous to CTE including the equations used (substituting β for α) this section will not be discussed in depth, as the same logic argued for CTE applies to CME as well.

Longitudinal moisture expansion coefficient, β_1 :

| | E-Glass/Epoxy | Kevlar 49/Epoxy | Carbon/Epoxy |
|-----------|---------------|-----------------|--------------|
| β_1 | 0 | 0 | 0.1 |
| level | 1 | 1 | -1 |

Transverse moisture expansion coefficient, β_2 :

| | E-Glass/Epoxy | Kevlar 49/Epoxy | Carbon/Epoxy |
|-----------|---------------|-----------------|--------------|
| β_2 | 0.2 | 0.3 | 0.2 |
| level | 1 | -1 | 1 |

Out-of-plane moisture expansion coefficient, β_3 :

| | E-Glass/Epoxy | Kevlar 49/Epoxy | Carbon/Epoxy |
|-----------|---------------|-----------------|--------------|
| β_3 | 0.2 | 0.3 | 0.2 |
| level | 1 | -1 | 1 |

3.3.9 Overwrap material selection

Summation of the assigned levels in the discussion above is shown in table 3.1:

| | E-Glass/Epoxy | Kevlar 49/Epoxy | Carbon/Epoxy |
|---------------|---------------|-----------------|--------------|
| Points | 1 | -11 | 14 |
| Rank | 2 | 3 | 1 |

Table 3.1: Overwrap material ranking by points based on material properties

Outcome: Due to the outcome of the above material property investigation *a carbon fiber epoxy overwrap will be utilized* in the design for this paper. The carbon fiber used will likely be Toray™ TORAYCA T-1000G high strength fiber as it is a tow commonly used by Blue Force Technologies, the company most likely to perform the filament winding of the COPVs. The white this material is given in appendix 6.2.2 [49].

3.4 Slosh Mitigation

Slosh within context of aero-systems is defined in the Slosh Design Handbook as “periodic motion of a contained liquid propellant”. Slosh occurs due to dynamic motion and is most commonly caused by “gust loads, control modes, and structural modes” [50]. The slosh Design Handbook continues to explain that “if any of these excitations have frequencies in the vicinity of the resonant frequency of a contained liquid violent sloshing will occur” [50]. Due to the large liquid mass of propellant within a rocket, slosh can lead to significant forces which must be taken into consideration to maintain planned trajectory [50].

The Slosh Design Handbook written by James R Roberts and Pei-Ying Chen was written to evaluate the efficacy of damper designs by examining their damping effect on eigen frequencies of contained fluids [50]. This trade study will focus primarily on the results obtained by Roberts and Chen as LRL does not currently have sufficient information to plan for specific load histories. Mathematical models for the most promising designs will be considered to ensure their likely efficacy within the context of the LRL launch vehicle projected flight profile. Design selection will be based on the designs that provide damping over the broadest spectrum of frequencies likely to occur within the LRL launch vehicle. All mathematical models will assume a fully rigid circular cylinder [50].

3.4.1 Existing slosh mitigation system designs

Sectioned tanks

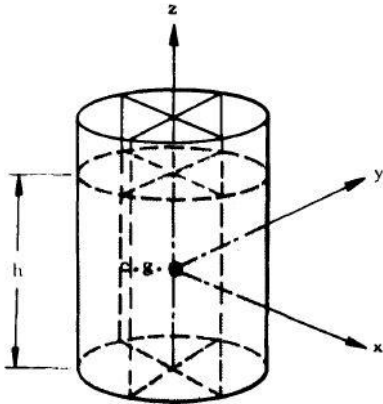


Figure 3.8: 90° sectored tank [50]

In the study performed by Abramson and Garza, water and methylene chloride were used as test liquids to examine partitioning effects on effective resonant frequency in the liquid and the damping ratio of the system [51]. It was found that 90° sector tanks with solid walls exhibit the lowest resonant frequency parameters of the three tanks

The general idea behind a sectioned tank is that it divides the fluid into discrete sections effectively forming a collective of smaller tanks. The following partition designs will be compared in terms of resonant frequencies and damping ratios. Resonant frequencies of given designs will be discussed in terms of resonant frequency parameter; Defined as “ $(\omega^2 d/a)$ where ω is the liquid natural frequency ... a is the acceleration field” and d is the tank diameter [51]. In the article frequencies and damping ratios were measured against excitation amplitude which is defined as (x_0/d) where x_0 is transnational excitation and d is the tanks diameter [51]. When discussing perforations, hole diameter ratio is used defined by (d_h/d) where d_h is perforation hole diameter and d is tank diameter [51].

examined. The 90° exhibited resonant frequency parameter values starting at around 5.5 and decreasing to approximately 4.85 as excitation amplitude increased [51]. It was discovered that in terms of resonant frequencies parameters 60° and 45° sectioned tanks performed similarly at low excitation amplitudes but started to diverge as excitation amplitude increased. The 45° sectioned tanks resonant frequency parameter leveled off at approximately 6.5 [51].

It was found that solid walled partitions offer little damping near resonant frequency with tested damping ratios averaging at 0.04. However “at frequencies below the resonant frequency the liquid sloshing is effectively damped” [51]. On the other hand studies showed that at resonant frequency, perforated partitions “with less than 10% open area will increase the damping ratio to approximately 0.1 while maintaining a liquid resonant frequency corresponding to a solid wall [sectioned] tank” [51].

When examining increased perforation percentages in the 45° sectioned tank, studies showed that maximum damping occurred in the range of 16-23% open area with a hole diameter ratio of 0.00278; “However, the excitation amplitude must be quite large to maintain the resonant frequency corresponding to solid-sector walls” [51]. When the hole diameter of high percentage perforation partitions were decreased to a ratio of 0.00139, the article states that they were able to obtain damping ratios 0.15 while maintaining the solid-walled resonant frequency at 23% perforation [51].

Results for the 60° and 90° sector tanks show similar trends. Both 60° and 90° tanks exhibited damping ratios of 0.12 at 16-23% perforation while maintaining solid walled frequency characteristics with lower excitation amplitudes corresponding to small diameter ratios and large excitation amplitudes corresponding to larger diameter ratios [51].

The main takeaways from this information is that tank sectioning is an effective means of resonant frequency control as well as slosh damping. Additionally that resonant frequency control can be maintained by relating the hole diameter ratio to particular excitation amplitudes [51, 50]. According to the Slosh Design Handbook studies “indicate that cross partitions have a greater effect on eigen frequencies than do concentric partitions” and that for “[90° sectioned tanks], the vibrating liquid mass is reduced to more than one-half of that of a [non-partitioned] circular cylindrical tank” [50].

Circumferential ring baffles

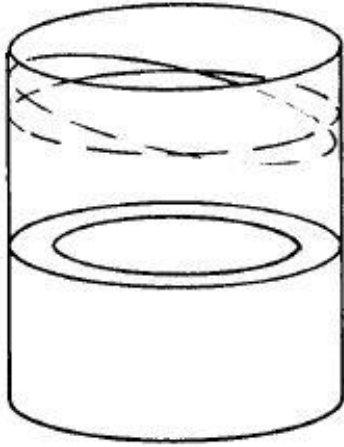


Figure 3.9: Ring baffle [50]

Another study was performed by Abramson and Garza in 1963 [52]. In this study they evaluated the efficacy of ring baffles within a cylindrical tank for damping slosh. The article explains that ring baffles primary utility is reducing liquid propellant motion caused by lateral forces [50, 52]. Their experiment aimed to investigate and measure the effect circumferential ring baffles have on slosh and the resonant frequencies that contribute to it.

In the study baffles 0.018 - 0.03 inches thick with a fixed width to radius ratio (W/R) of 0.157 were used [52]. In addition to solid baffles, perforated baffles with a baseline of 30% perforated area and 0.079 inch diameter holes were tested [52]. Liquid depth was held constant and was equal to the tanks diameter.

Resonant frequency was presented using the same dimensionless resonant frequency parameter ($\omega^2 d/a$) in the authors previous article. [51, 52]. Excitation amplitude (x_0/d) was also presented in the same form [51]. In the studies, excitation amplitude was varied from $0.00184 \leq x_0/d \leq 0.00823$, “then all data was presented in terms of RMS values” [52]. The authors also define a ratio (d_s/R) as the distance of the baffle below the liquids surface at equilibrium in relation to the tank radius [52].

The study resulted in the findings that “the liquid resonant frequency exhibits a maximum value when the baffle is located at the liquid free surface ($d_s/R=0$). Resonant frequency decreases to a minimum value near a baffle depth of $d_s/R=0.10$. At ring depths greater than $d_s/R=0.10$, the liquid resonant frequencies increase with (d_s/R), gradually approaching the first liquid resonant frequency for a bare-walled cylindrical tank” [52]. When an analysis of the liquids resonant frequency as a function of d_s/R was performed for the perforated baffle it was observed that “for baffle depths greater than $d_s/R=0.06$ ” the resonant frequency increased with an increase in percentage of perforated area as well as perforation hole size [52].

The findings on perforation effects were given in graphical form as seen in figures 3.10 and 3.11. As explained in the Slosh Design Handbook and is apparent by these plots, as perforation both in terms of hole diameter and area percentage increase damping factor decreases[50, 52]. Additionally effective resonant frequency increases with an increase in both metrics of perforation [50, 52] This indicates that there is no benefit to perforating circumferential ring baffles other than weight reduction; However there are more effective methods of accomplishing weight reduction, so as a general rule perforating ring baffles is not a good idea.

The article also offers a figure showing damping ratio for multiple circumferential baffles and resonant frequency on the same plot which can be seen in figure 3.12 [52]. This image shows that damping is greatest just below the baffles and that resonant frequency reaches a maximum at the baffles.

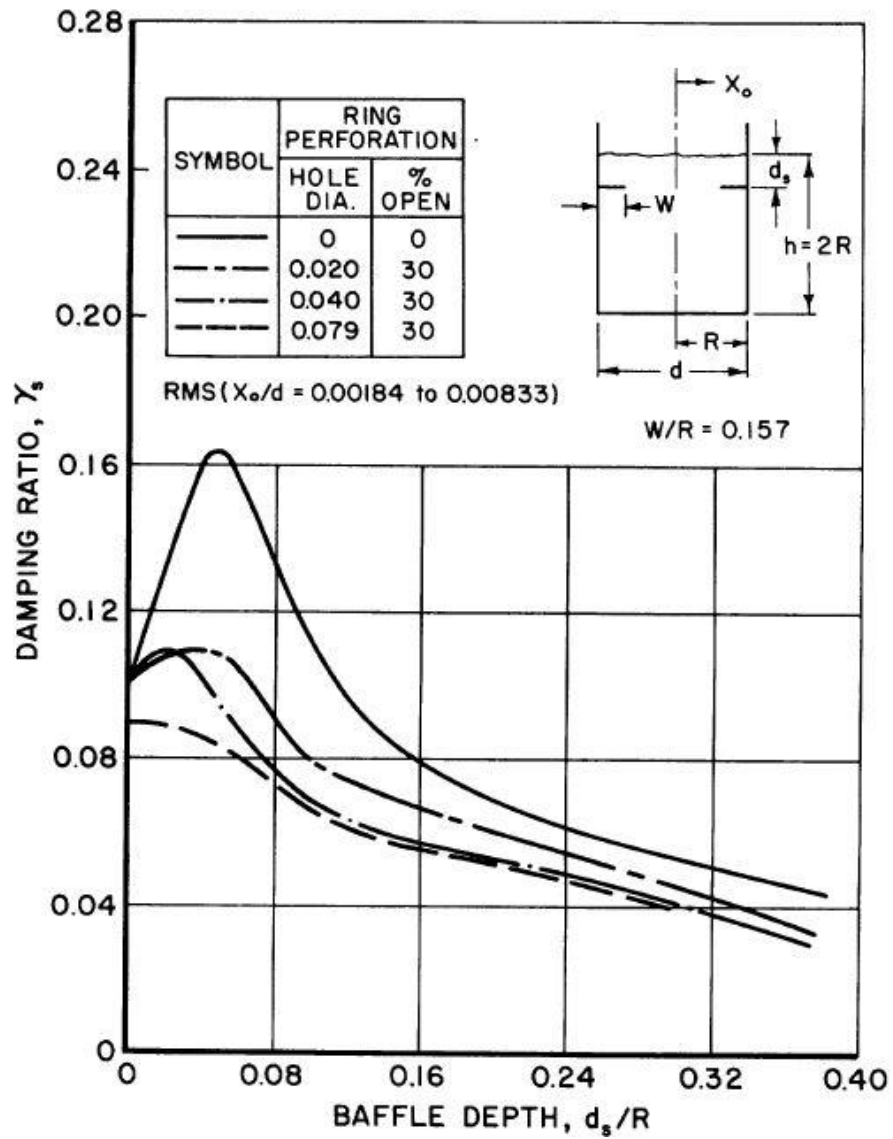


Figure 3.10: Effect perforation diameter on damping ratio for circumferential ring baffles [52]

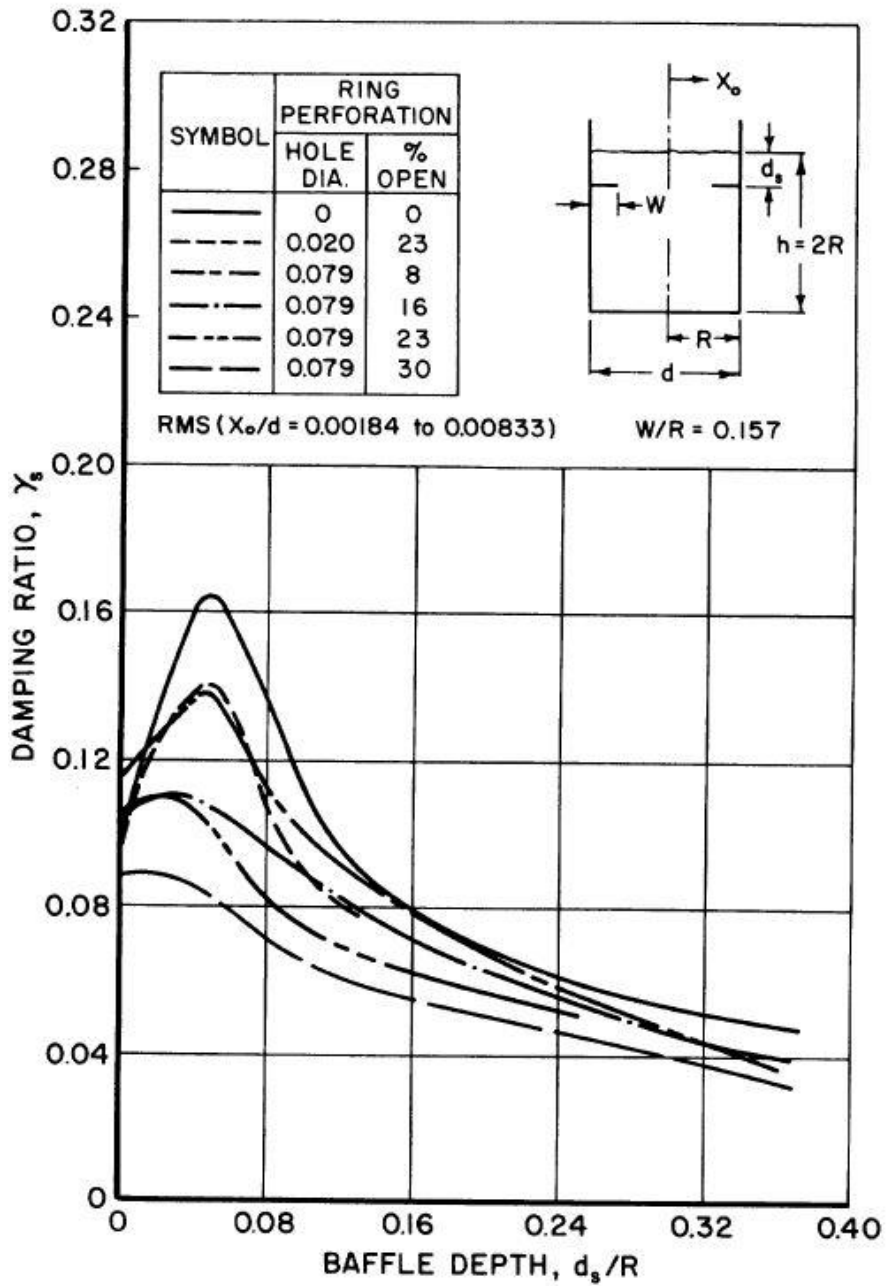


Figure 3.11: Effect perforation area percentage on damping ratio for circumferential ring baffles [52]

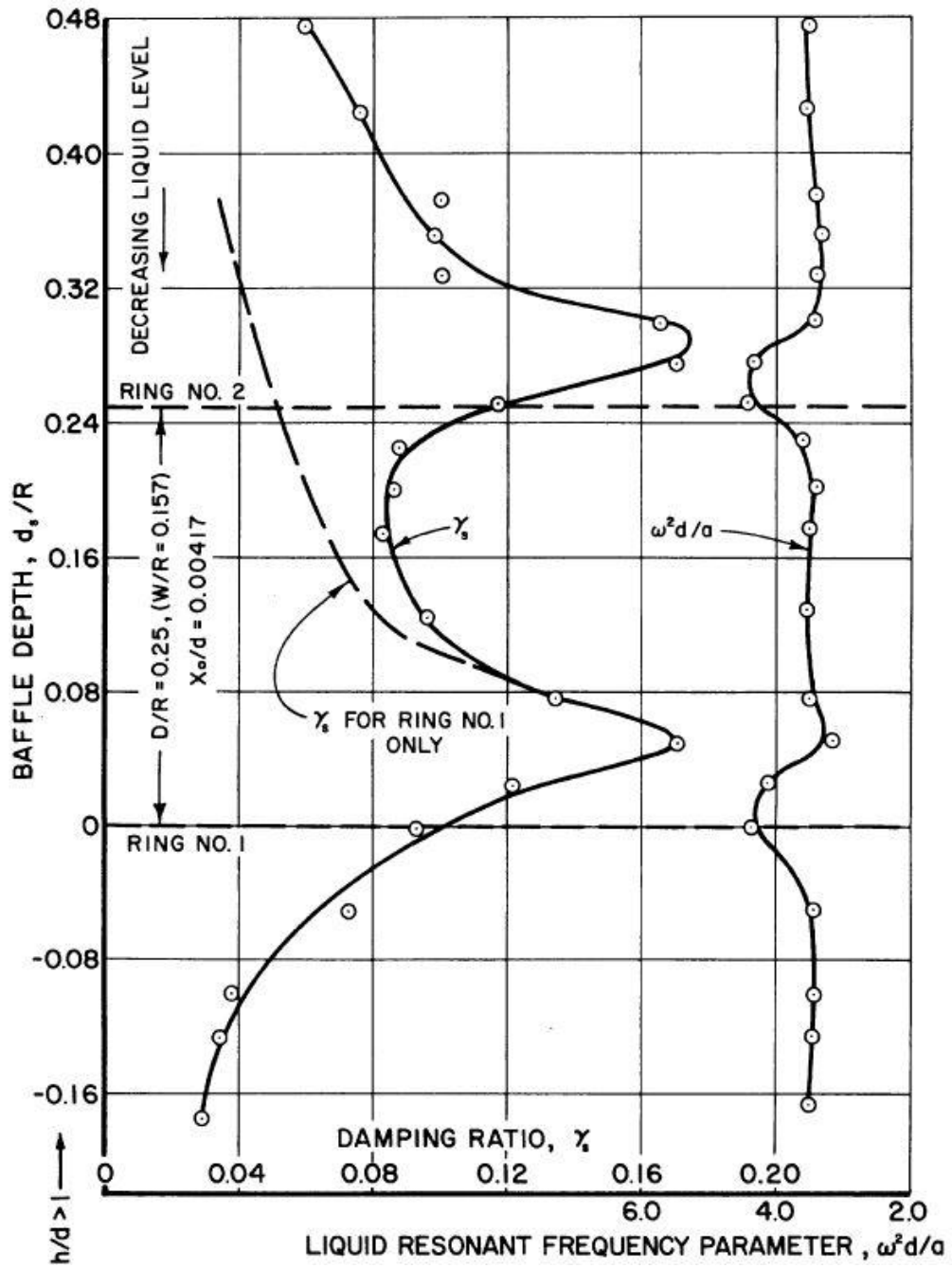


Figure 3.12: Effect of multiple circumferential ring baffles on damping ratio and resonant frequency [52]

Ring with radial clearance

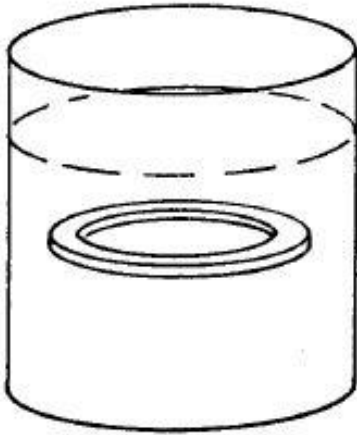


Figure 3.13: Ring-with-radial-clearance [50]

A 1961 study by Silveira et al. investigated the effect of flat ring baffles with radial clearance on damping and effective resonant frequency [53]. The study defines damping factor as $\delta = \frac{1}{n} \log_e \frac{M_o}{M_n}$ where “n is equal to number of cycles over which decay was measured, M_o equals the amplitude of a selected initial moment, and M_n represents the amplitude of a selected terminal moment after n cycles” [53].

For this study M_o was set to produce a wave amplitude equal to approximately one inch in a 12 inch diameter, 12 inch deep tank filled with water. M_n was set as $0.3M_o$ for general damping evaluation. To examine the effect of amplitude on damping M_n was set equal to $0.7M_o$ [53]. Using this test procedure baffle geometry was varied and tested in different states.

The geometric parameters changed were baffle clearance from the tanks walls (c) and the baffles width defined as the baffles outer radius minus its inner radius (w)[53]. Figure 3.14 shows the damping factor corresponding to each configuration plotted against (d/R) which represents the ratio of the baffles distance below the liquids equilibrium surface and the tanks radius [53]. Similarly frequency was measured as a function of baffle location for each of the geometry previously described. Results are shown in figure 3.15.

In the Slosh Design Handbook Roberts and Chen interpenetrate the findings of Silveira et al. as follows:

When radial clearance is held constant:

- “The damping factor increases as the baffle width increases” as show in figure 3.14 [50, 53]
- “The frequency increases as the baffle width decreases” as show in figure 3.15 [50, 53]

When baffle width is held constant:

- “The damping factor decreases as radial clearance increases” as show in figure 3.14 [50, 53]
- “The frequency increases as the radial clearance decreases” as show in figure 3.15 [50, 53]

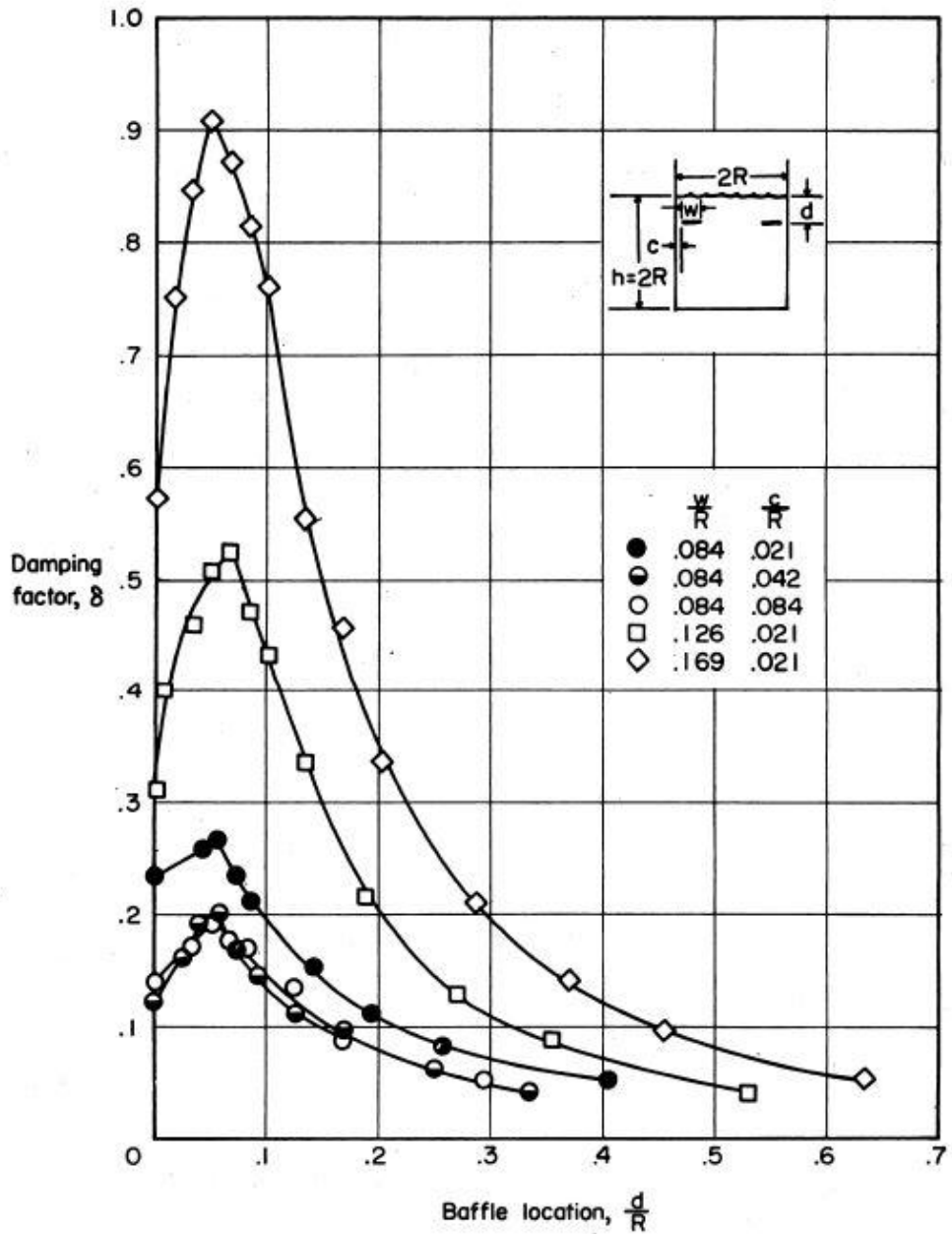


Figure 3.14: Ring with radial clearance study results [53]

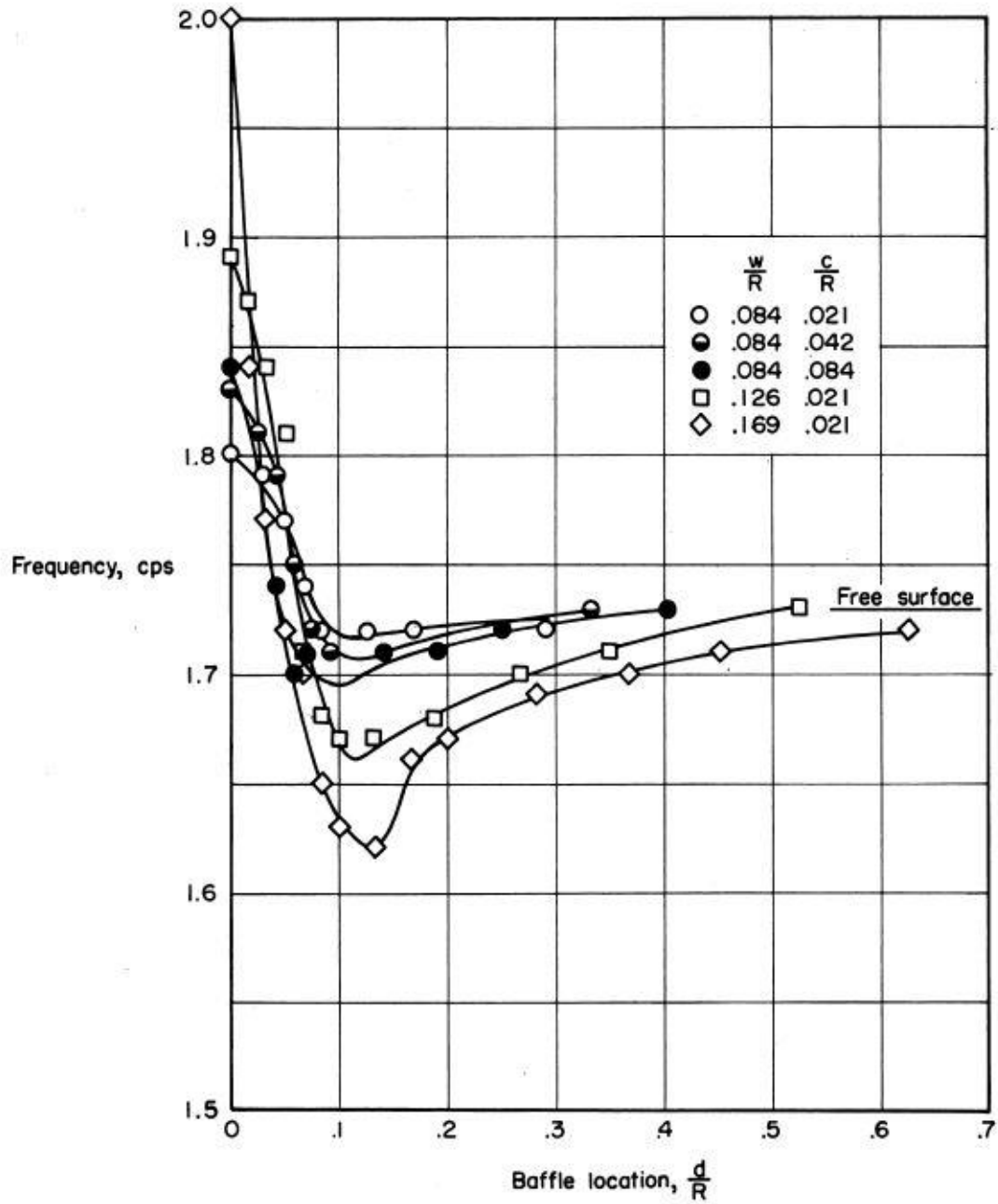


Figure 3.15: Ring with radial clearance study results [53]

Conic section baffles

In the previously cited article by Silveira et al. conic sections were also investigated using the same experimental design as described in the previous discussion. Conic section baffles were investigated in upright along with inverted orientations as shown in figure 3.16 using both perforated and non-perforated baffle material. All conic section baffles in the study were held at 45° and are sized with their radius as projected onto a plane [53].

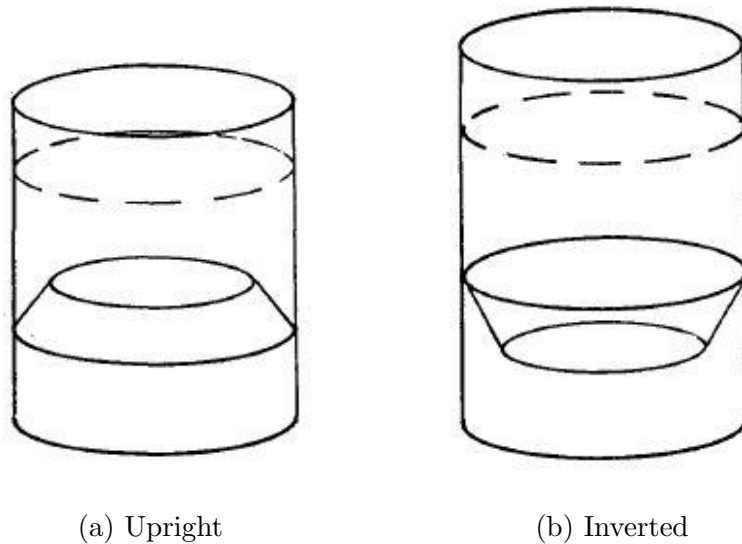


Figure 3.16: Conic section baffle designs [50]

Silveira et al. found that the damping results “are very similar to those of the flat rings... although the damping provided by the conic sections is slightly higher” [53]. It was found that maximum damping for upright conic section baffles occurs when the upright conic section baffle is just below the surface with a d/R ratio of about 0.085 where d is the measure from the top of the baffle to the static fluid surface [53]. The article continues to say that “the surface area of a conic section baffle having the same value of w/R as that for the fixed ring is considerably higher” [53]. This implies that the increase of mass for upright conic section baffles are not worth the increase in damping for rocketry applications.

When examining inverted conic section baffles Silveira et al. found that they perform nearly the same as upright conic section baffles with the same relations to flat ring baffles. “However, the maximum value of damping occurs when the baffle is approximately half submerged in the liquid ... [due to an] almost complete restriction of fluid motion in the region between the baffle and the tank wall” [53]. The inverted conic section appears to be less effective than both flat ring and upright conic section baffles [53]; Therefore this design will be eliminated from consideration. Silveira et al. found that adding perforations in the conic section baffles reduced the sharp curve seen in the damping factor vs. depth ratio plots, however damping efficiency also decreased by more than half compared with solid conic section baffles [53]. This indicates that use of perforated conic section baffles are also not worth considering.

Cruciform baffles

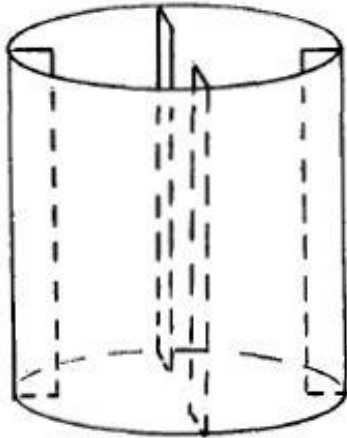


Figure 3.17: Cruciform-baffles [50]

Another baffle geometry covered by Silveira et al. in the same study are cruciform baffles. Two sizes of cruciform baffles were tested: One with $w/R = 0.169$ and the other with $w/R = 0.337$ [53]. Damping factor was measured 90° and 45° from the node line (fluid flow direction) yielding the following results [53]:

| w/R | Angle | δ |
|-------|------------|----------|
| 0.169 | 90° | 0.072 |
| 0.169 | 45° | 0.070 |
| 0.337 | 90° | 0.156 |
| 0.337 | 45° | 0.142 |

Cruciform baffles show the lowest damping of flat or conic baffle types as examined with the conventional slosh generation method used in the article authored by Silveira et al. [53].

However, the Slosh Design Handbook indicates that the primary utility of cruciform baffles is the prevention of rotational slosh [50] which can be caused by rotational movement of the container or by a vortex caused by drainage.

Can Floats

Floats are a damping methodology proposed in a 1958 article by Eulitz et al. [54]. The idea with a float is that it will rest atop the fluid and track the fluid level as it decreases. Examples of these floats can be seen in figure 3.18 which also acts as a visual aid to describe the test procedure. In the test, tanks were hung by their tops as shown in figure 3.18 [54]. The tanks were then oscillated. A load cell was attached to the bottom of the tanks and the reaction force caused by the oscillations was measured [54]. Damping factor in this experiment is the ratio of the maximum reaction force for a liquid contained by a slosh mitigation system to the maximum reaction force for a free liquid.

Figure 3.20 shows the resulting damping effects of different designs undergoing this test. On this chart the "Solid Liquid" line represents the ideal damping curve. The slosh mitigation mechanism that most closely resembles the ideal damping curve is the "Float, Cans" curve. The mechanism to which this refers is shown in figure 3.19. The article by Eulitz et al. describes the can as a cylinder of perforated aluminum in which a hollow aluminum sphere lies. The top and bottom of the cans are angled to prevent the sphere from falling out. The typical geometry for a can as described by Eulitz et al. can be seen in figure 3.19(b). Sizing guidelines for a can design is detailed in the Slosh Design Handbook.

DEVICES FLOATING ON THE LIQUID SURFACE

- A. BELL TYPE FLOAT
- B. MAT TYPE FLOAT
- C. CAN TYPE FLOAT

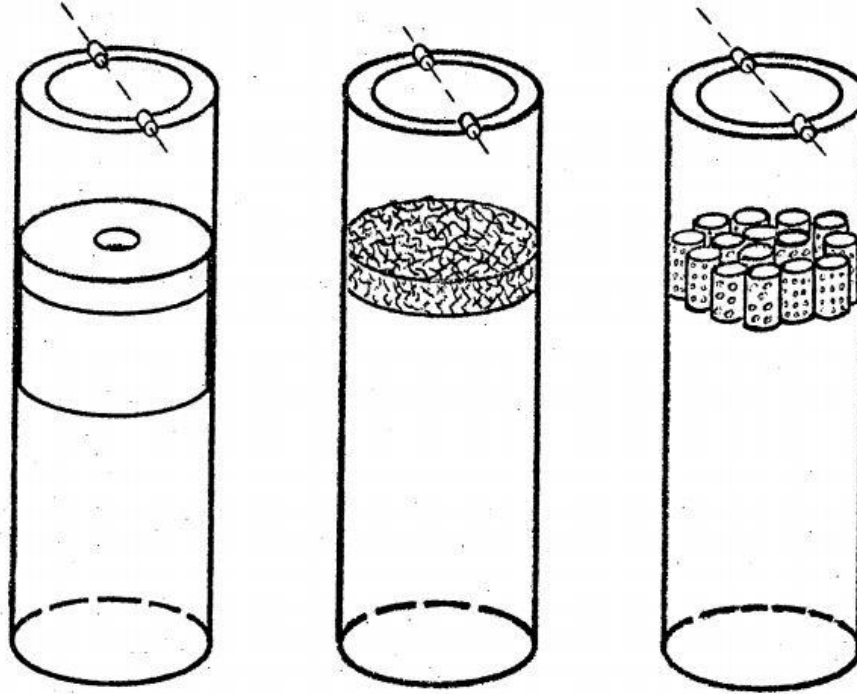
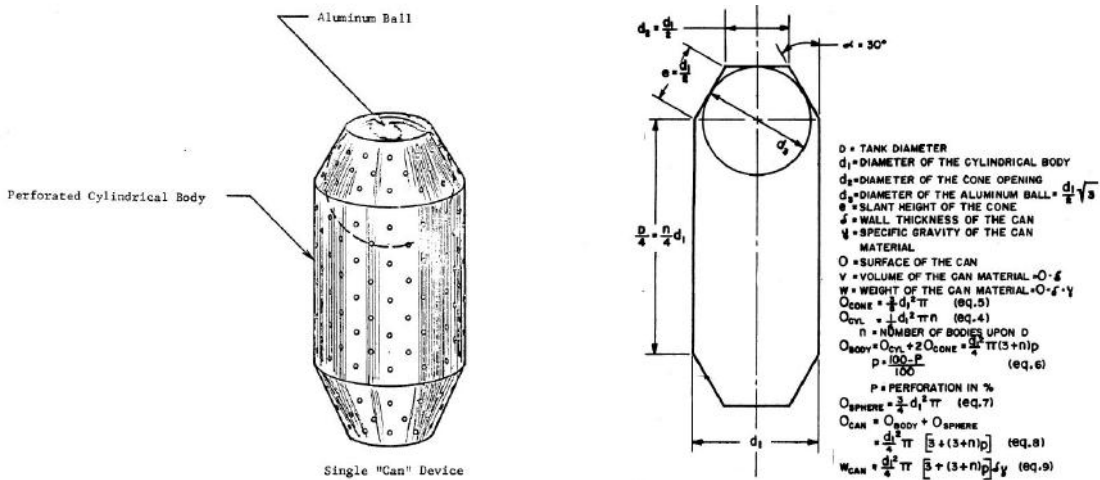


Figure 3.18: Float type slosh mitigation designs [54]



(a) Proposed can design

(b) Typical can dimensions

Figure 3.19: Can design proposed by Eulitz et al. [50, 54]

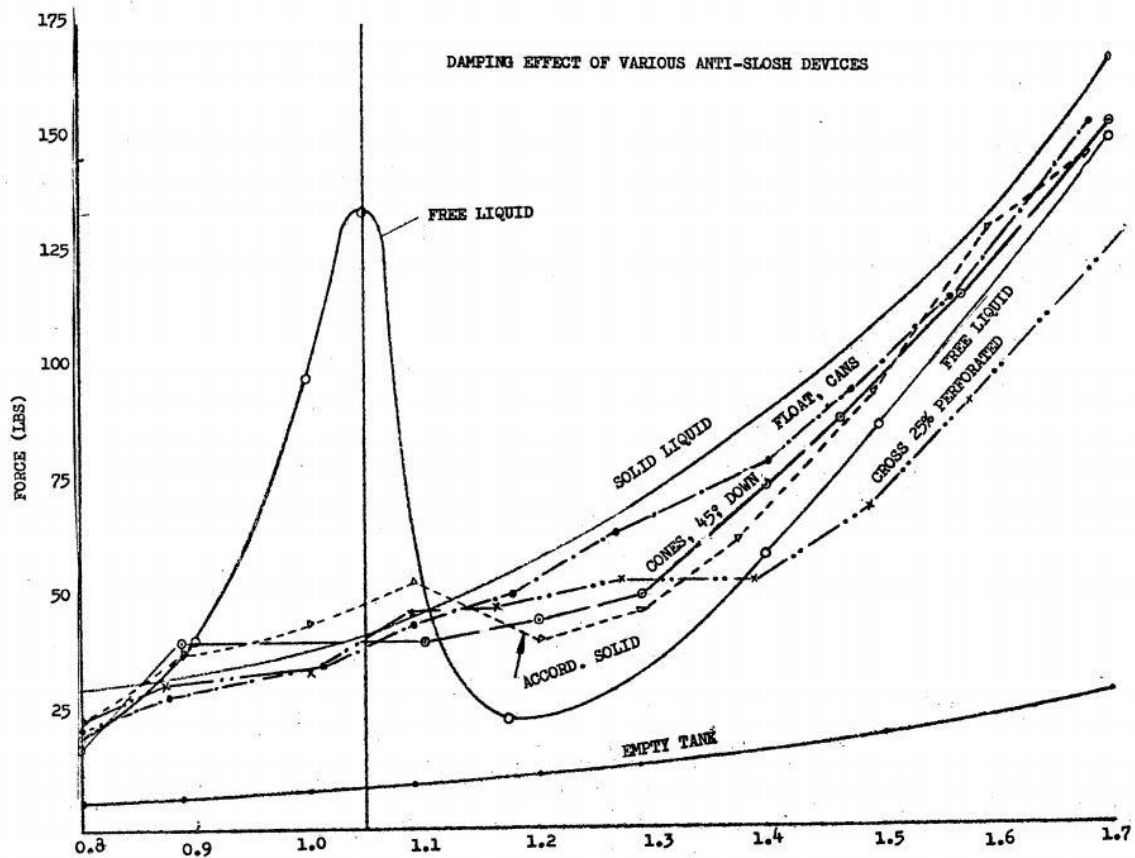


Figure 3.20: Damping comparison of several designs [54]

Though other float designs such as mat and bell type baffles were mentioned, there is not extensive explanation of the results for these damping mechanisms. In the slosh design handbook it was noted that the mat type was “highly effective in damping the liquid amplitude” but notes that it can easily become caught on internal tank features [50].

3.4.2 Slosh mitigation system selection

In the Slosh Design Handbook, Roberts and Chen give the recommendation that “the designer should start with solid circumferential ring baffles and use Miles’ expression for [the] first approximation of the damping factor” [50]. “Miles’ expression” refers to a semi-empirical relation derived by J. W. Miles for the damping factor of fixed ring baffles [55, 56, 53, 50]. The equation for this relationship is given in equation 3.1.

$$\delta = (2\pi)2.83e^{-4.60\frac{d}{R}\left(\frac{R^2-(R-w)^2}{R^2}\right)^{\frac{3}{2}}}\left(\frac{\zeta}{R}\right)^{\frac{1}{2}} \quad (3.3)$$

Semi-empirical relationship for damping factor: $d =$ Depth below static liquid surface, $R =$ Tank radius, $w =$ Width of baffle annulus projected on liquid surface, $\zeta =$ Wave amplitude [53]

Roberts and Chen suggest that the damping factor calculated by use of Miles’ expression be used as the basis for a “ball-park-figure for the spacing and width of the baffles” [50]. The Handbook then suggests that Bauer’s extension (a mathematically intensive expansion found in the Handbook) be used to refine the result of baffle distribution. Finally the handbook suggests that analysis of “pressure acting on the baffle will permit the optimization of thickness and material of each baffle and thus the calculation of the total weight added by the damping system” [50]. For pressure analysis a series of complex relations were used to estimate, however in 2020, FEA and CFD analysis techniques can be used to model the pressure on the baffles to ensure they do not plasticity deform or fail when in use.

Outcome: Because much is still unknown about the system including the oscillatory or vibrational loading, ***a circumferential ring baffle system will be utilized*** in the design for this paper. Should future testing reveal that greater damping be required or a greater shift in resonant frequency be required to adequately reduce slosh, this trade study can act as a basis for deeper investigation. In the design of the tanks, an effort will be made for the parametric modeling of the slosh mitigation system to provide ease of variability for future design alterations.

COPV Design

4.1 Design Selection

By evaluating design choices through trade studies the general COPV designs have been selected. The pressurant COPV will consist of an aluminum liner with hemispherical heads and a carbon fiber overwrap. By trade study it was concluded that the propellant COPVs will be two separate tanks rather than one tank sharing a common bulkhead. They too will have aluminum liners with hemispherical heads, and carbon overwraps. Additionally, the propellant tanks will have circumferential ring baffles as slosh mitigation mechanisms. The aluminum used will be 6061 with the assumption of T6 temper for analysis. The carbon used will be Toray T1000G unidirectional fiber and the matrix used will be 3501-6 Epoxy.

4.2 Stack Configuration

The stacking of the propellant tanks requires consideration. Placement of the fuel and oxidizer COPVs on top of one another has potential mass and stability ramifications. In terms of stability, tank placement will result in varying mass center location for the rocket throughout its flight. Because the propellants will be draining, the tanks mass center will shift downwards with the propellants until a minimum value is reached at which point the mass center will shift upwards again.

Rocket stability in its simplest form is ensuring that the rockets center of mass (CM) is positioned above its center of pressure (CP). In a state where the height of $CM > CP$, the system acts like a pendulum. The center of mass acts like the pendulums pivot and the center of pressure acts like the pendulums bob with an equilibrium position of the center of pressure directly below the center of mass. In a state where the height of $CM < CP$, the system acts like an inverted pendulum. The system is inherently unstable with the center of pressure wanting to topple the rocket.

However if the center of mass is too high, the rocket will be unstable on the launch pad and as it takes off. On the pad and as the rocket has just begun to gain velocity there is not sufficient aerodynamic pressure to keep a rocket with a high center of mass stable. Because of this a rockets center of mass should lie below its midpoint while traveling at low velocity.

To track the rockets center of mass throughout flight, the Matlab script shown in appendix 6.1.5 was written. Graphical outputs from that script are shown in figure 4.1 where spacing between the propellant tanks was varied.

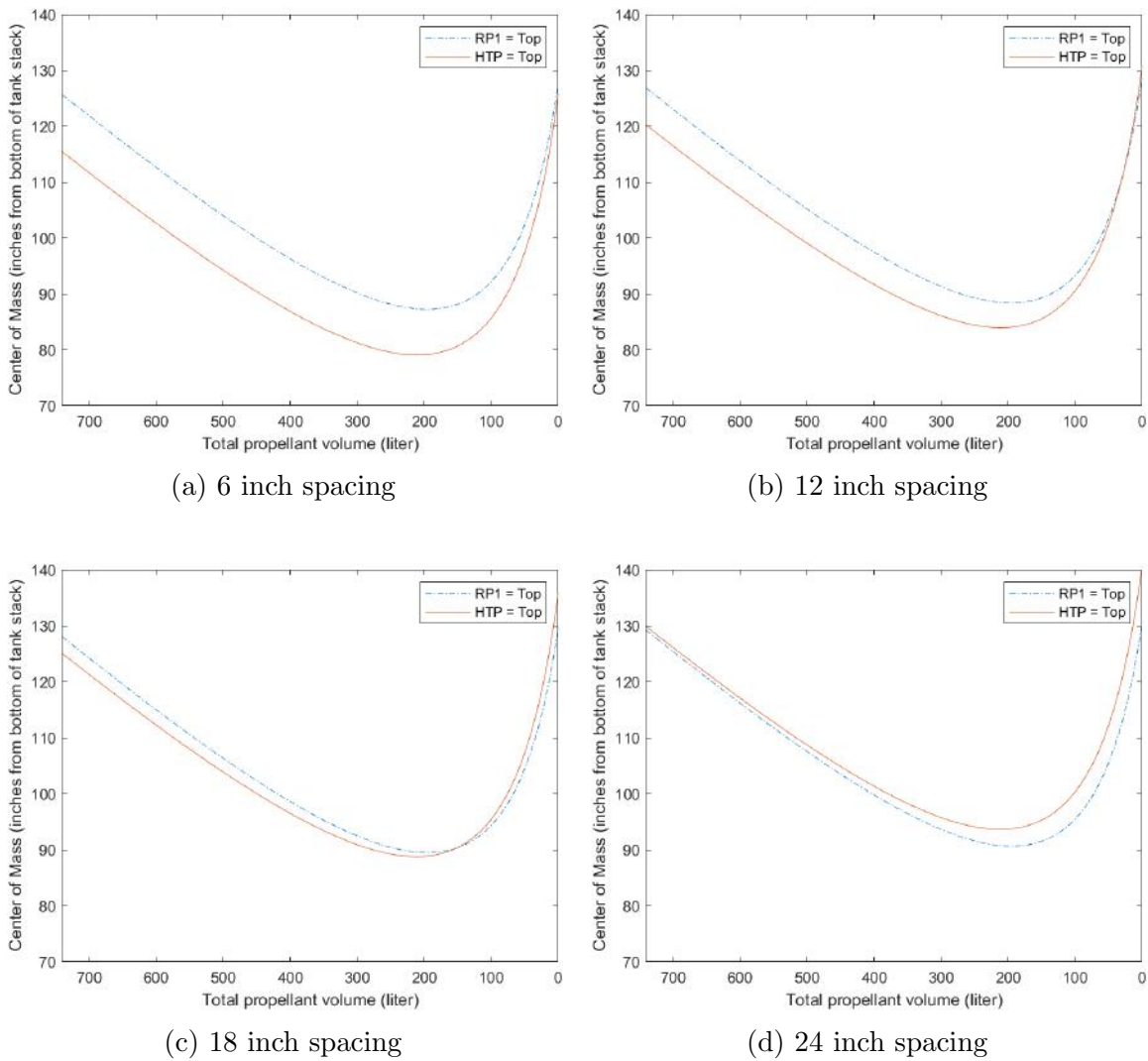


Figure 4.1: Center of Mass for two propellant tanks with varied spacing. HTP on top vs RP-1 on top. **Note: Spacing offers no mass contribution**

Figure 4.1 indicates that locating the RP-1 tank above the HTP tank will provide a higher CM for most of the burn time with tank spacing less than 18 inches. It is likely that tank spacing will be less than 18 inches, and the maximum CM height for either configuration is estimated to be less than half the final rocket height. Because of this the current assumption will be made that the RP-1 tank will go above the HTP tank. Should circumstances change as other rocket systems further in development, this decision can be re-evaluated.

4.3 Baffle Design

Using Miles Equation shown in eq. 3.1, initial geometric parameters can be determined. Because slosh amplitudes, resonant frequencies, and required damping factors have yet to be determined, baffle design must be approached symbolically. The biggest impact on design will be the number and spacing of the baffles within the tank. An initial estimate for this can be derived by solving miles equation for baffle depth as shown in equation 4.1.

$$d = -\frac{0.21739R*\log(0.056238\delta)}{\frac{\zeta}{R}^{1/2}*\left(\frac{R^2*(w-R)^2}{R^2}\right)^{\frac{3}{2}}} \quad (4.1)$$

Miles Equation solved for baffle depth: δ = Damping ratio, R = Tank radius, w = Width of baffle annulus projected on liquid surface, ζ = Wave amplitude

An alternative to Miles Equation is O'Neill's Extension which is shown in eq. 4.2. O'Neill's Extension gives damping factor in terms of lateral force and fluid density rather than in terms of wave amplitude [50].

$$\delta = (2\pi)2.16e^{-4.60\frac{d}{R}\left(\frac{R^2-(R-w)^2}{R^2}\right)^{\frac{3}{2}}}\left(\frac{F}{\rho g R^3}\right)^{\frac{1}{2}} \quad (4.2)$$

O'Neill's relationship for damping factor: d = Depth below static liquid surface, R = Tank radius, w = Width of baffle annulus projected on liquid surface, F = lateral force, ρ = fluid density, g = gravitational acceleration [50]

Similarly to Miles equation, O'Neill's equation can be rewritten to solve for baffle depth where lateral lateral force can be experimentally determined and used as a design parameter. This solution is shown in equation 4.3

$$d = -\frac{0.21739R*\log(0.073683\delta)}{\frac{F}{R^3 g \rho}^{1/2}*\left(\frac{R^2*(w-R)^2}{R^2}\right)^{\frac{3}{2}}} \quad (4.3)$$

O'Neill's Equation solved for baffle depth: δ = Damping ratio, R = Tank radius, w = Width of baffle annulus projected on liquid surface, F = lateral force, ρ = fluid density, g = gravitational acceleration

The result of these equations give the damping factor of a single baffle submerged at depth d which can give a good estimate. However, for a better estimate for a system of rings, Bauer's Extension must be used. According to the Slosh Design Handbook, Miles' Equation gives a higher estimate of damping factor than is actually observed because it assumes the fluid and baffle are in constant contact with one another. Additionally Bauer's Extension accounts for a system of baffles and their combined interaction with

the fluid [50]. The entire derivation and explanation of Bauer's Extension is shown in the Slosh design handbook, but for the sake of brevity, only the result will be presented in this paper. The result of Bauer's Extension is the conditional summation shown in equation 4.4 [50].

$$\delta = 2.83 \sqrt{\frac{\zeta}{R}} \left\{ \sum_{n=1}^N e^{-4.6(\frac{d}{R} + (n-1)\frac{D}{R})} \bar{\alpha}_n^{\frac{3}{2}} + \sum_{m=1}^M e^{-4.6(m\frac{D}{R} - \frac{d}{R})} \bar{\alpha}_m^{\frac{3}{2}} \right\} \quad (4.4)$$

Bauer's Extension relationship for damping factor: $d =$ Depth below static liquid surface, $R =$ Tank radius, $n = n^{\text{th}}$ baffle below the free fluid surface, $\bar{\alpha}_n =$ conditional effective baffle area for fully submerged baffle, $m = m^{\text{th}}$ baffle above the free fluid surface, $\bar{\alpha}_m =$ conditional effective baffle area for baffle impacted by slosh, $D =$ Distance between baffles, $\zeta =$ Wave amplitude

As noted in the equations caption $\bar{\alpha}_n$ and $\bar{\alpha}_m$ are conditional parameters depending on whether or not the baffles are coming into contact with the sloshing fluid. $\bar{\alpha}_n$ describes the effective area of a baffle submerged a depth $d + (n-1)D$ below the free surface and is given by equations 4.5 – 4.7 for various relations between the equations parameters (given in equation captions) [50]. $\bar{\alpha}_m$ describes the effective area of a non-submerged baffle above the free fluid surface level a distance of $D-d$ and is given by equations 4.8 – 4.10 for various relations between the equations parameters (given in equation captions) [50].

$$\bar{\alpha}_n = \frac{w}{R} \left(2 - \frac{w}{R} \right) \quad (4.5)$$

Bauer's Extension lower effective baffle area if $\frac{d}{R} + \frac{D}{R} \geq \frac{\zeta}{R}$: $d =$ Depth below static liquid surface, $R =$ Tank radius, $n = n^{\text{th}}$ baffle below the free fluid surface, $D =$ Distance between baffles, $\zeta =$ Wave amplitude, $w =$ Width of baffle annulus projected on liquid surface

$$\begin{aligned}
\bar{\alpha}_n &= \frac{w}{R} \left(2 - \frac{w}{R}\right) - \frac{1}{2} \left\{ 1 - \frac{\frac{d}{R} + (n-1)\frac{D}{R}}{\frac{\zeta}{R}} \right\} \\
&+ \frac{2}{\pi} \left[\frac{\frac{d}{R} + (n-1)\frac{D}{R}}{\frac{\zeta}{R}} \right] \cdot \ln \left\{ \frac{\frac{\zeta}{R} + \sqrt{\frac{\zeta^2}{R^2} - \left(\frac{d}{R} + (n-1)\frac{D}{R}\right)^2}}{\frac{d}{R} + (n-1)\frac{D}{R}} \right\} \\
&- \frac{1}{\pi} \left[\frac{\frac{d}{R} + (n-1)\frac{D}{R}}{\frac{\zeta}{R}} \right] \cdot \sqrt{\frac{\zeta^2}{R^2} - \left(\frac{d}{R} + (n-1)\frac{D}{R}\right)^2} \\
&+ \left(\frac{1}{\pi}\right) \arcsin \left(\frac{\frac{d}{R} + (n-1)\frac{D}{R}}{\frac{\zeta}{R}} \right) - \left(\frac{1}{2}\right) \left(\frac{\frac{d}{R} + (n-1)\frac{D}{R}}{\frac{\zeta}{R}} \right)
\end{aligned} \tag{4.6}$$

Bauer's Extension lower effective baffle area if $\frac{\zeta}{R}(1 - \frac{w}{R}) \leq \frac{d}{R} + \frac{D}{R} \leq \frac{\zeta}{R}$: d = Depth below static liquid surface, R =Tank radius, $n = n^{th}$ baffle below the free fluid surface, D = Distance between baffles, ζ =Wave amplitude, w = Width of baffle annulus projected on liquid surface

$$\begin{aligned}
\bar{\alpha}_n &= \frac{w}{R} \left(2 - \frac{w}{R} \right) - \frac{1}{2} \left\{ 1 - \frac{\frac{d}{R} + (n-1) \frac{D}{R}}{\frac{\zeta}{R}} \right\} \\
&+ \frac{2}{\pi} \left[\frac{\frac{d}{R} + (n-1) \frac{D}{R}}{\frac{\zeta}{R}} \right] \cdot \ln \left\{ \frac{\frac{\zeta}{R} + \sqrt{\frac{\zeta^2}{R^2} - \left(\frac{d}{R} + (n-1) \frac{D}{R} \right)^2}}{\frac{d}{R} + (n-1) \frac{D}{R}} \right\} \\
&- \frac{1}{\pi} \left[\frac{\frac{d}{R} + (n-1) \frac{D}{R}}{\frac{\zeta}{R}} \right] \cdot \sqrt{\frac{\zeta^2}{R^2} - \left(\frac{d}{R} + (n-1) \frac{D}{R} \right)^2} \\
&+ \left(\frac{1}{\pi} \right) \arcsin \left(\frac{\frac{d}{R} + (n-1) \frac{D}{R}}{\frac{\zeta}{R}} \right) - \left(\frac{1}{2} \right) \left(\frac{\frac{d}{R} + (n-1) \frac{D}{R}}{\frac{\zeta}{R}} \right) \\
&\quad + \frac{1}{2} \left(1 - \frac{w}{R} \right)^2 \left\{ 1 - \frac{\frac{d}{R} + (n-1) \frac{D}{R}}{\left(1 - \frac{w}{R} \right) \frac{\zeta}{R}} \right\} \\
&- \left(\frac{2}{\pi} \right) \left[\frac{\frac{d}{R} + (n-1) \frac{D}{R} \left(1 - \frac{w}{R} \right)}{\frac{\zeta}{R}} \right] \cdot \ln \left[\frac{\frac{\zeta}{R} + \sqrt{\left(\frac{\zeta}{R} \right)^2 - \left[\frac{\frac{d}{R} + (n-1) \frac{D}{R}}{1 - \frac{w}{R}} \left(\frac{D}{R} \right) \right]^2}}{\frac{\frac{d}{R} + (n-1) \frac{D}{R}}{1 - \frac{w}{R}}} \right] \\
&+ \left(\frac{1}{\pi} \right) \left[\frac{\frac{d}{R} + (n-1) \frac{D}{R} \left(1 - \frac{w}{R} \right)}{\frac{\zeta}{R}} \right] \sqrt{\left(\frac{\zeta}{R} \right)^2 - \left[\frac{\frac{d}{R} + (n-1) \frac{D}{R}}{1 - \frac{w}{R}} \right]^2} \\
&- \frac{1}{\pi} \left(1 - \frac{w}{R} \right)^2 \arcsin \left[\frac{\frac{d}{R} + (n-1) \frac{D}{R}}{\left(1 - \frac{w}{R} \right) \frac{\zeta}{R}} \right] + \frac{1}{2} \left(1 - \frac{w}{R} \right) \left[\frac{\frac{d}{R} + (n-1) \frac{D}{R}}{\frac{\zeta}{R}} \right]
\end{aligned} \tag{4.7}$$

Bauer's Extension lower effective baffle area if $\frac{d}{R} + \frac{D}{R} < \frac{\zeta}{R} \left(1 - \frac{w}{R} \right)$: d = Depth below static liquid surface, R = Tank radius, $n = n^{\text{th}}$ baffle below the free fluid surface, D = Distance between baffles, ζ = Wave amplitude, w = Width of baffle annulus projected on liquid surface

$$\bar{\alpha}_m = 0 \quad (4.8)$$

Bauer's Extension upper effective baffle area if $m\frac{D}{R} - \frac{d}{R} \geq \frac{\zeta}{R}$: d = Depth below static liquid surface, R =Tank radius, $m = m^{\text{th}}$ baffle above the free fluid surface, D = Distance between baffles, ζ =Wave amplitude, w = Width of baffle annulus projected on liquid surface

$$\begin{aligned} \bar{\alpha}_m = & \frac{1}{2} \left(1 - \frac{m\frac{D}{R} - \frac{d}{R}}{\frac{\zeta}{R}} \right) - \frac{2}{\pi} \left[\frac{m\frac{D}{R} - \frac{d}{R}}{\frac{\zeta}{R}} \right] \cdot \ln \left[\frac{\frac{\zeta}{R} + \sqrt{\left(\frac{\zeta}{R}\right)^2 - \left[m\frac{D}{R} - \frac{d}{R}\right]^2}}{m\frac{D}{R} - \frac{d}{R}} \right] \\ & + \frac{1}{\pi} \left[\frac{m\frac{D}{R} - \frac{d}{R}}{\left(\frac{\zeta}{R}\right)^2} \right] \sqrt{\left(\frac{\zeta}{R}\right)^2 - \left(m\frac{D}{R} - \frac{d}{R}\right)^2} - \frac{1}{\pi} \arcsin \left(\frac{m\frac{D}{R} - \frac{d}{R}}{\frac{\zeta}{R}} \right) \\ & + \frac{1}{2} \frac{\left(m\frac{D}{R} - \frac{d}{R}\right)}{\frac{\zeta}{R}} \end{aligned} \quad (4.9)$$

Bauer's Extension upper effective baffle area if $\frac{\zeta}{R}(1 - \frac{w}{R})/leq m\frac{D}{R} - \frac{d}{R} \leq \frac{\zeta}{R}$: d = Depth below static liquid surface, R =Tank radius, $m = m^{\text{th}}$ baffle above the free fluid surface, D = Distance between baffles, ζ =Wave amplitude, w = Width of baffle annulus projected on liquid surface

$$\begin{aligned}
\bar{\alpha}_m = & \frac{1}{2} \left(1 - \frac{m \frac{D}{R} - \frac{d}{R}}{\frac{\zeta}{R}} \right) - \frac{2}{\pi} \left[\frac{m \frac{D}{R} - \frac{d}{R}}{\frac{\zeta}{R}} \right] \cdot \ln \left[\frac{\frac{\zeta}{R} + \sqrt{\left(\frac{\zeta}{R}\right)^2 - \left[m \frac{D}{R} - \frac{d}{R}\right]^2}}{m \frac{D}{R} - \frac{d}{R}} \right] \\
& + \frac{1}{\pi} \left[\frac{m \frac{D}{R} - \frac{d}{R}}{\left(\frac{\zeta}{R}\right)^2} \right] \sqrt{\left(\frac{\zeta}{R}\right)^2 - \left(m \frac{D}{R} - \frac{d}{R}\right)^2} - \frac{1}{\pi} \arcsin \left(\frac{m \frac{D}{R} - \frac{d}{R}}{\frac{\zeta}{R}} \right) \\
& + \frac{1}{2} \frac{\left(m \frac{D}{R} - \frac{d}{R}\right)}{\frac{\zeta}{R}} - \frac{1}{2} \left(1 - \frac{w}{R}\right)^2 \left\{ 1 - \frac{\left(m \frac{D}{R} - \frac{d}{R}\right)}{\left(1 - \frac{w}{R}\right) \frac{\zeta}{R}} \right\} \\
& + \frac{2}{\pi} \left[\frac{\left(m \frac{D}{R} - \frac{d}{R}\right) \left(1 - \frac{w}{R}\right)}{\frac{\zeta}{R}} \right] \cdot \ln \left[\frac{\frac{\zeta}{R} + \sqrt{\left(\frac{\zeta}{R}\right)^2 - \left(\frac{m \frac{D}{R} - \frac{d}{R}}{\left(1 - \frac{w}{R}\right)^2}\right)^2}}{\frac{m \frac{D}{R} - \frac{d}{R}}{1 - \frac{w}{R}}} \right] \\
& - \frac{1}{\pi} \frac{\left(m \frac{D}{R} - \frac{d}{R}\right)}{\left(\frac{\zeta}{R}\right)^2} \sqrt{\left(\frac{\zeta}{R}\right)^2 - \left(\frac{m \frac{D}{R} - \frac{d}{R}}{\left(1 - \frac{w}{R}\right)^2}\right)^2} \\
& + \frac{1}{\pi} \left(1 - \frac{w}{R}\right)^2 \arcsin \left\{ \frac{\left(m \frac{D}{R} - \frac{d}{R}\right)}{\left(1 - \frac{w}{R}\right) \frac{\zeta}{R}} \right\} - \frac{1}{2} \left(1 - \frac{w}{R}\right) \frac{\left(m \frac{D}{R} - \frac{d}{R}\right)}{\frac{\zeta}{R}}
\end{aligned} \tag{4.10}$$

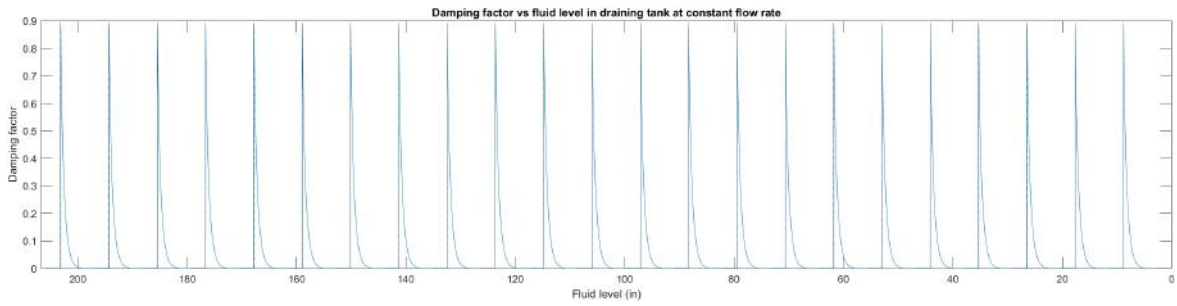
Bauer's Extension upper effective baffle area if $m \frac{D}{R} - \frac{d}{R} \leq \frac{\zeta}{R} \left(1 - \frac{w}{R}\right)$: d = Depth below static liquid surface, R =Tank radius, $m = m^{\text{th}}$ baffle above the free fluid surface, D = Distance between baffles, ζ =Wave amplitude, w = Width of baffle annulus projected on liquid surface

Parameters fixed by design are: D - the spacing between the baffles, w - the width of the baffles, and R - the tanks inner radius. Tank radius is primarily of aerodynamic concern and is dictated accordingly. This leaves D and w as the primary design parameters. ζ - the wave amplitude of the sloshing free fluid is almost entirely at the whim of flight and vibrational dynamics. For this reason ζ will be assigned a value within a realistic range for the sake of testing. Baffle depth 'd' is a function of baffle spacing and fluid flow rate. Using this set of relations and assumptions a Matlab script shown in code appendix 6.1.4 has been created to act a parametric model for baffle design. To obtain realistic values for parameters, an experiment must be conducted using vibratory modes and attitude adjustments that will be seen in flight. Figures 4.2a – 4.2d show damping factor vs tank level for a variety of baffle quantities and spacing.

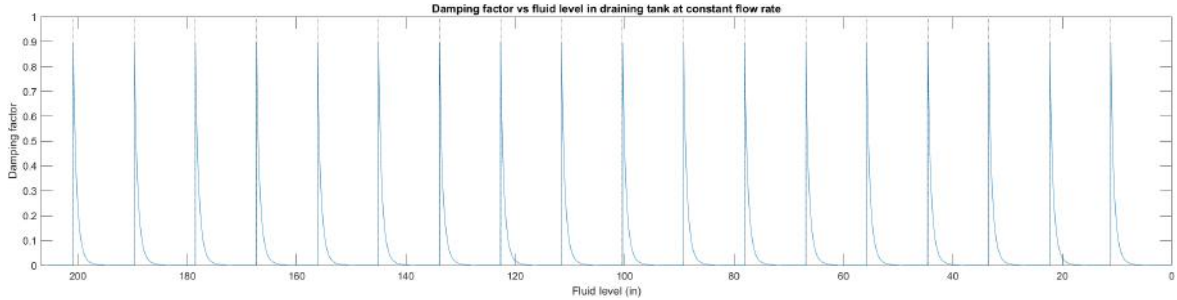
This analysis shows a problem with Bauer's model in the sense that it is not the best for tanks with few baffles as it defaults to a state of near linearity for large 'D' values; In the real world it is likely not the case that baffles above the fluid will provide significant damping if the slosh amplitude is less than the 'd' value. For large values of D, this situation is often the case. However Bauer's model seems to indicate that increases in baffles offer higher damping more frequently where less baffles provide room for intermediate damping. Due to the lack of information on actual parameter values along with evidence pointing towards increased quantities of baffles providing little benefit for damping of high amplitude slosh, 10 baffles will be used in the HTP tank with a spacing of D=24" within the cylindrical section of the tank.

The top baffle spacing will be increased to a maximum of 30 inches so that the top baffle ends at the end of the cylinder. Should the spacing exceed 30 inches, the baffle will be returned in its position to D=24" and an additional baffle will be placed at the top of the cylinder. Because the RP-1 tank has a short cylindrical section, baffles will be placed on the top and bottom of the cylinder. Should the cylinder for the RP-1 tank exceed 24 inches, the baffle will increase in spacing up to 6 inches ($D_{\max}=30$) at which point spacing of the two baffles will return to 24" and an additional baffle will be added. A baffle thickness of 0.1" was assumed, and will be designed as such. Future analysis will be done to determine if this thickness is sufficient. The baffles not only act as a slosh mitigation mechanism but also serve as a skeleton for the liner. This is the reason for the baffles on the end.

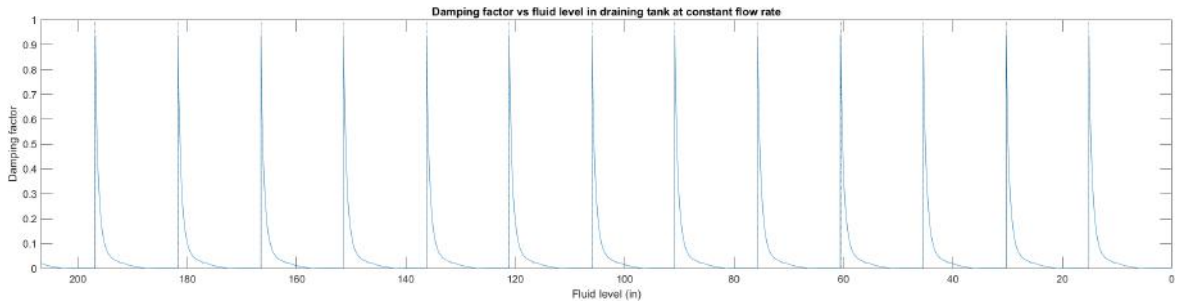
In addition to the circumferential baffles, longitudinal baffles will be added. These baffles will act more as a means of creating a framework than preventing slosh, however in the instance of roll events, they will offer marginal slosh mitigation. This framework will help stabilize the liner as it is being wound. Notches will be cut in the circumferential baffles for the longitudinal baffles to slot into. These longitudinal baffles will be made from 6061 angle oriented such that a single edge is coincident with the edge of the baffles with the "L" facing into the baffle to provide stiffness while maintaining light weight. This material can be purchased from Alro steel, the LRL metal supplier.



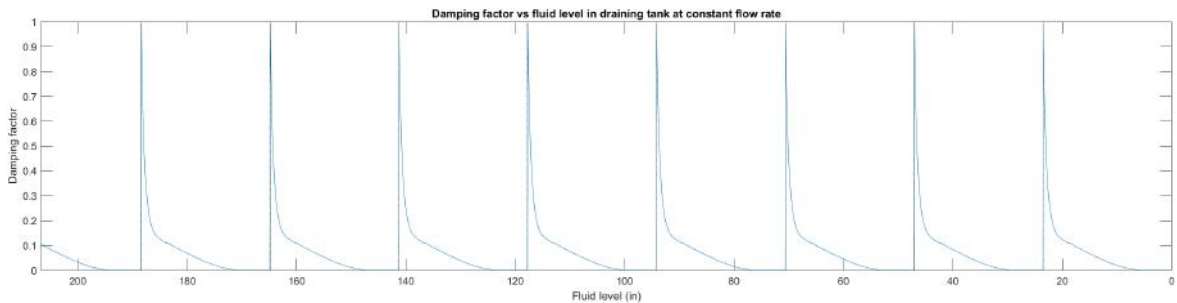
(a) HTP baffle system using Bauer's Expansion - 25 baffles:
 $\zeta = 6$ (in), $w = 2$ (in), $N = 19$, $M = 1$, $D = 8.83$ (in), $R = 7.8$ (in), $Weight = 20.83$ (lb)



(b) HTP baffle system using Bauer's Expansion - 20 baffles:
 $\zeta = 6$ (in), $w = 2$ (in), $N = 19$, $M = 1$, $D = 11.15$ (in), $R = 7.8$ (in), $Weight = 16.66$ (lb)



(c) HTP baffle system using Bauer's Expansion - 15 baffles:
 $\zeta = 6$ (in), $w = 2$ (in), $N = 14$, $M = 1$, $D = 15.14$ (in), $R = 7.8$ (in), $Weight = 12.50$ (lb)



(d) HTP baffle system using Bauer's Expansion - 10 baffles:
 $\zeta = 6$ (in), $w = 2$ (in), $N = 9$, $M = 1$, $D = 23.55$ (in), $R = 7.8$ (in), $Weight = 8.33$ (lb)

4.4 Liner Design

As previously noted the liners for all three COPVs will be made from 6061 sheet aluminum. The cylinders can be manufactured locally, and the hemispherical heads can be purchased online. The cylinders can be rolled and welded, and the heads can be welded to the completed cylinders. The baffle assembly will act as a supportive framework to which the liners cylinder can be affixed for welding.

While both the RP-1 and N₂ tanks will likely be small enough that the cylinders will be able to be made from a single piece of rolled aluminum, it is likely that the HTP tank cylinder will need to be made from multiple pieces. The number of pieces used should be minimized to reduce the amount of welding that needs to be done. Additionally, longitudinal welds should be performed 180 degrees to one another to reduce the amount of welds converging in a single location. To weld the cylinders, the use of an automated welder is suggested. Because welding of thin aluminum is notoriously difficult, use of an automated welder will ensure a uniform, airtight weld throughout the length of all weld seams while avoiding punch through.

All exterior welds should be performed atop baffles. In practice the baffle will act as a backer which will provide two benefits. First, the backer will help prevent punch through of the weld. Secondly, the baffle will become part of the joint and will help to reduce the load placed on the weld seam itself. The liner will also have to be welded to the other longitudinal baffles on the baffle structure. This can be done through the following process:

1. Fixture rolled cylinder around the baffle structure such that the open edges converge atop a longitudinal baffle
2. Tack weld the ends of the longitudinal baffle opposite to the the baffle where the open edges converge to the cylinder
3. Allow the cylinder material to open and weld along the length of the longitudinal baffle opposite the open edges
4. Perform this same process welding longitudinal angle baffles to the cylinder working towards the open edges. Check before and after each weld to ensure that the open edges of the liner still converge atop the baffle to which the cylinder material was originally aligned
5. After all other longitudinal baffles have been welded to the cylinder material, close the cylinder with a final weld along the longitudinal baffle to which the material was originally aligned

An additional consideration when discussing the design of the liner is the forces it faces during the filament winding process. Because the fiber requires compaction, which in filament winding is provided by tension in the filament itself, there will be significant inward pressure on the liner while it is being wound. To counteract this pressure, the liner must be pressurized to provide equal and opposite force to maintain the tanks geometry during winding. An analogy to this is the pressure inside of a beverage can which keeps it from becoming dented in transit.

4.5 Overwrap Design

The carbon used will be Toray T1000G unidirectional fiber, however full properties are unavailable, so remaining properties will be supplemented using AS4 properties, a lower property fiber. The matrix used will be 3501-6 epoxy.

The COPV analysis Matlab scripts shown in the code appendices 6.1.1 and 6.1.2 gives the following lamina level material properties for a unit sample of the composite using the supplemented T1000G reinforcement in a 3501-6 epoxy matrix :

| | |
|---|------------------------------|
| Longitudinal Modulus (E1) | 26.4732 Msi |
| Transverse Modulus (E2) | 1.1041 Msi |
| Shear Modulus (G12) | 544.5523 ksi |
| Poissons ratio (v12) | 0.2585 |
| Longitudinal CTE | -0.3648 ($\frac{10^6}{F}$) |
| Transverse CTE | 18.2466 ($\frac{10^6}{F}$) |
| Longitudinal tensile strength (F1t) | 563.6400 ksi |
| Longitudinal compressive strength (F1c) | 595.0256 ksi |
| Transverse tensile strength (F2t) | 6.5785 ksi |
| Transverse compressive strength (F2c) | 19.0682 ksi |
| In-plane shear strength (F6) | 5.8176 ksi |

Material deposition direction is the variable that dictates the overwraps performance in a specific loading case. For pressure vessels, stress components are considered in the the hoop 4.11 and longitudinal 4.12 directions. The stresses are described by the following equations in which σ_{hoop} and σ_{long} are mutually orthogonal:

$$\sigma_{hoop} = \frac{Pr}{t} \quad (4.11)$$

$$\sigma_{long} = \frac{Pr}{2t} \quad (4.12)$$

Because the fiber is deposited at an angle α , the area relationships shown in figure 4.3 exist. Because stress is defined as force divided by area, the orientation of the fibers area components drive the way stress is distributed into the fiber. Figure 4.3 indicates that $A_{long} = \sec(\alpha)$. Similarly, figure 4.3 shows $A_{hoop} = \csc(\alpha)$. From these relations and the definition of stress we get equations 4.14 and 4.13.

$$\sigma_{long} = \frac{F_{long}}{A_{long}} = \frac{\sigma_f A_f \cdot \cos(\alpha)}{A_f \cdot \sec(\alpha)} = \sigma_f \cdot \cos^2(\alpha) \quad (4.13)$$

$$\sigma_{hoop} = \frac{F_{hoop}}{A_{hoop}} = \frac{\sigma_f A_f \cdot \sin(\alpha)}{A_f \cdot \csc(\alpha)} = \sigma_f \cdot \sin^2(\alpha) \quad (4.14)$$

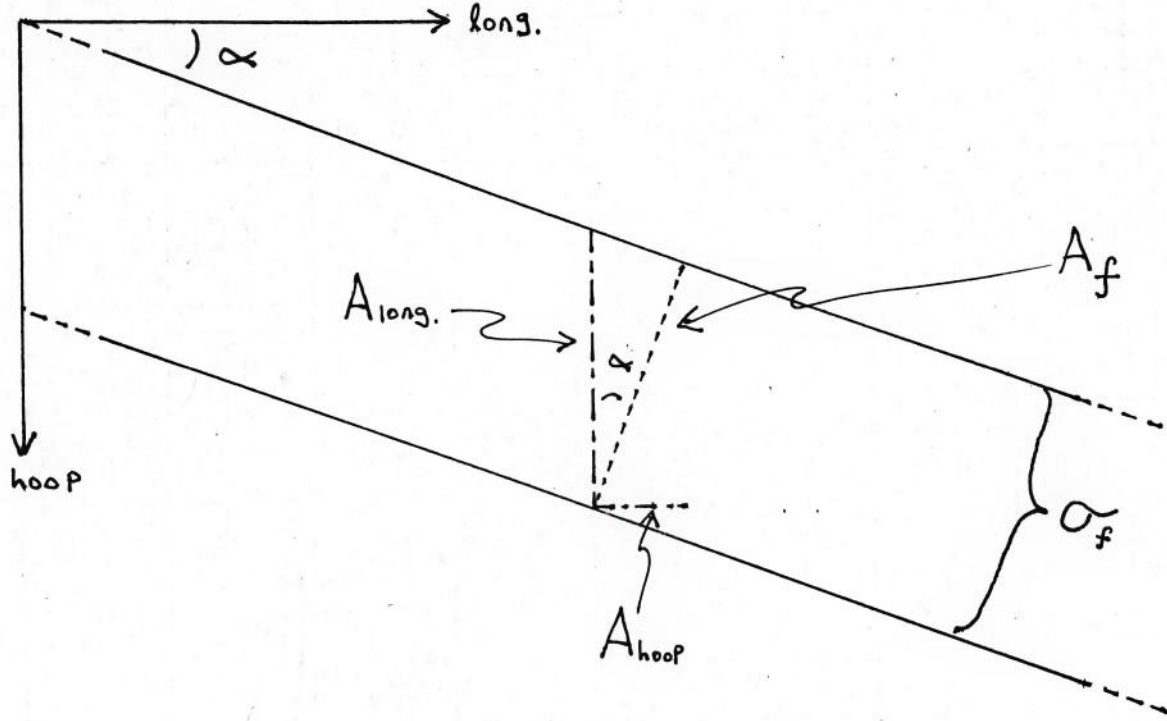


Figure 4.3: Illustration of fiber loading area components

By referring to equations 4.11 and 4.12 one can see that hoop stress is double that of longitudinal stress indicating the relationship between the two stresses shown in equation 4.15. This results in the outcome shown in equation 4.16.

$$\frac{\sigma_{hoop}}{\sigma_{long}} = \frac{\sigma_f \cdot \sin^2(\alpha)}{\sigma_f \cdot \cos^2(\alpha)} = \tan^2(\alpha) = 2 \quad (4.15)$$

$$\tan^2(\alpha) = 2 \therefore \tan^{-1}(\sqrt{2}) = \alpha \implies \boxed{\alpha \approx 54.74^\circ} \quad (4.16)$$

This relationship has been discussed in many articles including [57, 58, 59] and is generally regarded as the ideal loading angle for thin walled pressure vessels within a single lamina. This will be the initial orientation considered during the analysis of the pressure vessel. However, in reality to achieve even coating of the liner, the filament winding angle must vary such that the layers do not continually deposit material on the same paths. To compensate for this the mathematical relation shown in equations 4.17 and 4.18 applies for a multilayered overwrap with varying orientation and thickness [57].

$$\sigma_{hoop}(t_1 + t_2 + \dots + t_n) = \sigma_{f1}t_1 \cdot \sin^2(\alpha) + \sigma_{f2}t_2 \cdot \sin^2(\alpha) + \dots + \sigma_{fn}t_n \cdot \sin^2(\alpha) \quad (4.17)$$

$$\sigma_{long}(t_1 + t_2 + \dots + t_n) = \sigma_{f1}t_1 \cdot \cos^2(\alpha) + \sigma_{f2}t_2 \cdot \cos^2(\alpha) + \dots + \sigma_{fn}t_n \cdot \cos^2(\alpha) \quad (4.18)$$

Using these relations given by [57] one can generate a symmetric layup of fibers which average to 54.74° emulating conditions of a 54.74° lamina. Because access to filament winding software is cost prohibitive, the assumption that the dictated laminate will be manufacturable with slight alteration by Blue Force Technologies is made. Without access to filament winding software one is unable to determine the completed surface profile.

The COPV analysis scripts shown in code appendices 6.1.1 and 6.1.2 give an initial estimate for a composite structure that would meet the requirements for each COPV. Because both of the propellant tanks are under the same load, they have the same layups. The initial estimate of a working layup for the propellant tanks is $[\pm 54.7_5]_s$. The initial estimate of a working layup for the pressurant tank is $[\pm 54.7_{23}]_s$. This analysis tool was built using classic laminate theory and analyzed using Tsai-Hill failure criteria. This initial laminate design is only a starting place for laminate architecture and analysis will reveal opportunities for improvement.

4.6 Parametric Model

To aid in revision of the design as the research on other parts of the rocket progress, all COPVs have been modeled parametrically. Additionally, the information architecture has been constructed in such that the update sequence is straight forward. This update sequence is detailed in appendix 6.2.4. The highest level of the design starts with the COPV analysis scripts (6.1.1, 6.1.2) entitled “Pressurant_COPV.m” and “Propellant_COPVs.m”. These scripts perform an analysis of material usage, sizing, and composite failure using classical laminate theory. The option exists to write the outputs of these analysis scripts to the “Master.xlsx” Excel spreadsheet. The Master spreadsheet contains all of the necessary information for the parametric model to update to the design validated using the COPV analysis scripts.

The Master spreadsheet is linked in all of the design tables within the SolidWorks part files. This allows for the user to easily update the CAD model based on the most recent design verified as functional in the Matlab analysis scripts. Once all parts have been updated as per the update sequence in appendix 6.2.4, all configurations will update to meet the new design. This process streamlines iterative design by eliminating the need for re-modeling. However, large alterations to the design will require hand updates of the models sketches and all related updates to configurations within the design tables.

4.7 Analysis and Revision

4.7.1 Loading Validation

When considering loading validation of a composite, a failure criteria must be selected. Failure criteria, based on individual ply failure take three main forms: maximum stress, maximum strain, and interactive models. The earliest and simplest forms of failure analysis are max stress and max strain, which are exactly as they sound. These methods analyze failure directly on the failure strengths and strains of the material. Whichever loading component be it tensile, compressive, or shear (stress or strain) reaches its limit first is the basis for ply failure. The interactive models consider the affect that each loading component has simultaneously and bases ply failure on exceeding a laminate failure mode index value of one for which the terms of the interactive models sum to. The most commonly used interactive models are the Tsai-Hill and Tsai-Wu models.

Image 4.4 shows a direct comparison of the shear failure estimates using each of the four aforementioned failure criteria. Image 4.5 is a comparison of the predicted tensile failure loads. Tsai-Hill has been selected for testing as it offers a conservative value for tensile failure which is the primary loading condition the overwraps will face in this analysis. Additionally, the Tsai-Hill criteria offers a conservative estimate for shear for angles less than $\approx 40^\circ$ and greater than $\approx 50^\circ$.

For interactive models such as Tsai-Hill and Tsai-Wu, ply failure is indicated through use of a laminate failure index. Each term in these interactive models which represent stresses sum to produce this laminate failure index. Ply failure, occurs when the value of the laminate failure index exceeds a value of 1. In this analysis, laminate failure will be declared if any lamina within the laminate fails. All FEA images shown within this analysis show the laminates failure index using this criteria.

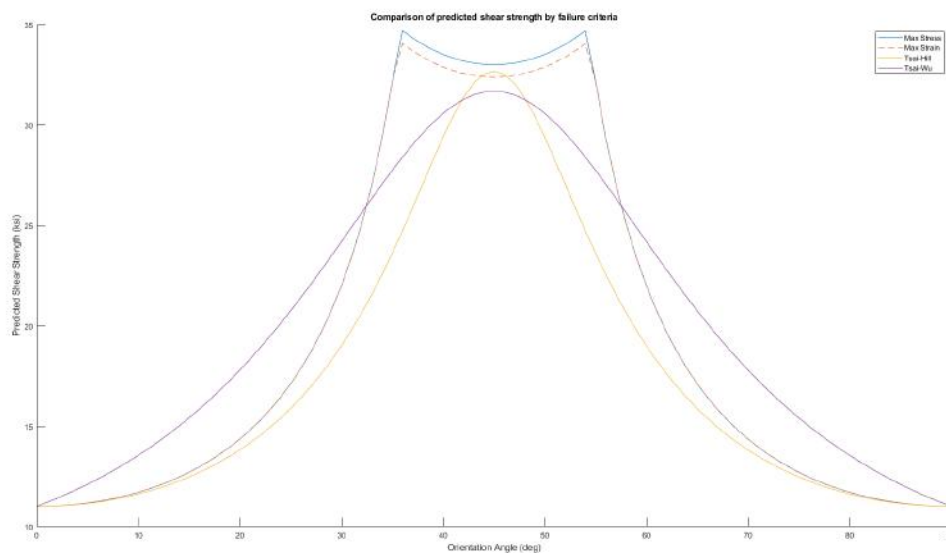


Figure 4.4: Failure criteria shearing failure load comparison for AS4/3051-6 unidirectional composite

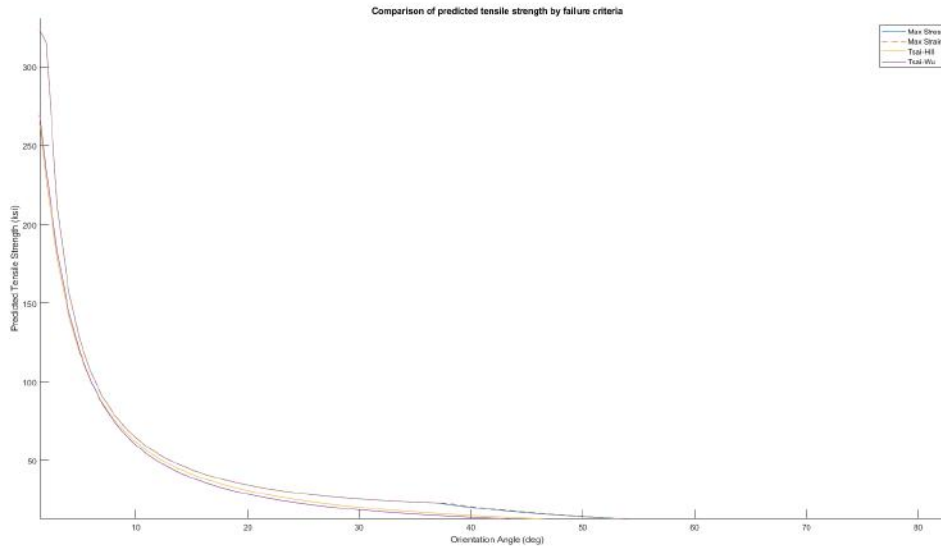


Figure 4.5: Failure criteria tensile failure load comparison for AS4/3051-6 unidirectional composite

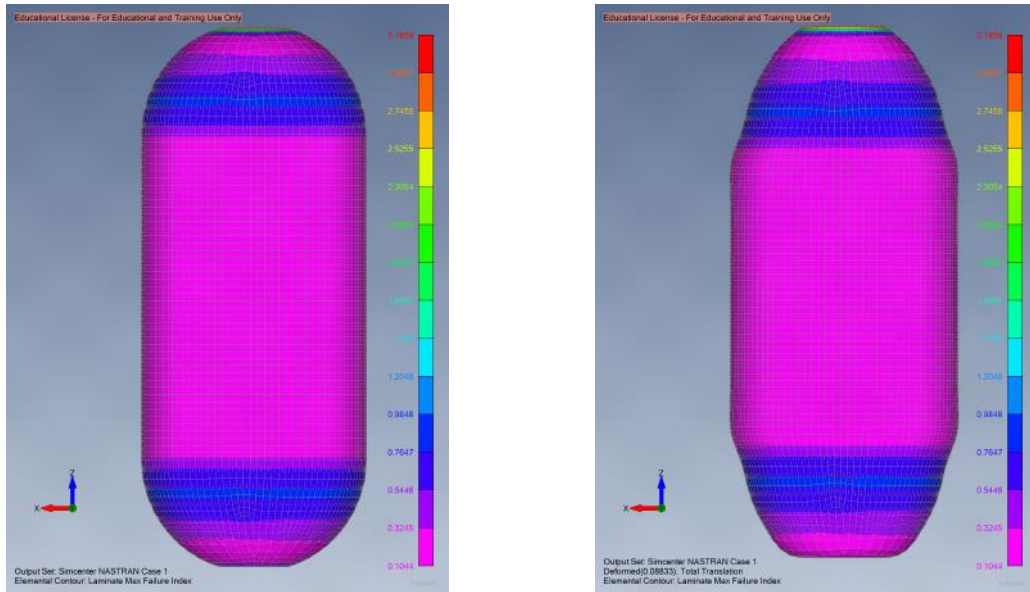
Because this overview of failure criteria has been high level and brief, it is suggested that before the reader performs an analysis of their own, a study on these criteria should be done to gain a full understanding before selection for a given case. Mechanical analysis was performed using FEMAP, a CAE software with robust composite analysis features. Because FEMAP uses the same classical laminate theory as the COPV analysis Matlab scripts, in code appendices 6.1.1 and 6.1.2, the results between the two analysis are very similar.

However, FEMAP offers a visualization of the analysis which the tool cannot provide. Additionally, the output is given in a GUI which gives the user an opportunity to vary the laminate architecture relatively simply. Potentially the most important advantage of a finite element analysis tool over the Matlab analysis scripts is that the FEA software accounts for part geometry. Because the analysis scripts consider only a planar, unit section with planar loading, part complexities such as holes or curvature cannot be accounted for.

The first iteration of analysis was performed on the initial design previously stated. Because FEMAP was able to account for part geometry where the analysis tool could not, the initial laminate architectures failed the analysis. Because both propellant tanks face the same pressures and have the same overwrap architecture, the output from FEMAP was identical between the two with the only difference being a longer midsection for the HTP tank. Because of this, both propellant tanks will be discussed interchangeably, and the images of each apply to the other.

In the first analysis, a uniform internal pressure of MEOP was applied to both the propellant and pressurant overwraps. The results of this analysis can be seen in figures 4.6 and 4.7. As can be seen in these images, the laminate failure mode index, and by virtue stress has an uneven distribution with concentrations at the transition from the cylinder to the hemispherical tank head and around the constrained openings.

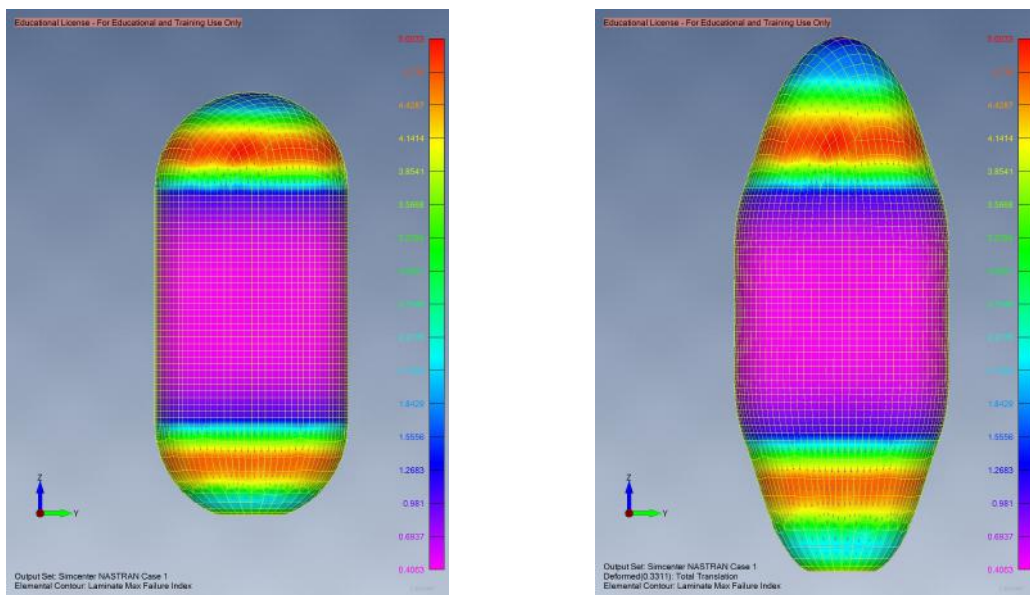
This uneven distribution of stress is purely geometric. If one considers a single lamina as has been explained previously one would expect the optimal fiber orientation to be $\tan^{-1}(\sqrt{2})$. When a laminate is created the average optimal orientation becomes $\tan^{-1}(\sqrt{2})$; However, variance of lamina to angles other than $\tan^{-1}(\sqrt{2})$ but average to $\tan^{-1}(\sqrt{2})$ provides the opportunity for a thinner laminate that meets loading requirements.



(a) undeformed

(b) deformed

Figure 4.6: RP1 overwrap design 1 FEA results 1000 psi



(a) undeformed

(b) deformed

Figure 4.7: N2 overwrap design 1 FEA results 1000 psi

This uneven distribution of stress is more pronounced in the N2 tank shown in figure 4.7 because the testing pressure is higher, and therefore the thickness of the laminate is greater. To combat this uneven distribution of stress and as a result wasted material, the composites angles were varied. To accomplish this, Excel solver was used to predict the number of plies in each direction that would produce the best results.

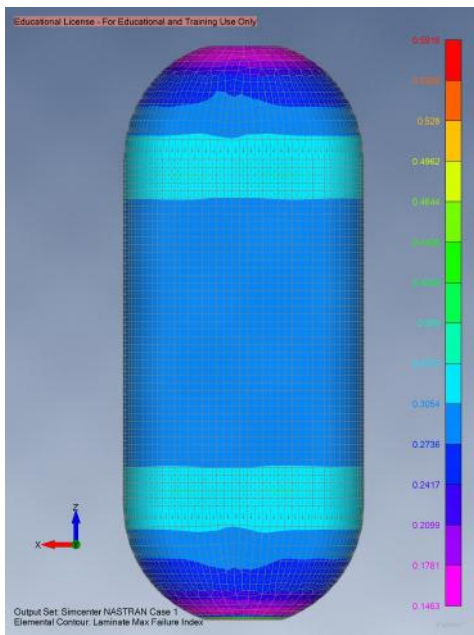
In Excel, orientation angle limits were set at $15^\circ \leq \alpha \leq 75^\circ$ and this condition was applied to two variable angles α_1 and α_2 . Ply count limits for each angle were set to 10, and all values (both ply count and angle) were constrained to integer values. The objective was then set to 55 degrees. The function to optimize was $\alpha = (\alpha_1 \cdot count_1 + \alpha_2 \cdot count_2) / (count_1 + count_2)$. The result was $\alpha_1 = 15^\circ$ at 5 plies and $\alpha_2 = 75^\circ$ at 10 plies. It is not surprising that the count for the fiber primarily reinforcing the hoop direction was double that of the fiber count for the orientation primarily reinforcing the longitudinal direction.

Using this as a basis some experimentation was done to find the best placement of the lamina within the laminate in the approximate proportion output by the Excel solver to find the most even stress distribution with the thinnest symmetric overwrap. It turned out that the stress distribution is most even when the longitudinal reinforcements ($\alpha = 15^\circ$) are furthest from the plane of symmetry meaning that they are the first and last plies laid, and the hoop reinforcement ($\alpha = 75^\circ$) was in the middle of the laminate. This pattern for ply distribution is common for both propellant and pressurant overwraps.

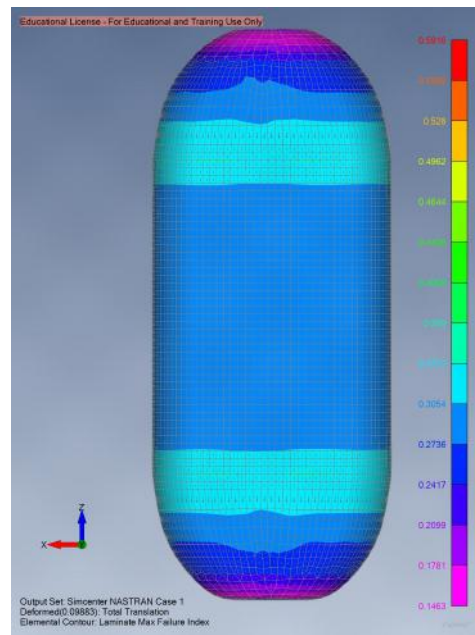
Through experimentation using the aforementioned technique, a laminate structure of $[\pm 15 / \pm 75_3]_s$ for the propellant overwrap and $[\pm 15_{10} / -15 / \pm 75_{12} / 75]_s$ for the pressurant overwrap was developed. This structure eliminates 4 plies from the propellant tanks and 24 plies from the pressurant tank resulting in an approximate weight savings of 25.95lb from the HTP tank, 5.65lb from the RP-1 tank, and 21.10lb from the N2 tank or a combined weight of 52.69lb while producing stronger and more evenly stress distributed overwraps. Results of these FEMAP analyses at MEOP can be seen in images 4.8 and 4.9.

As per the system constrain 2.1.4 the tanks must be rated with a safety factor of 1.426 meaning that the propellant overwraps must be validated to a pressure of 1426 psi and the pressurant overwrap must be validated to a pressure of 8550 psi. The results of these FEMAP analyses are shown in figures 4.10, 4.11, and 4.12 for RP-1, HTP, and N2 overwraps respectively.

At this time LRL has yet to complete the dynamic model to give an estimate of maximum acceleration. Additionally, the design of the airframe sections connecting the COPVs to one another and to other components of the rocket have yet to be designed. Therefore, compression analysis cannot be done to evaluate the validity of the COPVs acting as structural sections. After the dynamic model is completed, and after a rough estimate of the rockets component masses along with a full stack layout has been designed, compressive simulation and related design adaptation can commence. Additionally it will be important to model the COPVs with the liners. The setup for this within FEMAP is more difficult and is currently in progress.

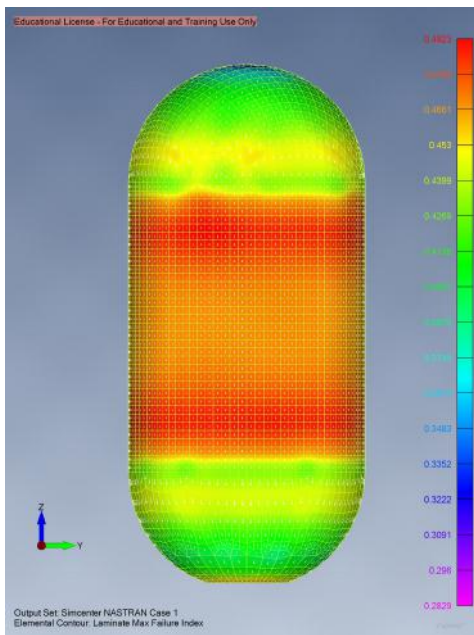


(a) undeformed

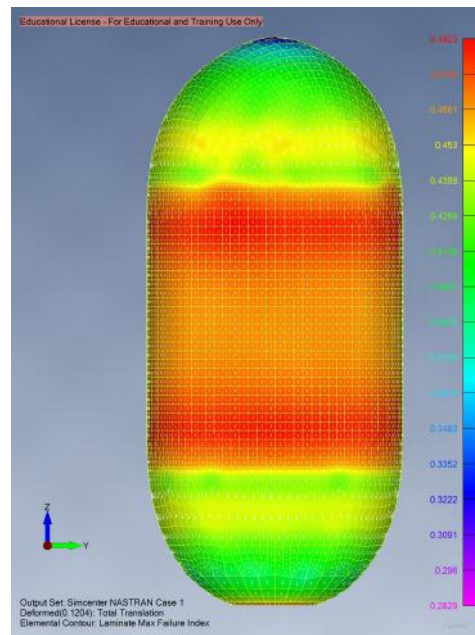


(b) deformed

Figure 4.8: RP1 overwrap design 2 FEA results 1000 psi



(a) undeformed



(b) deformed

Figure 4.9: N2 overwrap design 2 FEA results 6000 psi

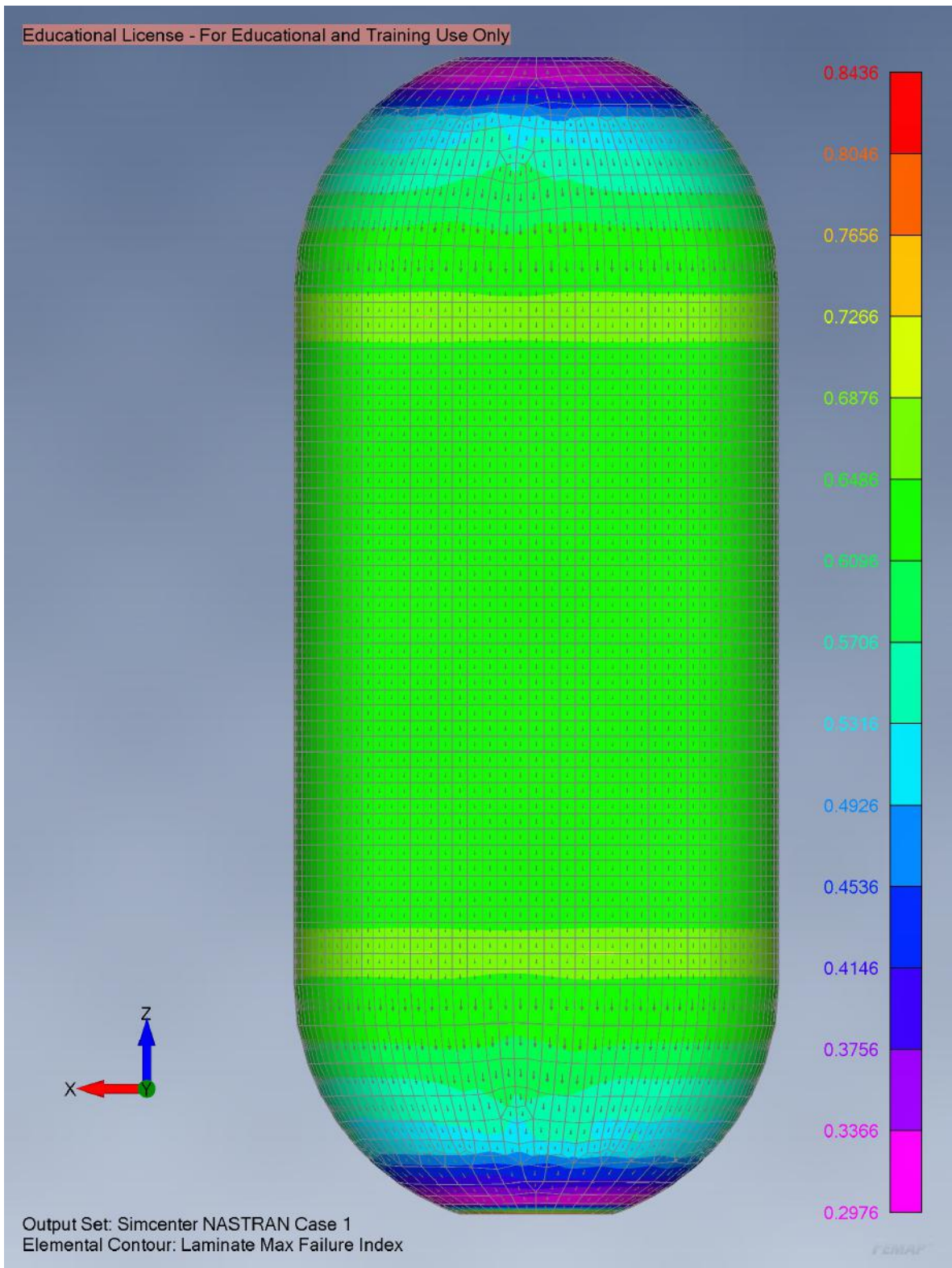


Figure 4.10: Undeformed RP1 overwrap design 2 FEA results at 1426 psi

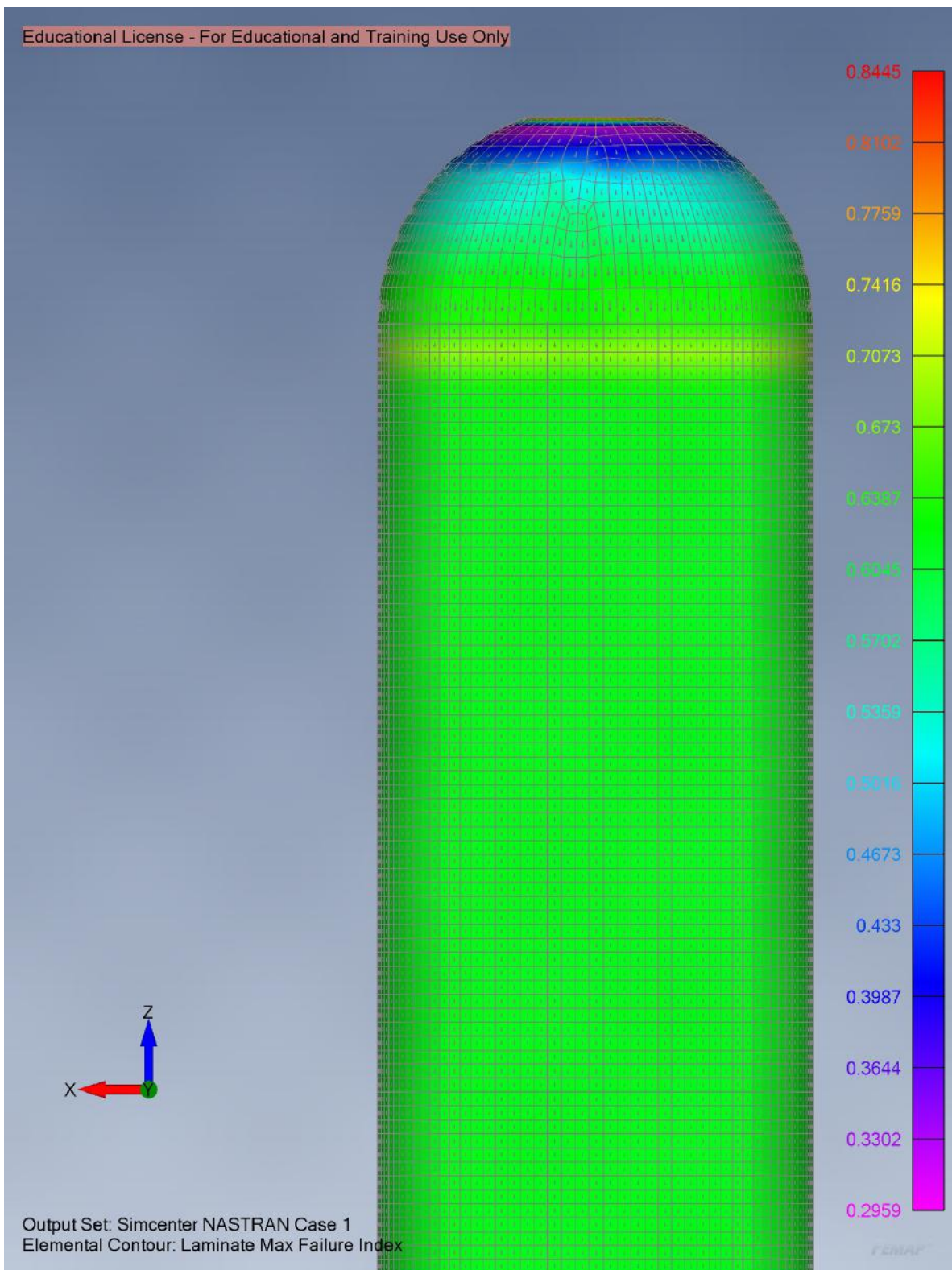


Figure 4.11: Undeformed HTP overwrap design 2 FEA results at 1426 psi

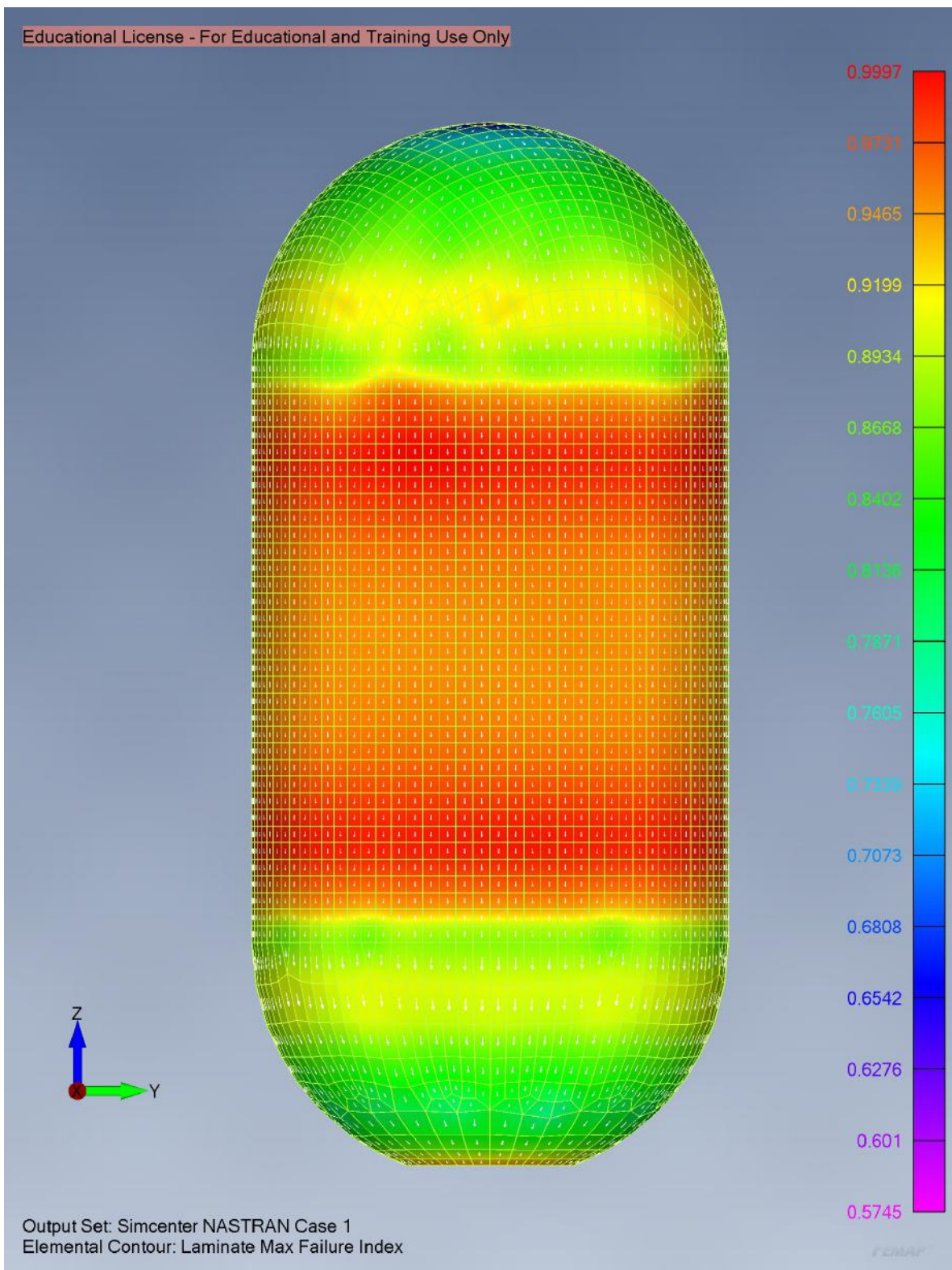


Figure 4.12: Undeformed N2 overwrap design 2 FEA results at 8550 psi

4.7.2 Flow Analysis

Implementing flow analysis through the use of computational fluid dynamics (CFD) allows for a study of fluid motion within the propellant tanks. The most applicable study type for this application is a transient analysis examining the fluid characteristics within a draining vessel. The analysis performed was conducted within SolidWorks Flow Simulation. An attempt was made to perform the analysis within Ansys Fluent, however due to the relatively small feature sizes of the baffling system in comparison to the relatively large size of the HTP tank, meshing exceeded the RAM of available computers. Because Fluent utilizes a more detailed engine than SolidWorks Flow Simulation, it is likely that available computers would not possess sufficient processing power to run the simulation within Fluent in a reasonable time as it took nearly 24 hours in SolidWorks.

Setting up the simulation, water was used in place of HTP and RP-1 as sufficient material information was not available. This should not have appreciable affect in the result of the transient analysis but should be noted. Because N₂ flow into the propellant tanks will be regulated to 1000 psi, a static pressure condition was applied to each of the tanks. The volumetric flow rate of the waters expulsion was limited to the volumetric flow rates for each propellant into the engine. The simulation was run for 105 seconds to evaluate the tanks performance throughout the entirety of a burn cycle.

The immediately apparent fluid concern that arose as a result of the CFD analysis was the intense disruption of the fluids surface with a high fluid level in the tank. Figure 4.13 shows the fluid surface of the HTP approximately four seconds into the burn cycle. It is clear that the nitrogen is flowing into the tank at a high velocity creating a disruption in the fluids surface. This disruption may be a source for slosh. Additionally the high velocity of the nitrogen may infuse the HTP with nitrogen bubbles possibly causing combustion instability near the end of the burn cycle.

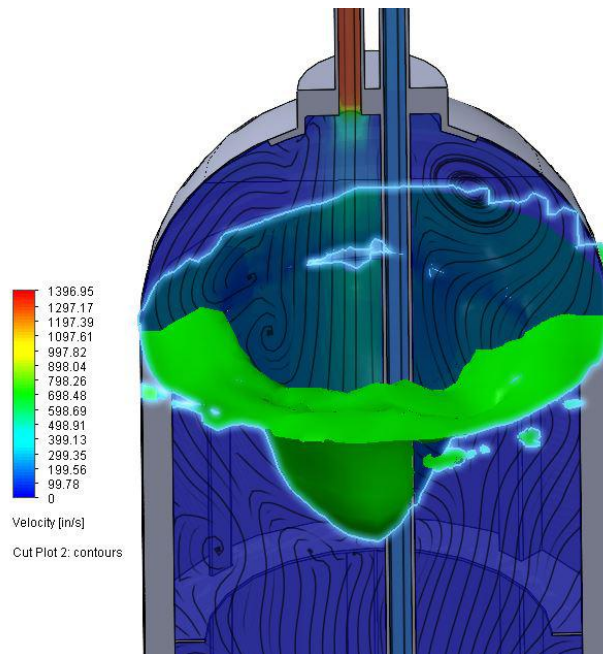


Figure 4.13: Isosurface for high fluid level HTP

The disruption within the HTP tank is caused by the high volumetric flow rate of the HTP (approximately $395.13 \text{ in}^3/\text{sec}$) creating a void within the tank which must be filled. An image depicting the discrepancy in flow velocity between the two propellants is shown in figure 4.15. Nitrogen rushes in to fill this void at a high velocity which in turn creates disruption. To overcome this disruption a diffuser can be used. A diffuser acts to distribute the incoming gas over a greater area rather than in a single stream in turn distributing and dampening the disruption. As the tank level lowers the stream of incoming nitrogen becomes more diffuse. By about 20 seconds into the burn the surface of the HTP becomes stable. This stability is shown in Figure 4.14.

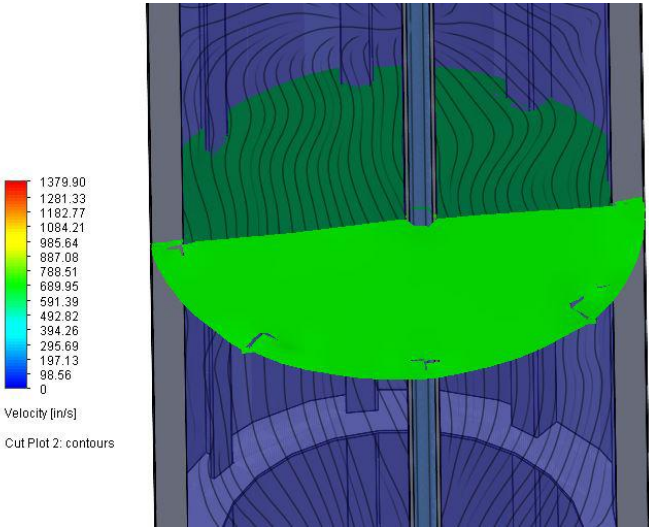


Figure 4.14: Stabilized isosurface for HTP

Because the RP-1 tank has relatively low volumetric flow rate of approximately $56.45 \text{ in}^3/\text{sec}$, or $1/7^{\text{th}}$ of the HTP flow rate, the surface remains relatively stable throughout the entirety of the burn cycle. Because less volume needs to be replaced the velocity of the incoming N_2 is much lower. However it is recommended that both the HTP and RP-1 tanks implement check valves or similar one way flow systems to avoid backflow into the pressurant lines where the propellants could potentially mix. The design of both diffusers and one way flow mechanisms will be the focus of future studies.

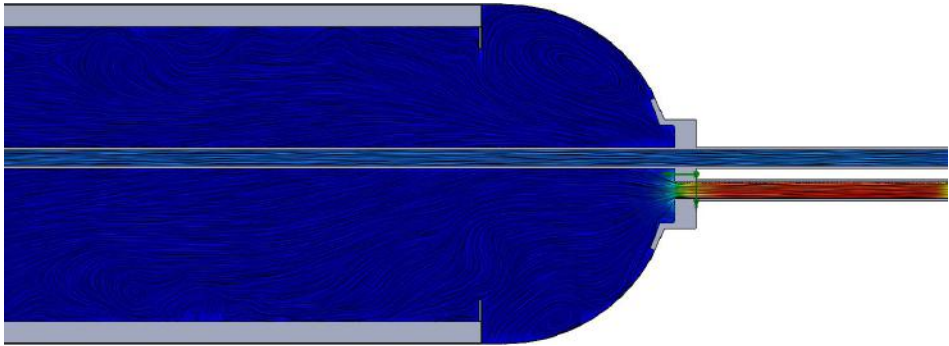


Figure 4.15: Propellant exit velocity at engine inlet



Figure 4.16: Fluid velocity within the RP1 tank with fluid level near top baffle

In both propellant tanks the liquid forms vortices and recirculates beneath the circumferential baffles as shown in figure 4.16. Because neither heat transfer nor mid tank flow state are of great concern the formation of these vortices should not pose a problem; However they are noteworthy in the event that requirements change in the future. This simulation implies that the tank design provides no undue restriction of flow fulfilling the functional requirement for mass flow rate 2.1.3. Additionally this partially satisfies the constraint of functionality at MEOP 2.1.1.

4.8 Conclusion

4.8.1 Final Designs

RP1 Tank



Figure 4.17: Final RP1 tank design cross section

| Specification | Value | Unit |
|--------------------------|-------------------------|------|
| Weight | 33.27 | lb |
| Total Height | 21.991 | in |
| Overwrap fiber | Toray T1000G | - |
| Overwrap matrix | Epoxy 3501-6 | - |
| Laminate structure | $[\pm 15 / \pm 75_3]_s$ | - |
| Overwrap outer radius | 8.000 | in |
| Lamina count | 16 | ct |
| Lamina thickness | 0.010 | in |
| Laminate thickness | 0.160 | in |
| Liner material | 6061 aluminum | - |
| Liner outer radius | 7.840 | in |
| Liner inner radius | 7.800 | in |
| Liner thickness | 0.040 | in |
| Cylinder length | 20.133 | in |
| Baffle material | 6061 aluminum | - |
| Baffle count | 2 | ct |
| Baffle thickness | 0.100 | in |
| Baffle outer radius | 7.800 | in |
| Baffle width | 2.000 | in |
| Baffle spacing | 20.133 | in |
| Vertical baffle material | 6061 aluminum | - |
| Vertical baffle count | 8 | ct |
| Vertical baffle shape | Angle | - |
| Vertical angle thickness | 0.125 | in |
| Vertical angle width | 1.000 | in |
| Vertical angle length | 20.133 | in |

Drawings for this assembly can be found in appendix 6.2.1.

HTP Tank



| Specification | Value | Unit |
|--------------------------|-------------------------|------|
| Weight | 188.82 | lb |
| Total Height | 220.895 | in |
| Overwrap fiber | Toray T1000G | - |
| Overwrap matrix | Epoxy 3501-6 | - |
| Laminate structure | $[\pm 15 / \pm 75_3]_s$ | - |
| Overwrap outer radius | 8.000 | in |
| Lamina count | 16 | ct |
| Lamina thickness | 0.010 | in |
| Laminate thickness | 0.160 | in |
| Liner material | 6061 aluminum | - |
| Liner outer radius | 7.840 | in |
| Liner inner radius | 7.800 | in |
| Liner thickness | 0.040 | in |
| Cylinder length | 201.118 | in |
| Baffle material | 6061 aluminum | - |
| Baffle count | 10 | ct |
| Baffle thickness | 0.100 | in |
| Baffle outer radius | 7.800 | in |
| Baffle width | 2.000 | in |
| Baffle spacing | 201.118 | in |
| Vertical baffle material | 6061 aluminum | - |
| Vertical baffle count | 8 | ct |
| Vertical baffle shape | Angle | - |
| Vertical angle thickness | 0.125 | in |
| Vertical angle width | 1.000 | in |
| Vertical angle length | 201.118 | in |

Drawings for this assembly can be found in appendix 6.2.1.

Figure 4.18: Final RP1 tank design

N2 Tank



Figure 4.19: Final RP1 tank design

| Specification | Value | Unit |
|-----------------------|---|------|
| Weight | 64.59 | lb |
| Total Height | 31.987 | in |
| Overwrap fiber | Toray T1000G | - |
| Overwrap matrix | Epoxy 3501-6 | - |
| Laminate structure | $[\pm 15_{10} / - 15 / \pm 75_{12} / 75]_s$ | - |
| Overwrap outer radius | 8.000 | in |
| Lamina count | 72 | ct |
| Lamina thickness | 0.010 | in |
| Laminate thickness | 0.720 | in |
| Liner material | 6061 aluminum | - |
| Liner outer radius | 7.280 | in |
| Liner inner radius | 7.240 | in |
| Liner thickness | 0.040 | in |
| Cylinder length | 13.693 | in |

Drawings for this assembly can be found in appendix 6.2.1.

4.8.2 Future work

Because the design created within this project is preliminary, there is substantial work left to be done before the design can be manufactured. More in-depth analysis must be performed on the system. A full pressure analysis considering the interaction between the liner and overwrap is the next step as all information is present to complete this. This analysis is underway, however current limitations are access to computing power and time. As COVID-19 restrictions ease, access to more powerful computers will become available.

Another analysis that must be performed in the future is combined loading analysis. Once the dynamic model for the rocket has been created, a time dependent loading model must be developed to determine maximum loading conditions throughout the flight. These include inertial compressive loads and bending moments which may be imposed due to GNC systems, gust, or normal aerodynamic loads.

Vibratory data must be collected from the engine during hot static fires to determine engine vibration frequency. Ideally a scale model of the rocket will be wind tunnel tested to determine if there is resonant drag instability. With knowledge of these vibratory modes, the system can be designed to avoid matching resonant frequencies. This will include possible alteration to baffling to avoid slosh.

Airframe integration is another area of work that must be focused on. Several concepts have been developed by LRL structures team members, but before the COPVs can be produced, a fully developed plan for integration must be laid out. This too will affect loading conditions as it will define the constraints through which loads are transmitted to the COPVs.

Yet another line of inquiry that must be pursued is plumbing integration. The propulsion team must work with the structures team to determine how this will happen. These decisions will change the polar boss design. Stainless steel plumbing will require a material transition from the aluminum boss. Additionally, expansion and contraction of the system must be considered as lines run through both of the propellant tanks meaning all joints cannot be welded. This will likely require the use of a mix of welds or threads and expansion joints at the orifices in the polar bosses. Material mismatch between the aluminum bosses and stainless plumbing will be another challenge to overcome.

Finally as LRL is in transition from SolidWorks to Siemens NX, the parametric model must be recreated within NX. Though not particularly difficult, this task requires considerable thought to ensure that updates do not break the model. Because almost none of LRL's membership have experience with NX, this exercise may be useful as a training tool for proper modeling and assembly management techniques.

4.8.3 Closing summary

This report has been an extensive study to create a preliminary design of COPVs for the Liquid Rocketry Lab launch vehicle. This report presented specifications for which the COPVs must adhere to maintain functionality. This definition of specifications derived from the problem space helped define possibilities within a solution space.

The report continued to trade studies to narrow the solution space through careful examination of options with demonstrated utility in similar applications. In these trade studies were an exhaustive look at some of the tough questions which needed to be answered to come up with a feasible design. Conclusion of these trade studies marked entrance into the design phase and provided a foundation to design from.

The design stage commenced with conceptualization of the design by evaluating realities of the application. The conceptualized design was then parametrically modeled in SolidWorks. This design was analyzed for its viability, and corrections were made to the design to update it based on discoveries made in analysis. This analysis and update cycle will continue as more information on the application is realized. Suggestions for future work to conduct before manufacturing have been suggested to aid in project continuity.

References

- [1] National Aeronautics and Space Administration. Pressure Vessels Improve Transportation of Liquid Fuels. [Online]. Available: https://spinoff.nasa.gov/Spinoff2020/t_1.html#:~:text=NASA%20pioneered%20COPVs%20in%20the,to%20make%20a%20better%20COPV.
- [2] Pat B. McLaughlan, P.E., Scott C. Forth, PhD, and Lorie Grimes-Ledesma, Ph.D, “Composite Overwrapped Pressure Vessels, A Primer,” p. 30. [Online]. Available: <https://core.ac.uk/download/pdf/154739071.pdf>
- [3] Michael Legault. Pressure vessel tank types. [Online]. Available: <https://www.compositesworld.com/articles/pressure-vessel-tank-types>
- [4] M. Legault, “The first commercial Type V composite pressure vessel.” [Online]. Available: <https://www.compositesworld.com/articles/next-generation-pressure-vessels>
- [5] Tom Benson. Ideal Rocket Equation. [Online]. Available: <https://www.grc.nasa.gov/WWW/K-12/rocket/rktpow.html>
- [6] Lorie Grimes-Ledesma, Pappu L*N. Murthy, John P. Gvekenvesi, and S.L. Phoenix, “Reliability Considerations for Composite Overwrapped Pressure Vessels on Spacecraft,” p. 2.
- [7] Lorie Grimes-Ledesma, S. Leigh Phoenix, Harold Beeson, Tommy Yoder, and Nathaniel Greene, “Testing of Carbon Fiber Composite Overwrapped Pressure Vessel Stress-Rupture Lifetime.” [Online]. Available: <http://citeseerx.ist.psu.edu/viewdoc/download?doi=10.1.1.486.6361&rep=rep1&type=pdf>
- [8] A. Engelbrecht-Wiggans and S. L. Phoenix, “Comparison of probabilistic models for stress rupture failure in continuous unidirectional fiber composite structures,” vol. 53, no. 10, pp. 7431–7452. [Online]. Available: <http://link.springer.com/10.1007/s10853-018-2101-2>
- [9] Dr. Philip Bradford, “NCSU TE-565 Textile Composites Lecture: Statistical approach to fiber failure modeling.”
- [10] J. B. Chang, “Implementation Guidelines for ANSI/AIAA S-081: Space Systems Composite Overwrapped Pressure Vessels:.” [Online]. Available: <http://www.dtic.mil/docs/citations/ADA413531>

- [11] Don Pettit, “The Tyranny of the Rocket Equation.” [Online]. Available: https://www.nasa.gov/mission_pages/station/expeditions/expedition30/tryanny.html#
- [12] Julian Jeffrey-Wilensky, “LRL Recovery System Preliminary Calculations,” Liquid Rocketry Lab, Inc.
- [13] Brian Alonso, “Atmos_properties,” Liquid Rocketry Lab, Inc.
- [14] J. L. Hall, “A Review of Ballute Technology for Planetary Aerocapture,” p. 10.
- [15] National Aeronautics and Space Administration, “Orion Parachute System.” [Online]. Available: https://www.nasa.gov/sites/default/files/atoms/files/orion_parachutes.pdf
- [16] “What is stress corrosion? Stress corrosion cracking/Stress cracking: Electrochemical Corrosion.” [Online]. Available: https://www.youtube.com/watch?v=pnsExPkHbI0&ab_channel=RevathiPurushothaman
- [17] OzoneLab, “Material Compatibility with Hydrogen Peroxide (H₂O₂).” [Online]. Available: <http://www.ozoneservices.com/articles/004.htm>
- [18] Is Med Specialties, “Hydrogen Peroxide Material Compatability Chart.” [Online]. Available: ismedspec.com
- [19] Parabilis Space Technologies, “Metallic H₂O₂ Material Compatibility Overview.”
- [20] Kaufman, J. Gilbert, *Aluminum Alloy Database*. Knovel, 2004; 2009; 2015. [Online]. Available: <https://app.knovel.com/hotlink/toc/id:kpAAD00001/aluminum-alloy-database/aluminum-alloy-database>
- [21] H. Barthelemy, M. Weber, and F. Barbier, “Hydrogen storage: Recent improvements and industrial perspectives,” vol. 42, no. 11, pp. 7254–7262. [Online]. Available: <https://linkinghub.elsevier.com/retrieve/pii/S0360319916305559>
- [22] G. Sutton, *History of Liquid Propellant Rocket Engines*, ser. Library of Flight Series. American Institute of Aeronautics and Astronautics. [Online]. Available: <https://books.google.com/books?id=s1C9Oo2I4VYC>
- [23] Robert A. Braeunig, “Rocket Propellants,” 1996, 2005, 2006, 2008. [Online]. Available: <http://www.braeunig.us/space/propel.htm>
- [24] Davis Instruments, “Kerosene Chemical Compatibility Results.” [Online]. Available: <http://www.davis.com/Chemical-Resistance>
- [25] Malachi Lloyd Green, “Kerosene: The Advantages & Disadvantages.” [Online]. Available: <https://itstillruns.com/kerosene-advantages-disadvantages-8319651.html>
- [26] Alan Fletcher, Larry Perkins, and Steven Anderson, “Fuel and Fuel System Materials Compatibility Test Program for a JP-8+100 Fuel Additive.” [Online]. Available: <https://apps.dtic.mil/dtic/tr/fulltext/u2/a417475.pdf>

- [27] Rick Newlands, Martin Heywood, and Andy Lee, “Rocket vehicle loads and airframe design.”
- [28] E. W. Weisstein, “Circle Packing.” [Online]. Available: <https://mathworld.wolfram.com/CirclePacking.html>
- [29] Space Exploration Technologies Corp., “Falcon User’s Guide.” [Online]. Available: https://www.spacex.com/media/Falcon_Users_Guide_082020.pdf
- [30] Ed Kyle, “Vulcan Data Sheet.” [Online]. Available: <https://www.spacelaunchreport.com/vulcan.html>
- [31] Blue Origin, “New Glenn Payload User’s Guide.”
- [32] S. S. Pietrobon, “Analysis of Propellant Tank Masses,” p. 9.
- [33] “Saturn Illustrated Chronology - Part 8 January 1967 through December 1967.” [Online]. Available: <https://history.nasa.gov/MHR-5/part-8.htm>
- [34] Philip Sloss, “NASA, Boeing rewriting the book on building the SLS Core Stage.” [Online]. Available: <https://www.nasaspaceflight.com/2018/02/nasa-boeing-rewriting-book-building-sls-core-stage/>
- [35] Michael Neufeld, “Robert Goddard and the First Liquid-Propellant Rocket.”
- [36] Explore the World of Piping, “Introduction to Spherical and Cylindrical Pressure Vessels.” [Online]. Available: <http://www.wermac.org/equipment/pressurevessel.html>
- [37] Cameron Moore and Michael Tomlinson. Comparison Between Head Types: Hemi, SE, F&D and Flat. [Online]. Available: <https://www.pveng.com/home/asme-code-design/comparison-between-head-types-hemi-se-fd-and-flat/>
- [38] S. Lawate and B. B. Deshmukh, “Analysis of Heads of Pressure Vessel,” vol. 4, no. 2, p. 7.
- [39] Baker Tankhead Inc., “2:1 Semi-Elliptical Tank Heads.” [Online]. Available: <https://www.bakertankhead.com/products/tank-heads/>
- [40] —, “ASME Flanged & Dished Tank Heads.” [Online]. Available: <https://www.bakertankhead.com/products/tank-heads/>
- [41] M. J. Thattil and C. Pany, “Design and Analysis of Pressure Vessel with different end domes,” vol. 06, no. 08, p. 9.
- [42] L. Brundrett and Michael Tomlinson, “Comparison of Four Head Types,” p. 14.
- [43] Keith Kachelhofer, “Decoding pressure vessel design: Bridging the gap between users’ and manufacturers’ responsibilities for the ASME pressure vessel code,” vol. 117, no. 6, pp. 28–35.

- [44] Aerospace Specification Metals Inc., “Aluminum 6061-T6; 6061-T651.” [Online]. Available: <http://asm.matweb.com/search/SpecificMaterial.asp?bassnum=MA6061T6>
- [45] —, “AISI Type 304 Stainless Steel.” [Online]. Available: <http://asm.matweb.com/search/SpecificMaterial.asp?bassnum=MQ304A>
- [46] Polymer Database, “Rigid Polyvinyl Chloride (PVC).” [Online]. Available: <https://polymerdatabase.com/Commercial%20Polymers/PVC.html>
- [47] I. M. Daniel and O. Ishai, *Engineering Mechanics of Composite Materials*, 2nd ed. Oxford University Press.
- [48] A. Poenninger and B. Defoort, “Determination of the coefficient of moisture expansion (CME),” pp. p. 567 – 572.
- [49] Toray Composite Materials America, Inc., “Toray T1000G fiber white sheet.”
- [50] J. R. Roberts and P.-Y. Chen, “Slosh Design Handbook I,” p. 328.
- [51] H. N. Abramson and L. R. Garza, “Liquid frequencies and damping in compartmented cylindrical tanks,” vol. 2, no. 3, pp. 453–455. [Online]. Available: <https://arc.aiaa.org/doi/10.2514/3.28203>
- [52] Abramson, H. N. and Garza, L. R., “Measurements of Liquid Damping Provided by Ring Baffles in Cylindrical Tanks.”
- [53] M. A. Silveira, D. G. Stephens, and H. W. Leonard, “An Experimental Investigation of the Damping of Liquid Oscillations in Cylindrical Tanks with Various Baffles,” p. 33.
- [54] Werner R. Eulitz and Herman Beduefrftig, “Experimental Investigation of the Responses of a Liquid in an Oscilating Container,” pp. 43–104. [Online]. Available: <https://apps.dtic.mil/dtic/tr/fulltext/u2/a417178.pdf>
- [55] J.P. O’Neill, “Semiannual Report on Experimental Investigation of Sloshing,” p. 32.
- [56] J.W. Miles, “Ring Damping of Free Surface Oscillations in a Circular Tank,” vol. 25, no. 2, pp. 274–276.
- [57] Suong V. Hoa, “Chapter 5: Filament Winding and Fiber Placement,” in *Principles of the Manufacturing of Composite Materials*. DEStech Publications, Inc.
- [58] S. Sulaiman, S. Borazjani, and S. H. Tang, “Finite element analysis of filament-wound composite pressure vessel under internal pressure,” vol. 50, p. 012061. [Online]. Available: <https://iopscience.iop.org/article/10.1088/1757-899X/50/1/012061>
- [59] H. Y. Hong, “Burst Strength Analysis of Composite Pressure Vessel using Finite Element Method,” p. 57.

Appendices

6.1 Code

6.1.1 Propellant COPV Analysis Script - MATLAB

```
1 %% Liquid Rocketry Lab           John Slugg           10/23/2020
2
3 %%                               Propellant COPVs
4 clear;
5 clc;
6
7 % Write output to Excel?      1 = Yes, 0 = No
8
9 Write_to_Excel = 0;
10
11                               %% ROCKET RADIUS INPUT
12
13                               Aero_Optimum_Radius = 8; %inches
14
15 fprintf('Rocket external radius           = %0.4f in\n',...
16         Aero_Optimum_Radius)
17 fprintf('%s\n','')
18 %% PROPELLANT COPV CALCULATIONS
19 fprintf('%s\n','----- Propellant COPVs -----')
20 %%%%%%%%%%%%%%%%%%%%%%%%%%%%%%%%%%%%%%%%%%%%%%%%%%%%%%%%%%%%%%%%%%%%%%%%%
21
22 %% Initial Conditions
23
24 HTP_Vol_L = 647.5; %.....Liters
25 HTP_Volume = HTP_Vol_L* 61.0237; %.....in^3
26 HTP_Density = 0.02926311; %.....lb/in^3
27 HTP_Mass = HTP_Density*HTP_Volume; %.....lbm
28 HTP_Kg = HTP_Mass*0.453592; %.....Kg
29
30 RP1_Vol_L = 92.5; %.....Liters
31 RP1_Volume = RP1_Vol_L* 61.0237; %.....in^3
32 RP1_Density = 0.0520233; %.....lb/in^3
33 RP1_Mass = RP1_Density*RP1_Volume; %.....lbm
34 RP1_Kg = RP1_Mass*0.453592; %.....Kg
35
36 Total_Propellant_Mass = HTP_Mass + RP1_Mass; %.....lbm
37
38 Propellant_Mix_Ratio_Vol = (HTP_Vol_L/RP1_Vol_L);
39 fprintf('Propellant mix ratio by volume (HTP:RP-1)           = %0.2f:\n',...
40         Propellant_Mix_Ratio_Vol)
41
42
```

```

43 %% Laminate Properties
44
45 % NOTE: ORIENTATION AUTOMATICALLY PRODUCES A SYMMETRIC MATRIX. TO AVOID
46 % THIS COMMENT OUT THE LINES THAT ARE FOLLOWED BY THE COMMENT "symmetry"
47
48 Orientation = [15 -15 75 -75 75 -75 75 -75]; %.....degrees
49
50 %Orientation = [15 -15 75 -75 75 -75 75 -75]; %.....degrees
51
52 Orientation_flip = fliplr(Orientation); %symmetry
53 Orientation = [Orientation Orientation_flip]; %symmetry
54
55 Lamina_Thickness = cell(1,length(Orientation));
56 for k = 1:length(Orientation)
57
58         Lamina_Thickness{k} = 0.01; %.....in
59
60 end
61
62 Laminate_Thickness = sum(cat(3,Lamina_Thickness{:}),3);
63
64 Number_of_plyies = numel(Orientation);
65 Fiber_Volume_Fraction = 0.61;
66 Matrix_Volume_Fraction = 1 - Fiber_Volume_Fraction;
67
68 %% Tank Properties
69 MEOP = 1000; %Psi
70 Liner_thickness = 0.040; %in
71 Radius = Aero_Optimum_Radius-Laminate_Thickness; %.....in
72 Inner_Radius = Radius - Liner_thickness; %.....in
73 Midsection_Height_RP1 = (RP1_Volume - ((4/3)*pi()*Inner_Radius^3)/2)/...
74         (pi()*Inner_Radius^2); %.....in
75 Midsection_Height_HTP = (HTP_Volume - ((4/3)*pi()*Inner_Radius^3)/2)/...
76         (pi()*Inner_Radius^2); %.....in
77
78 Liner_Material = 1;
79
80 %Liner material options
81 % 1 = Aluminum
82 % 2 = Stainless
83 % 3 = PVC
84
85 %Common Bulkhead Tank Dimensions
86 %Hemispherical tank head assumed
87 Height_HTP_CB = Aero_Optimum_Radius + Midsection_Height_HTP; %.....in
88 Height_RP1_CB = Aero_Optimum_Radius + Midsection_Height_RP1; %.....in
89 Total_Tank_Height_CB = Height_RP1_CB + Height_HTP_CB; %in
90 Midsection_Height_CB = Midsection_Height_HTP + Midsection_Height_RP1; %in
91
92 %Individual Tank Dimensions
93 %Hemispherical tank head assumed
94 Height_HTP_IT = 2*Aero_Optimum_Radius + Midsection_Height_HTP; %....in
95 Height_RP1_IT = 2*Aero_Optimum_Radius + Midsection_Height_RP1; %....in
96 Combine_Tank_Height_IT = Height_RP1_IT + Height_HTP_IT; %.....in
97 Midsection_Height_IT = Midsection_Height_HTP + Midsection_Height_RP1; %in
98
99
100 %% Baffle System volume and mass contribution
101
102 Vertical_Angle_Count = 8;

```

```

103 Vertical_Angle_Width = 1; %in
104 Vertical_Angle_Thickness = 0.125; %in
105 Verticle_Angle_Area = 2*(Vertical_Angle_Width*Vertical_Angle_Thickness)...
106     - Vertical_Angle_Thickness^2; %in
107
108 Baffle_Width = 2; %in
109 Baffle_Thickness = .125; %in
110 Baffle_Spacing = 24; %in
111 Baffle_Volume = pi()*(Inner_Radius^2 - (Inner_Radius-Baffle_Width)^2);%in^3
112
113
114 Volume_difference_HTP = 1;
115 Volume_difference_RP1 = 1;
116 while Volume_difference_RP1 < 99 | Volume_difference_RP1 > 101
117
118 Vertical_Angle_Length_RP1 = Midsection_Height_RP1; %in
119 Vertical_Angle_Volume_RP1 = Verticle_Angle_Area*Vertical_Angle_Length_RP1;%in^3
120
121 Baffle_Count_RP1 = floor(Midsection_Height_RP1/Baffle_Spacing)+1;%in^3
122 Baffle_Volume_RP1 = Baffle_Volume*Baffle_Count_RP1; %in^3
123
124 Baffle_System_Volume_RP1 = Baffle_Volume_RP1+Vertical_Angle_Volume_RP1;%in^3
125
126 Volume_difference_RP1 = ((4/3)*pi()*Inner_Radius^3)+...
127     Midsection_Height_RP1*pi()*Inner_Radius^2-...
128     (RP1_Volume+Baffle_System_Volume_RP1);
129
130 if Volume_difference_RP1 < 99
131     Midsection_Height_RP1 = Midsection_Height_RP1 + 0.01;
132 elseif Volume_difference_RP1 > 101
133     Midsection_Height_RP1 = Midsection_Height_RP1 - 0.01;
134 end
135 end
136
137 while Volume_difference_HTP < 99 | Volume_difference_HTP > 101
138
139 Vertical_Angle_Length_HTP = Midsection_Height_HTP; %in
140 Vertical_Angle_Volume_HTP = Verticle_Angle_Area*Vertical_Angle_Length_HTP;%in^3
141
142 Baffle_Count_HTP = floor(Midsection_Height_HTP/Baffle_Spacing)+1;%in^3
143 Baffle_Volume_HTP = Baffle_Volume*Baffle_Count_HTP; %in^3
144
145 Baffle_System_Volume_HTP = Baffle_Volume_HTP+Vertical_Angle_Volume_HTP;%in^3
146
147 Volume_difference_HTP = ((4/3)*pi()*Inner_Radius^3)+...
148     Midsection_Height_HTP*pi()*Inner_Radius^2-...
149     (HTP_Volume+Baffle_System_Volume_HTP);
150
151 if Volume_difference_HTP < 99
152     Midsection_Height_HTP = Midsection_Height_HTP + 0.01;
153 elseif Volume_difference_HTP > 101
154     Midsection_Height_HTP = Midsection_Height_HTP - 0.01;
155 end
156 end
157
158 %% Probability of Failure Analysis
159 % Variable Initiation
160 Material = 1;
161 %     1 = Carbon Fiber / Epoxy
162 %     2 = Kevlar Fiber / Epoxy

```



```

163 %      3 = Glass Fiber / Epoxy
164
165 Expected_Burst_Strength = MEOP*1.075; %.....Psi
166 Percent_ULT = (MEOP/Expected_Burst_Strength)*100;
167 Loading_Time = 1; %.....Hours
168
169 if Material == 1
170     fprintf('Material:  Carbon Fiber / Epoxy\n')
171     Alpha = 0.20;
172     Beta = (1.4*(10^51))*(10^(-0.515*Percent_ULT));
173 else if Material == 2
174     fprintf('Material:  Kevlar Fiber / Epoxy\n')
175     Alpha = 0.93;
176     Beta = (2.0*(10^18))*(10^(-0.198*Percent_ULT));
177 else if Material == 3
178     fprintf('Material:  Glass Fiber / Epoxy\n')
179     Alpha = 1.00;
180     Beta = (1.4*(10^13))*(10^(-0.158*Percent_ULT));
181 else
182     fprintf('Error: Please Select Material Option\n')
183 end
184 end
185 end
186 fprintf('Maximum Expected Operating Pressure           = %0.2f Psi\n',...
187                                     MEOP)
188 % fprintf('Expected Burst Pressure                       = %0.2f Psi\n',...
189 %         Expected_Burst_Strength)
190 fprintf('Percent loading of ultimate burst strength     = %0.3f \n',...
191         Percent_ULT)
192
193 Probability_of_Survival = exp(-((Loading_Time/Beta))^Alpha);
194
195 while Probability_of_Survival<0.999
196 Percent_ULT = (MEOP/Expected_Burst_Strength)*100;
197 if Material == 1
198     Alpha = 0.20;
199     Beta = (1.4*(10^51))*(10^(-0.515*Percent_ULT));
200 else if Material == 2
201     Alpha = 0.93;
202     Beta = (2.0*(10^18))*(10^(-0.198*Percent_ULT));
203 else if Material == 3
204     Alpha = 1.00;
205     Beta = (1.4*(10^13))*(10^(-0.158*Percent_ULT));
206 else
207     fprintf('Error: Please Select Material Option\n')
208 end
209 end
210 end
211 Probability_of_Survival = exp(-((Loading_Time/Beta))^Alpha);
212 Expected_Burst_Strength = Expected_Burst_Strength+1; %.....Psi
213 end
214 fprintf('Required Burst Strength Survive Prob. of 0.999 = %0.2f Psi\n',...
215         Expected_Burst_Strength)
216 Pressure = Expected_Burst_Strength;
217 %% Material Properties
218 % Reference: Daniel, I. M., and Ishai, O., 2006, Engineering Mechanics
219 %           of Composite Materials, Oxford University Press, New York.
220 %           Table A.2 & Table A.3
221
222 %% Reinforcement: AS4 Carbon Fiber

```

```

223 %   Fiber_Density = 0.0647; %.....lb/in^3
224 %   Fiber_Longitudinal_Modulus = 3.408*(10^7); %.....Psi
225 %   Fiber_Transverse_Modulus = 2.176*(10^6); %.....Psi
226 %   Fiber_Axial_Shear_Modulus = 3.916*(10^6); %.....Psi
227 %   Fiber_Transverse_Shear_Modulus = 1.015*(10^6); %.....Psi
228 %   Fiber_Poissons_Ratio = 0.2;
229 %   Fiber_Longitudinal_Tensile_Strength = 536640; %.....Psi;
230 %   Fiber_Longitudinal_CTE = -0.3; %((10^-6)/F)
231 %   Fiber_Transverse_CTE = 8.3; %((10^-6)/F)
232
233 %% Reinforcement: Toray T1000G Carbon Fiber
234 Fiber_Density = 0.0650291; %.....lb/in^3
235 Fiber_Longitudinal_Modulus = 43*(10^6); %.....Psi
236 Fiber_Transverse_Modulus = 2.176*(10^6); %.....Psi
237 Fiber_Axial_Shear_Modulus = 3.916*(10^6); %.....Psi
238 Fiber_Transverse_Shear_Modulus = 1.015*(10^6); %.....Psi
239 Fiber_Poissons_Ratio = 0.2;
240 Fiber_Longitudinal_Tensile_Strength = 924000; %.....Psi;
241 Fiber_Longitudinal_CTE = -0.6; %.....(10^-6)/F
242 Fiber_Transverse_CTE = 8.3; %.....(10^-6)/F
243
244 %% Matrix: 3501-6 Epoxy
245 Matrix_Density = 0.0361273; %.....lb/in^3
246 Matrix_Youngs_Modulus = 623662; %.....Psi
247 Matrix_Shear_Modulus = 232060; %.....Psi
248 Matrix_Poissons_Ratio = 0.35;
249 Matrix_Tensile_Strength = 10007.6; %.....Psi
250 Matrix_Compressive_Strength = 29007.5; %.....Psi
251 Matrix_Shear_Strength = 14503.8; %.....Psi
252 Matrix_CTE = 25; %.....(10^-6)/F
253 Matrix_Glass_Transition_Temperture = 390; %.....(10^-6)/F
254 Matrix_Maximum_Use_Temperature = 300; %.....F
255
256 %% Liner
257
258 if Liner_Material == 1;
259     % 6061-T6 Almuninum
260     Liner_Density = 0.0975; %lb/in^3
261     Liner_Youngs_Modulus = 1*(10^7); %Psi
262     Liner_Shear_Modulus = 3770000; %Psi
263     Liner_Tensile_Yeild_Strength = 40000; %Psi
264     Liner_Shear_Strength = 30000; %Psi
265     Liner_Poissons_Ratio = 0.33;
266
267 else if Liner_Material == 2;
268     % 304 Stainless Steel
269     Liner_Density = 0.289; %lb/in^3
270     Liner_Youngs_Modulus = 2.8*(10^7); %Psi
271     Liner_Shear_Modulus = 1.25*(10^7); %Psi
272     Liner_Tensile_Yeild_Strength = 31200; %Psi
273     Liner_Poissons_Ratio = 0.29;
274
275 else
276     % Rigid PVC
277     Liner_Density = 0.050; %lb/in^3
278     Liner_Youngs_Modulus = 435113; %Psi
279     Liner_Tensile_Yeild_Strength = 5801; %Psi
280     Liner_Poissons_Ratio = 0.32;
281     end
282 end

```

```

283
284 %% Thermal Conditions
285 Cure_Temperature = 300; %F
286 Testing_Temperature = 72; %F
287
288 %% Variable Definitions
289 lt = Lamina_Thickness;%inches
290 Lt = Laminate_Thickness;%inches
291 Vf = Fiber_Volume_Fraction;
292 Vm = Matrix_Volume_Fraction;
293 E1f = Fiber_Longitudinal_Modulus;%Psi
294 E2f = Fiber_Transverse_Modulus;%Psi
295 G12f = Fiber_Axial_Shear_Modulus;%Psi
296 G23f = Fiber_Transverse_Shear_Modulus;%Psi
297 v12f = Fiber_Poissons_Ratio;
298 F1ft = Fiber_Longitudinal_Tensile_Strength;%Psi
299 a1f = Fiber_Longitudinal_CTE*10^-6;%(/F)
300 a2f = Fiber_Transverse_CTE*10^-6;%(/F)
301 pm = Matrix_Density;%lb/in^3
302 Em = Matrix_Youngs_Modulus;%Psi
303 Gm = Matrix_Shear_Modulus;%Psi
304 vm = Matrix_Poissons_Ratio;
305 Fmt = Matrix_Tensile_Strength;%Psi
306 Fmc = Matrix_Compressive_Strength;%Psi
307 Fms = Matrix_Shear_Strength;%Psi
308 am = Matrix_CTE*10^-6;%((10^-6)/F)
309 Tg = Matrix_Glass_Transition_Temperture;%F
310 Tmax = Matrix_Maximum_Use_Temperature;%F
311 Ttest = Testing_Temperature;%F
312 Tcure = Cure_Temperature;%F
313
314 %% Lamina Level Properties
315
316 E1 = Vf*E1f+Vm*Em;
317 E2 = (Em*E2f)/(Vf*Em+Vm*E2f);
318 G12 = (Gm*G12f)/(Vf*Gm+Vm*G12f);
319 v12 = Vf*v12f+Vm*vm;
320 v21 = (E2*v12)/E1;
321
322 Q11 = (E1./(1-v12.*v21));
323 Q12 = (v12.*E2)./(1-v12.*v21);
324 Q22 = (E2./(1-v12.*v21));
325 Q66 = G12;
326
327 m = cosd(Orientation);
328 n = sind(Orientation);
329
330
331
332 Zero = zeros(1,Number_of_plies);
333 One = ones(1,Number_of_plies);
334 for k = 1:Number_of_plies
335 Qp = [Q11*One Q12*One Zero;Q12*One Q22*One Zero;Zero Zero Q66*One];
336 end
337 for k = 1:Number_of_plies
338 Q{k} = Qp(:, [k k+Number_of_plies k+2*Number_of_plies]);
339 end
340
341 Q11bar = Q11.*(m.^4)+2*(Q12+2*Q66).*(m.^2).*(n.^2)+Q22.*(n.^4);
342 Q12bar = (Q11+Q22-4*Q66).*(m.^2).*(n.^2)+Q12.*((n.^4)+(m.^4));

```

```

343 Q22bar = Q11.*(n.^4)+2*(Q12+2*Q66).*(m.^2).*(n.^2)+Q22.*(m.^4);
344 Q16bar = (Q11-Q12-2*Q66).*(m.^3).*n+(Q12-Q22+2*Q66).*m.*(n.^3);
345 Q26bar = (Q11-Q12-2*Q66).*(m.^3).*m+(Q12-Q22+2*Q66).*n.*(m.^3);
346 Q66bar = (Q11+Q22-2*Q12-2*Q66).*(m.^2).*(n.^2)+Q66.*((n.^4)+(m.^4));
347
348 Qb = [Q11bar Q12bar Q16bar;Q12bar Q22bar Q26bar;Q16bar Q26bar Q66bar];
349 Qbar = cell(Number_of_plyies,1);
350 for k = 1:Number_of_plyies
351 Qbar{k} = Qb(:,[k k+Number_of_plyies k+2*Number_of_plyies]);
352 end
353
354
355 %% Lamina Properties Text Output
356 % fprintf('%s\n','----- Principal Lamina Level Properties -----')
357 % fprintf('Longitudinal Modulus (E1) = %0.4f Psi\n',E1(:,1))
358 % fprintf('Transverse Modulus (E2) = %0.4f Psi\n',E2(:,1))
359 % fprintf('Shear Modulus (G12) = %0.4f Psi\n',G12(:,1))
360 % fprintf('Poissons ratio (v12) = %0.4f \n',v12(:,1))
361
362 %% Lamina Thermal Properties
363 a1 = (E1f*a1f*Vf+Em*am*Vm)/(E1f*Vf+Em*Vm);
364 a2 = a2f*Vf*(1+v12f*(a1f/a2f))+am*Vm*(1+vm)-(v12f*Vf+vm*Vm)*...
365 ((E1f*a1f*Vf+Em*am*Vm)./E1);
366 %% Lamina Thermal Properties Text Output
367 % fprintf('Longitudinal CTE = %0.4f (10^-6/F) \n',a1(:,1)*10^6)
368 % fprintf('Transverse CTE = %0.4f (10^-6/F) \n',a2(:,1)*10^6)
369
370 %% Lamina Strengths
371 %% Principal Longitudinal Tension
372 % Fiber First Criteria
373 F1t_ff = F1ft*Vf; % for E1f >> Em
374 % Matrix first Criteria
375 F1t_mf = Fmt*(Vf*(E1f/Em)+Vm); %for strain ult(fiber > matrix)
376
377 % Failure mode
378 if E1f > Em*10
379 F1t = F1t_ff;
380 else F1t = F1t_mf;
381 end
382
383 %% Principal Longitudinal Compression
384 % High Fiber Volume Fraction
385 F1c_LVf = 2*Vf*((Em*E1f*Vf)/(3*Vm))^(1/2);
386 % Low Fiber Volume Fraction
387 F1c_HVf = Gm/(Vm);
388
389 % Failure mode
390 if Vf >= 0.30
391 F1c = F1c_HVf;
392 else
393 F1c = F1c_LVf;
394 end
395
396 %% Principal Transverse Tension
397 K_sigma = (1-Vf*(1-(Em/E2f)))/(1-((4*Vf)/pi())^(1/2)*(1-(Em/E2f)));
398 K_epsilon = 1/(1-((4*Vf)/pi())^(1/2)*(1-(Em/E2f)));
399 % assuming no residual radial stress
400 F2t = (1/K_sigma)*Fmt;
401
402 %% Principal Transverse Compression

```

```

403         % assuming no residual radial stress
404         F2c = Fmc/K_sigma;
405
406     %% Principal In-Plane Shear
407         K_tau = (1-Vf*(1-(Gm/G12f)))/(1-((4*Vf)/pi()^(1/2)*(1-(Gm/G12f))));
408         F6 = Fms/K_tau;
409
410     %% Lamina Strength Text Output
411
412     %         fprintf('Longitudinal tensile strength (F1t) = %0.4f Psi\n',F1t)
413     %         fprintf('Longitudinal compressive strength (F1c) = %0.4f Psi\n',F1c)
414     %         fprintf('Transverse tensile strength (F2t) = %0.4f Psi\n',F2t)
415     %         fprintf('Transverse compressive strength (F2c) = %0.4f Psi\n',F2c)
416     %         fprintf('In-plane shear strength (F6) = %0.4f Psi\n',F6)
417
418     %% Laminate ABD Matrix
419     % fprintf('%s\n','')
420     % fprintf('----- Laminate ABD Matrix -----')
421
422     zk = cell(Number_of_plyies,1);
423     zk{1} = lt{1};
424     for k = 2:Number_of_plyies
425         zk{k} = lt{k} + zk{k-1};
426     end
427     zk = cell2mat(zk) - Lt/2;
428     zk_1 = zk - cell2mat(reshape(lt,[Number_of_plyies,1]));
429     zk = num2cell(zk);
430     zk_1 = num2cell(zk_1);
431
432     A = cell(Number_of_plyies,1);
433     for k = 1:Number_of_plyies
434         A{k} = Qbar{k}*(zk{k}-zk_1{k});
435     end
436     A = sum(cat(3,A{:}),3);
437     A(A < 10^-12 & A > -10^-12) = 0;
438
439     B = cell(Number_of_plyies,1);
440     for k = 1:Number_of_plyies
441         B{k} = 1/2.*(Qbar{k}*(zk{k}.^2 - zk_1{k}.^2));
442     end
443     B = sum(cat(3,B{:}),3);
444     B(B < 10^-12 & B > -10^-12) = 0;
445
446     D = cell(Number_of_plyies,1);
447     for k = 1:Number_of_plyies
448         D{k} = 1/3.*(Qbar{k}*(zk{k}.^3 - zk_1{k}.^3));
449     end
450     D = sum(cat(3,D{:}),3);
451     D(D < 10^-12 & D > -10^-12) = 0;
452
453     ABD = [A B;B D];
454
455
456     %% Laminate Compliance Matrix
457
458     B_star = -(inv(A))*B;
459     B_star(B_star < 10^-12 & B_star > -10^-12) = 0;
460     C_star = B*(inv(A));
461     C_star(C_star < 10^-12 & C_star > -10^-12) = 0;
462     D_star = D - C_star*B;

```

```

463 D_star(D_star < 10^-12 & D_star > -10^-12) = 0;
464
465 a = (inv(A))-(B_star*(inv(D_star)))*C_star;
466 b = B_star*(inv(D_star));
467 c = -(inv(D_star))*C_star;
468 d = inv(D_star);
469
470 %% Effective Laminate Properties
471
472 % fprintf('%s\n','')
473 % fprintf('%s\n','----- Effective Laminate Properties -----')
474
475 E_x = 1/(Lt*a(1,1));
476 E_y = 1/(Lt*a(2,2));
477 G_xy = 1/(Lt*a(3,3));
478 v_xy = -(a(2,1)/a(1,1));
479 v_yx = -(a(1,2)/a(2,2));
480 n_sx = a(1,3)/a(3,3);
481 if n_sx < 10^-12 & n_sx > -10^-12
482     n_sx = 0;
483 end
484 n_xs = a(3,1)/a(1,1);
485 if n_xs < 10^-12 & n_xs > -10^-12
486     n_xs = 0;
487 end
488 n_ys = a(3,2)/a(2,2);
489 if n_ys < 10^-12 & n_ys > -10^-12
490     n_ys = 0;
491 end
492 n_sy = a(2,3)/a(3,3);
493 if n_sy < 10^-12 & n_sy > -10^-12
494     n_sy = 0;
495 end
496
497 %% Composite Density
498 Composite_Density = Vf*Fiber_Density + Vm*Matrix_Density;
499
500 %% Laminate Level Properties Output
501
502 %     fprintf('Axial modulus (Ex) = %0.4f Psi\n',E_x)
503 %     fprintf('Transverse modulus (Ey) = %0.4f Psi\n',E_y)
504 %     fprintf('Shear modulus (Gxy) = %0.4f Psi\n',G_xy)
505 %     fprintf('Poissons ratio xy (vxy) = %0.4f\n',v_xy)
506 %     fprintf('Poissons ratio yx (vyx) = %0.4f\n',v_yx)
507 %     fprintf('Shear coupling coefficient (nsx) = %0.4f\n',n_sx)
508 %     fprintf('Shear coupling coefficient (nxs) = %0.4f\n',n_xs)
509 %     fprintf('Shear coupling coefficient (nsy) = %0.4f\n',n_sy)
510 %     fprintf('Shear coupling coefficient (nys) = %0.4f\n',n_ys)
511 %     fprintf('Composite Density = %0.4f lb/in^3\n',Composite_Density)
512
513 %% Thermal Analysis
514
515     %% Global CTEs
516     ax = a1.*(m.^2)+a2.*(n.^2);
517     ay = a1.*(n.^2)+a2.*(m.^2);
518     axy = 2*(a1-a2).*m.*n;
519     dT = Cure_Temperature - Testing_Temperature;
520     ex = ax*dT;
521     ey = ay*dT;
522     exy = axy*dT;

```

```

523
524     avg_ax = sum(ax)/Number_of_plyies;
525     avg_ay = sum(ay)/Number_of_plyies;
526 %fprintf('Axial coefficient of thermal expansion = %0.4f\n',avg_ax*10^6)
527 %fprintf('Transverse coefficient of thermal expansion = %0.4f\n',avg_ay*10^6)
528
529     ET = [ex;ey;exy];
530     eT = cell(Number_of_plyies,1);
531     for k = 1:Number_of_plyies
532         eT{k} = ET(:,[k]);
533     end
534
535     %% Thermal Forces
536     NT = cell(Number_of_plyies,1);
537     for k = 1:Number_of_plyies
538         NT{k} = Qbar{k}*(eT{k})*lt{k};
539     end
540     NT = sum(cat(3,NT{:}),3);
541     NT(NT < 10^-12 & NT > -10^-12) = 0;
542
543     %% Thermal Moments
544
545     zk_bar = cell2mat(reshape(zk,[1,Number_of_plyies])) - cell2mat(lt)/2;
546     zk_bar(zk_bar < 10^-12 & zk_bar > -10^-12) = 0;
547     zk_bar = num2cell(zk_bar);
548
549     MT = cell(Number_of_plyies,1);
550     for k = 1:Number_of_plyies
551         MT{k} = Qbar{k}*(eT{k})*zk_bar{k}*lt{k};
552     end
553     MT = sum(cat(3,MT{:}),3);
554     MT(MT < 10^-12 & MT > -10^-12) = 0;
555
556     %% Thermal Midplane Strain - Global Coordinates
557     Epsilon_0_T_xy = a*NT+b*MT;
558     Epsilon_0_T_xy(isnan(Epsilon_0_T_xy)) = 0;
559     Epsilon_0_T_xy(Epsilon_0_T_xy < 10^-12 & Epsilon_0_T_xy > -10^-12) = 0;
560
561     %% Thermal Midplane Curvature - Global Coordinates
562     Kappa_T_xy = c*NT+d*MT;
563     Kappa_T_xy(isnan(Kappa_T_xy)) = 0;
564     Kappa_T_xy(Kappa_T_xy < 10^-12 & Kappa_T_xy > -10^-12) = 0;
565
566     %% Net Thermal Strains in Lamina - Global Coordinates
567     Epsilon_T_xy = cell(Number_of_plyies,1);
568     for k = 1:Number_of_plyies
569         Epsilon_T_xy{k} = Epsilon_0_T_xy+lt{k}*zk{k}*Kappa_T_xy;
570     end
571
572     %% Thermal Elastic Strains in Lamina - Global Coordinates
573     Epsilon_Te_xy = cell(Number_of_plyies,1);
574     for k = 1:Number_of_plyies
575         Epsilon_Te_xy{k} = Epsilon_T_xy{k}-eT{k};
576     end
577
578     %% Residual Thermal Strains in Lamina - Principal Coordinates
579     T11 = m.^2;
580     T12 = n.^2;
581     T13 = 2*m.*n;
582     T23 = -2*m.*n;

```

```

583     T31 = -m.*n;
584     T32 = m.*n;
585     T33 = (m.^2)-(n.^2);
586     trans = [T11 T12 T13;T12 T11 T23;T31 T32 T33];
587     T = cell(Number_of_plies,1);
588     for k = 1:Number_of_plies
589     T{k} = trans(:, [k k+Number_of_plies k+2*Number_of_plies]);
590     end
591
592     Epsilon_T_12 = cell(Number_of_plies,1);
593     for k = 1:Number_of_plies
594     Epsilon_T_12{k} = T{k}*Epsilon_T_xy{k};
595     end
596
597     %% Residual Thermal Stresses in Lamina - Principal Coordinates
598     Sigma_T_12 = cell(Number_of_plies,1);
599     for k = 1:Number_of_plies
600     Sigma_T_12{k} = Q{k}*Epsilon_T_12{k};
601     end
602     Sig_T_12 = (cell2mat(Sigma_T_12));
603     Sig_T_12(isnan(Sig_T_12)) = 0;
604     threes = 3*ones(1,Number_of_plies);
605     Sigma_T_12 = mat2cell(Sig_T_12,threes,[1]);
606
607     for k = 1:Number_of_plies
608     Net_Sig_Therm{k} = Qbar{k}*Epsilon_T_xy{k};
609     end
610     Net_Thermal_Stress = sum(cat(3,Net_Sig_Therm{:}),3);
611
612     %% Mechanical Analysis
613
614     %% Mechanical Stress in Laminate - Global Coordinates
615     Sigma_Long = (Pressure*Radius)/(2*Laminate_Thickness);
616     Sigma_Hoop = (Pressure*Radius)/Laminate_Thickness;
617
618     Sigma_xy = [Sigma_Long; Sigma_Hoop; 0];
619
620     %% Mecanical Strains in Laminate - Global Coordinates
621
622     Inverse_Modulus_Matrix = [1/E_x -v_yx/E_y n_sx/G_xy;...
623                               -v_xy/E_x 1/E_y n_sy/G_xy;...
624                               n_xs/E_x n_ys/E_y 1/G_xy];
625
626     Epsilon_xy = Inverse_Modulus_Matrix * Sigma_xy;
627
628     %% Net Mechanical Strains in Lamina - Principal Coordinates
629     T11 = m.^2;
630     T12 = n.^2;
631     T13 = 2*m.*n;
632     T23 = -2*m.*n;
633     T31 = -m.*n;
634     T32 = m.*n;
635     T33 = (m.^2)-(n.^2);
636     trans = [T11 T12 T13;T12 T11 T23;T31 T32 T33];
637     T = cell(Number_of_plies,1);
638     for k = 1:Number_of_plies
639     T{k} = trans(:, [k k+Number_of_plies k+2*Number_of_plies]);
640     end
641
642     Epsilon_12 = cell(Number_of_plies,1);

```



```

643     for k = 1:Number_of_plies
644         Epsilon_12{k} = T{k}*Epsilon_xy;
645     end
646
647     %% Mechanical Stresses in Lamina - Principal Coordinates
648         Sigma_12 = cell(Number_of_plies,1);
649     for k = 1:Number_of_plies
650         Sigma_12{k} = Q{k}*Epsilon_12{k};
651     end
652
653     %% Net Stress in Lamina - Principal Coordinates
654         Net_Sigma_12 = cell(Number_of_plies,1);
655     for k = 1:Number_of_plies
656         Net_Sigma_12{k} = Sigma_12{k}+Sigma_T_12{k};
657     end
658
659     Net_Sigma_12 = reshape(Net_Sigma_12,[1 Number_of_plies]);
660     stress_mat = cell2mat(Net_Sigma_12);
661     Sigma_1 = stress_mat(1,:);
662     Sigma_2 = stress_mat(2,:);
663     Tau_6 = stress_mat(3,:);
664
665     %% Net Strain in Lamina - Principal Coordinates
666         Net_Epsilon_12 = cell(Number_of_plies,1);
667     for k = 1:Number_of_plies
668         Net_Epsilon_12{k} = Epsilon_12{k}+Epsilon_T_12{k};
669     end
670
671     Net_Epsilon_12 = reshape(Net_Epsilon_12,[1 Number_of_plies]);
672     Strain_mat = cell2mat(Net_Epsilon_12);
673     Epsilon_1 = Strain_mat(1,:);
674     Epsilon_2 = Strain_mat(2,:);
675     Gamma_6 = Strain_mat(3,:);
676     %% Tsai-Wu failure analysis
677     f1 = (1/F1t)-(1/F1c);
678     f11 = 1/(F1t*F1c);
679     f2 = (1/F2t)-(1/F2c);
680     f22 = 1/(F2t*F2c);
681     f6 = 1/(F6^2);
682     f12 = -(1/2)*((f11*f22)^(1/2));
683     a_TW = f11.*(Sigma_1.^2)+f22.*(Sigma_2.^2)+...
684         f6.*(Tau_6.^2)+2.*f12.*Sigma_1.*Sigma_2;
685     b_TW = f1.*Sigma_1+f2.*Sigma_2;
686
687     Tsai_Wu_quadratic = a_TW+b_TW-1 == 0;
688
689     Sft_TW = (-b_TW+(((b_TW.^2)+4.*a_TW).^(1/2)))./(2.*a_TW);
690     Sft_TW(isnan(Sft_TW)) = 0;
691     Sfc_TW = abs(-b_TW-(((b_TW.^2)+4.*a_TW).^(1/2)))./(2.*a_TW);
692     Sfc_TW(isnan(Sfc_TW)) = 0;
693
694     Tension_Test_Pass = [Sft_TW > 1];
695     Tension_Test_Fail = [Sft_TW < 1];
696     Compression_Test_Pass = [Sfc_TW > 1];
697     Compression_Test_Fail = [Sfc_TW < 1];
698
699     %% Maximum Stress failure analysis
700     Failure_Stress_1_Direction = cell(Number_of_plies,1);
701     for k = 1:Number_of_plies
702         if Sigma_1(k)>0

```

```

703 Failure_Stress_1_Direction{k} = F1t/(cos(Orientation(k))^2);
704 else
705 Failure_Stress_1_Direction{k} = F1c/(cos(Orientation(k))^2);
706 end
707 end
708
709 Failure_Stress_2_Direction = cell(Number_of_plyies,1);
710 for k = 1:Number_of_plyies
711 if Sigma_2(k)>0
712 Failure_Stress_2_Direction{k} = F2t/(sin(Orientation(k))^2);
713 else
714 Failure_Stress_2_Direction{k} = F2c/(sin(Orientation(k))^2);
715 end
716 end
717
718 Failure_Stress_6_Direction = cell(Number_of_plyies,1);
719 for k = 1:Number_of_plyies
720 if Tau_6(k)>0
721 Failure_Stress_6_Direction{k} = F6/(cos(Orientation(k))*sin(Orientation(k)));
722 else
723 Failure_Stress_6_Direction{k} = F6/(cos(Orientation(k))*sin(Orientation(k)));
724 end
725 end
726
727 Max_Stress_Pass_1_Direction = cell(Number_of_plyies,1);
728 for k = 1:Number_of_plyies
729 if Failure_Stress_1_Direction{k} > 0
730 if Failure_Stress_1_Direction{k} - Sigma_1(k)>0
731 Max_Stress_Pass_1_Direction{k} = 1;
732 else
733 Max_Stress_Pass_1_Direction{k} = 0;
734 end
735 else
736 if Failure_Stress_1_Direction{k} - Sigma_1(k)<0
737 Max_Stress_Pass_1_Direction{k} = 1;
738 else
739 Max_Stress_Pass_1_Direction{k} = 0;
740 end
741 end
742 end
743
744 Max_Stress_Pass_2_Direction = cell(Number_of_plyies,1);
745 for k = 1:Number_of_plyies
746 if Failure_Stress_2_Direction{k} > 0
747 if Failure_Stress_2_Direction{k} - Sigma_2(k)>0
748 Max_Stress_Pass_2_Direction{k} = 1;
749 else
750 Max_Stress_Pass_2_Direction{k} = 0;
751 end
752 else
753 if Failure_Stress_2_Direction{k} - Sigma_2(k)<0
754 Max_Stress_Pass_2_Direction{k} = 1;
755 else
756 Max_Stress_Pass_2_Direction{k} = 0;
757 end
758 end
759 end
760
761 Max_Stress_Pass_6_Direction = cell(Number_of_plyies,1);
762 for k = 1:Number_of_plyies

```

```

763 if Failure_Stress_6_Direction{k} > 0
764 if Failure_Stress_6_Direction{k} - Tau_6(k)>0
765 Max_Stress_Pass_6_Direction{k} = 1;
766 else
767 Max_Stress_Pass_6_Direction{k} = 0;
768 end
769 else
770 if Failure_Stress_6_Direction{k} - Tau_6(k)<0
771 Max_Stress_Pass_6_Direction{k} = 1;
772 else
773 Max_Stress_Pass_6_Direction{k} = 0;
774 end
775 end
776 end
777
778 if sum(cell2mat(Max_Stress_Pass_1_Direction)) == Number_of_plies &&...
779     sum(cell2mat(Max_Stress_Pass_2_Direction)) == Number_of_plies &&...
780     sum(cell2mat(Max_Stress_Pass_6_Direction)) == Number_of_plies
781 Max_Stress_Failure_Analysis = 1;
782 else
783 Max_Stress_Failure_Analysis = 0;
784 end
785
786 %% Maximum Strain failure analysis
787 Failure_Strain_1_Direction = cell(Number_of_plies,1);
788 for k = 1:Number_of_plies
789 if Epsilon_1(k)>0
790 Failure_Strain_1_Direction{k} = F1t/E1;
791 else
792 Failure_Strain_1_Direction{k} = -F1c/E1;
793 end
794 end
795
796 Failure_Strain_2_Direction = cell(Number_of_plies,1);
797 for k = 1:Number_of_plies
798 if Epsilon_2(k)>0
799 Failure_Strain_2_Direction{k} = F2t/E2;
800 else
801 Failure_Strain_2_Direction{k} = -F2c/E2;
802 end
803 end
804
805 Failure_Strain_6_Direction = cell(Number_of_plies,1);
806 for k = 1:Number_of_plies
807 Failure_Strain_6_Direction{k} = F6/G12;
808 end
809
810 Max_Strain_Pass_1_Direction = cell(Number_of_plies,1);
811 for k = 1:Number_of_plies
812 if Failure_Strain_1_Direction{k} > 0
813 if Failure_Strain_1_Direction{k} - Epsilon_1(k)>0
814 Max_Strain_Pass_1_Direction{k} = 1;
815 else
816 Max_Strain_Pass_1_Direction{k} = 0;
817 end
818 else
819 if Failure_Strain_1_Direction{k} - Epsilon_1(k)<0
820 Max_Strain_Pass_1_Direction{k} = 1;
821 else
822 Max_Strain_Pass_1_Direction{k} = 0;

```

```

823 end
824 end
825 end
826
827 Max_Strain_Pass_2_Direction = cell(Number_of_plies,1);
828 for k = 1:Number_of_plies
829 if Failure_Strain_2_Direction{k} > 0
830 if Failure_Strain_2_Direction{k} - Epsilon_2(k)>0
831 Max_Strain_Pass_2_Direction{k} = 1;
832 else
833 Max_Strain_Pass_2_Direction{k} = 0;
834 end
835 else
836 if Failure_Strain_2_Direction{k} - Epsilon_2(k)<0
837 Max_Strain_Pass_2_Direction{k} = 1;
838 else
839 Max_Strain_Pass_2_Direction{k} = 0;
840 end
841 end
842 end
843
844 Max_Strain_Pass_6_Direction = cell(Number_of_plies,1);
845 for k = 1:Number_of_plies
846 if Failure_Strain_6_Direction{k} > 0
847 if Failure_Strain_6_Direction{k} - Gamma_6(k)>0
848 Max_Strain_Pass_6_Direction{k} = 1;
849 else
850 Max_Strain_Pass_6_Direction{k} = 0;
851 end
852 else
853 if Failure_Strain_6_Direction{k} - Gamma_6(k)<0
854 Max_Strain_Pass_6_Direction{k} = 1;
855 else
856 Max_Strain_Pass_6_Direction{k} = 0;
857 end
858 end
859 end
860
861 if sum(cell2mat(Max_Strain_Pass_1_Direction)) == Number_of_plies &&...
862     sum(cell2mat(Max_Strain_Pass_2_Direction)) == Number_of_plies &&...
863     sum(cell2mat(Max_Strain_Pass_6_Direction)) == Number_of_plies
864 Max_Strain_Failure_Analysis = 1;
865 else
866 Max_Strain_Failure_Analysis = 0;
867 end
868
869 % Tsai-Hill failure analysis
870
871 F1_TH = cell(Number_of_plies,1);
872 for k = 1:Number_of_plies
873 if Sigma_1(k)>0
874 F1_TH{k} = F1t;
875 else
876 F1_TH{k} = F1c;
877 end
878 end
879
880 F2_TH = cell(Number_of_plies,1);
881 for k = 1:Number_of_plies
882 if Sigma_1(k)>0

```

```

883 F2_TH{k} = F2t;
884 else
885 F2_TH{k} = F2c;
886 end
887 end
888
889 F6_TH = cell(Number_of_plies,1);
890 for k = 1:Number_of_plies
891 F6_TH{k} = F6;
892 end
893
894 A_TH = 1./((cell2mat(F1_TH)')).^2);
895 B_TH = 1./((cell2mat(F2_TH)')).^2);
896 C_TH = -1./((cell2mat(F1_TH)')).^2);
897 D_TH = 1./((cell2mat(F6_TH)')).^2);
898
899
900 Tsai_Hill_Pass_Fail = cell(Number_of_plies,1);
901 for k = 1:Number_of_plies
902 Tsai_Hill_Pass_Fail{k} = (A_TH(k)*Sigma_1(k)^2)+(B_TH(k)*Sigma_2(k)^2)+...
903 (C_TH(k)*Sigma_1(k)*Sigma_2(k))+...
904 (D_TH(k)*Tau_6(k)^2);
905 end
906
907 if sum(cell2mat(Tsai_Hill_Pass_Fail)) < Number_of_plies
908 Tsai_Hill_Failure_Analysis = 1;
909 else
910 Tsai_Hill_Failure_Analysis = 0;
911 end
912
913 %% FAILURE ANALYSIS CRITERIA SELECTION
914
915 % Tsai_Wu = 1
916 % Maximum_Stress = 2
917 % Maximum_Strain = 3
918 % Tsai_Hill = 4
919
920 Failure_Mode_Analysis_Criteria = 1 ;
921
922 %% Results
923 fprintf('%s\n','')
924
925 if Failure_Mode_Analysis_Criteria == 1
926     if Tension_Test_Pass == One & Compression_Test_Pass == One
927         fprintf('For Tsai-Wu failure criteria tank = Pass\n')
928     else fprintf('For Tsai-Wu failure criteria tank = Fail\n')
929     end
930
931 elseif Failure_Mode_Analysis_Criteria == 2
932     if Max_Stress_Failure_Analysis == 1
933         fprintf('For maximum stress failure criteria tank = Pass\n')
934     else fprintf('For maximum stress failure criteria tank = Fail\n')
935     end
936
937 elseif Failure_Mode_Analysis_Criteria == 3
938     if Max_Strain_Failure_Analysis == 1
939         fprintf('For maximum strain failure criteria tank = Pass\n')
940     else fprintf('For maximum strain failure criteria tank = Fail\n')
941     end
942

```

```

943 elseif Failure_Mode_Analysis_Criteria == 4
944     if Tsai_Hill_Failure_Analysis == 1
945         fprintf('For Tsai-Hill failure criteria tank = Pass\n')
946     else fprintf('For Tsai-Hill failure criteria tank = Fail\n')
947     end
948 else fprintf('Please select failure analysis criteria\n')
949 end
950 fprintf('%s\n','')
951 fprintf('Common bulkhead tank height                = %0.4f in\n',...
952     Total_Tank_Height_CB)
953 fprintf('%s\n','')
954
955 fprintf('Combined individual tank heights            = %0.4f in\n',...
956     Combine_Tank_Height_IT)
957 fprintf('Individual HTP tank height                  = %0.4f in\n',...
958     Height_HTP_IT)
959 fprintf('Individual RP-1 tank height                  = %0.4f in\n',...
960     Height_RP1_IT)
961 fprintf('%s\n','')
962 %% Weight Calculation
963
964 Outer_Radius = Radius+Laminate_Thickness;
965
966 %Common Bulkhead Calculation
967 Liner_Volume_CB = 1.5*(4/3)*pi()*((Radius^3)-(Inner_Radius^3))+ ...
968     pi()*Midsection_Height_CB*((Radius^2)-(Inner_Radius^2));
969 Liner_Weight_CB = Liner_Density*Liner_Volume_CB;
970 Composite_Volume = (4/3)*pi()*((Outer_Radius^3)-(Radius^3))+ ...
971     pi()*Midsection_Height_CB*((Outer_Radius^2)-(Radius^2));
972 Composite_Weight = Composite_Density*Composite_Volume;
973 if Tension_Test_Pass == One & Compression_Test_Pass == One
974     Total_Weight_CB = Liner_Weight_CB+Composite_Weight;
975 else Total_Weight_CB = nan
976 end
977
978 %Individual Tank Calculation
979 Liner_Volume_IT = 2*(4/3)*pi()*((Radius^3)-(Inner_Radius^3))+ ...
980     pi()*Midsection_Height_IT*((Radius^2)-(Inner_Radius^2));
981 Liner_Weight_IT = Liner_Density*Liner_Volume_IT;
982 Composite_Volume = 2*(4/3)*pi()*((Outer_Radius^3)-(Radius^3))+ ...
983     pi()*Midsection_Height_IT*((Outer_Radius^2)-(Radius^2));
984
985 Composite_Vol_HTP = 2*(4/3)*pi()*((Outer_Radius^3)-(Radius^3))+ ...
986     pi()*Midsection_Height_HTP*((Outer_Radius^2)-(Radius^2));
987 Composite_Vol_RP1 = 2*(4/3)*pi()*((Outer_Radius^3)-(Radius^3))+ ...
988     pi()*Midsection_Height_RP1*((Outer_Radius^2)-(Radius^2));
989
990 Liner_Volume_HTP = (4/3)*pi()*((Radius^3)-(Inner_Radius^3))+ ...
991     pi()*Midsection_Height_HTP*((Radius^2)-(Inner_Radius^2));
992 Liner_Volume_RP1 = (4/3)*pi()*((Radius^3)-(Inner_Radius^3))+ ...
993     pi()*Midsection_Height_RP1*((Radius^2)-(Inner_Radius^2));
994
995 Liner_Weight_HTP = Liner_Density*Liner_Volume_HTP;
996 Liner_Weight_RP1 = Liner_Density*Liner_Volume_RP1;
997
998 Composite_Weight = Composite_Density*Composite_Volume;
999 Composite_Weight_HTP = Composite_Density*Composite_Vol_HTP; %1b
1000 Composite_Weight_RP1 = Composite_Density*Composite_Vol_RP1; %1b
1001
1002 Weight_HTP_IT = Composite_Weight_HTP+Liner_Weight_HTP; %kg

```

```

1003 Weight_RP1_IT = Composite_Weight_RP1+Liner_Weight_RP1; %kg
1004
1005 if Tension_Test_Pass == One & Compression_Test_Pass == One
1006 Total_Weight_IT = Liner_Weight_IT+Composite_Weight;
1007 else Total_Weight_IT = nan
1008 end
1009
1010 Estimate_Buffering_Factor = 1.5;
1011 Propellant_COPV_Safe_Weight_CB = Total_Weight_CB*Estimate_Buffering_Factor;
1012
1013 fprintf('Propellant tank weight common bulkhead design = %0.4f Lb\n',...
1014         Total_Weight_CB)
1015 fprintf('                                     = %0.4f Kg\n',...
1016         Total_Weight_CB*0.453592)
1017
1018 fprintf('Individual HTP tank weight           = %0.4f Lb\n',...
1019         Weight_HTP_IT)
1020 fprintf('                                     = %0.4f Kg\n',...
1021         Weight_HTP_IT*0.453592)
1022 fprintf('Individual RP-1 tank weight          = %0.4f Lb\n',...
1023         Weight_RP1_IT)
1024 fprintf('                                     = %0.4f Kg\n',...
1025         Weight_RP1_IT*0.453592)
1026
1027 fprintf('Combined tank weight individual tank design = %0.4f Lb\n',...
1028         Total_Weight_IT)
1029 fprintf('                                     = %0.4f Kg\n',...
1030         Total_Weight_IT*0.453592)
1031
1032 fprintf('%s\n', '')
1033
1034
1035 %% Excel Output
1036 if Tension_Test_Pass == One & Compression_Test_Pass == One
1037 if Write_to_Excel == 0
1038 return
1039 end
1040 else
1041     fprintf('ERROR HAS OCCURED. CHECK INPUT VALUES AND LOOK FOR "NaN"')
1042     return
1043 end
1044 %%%%%%%%%%%%%%%%%%%%%%%%%%%%%%%%%%%%%%%%%%%%%%%%%%%%%%%%%%%%%%%%%%%%%%%%%%%%%%%%%%%%%%%%%%%%%%%%%%%%%%%%%%%%%%%%%%%%%%%%%%%%%%%%%%%%%%%%%%%%%%%%%
1045 %% General Rocket Info
1046 xlswrite('Master.xlsx',Aero_Optimum_Radius, 'Rocket_Main', 'C3');
1047 xlswrite('Master.xlsx',Radius, 'Rocket_Main', 'C6');
1048 xlswrite('Master.xlsx',Inner_Radius, 'Rocket_Main', 'C7');
1049 xlswrite('Master.xlsx',HTP_Volume, 'Rocket_Main', 'C10');
1050 xlswrite('Master.xlsx',HTP_Density, 'Rocket_Main', 'C11');
1051 xlswrite('Master.xlsx',HTP_Mass, 'Rocket_Main', 'C12');
1052 xlswrite('Master.xlsx',Midsection_Height_HTP, 'Rocket_Main', 'C13');
1053 xlswrite('Master.xlsx',RP1_Volume, 'Rocket_Main', 'C14');
1054 xlswrite('Master.xlsx',RP1_Density, 'Rocket_Main', 'C15');
1055 xlswrite('Master.xlsx',RP1_Mass, 'Rocket_Main', 'C16');
1056 xlswrite('Master.xlsx',Midsection_Height_RP1, 'Rocket_Main', 'C17');
1057 xlswrite('Master.xlsx',Total_Propellant_Mass, 'Rocket_Main', 'C18');
1058 xlswrite('Master.xlsx',MEOP, 'Rocket_Main', 'C19');
1059
1060 %% Composite Properties
1061
1062 % Reinforcement: Toray T1000G Carbon Fiber

```

```

1063 xlswrite('Master.xlsx',Fiber_Density, 'Composite','C3');
1064 xlswrite('Master.xlsx',Fiber_Longitudinal_Modulus, 'Composite','C4');
1065 xlswrite('Master.xlsx',Fiber_Transverse_Modulus, 'Composite','C5');
1066 xlswrite('Master.xlsx',Fiber_Axial_Shear_Modulus, 'Composite','C6');
1067 xlswrite('Master.xlsx',Fiber_Transverse_Shear_Modulus, 'Composite','C7');
1068 xlswrite('Master.xlsx',Fiber_Poissons_Ratio, 'Composite','C8');
1069 xlswrite('Master.xlsx',Fiber_Longitudinal_Tensile_Strength, 'Composite','C9');
1070 xlswrite('Master.xlsx',Fiber_Longitudinal_CTE, 'Composite','C10');
1071 xlswrite('Master.xlsx',Fiber_Transverse_CTE, 'Composite','C11');
1072
1073 % Matrix: 3501-6 Epoxy
1074 xlswrite('Master.xlsx',Matrix_Density, 'Composite','C14');
1075 xlswrite('Master.xlsx',Matrix_Youngs_Modulus, 'Composite','C15');
1076 xlswrite('Master.xlsx',Matrix_Shear_Modulus, 'Composite','C16');
1077 xlswrite('Master.xlsx',Matrix_Poissons_Ratio, 'Composite','C17');
1078 xlswrite('Master.xlsx',Matrix_Tensile_Strength, 'Composite','C18');
1079 xlswrite('Master.xlsx',Matrix_Compressive_Strength, 'Composite','C19');
1080 xlswrite('Master.xlsx',Matrix_Shear_Strength, 'Composite','C20');
1081 xlswrite('Master.xlsx',Matrix_CTE, 'Composite','C21');
1082 xlswrite('Master.xlsx',Matrix_Glass_Transition_Temperture, 'Composite','C22');
1083 xlswrite('Master.xlsx',Matrix_Maximum_Use_Temperature, 'Composite','C23');
1084
1085 % Composite Lamina Properties
1086 xlswrite('Master.xlsx',Number_of_plies, 'Composite','C26');
1087 xlswrite('Master.xlsx',Fiber_Volume_Fraction, 'Composite','C27');
1088 xlswrite('Master.xlsx',Lamina_Thickness(1,1), 'Composite','C28');
1089 xlswrite('Master.xlsx',E1, 'Composite','C29');
1090 xlswrite('Master.xlsx',E2, 'Composite','C30');
1091 xlswrite('Master.xlsx',G12, 'Composite','C31');
1092 xlswrite('Master.xlsx',v12, 'Composite','C32');
1093 xlswrite('Master.xlsx',a1, 'Composite','C33');
1094 xlswrite('Master.xlsx',a2, 'Composite','C34');
1095 xlswrite('Master.xlsx',F1t, 'Composite','C35');
1096 xlswrite('Master.xlsx',F1c, 'Composite','C36');
1097 xlswrite('Master.xlsx',F2t, 'Composite','C37');
1098 xlswrite('Master.xlsx',F2c, 'Composite','C38');
1099 xlswrite('Master.xlsx',F6, 'Composite','C39');
1100
1101 % Laminate Structure
1102 xlswrite('Master.xlsx',Orientation, 'Composite','G25');
1103
1104 % Composite Laminate Properties
1105 xlswrite('Master.xlsx',E_x, 'Composite','C42');
1106 xlswrite('Master.xlsx',E_y, 'Composite','C43');
1107 xlswrite('Master.xlsx',G_xy, 'Composite','C44');
1108 xlswrite('Master.xlsx',v_xy, 'Composite','C45');
1109 xlswrite('Master.xlsx',v_yx, 'Composite','C46');
1110 xlswrite('Master.xlsx',n_sx, 'Composite','C47');
1111 xlswrite('Master.xlsx',n_xs, 'Composite','C48');
1112 xlswrite('Master.xlsx',n_sy, 'Composite','C49');
1113 xlswrite('Master.xlsx',n_ys, 'Composite','C50');
1114 xlswrite('Master.xlsx',Composite_Density, 'Composite','C51');
1115 xlswrite('Master.xlsx',avg_ax*10^6, 'Composite','C52');
1116 xlswrite('Master.xlsx',avg_ay*10^6, 'Composite','C53');

```


6.1.2 Pressurant COPV Analysis Script - MATLAB

```

1 %% Liquid Rocketry Lab           John Slugg           10/23/2020
2
3 %%                               Propellant COPVs
4 clear;
5 clc;
6
7 % Write output to Excel?      1 = Yes, 0 = No
8
9 Write_to_Excel = 0;
10
11                               %% ROCKET RADIUS INPUT
12
13                               Aero_Optimum_Radius = 8; %inches
14
15 fprintf('Rocket external radius           = %0.4f in\n',...
16         Aero_Optimum_Radius)
17 fprintf('%s\n','')
18 %% PROPELLANT COPV CALCULATIONS
19 fprintf('%s\n','----- Propellant COPVs -----')
20 %%%%%%%%%%%%%%%%%%%%%%%%%%%%%%%%%%%%%%%%%%%%%%%%%%%%%%%%%%%%%%%%%%%%%%%%%
21
22 %% Initial Conditions
23
24 HTP_Vol_L = 647.5; %.....Liters
25 HTP_Volume = HTP_Vol_L* 61.0237; %.....in^3
26 HTP_Density = 0.02926311; %.....lb/in^3
27 HTP_Mass = HTP_Density*HTP_Volume; %.....lbm
28 HTP_Kg = HTP_Mass*0.453592; %.....Kg
29
30 RP1_Vol_L = 92.5; %.....Liters
31 RP1_Volume = RP1_Vol_L* 61.0237; %.....in^3
32 RP1_Density = 0.0520233; %.....lb/in^3
33 RP1_Mass = RP1_Density*RP1_Volume; %.....lbm
34 RP1_Kg = RP1_Mass*0.453592; %.....Kg
35
36 Total_Propellant_Mass = HTP_Mass + RP1_Mass; %.....lbm
37
38 Propellant_Mix_Ratio_Vol = (HTP_Vol_L/RP1_Vol_L);
39 fprintf('Propellant mix ratio by volume (HTP:RP-1)           = %0.2f:1\n',...
40         Propellant_Mix_Ratio_Vol)
41
42
43 %% Laminate Properties
44
45 % NOTE: ORIENTATION AUTOMATICALLY PRODUCES A SYMMETRIC MATRIX. TO AVOID
46 % THIS COMMENT OUT THE LINES THAT ARE FOLLOWED BY THE COMMENT "symmetry"
47
48 Orientation = [15 -15 75 -75 75 -75 75 -75]; %.....degrees
49
50 %Orientation = [15 -15 75 -75 75 -75 75 -75]; %.....degrees
51
52 Orientation_flip = fliplr(Orientation);           %symmetry
53 Orientation = [Orientation Orientation_flip];           %symmetry
54
55 Lamina_Thickness = cell(1,length(Orientation));
56 for k = 1:length(Orientation)
57
58         Lamina_Thickness{k} = 0.01; %.....in

```

```

59
60 end
61
62 Laminate_Thickness = sum(cat(3,Lamina_Thickness{:}),3);
63
64 Number_of_plies = numel(Orientation);
65 Fiber_Volume_Fraction = 0.61;
66 Matrix_Volume_Fraction = 1 - Fiber_Volume_Fraction;
67
68 %% Tank Properties
69 MEOP = 1000; %Psi
70 Liner_thickness = 0.040; %in
71 Radius = Aero_Optimum_Radius-Laminate_Thickness; %.....in
72 Inner_Radius = Radius - Liner_thickness; %.....in
73 Midsection_Height_RP1 = (RP1_Volume - ((4/3)*pi()*Inner_Radius^3)/2)/...
74 (pi()*Inner_Radius^2); %.....in
75 Midsection_Height_HTP = (HTP_Volume - ((4/3)*pi()*Inner_Radius^3)/2)/...
76 (pi()*Inner_Radius^2); %.....in
77
78 Liner_Material = 1;
79
80 %Liner material options
81 % 1 = Aluminum
82 % 2 = Stainless
83 % 3 = PVC
84
85 %Common Bulkhead Tank Dimensions
86 %Hemispherical tank head assumed
87 Height_HTP_CB = Aero_Optimum_Radius + Midsection_Height_HTP; %.....in
88 Height_RP1_CB = Aero_Optimum_Radius + Midsection_Height_RP1; %.....in
89 Total_Tank_Height_CB = Height_RP1_CB + Height_HTP_CB; %in
90 Midsection_Height_CB = Midsection_Height_HTP + Midsection_Height_RP1; %in
91
92 %Individual Tank Dimensions
93 %Hemispherical tank head assumed
94 Height_HTP_IT = 2*Aero_Optimum_Radius + Midsection_Height_HTP; %....in
95 Height_RP1_IT = 2*Aero_Optimum_Radius + Midsection_Height_RP1; %....in
96 Combine_Tank_Height_IT = Height_RP1_IT + Height_HTP_IT; %.....in
97 Midsection_Height_IT = Midsection_Height_HTP + Midsection_Height_RP1; %in
98
99
100 %% Baffle System volume and mass contribution
101
102 Vertical_Angle_Count = 8;
103 Vertical_Angle_Width = 1; %in
104 Vertical_Angle_Thickness = 0.125; %in
105 Vertical_Angle_Area = 2*(Vertical_Angle_Width*Vertical_Angle_Thickness)...
106 - Vertical_Angle_Thickness^2; %in
107
108 Baffle_Width = 2; %in
109 Baffle_Thickness = .125; %in
110 Baffle_Spacing = 24; %in
111 Baffle_Volume = pi()*(Inner_Radius^2 - (Inner_Radius-Baffle_Width)^2);%in^3
112
113
114 Volume_difference_HTP = 1;
115 Volume_difference_RP1 = 1;
116 while Volume_difference_RP1 < 99 | Volume_difference_RP1 > 101
117
118 Vertical_Angle_Length_RP1 = Midsection_Height_RP1; %in

```

```

119 Vertical_Angle_Volume_RP1 = Verticle_Angle_Area*Vertical_Angle_Length_RP1;%in^3
120
121 Baffle_Count_RP1 = floor(Midsection_Height_RP1/Baffle_Spacing)+1;%in^3
122 Baffle_Volume_RP1 = Baffle_Volume*Baffle_Count_RP1; %in^3
123
124 Baffle_System_Volume_RP1 = Baffle_Volume_RP1+Vertical_Angle_Volume_RP1;%in^3
125
126 Volume_difference_RP1 = ((4/3)*pi()*Inner_Radius^3)+...
127 Midsection_Height_RP1*pi()*Inner_Radius^2-...
128 (RP1_Volume+Baffle_System_Volume_RP1);
129
130 if Volume_difference_RP1 < 99
131     Midsection_Height_RP1 = Midsection_Height_RP1 + 0.01;
132 elseif Volume_difference_RP1 > 101
133     Midsection_Height_RP1 = Midsection_Height_RP1 - 0.01;
134 end
135 end
136
137 while Volume_difference_HTP < 99 | Volume_difference_HTP > 101
138
139 Vertical_Angle_Length_HTP = Midsection_Height_HTP; %in
140 Vertical_Angle_Volume_HTP = Verticle_Angle_Area*Vertical_Angle_Length_HTP;%in^3
141
142 Baffle_Count_HTP = floor(Midsection_Height_HTP/Baffle_Spacing)+1;%in^3
143 Baffle_Volume_HTP = Baffle_Volume*Baffle_Count_HTP; %in^3
144
145 Baffle_System_Volume_HTP = Baffle_Volume_HTP+Vertical_Angle_Volume_HTP;%in^3
146
147 Volume_difference_HTP = ((4/3)*pi()*Inner_Radius^3)+...
148 Midsection_Height_HTP*pi()*Inner_Radius^2-...
149 (HTP_Volume+Baffle_System_Volume_HTP);
150
151 if Volume_difference_HTP < 99
152     Midsection_Height_HTP = Midsection_Height_HTP + 0.01;
153 elseif Volume_difference_HTP > 101
154     Midsection_Height_HTP = Midsection_Height_HTP - 0.01;
155 end
156 end
157
158 %% Probability of Failure Analysis
159 % Variable Initiation
160 Material = 1;
161 % 1 = Carbon Fiber / Epoxy
162 % 2 = Kevlar Fiber / Epoxy
163 % 3 = Glass Fiber / Epoxy
164
165 Expected_Burst_Strength = MEOP*1.075; %.....Psi
166 Percent_ULT = (MEOP/Expected_Burst_Strength)*100;
167 Loading_Time = 1; %.....Hours
168
169 if Material == 1
170     fprintf('Material: Carbon Fiber / Epoxy\n')
171     Alpha = 0.20;
172     Beta = (1.4*(10^51))*(10^(-0.515*Percent_ULT));
173 else if Material == 2
174     fprintf('Material: Kevlar Fiber / Epoxy\n')
175     Alpha = 0.93;
176     Beta = (2.0*(10^18))*(10^(-0.198*Percent_ULT));
177 else if Material == 3
178     fprintf('Material: Glass Fiber / Epoxy\n')

```

```

179     Alpha = 1.00;
180     Beta = (1.4*(10^13))*(10^(-0.158*Percent_ULT));
181 else
182     fprintf('Error: Please Select Material Option\n')
183 end
184 end
185 end
186 fprintf('Maximum Expected Operating Pressure           = %0.2f Psi\n',...
187         MEOP)
188 % fprintf('Expected Burst Pressure                       = %0.2f Psi\n',...
189 %     Expected_Burst_Strength)
190 fprintf('Percent loading of ultimate burst strength     = %0.3f \n',...
191         Percent_ULT)
192
193 Probability_of_Survival = exp(-((Loading_Time/Beta))^Alpha);
194
195 while Probability_of_Survival < 0.999
196 Percent_ULT = (MEOP/Expected_Burst_Strength)*100;
197 if Material == 1
198     Alpha = 0.20;
199     Beta = (1.4*(10^51))*(10^(-0.515*Percent_ULT));
200 else if Material == 2
201     Alpha = 0.93;
202     Beta = (2.0*(10^18))*(10^(-0.198*Percent_ULT));
203 else if Material == 3
204     Alpha = 1.00;
205     Beta = (1.4*(10^13))*(10^(-0.158*Percent_ULT));
206 else
207     fprintf('Error: Please Select Material Option\n')
208 end
209 end
210 end
211 Probability_of_Survival = exp(-((Loading_Time/Beta))^Alpha);
212 Expected_Burst_Strength = Expected_Burst_Strength+1; %.....Psi
213 end
214 fprintf('Required Burst Strength Survive Prob. of 0.999 = %0.2f Psi\n',...
215         Expected_Burst_Strength)
216 Pressure = Expected_Burst_Strength;
217 %% Material Properties
218 % Reference: Daniel, I. M., and Ishai, O., 2006, Engineering Mechanics
219 %           of Composite Materials, Oxford University Press, New York.
220 %           Table A.2 & Table A.3
221
222 %% Reinforcement: AS4 Carbon Fiber
223 %   Fiber_Density = 0.0647; %.....lb/in^3
224 %   Fiber_Longitudinal_Modulus = 3.408*(10^7); %.....Psi
225 %   Fiber_Transverse_Modulus = 2.176*(10^6); %.....Psi
226 %   Fiber_Axial_Shear_Modulus = 3.916*(10^6); %.....Psi
227 %   Fiber_Transverse_Shear_Modulus = 1.015*(10^6); %.....Psi
228 %   Fiber_Poissons_Ratio = 0.2;
229 %   Fiber_Longitudinal_Tensile_Strength = 536640; %.....Psi;
230 %   Fiber_Longitudinal_CTE = -0.3; %((10^-6)/F)
231 %   Fiber_Transverse_CTE = 8.3; %((10^-6)/F)
232
233 %% Reinforcement: Toray T1000G Carbon Fiber
234 Fiber_Density = 0.0650291; %.....lb/in^3
235 Fiber_Longitudinal_Modulus = 43*(10^6); %.....Psi
236 Fiber_Transverse_Modulus = 2.176*(10^6); %.....Psi
237 Fiber_Axial_Shear_Modulus = 3.916*(10^6); %.....Psi
238 Fiber_Transverse_Shear_Modulus = 1.015*(10^6); %.....Psi

```

```

239 Fiber_Poissons_Ratio = 0.2;
240 Fiber_Longitudinal_Tensile_Strength = 924000; %.....Psi;
241 Fiber_Longitudinal_CTE = -0.6; %.....(10^-6)/F
242 Fiber_Transverse_CTE = 8.3; %.....(10^-6)/F
243
244 %% Matrix: 3501-6 Epoxy
245 Matrix_Density = 0.0361273; %.....lb/in^3
246 Matrix_Youngs_Modulus = 623662; %.....Psi
247 Matrix_Shear_Modulus = 232060; %.....Psi
248 Matrix_Poissons_Ratio = 0.35;
249 Matrix_Tensile_Strength = 10007.6; %.....Psi
250 Matrix_Compressive_Strength = 29007.5; %.....Psi
251 Matrix_Shear_Strength = 14503.8; %.....Psi
252 Matrix_CTE = 25; %.....(10^-6)/F
253 Matrix_Glass_Transition_Temperture = 390; %.....(10^-6)/F
254 Matrix_Maximum_Use_Temperature = 300; %.....F
255
256 %% Liner
257
258 if Liner_Material == 1;
259     % 6061-T6 Aluminum
260     Liner_Density = 0.0975; %lb/in^3
261     Liner_Youngs_Modulus = 1*(10^7); %Psi
262     Liner_Shear_Modulus = 3770000; %Psi
263     Liner_Tensile_Yeild_Strength = 40000; %Psi
264     Liner_Shear_Strength = 30000; %Psi
265     Liner_Poissons_Ratio = 0.33;
266
267 else if Liner_Material == 2;
268     % 304 Stainless Steel
269     Liner_Density = 0.289; %lb/in^3
270     Liner_Youngs_Modulus = 2.8*(10^7); %Psi
271     Liner_Shear_Modulus = 1.25*(10^7); %Psi
272     Liner_Tensile_Yeild_Strength = 31200; %Psi
273     Liner_Poissons_Ratio = 0.29;
274
275 else
276     % Rigid PVC
277     Liner_Density = 0.050; %lb/in^3
278     Liner_Youngs_Modulus = 435113; %Psi
279     Liner_Tensile_Yeild_Strength = 5801; %Psi
280     Liner_Poissons_Ratio = 0.32;
281     end
282 end
283
284 %% Thermal Conditions
285 Cure_Temperature = 300; %F
286 Testing_Temperature = 72; %F
287
288 %% Variable Definitions
289 lt = Lamina_Thickness;%inches
290 Lt = Laminate_Thickness;%inches
291 Vf = Fiber_Volume_Fraction;
292 Vm = Matrix_Volume_Fraction;
293 E1f = Fiber_Longitudinal_Modulus;%Psi
294 E2f = Fiber_Transverse_Modulus;%Psi
295 G12f = Fiber_Axial_Shear_Modulus;%Psi
296 G23f = Fiber_Transverse_Shear_Modulus;%Psi
297 v12f = Fiber_Poissons_Ratio;
298 F1ft = Fiber_Longitudinal_Tensile_Strength;%Psi

```

```

299 a1f = Fiber_Longitudinal_CTE*10^-6;%(/F)
300 a2f = Fiber_Transverse_CTE*10^-6;%(/F)
301 pm = Matrix_Density;%lb/in^3
302 Em = Matrix_Youngs_Modulus;%Psi
303 Gm = Matrix_Shear_Modulus;%Psi
304 vm = Matrix_Poissons_Ratio;
305 Fmt = Matrix_Tensile_Strength;%Psi
306 Fmc = Matrix_Compressive_Strength;%Psi
307 Fms = Matrix_Shear_Strength;%Psi
308 am = Matrix_CTE*10^-6;%((10^-6)/F)
309 Tg = Matrix_Glass_Transition_Temperture;%F
310 Tmax = Matrix_Maximum_Use_Temperature;%F
311 Ttest = Testing_Temperature;%F
312 Tcure = Cure_Temperature;%F
313
314 %% Lamina Level Properties
315
316 E1 = Vf*E1f+Vm*Em;
317 E2 = (Em*E2f)/(Vf*Em+Vm*E2f);
318 G12 = (Gm*G12f)/(Vf*Gm+Vm*G12f);
319 v12 = Vf*v12f+Vm*vm;
320 v21 = (E2*v12)/E1;
321
322 Q11 = (E1./(1-v12.*v21));
323 Q12 = (v12.*E2)/(1-v12.*v21);
324 Q22 = (E2./(1-v12.*v21));
325 Q66 = G12;
326
327 m = cosd(Orientation);
328 n = sind(Orientation);
329
330
331
332 Zero = zeros(1,Number_of_plies);
333 One = ones(1,Number_of_plies);
334 for k = 1:Number_of_plies
335 Qp = [Q11*One Q12*One Zero;Q12*One Q22*One Zero;Zero Zero Q66*One];
336 end
337 for k = 1:Number_of_plies
338 Q{k} = Qp(:,[k k+Number_of_plies k+2*Number_of_plies]);
339 end
340
341 Q11bar = Q11.*(m.^4)+2*(Q12+2*Q66).*(m.^2).*(n.^2)+Q22.*(n.^4);
342 Q12bar = (Q11+Q22-4*Q66).*(m.^2).*(n.^2)+Q12.*((n.^4)+(m.^4));
343 Q22bar = Q11.*(n.^4)+2*(Q12+2*Q66).*(m.^2).*(n.^2)+Q22.*(m.^4);
344 Q16bar = (Q11-Q12-2*Q66).*(m.^3).*n+(Q12-Q22+2*Q66).*m.*(n.^3);
345 Q26bar = (Q11-Q12-2*Q66).*(n.^3).*m+(Q12-Q22+2*Q66).*n.*(m.^3);
346 Q66bar = (Q11+Q22-2*Q12-2*Q66).*(m.^2).*(n.^2)+Q66.*((n.^4)+(m.^4));
347
348 Qb = [Q11bar Q12bar Q16bar;Q12bar Q22bar Q26bar;Q16bar Q26bar Q66bar];
349 Qbar = cell(Number_of_plies,1);
350 for k = 1:Number_of_plies
351 Qbar{k} = Qb(:,[k k+Number_of_plies k+2*Number_of_plies]);
352 end
353
354
355 %% Lamina Properties Text Output
356 % fprintf('%s\n','----- Principal Lamina Level Properties -----')
357 % fprintf('Longitudinal Modulus (E1) = %0.4f Psi\n',E1(:,1))
358 % fprintf('Transverse Modulus (E2) = %0.4f Psi\n',E2(:,1))

```

```

359 %     fprintf('Shear Modulus (G12) = %0.4f Psi\n',G12(:,1))
360 %     fprintf('Poissons ratio (v12) = %0.4f \n',v12(:,1))
361
362 %% Lamina Thermal Properties
363 a1 = (E1f*a1f*Vf+Em*am*Vm)/(E1f*Vf+Em*Vm);
364 a2 = a2f*Vf*(1+v12f*(a1f/a2f))+am*Vm*(1+vm)-(v12f*Vf+vm*Vm)*...
365     ((E1f*a1f*Vf+Em*am*Vm)./E1);
366     %% Lamina Thermal Properties Text Output
367 %     fprintf('Longitudinal CTE = %0.4f (10^-6/F) \n',a1(:,1)*10^6)
368 %     fprintf('Transverse CTE = %0.4f (10^-6/F) \n',a2(:,1)*10^6)
369
370 %% Lamina Strengths
371     %% Principal Longitudinal Tension
372     % Fiber First Criteria
373     F1t_ff = F1ft*Vf; % for E1f >> Em
374     % Matrix first Criteria
375     F1t_mf = Fmt*(Vf*(E1f/Em)+Vm); %for strain ult(fiber > matrix)
376
377     % Failure mode
378     if E1f > Em*10
379         F1t = F1t_ff;
380     else F1t = F1t_mf;
381     end
382
383     %% Principal Longitudinal Compression
384     % High Fiber Volume Fraction
385     F1c_LVf = 2*Vf*((Em*E1f*Vf)/(3*Vm))^(1/2);
386     % Low Fiber Volume Fraction
387     F1c_HVf = Gm/(Vm);
388
389     % Failure mode
390     if Vf >= 0.30
391         F1c = F1c_HVf;
392     else
393         F1c = F1c_LVf;
394     end
395
396     %% Principal Transverse Tension
397     K_sigma = (1-Vf*(1-(Em/E2f)))/(1-((4*Vf)/pi())^(1/2)*(1-(Em/E2f)));
398     K_epsilon = 1/(1-((4*Vf)/pi())^(1/2)*(1-(Em/E2f)));
399     % assuming no residual radial stress
400     F2t = (1/K_sigma)*Fmt;
401
402     %% Principal Transverse Compression
403     % assuming no residual radial stress
404     F2c = Fmc/K_sigma;
405
406     %% Principal In-Plane Shear
407     K_tau = (1-Vf*(1-(Gm/G12f)))/(1-((4*Vf)/pi())^(1/2)*(1-(Gm/G12f)));
408     F6 = Fms/K_tau;
409
410     %% Lamina Strength Text Output
411
412 %     fprintf('Longitudinal tensile strength (F1t) = %0.4f Psi\n',F1t)
413 %     fprintf('Longitudinal compressive strength (F1c) = %0.4f Psi\n',F1c)
414 %     fprintf('Transverse tensile strength (F2t) = %0.4f Psi\n',F2t)
415 %     fprintf('Transverse compressive strength (F2c) = %0.4f Psi\n',F2c)
416 %     fprintf('In-plane shear strength (F6) = %0.4f Psi\n',F6)
417
418 %% Laminate ABD Matrix

```

```

419 % fprintf('%s\n','')
420 % fprintf('----- Laminate ABD Matrix -----')
421
422 zk = cell(Number_of_plies,1);
423 zk{1} = lt{1};
424 for k = 2:Number_of_plies
425     zk{k} = lt{k} + zk{k-1};
426 end
427 zk = cell2mat(zk) - Lt/2;
428 zk_1 = zk - cell2mat(reshape(lt,[Number_of_plies,1]));
429 zk = num2cell(zk);
430 zk_1 = num2cell(zk_1);
431
432 A = cell(Number_of_plies,1);
433 for k = 1:Number_of_plies
434     A{k} = Qbar{k}*(zk{k}-zk_1{k});
435 end
436 A = sum(cat(3,A{:}),3);
437 A(A < 10^-12 & A > -10^-12) = 0;
438
439 B = cell(Number_of_plies,1);
440 for k = 1:Number_of_plies
441     B{k} = 1/2.*(Qbar{k}*(zk{k}.^2 - zk_1{k}.^2));
442 end
443 B = sum(cat(3,B{:}),3);
444 B(B < 10^-12 & B > -10^-12) = 0;
445
446 D = cell(Number_of_plies,1);
447 for k = 1:Number_of_plies
448     D{k} = 1/3.*(Qbar{k}*(zk{k}.^3 - zk_1{k}.^3));
449 end
450 D = sum(cat(3,D{:}),3);
451 D(D < 10^-12 & D > -10^-12) = 0;
452
453 ABD = [A B;B D];
454
455
456 %% Laminate Compliance Matrix
457
458 B_star = -(inv(A))*B;
459 B_star(B_star < 10^-12 & B_star > -10^-12) = 0;
460 C_star = B*(inv(A));
461 C_star(C_star < 10^-12 & C_star > -10^-12) = 0;
462 D_star = D - C_star*B;
463 D_star(D_star < 10^-12 & D_star > -10^-12) = 0;
464
465 a = (inv(A))-(B_star*(inv(D_star)))*C_star;
466 b = B_star*(inv(D_star));
467 c = -(inv(D_star))*C_star;
468 d = inv(D_star);
469
470 %% Effective Laminate Properties
471
472 % fprintf('%s\n','')
473 % fprintf('----- Effective Laminate Properties -----')
474
475 E_x = 1/(Lt*a(1,1));
476 E_y = 1/(Lt*a(2,2));
477 G_xy = 1/(Lt*a(3,3));
478 v_xy = -(a(2,1)/a(1,1));

```



```

479 v_yx = -(a(1,2)/a(2,2));
480 n_sx = a(1,3)/a(3,3);
481 if n_sx < 10^-12 & n_sx > -10^-12
482     n_sx = 0;
483 end
484 n_xs = a(3,1)/a(1,1);
485 if n_xs < 10^-12 & n_xs > -10^-12
486     n_xs = 0;
487 end
488 n_ys = a(3,2)/a(2,2);
489 if n_ys < 10^-12 & n_ys > -10^-12
490     n_ys = 0;
491 end
492 n_sy = a(2,3)/a(3,3);
493 if n_sy < 10^-12 & n_sy > -10^-12
494     n_sy = 0;
495 end
496
497 %% Composite Density
498 Composite_Density = Vf*Fiber_Density + Vm*Matrix_Density;
499
500 %% Laminate Level Properties Output
501
502 %     fprintf('Axial modulus (Ex) = %0.4f Psi\n',E_x)
503 %     fprintf('Transverse modulus (Ey) = %0.4f Psi\n',E_y)
504 %     fprintf('Shear modulus (Gxy) = %0.4f Psi\n',G_xy)
505 %     fprintf('Poissons ratio xy (vxy) = %0.4f\n',v_xy)
506 %     fprintf('Poissons ratio yx (vyx) = %0.4f\n',v_yx)
507 %     fprintf('Shear coupling coefficient (nsx) = %0.4f\n',n_sx)
508 %     fprintf('Shear coupling coefficient (nxs) = %0.4f\n',n_xs)
509 %     fprintf('Shear coupling coefficient (nsy) = %0.4f\n',n_sy)
510 %     fprintf('Shear coupling coefficient (nys) = %0.4f\n',n_ys)
511 %     fprintf('Composite Density = %0.4f lb/in^3\n',Composite_Density)
512
513 %% Thermal Analysis
514
515     %% Global CTEs
516     ax = a1.*(m.^2)+a2.*(n.^2);
517     ay = a1.*(n.^2)+a2.*(m.^2);
518     axy = 2*(a1-a2).*m.*n;
519     dT = Cure_Temperature - Testing_Temperature;
520     ex = ax*dT;
521     ey = ay*dT;
522     exy = axy*dT;
523
524     avg_ax = sum(ax)/Number_of_plyies;
525     avg_ay = sum(ay)/Number_of_plyies;
526 %fprintf('Axial coefficient of thermal expansion = %0.4f\n',avg_ax*10^6)
527 %fprintf('Transverse coefficient of thermal expansion = %0.4f\n',avg_ay*10^6)
528
529     ET = [ex;ey;exy];
530     eT = cell(Number_of_plyies,1);
531     for k = 1:Number_of_plyies
532         eT{k} = ET(:,[k]);
533     end
534
535     %% Thermal Forces
536     NT = cell(Number_of_plyies,1);
537     for k = 1:Number_of_plyies
538         NT{k} = Qbar{k}*(eT{k})*lt{k};

```

```

539     end
540     NT = sum(cat(3,NT{:}),3);
541     NT(NT < 10^-12 & NT > -10^-12) = 0;
542
543     %% Thermal Moments
544
545     zk_bar = cell2mat(reshape(zk,[1,Number_of_plies])) - cell2mat(lt)/2;
546     zk_bar(zk_bar < 10^-12 & zk_bar > -10^-12) = 0;
547     zk_bar = num2cell(zk_bar);
548
549     MT = cell(Number_of_plies,1);
550     for k = 1:Number_of_plies
551         MT{k} = Qbar{k}*(eT{k})*zk_bar{k}*lt{k};
552     end
553     MT = sum(cat(3,MT{:}),3);
554     MT(MT < 10^-12 & MT > -10^-12) = 0;
555
556     %% Thermal Midplane Strain - Global Coordinates
557     Epsilon_0_T_xy = a*NT+b*MT;
558     Epsilon_0_T_xy(isnan(Epsilon_0_T_xy)) = 0;
559     Epsilon_0_T_xy(Epsilon_0_T_xy < 10^-12 & Epsilon_0_T_xy > -10^-12) = 0;
560
561     %% Thermal Midplane Curvature - Global Coordinates
562     Kappa_T_xy = c*NT+d*MT;
563     Kappa_T_xy(isnan(Kappa_T_xy)) = 0;
564     Kappa_T_xy(Kappa_T_xy < 10^-12 & Kappa_T_xy > -10^-12) = 0;
565
566     %% Net Thermal Strains in Lamina - Global Coordinates
567     Epsilon_T_xy = cell(Number_of_plies,1);
568     for k = 1:Number_of_plies
569         Epsilon_T_xy{k} = Epsilon_0_T_xy+lt{k}*zk{k}*Kappa_T_xy;
570     end
571
572     %% Thermal Elastic Strains in Lamina - Global Coordinates
573     Epsilon_Te_xy = cell(Number_of_plies,1);
574     for k = 1:Number_of_plies
575         Epsilon_Te_xy{k} = Epsilon_T_xy{k}-eT{k};
576     end
577
578     %% Residual Thermal Strains in Lamina - Principal Coordinates
579     T11 = m.^2;
580     T12 = n.^2;
581     T13 = 2*m.*n;
582     T23 = -2*m.*n;
583     T31 = -m.*n;
584     T32 = m.*n;
585     T33 = (m.^2)-(n.^2);
586     trans = [T11 T12 T13;T12 T11 T23;T31 T32 T33];
587     T = cell(Number_of_plies,1);
588     for k = 1:Number_of_plies
589         T{k} = trans(:,[k k+Number_of_plies k+2*Number_of_plies]);
590     end
591
592     Epsilon_T_12 = cell(Number_of_plies,1);
593     for k = 1:Number_of_plies
594         Epsilon_T_12{k} = T{k}*Epsilon_T_xy{k};
595     end
596
597     %% Residual Thermal Stresses in Lamina - Principal Coordinates
598     Sigma_T_12 = cell(Number_of_plies,1);

```

```

599     for k = 1:Number_of_plies
600     Sigma_T_12{k} = Q{k}*Epsilon_T_12{k};
601     end
602     Sig_T_12 = (cell2mat(Sigma_T_12));
603     Sig_T_12(isnan(Sig_T_12)) = 0;
604     threes = 3*ones(1,Number_of_plies);
605     Sigma_T_12 = mat2cell(Sig_T_12,threes,[1]);
606
607     for k = 1:Number_of_plies
608     Net_Sig_Therm{k} = Qbar{k}*Epsilon_T_xy{k};
609     end
610     Net_Thermal_Stress = sum(cat(3,Net_Sig_Therm{:}),3);
611
612 %% Mechanical Analysis
613
614 %% Mechanical Stress in Laminate - Global Coordinates
615 Sigma_Long = (Pressure*Radius)/(2*Laminate_Thickness);
616 Sigma_Hoop = (Pressure*Radius)/Laminate_Thickness;
617
618 Sigma_xy = [Sigma_Long; Sigma_Hoop; 0];
619
620 %% Mechanical Strains in Laminate - Global Coordinates
621
622 Inverse_Modulus_Matrix = [1/E_x -v_yx/E_y n_sx/G_xy;...
623                          -v_xy/E_x 1/E_y n_sy/G_xy;...
624                          n_xs/E_x n_ys/E_y 1/G_xy];
625
626 Epsilon_xy = Inverse_Modulus_Matrix * Sigma_xy;
627
628 %% Net Mechanical Strains in Lamina - Principal Coordinates
629 T11 = m.^2;
630 T12 = n.^2;
631 T13 = 2*m.*n;
632 T23 = -2*m.*n;
633 T31 = -m.*n;
634 T32 = m.*n;
635 T33 = (m.^2)-(n.^2);
636 trans = [T11 T12 T13;T12 T11 T23;T31 T32 T33];
637 T = cell(Number_of_plies,1);
638 for k = 1:Number_of_plies
639 T{k} = trans(:,[k k+Number_of_plies k+2*Number_of_plies]);
640 end
641
642 Epsilon_12 = cell(Number_of_plies,1);
643 for k = 1:Number_of_plies
644 Epsilon_12{k} = T{k}*Epsilon_xy;
645 end
646
647 %% Mechanical Stresses in Lamina - Principal Coordinates
648 Sigma_12 = cell(Number_of_plies,1);
649 for k = 1:Number_of_plies
650 Sigma_12{k} = Q{k}*Epsilon_12{k};
651 end
652
653 %% Net Stress in Lamina - Principal Coordinates
654 Net_Sigma_12 = cell(Number_of_plies,1);
655 for k = 1:Number_of_plies
656 Net_Sigma_12{k} = Sigma_12{k}+Sigma_T_12{k};
657 end
658

```

```

659 Net_Sigma_12 = reshape(Net_Sigma_12,[1 Number_of_plyies]);
660 stress_mat = cell2mat(Net_Sigma_12);
661 Sigma_1 = stress_mat(1,:);
662 Sigma_2 = stress_mat(2,:);
663 Tau_6 = stress_mat(3,:);
664
665     %% Net Strain in Lamina - Principal Coordinates
666     Net_Epsilon_12 = cell(Number_of_plyies,1);
667     for k = 1:Number_of_plyies
668         Net_Epsilon_12{k} = Epsilon_12{k}+Epsilon_T_12{k};
669     end
670
671 Net_Epsilon_12 = reshape(Net_Epsilon_12,[1 Number_of_plyies]);
672 Strain_mat = cell2mat(Net_Epsilon_12);
673 Epsilon_1 = Strain_mat(1,:);
674 Epsilon_2 = Strain_mat(2,:);
675 Gamma_6 = Strain_mat(3,:);
676 %% Tsai-Wu failure analysis
677 f1 = (1/F1t)-(1/F1c);
678 f11 = 1/(F1t*F1c);
679 f2 = (1/F2t)-(1/F2c);
680 f22 = 1/(F2t*F2c);
681 f6 = 1/(F6^2);
682 f12 = -(1/2)*((f11*f22)^(1/2));
683 a_TW = f11.*(Sigma_1.^2)+f22.*(Sigma_2.^2)+...
684         f6.*(Tau_6.^2)+2.*f12.*Sigma_1.*Sigma_2;
685 b_TW = f1.*Sigma_1+f2.*Sigma_2;
686
687 Tsai_Wu_quadratic = a_TW+b_TW-1 == 0;
688
689 Sft_TW = (-b_TW+(((b_TW.^2)+4.*a_TW).^(1/2)))/(2.*a_TW);
690 Sft_TW(isnan(Sft_TW)) = 0;
691 Sfc_TW = abs(-b_TW-(((b_TW.^2)+4.*a_TW).^(1/2)))/(2.*a_TW);
692 Sfc_TW(isnan(Sfc_TW)) = 0;
693
694 Tension_Test_Pass = [Sft_TW > 1];
695 Tension_Test_Fail = [Sft_TW < 1];
696 Compression_Test_Pass = [Sfc_TW > 1];
697 Compression_Test_Fail = [Sfc_TW < 1];
698
699 %% Maximum Stress failure analysis
700 Failure_Stress_1_Direction = cell(Number_of_plyies,1);
701 for k = 1:Number_of_plyies
702     if Sigma_1(k)>0
703         Failure_Stress_1_Direction{k} = F1t/(cos(Orientation(k))^2);
704     else
705         Failure_Stress_1_Direction{k} = F1c/(cos(Orientation(k))^2);
706     end
707 end
708
709 Failure_Stress_2_Direction = cell(Number_of_plyies,1);
710 for k = 1:Number_of_plyies
711     if Sigma_2(k)>0
712         Failure_Stress_2_Direction{k} = F2t/(sin(Orientation(k))^2);
713     else
714         Failure_Stress_2_Direction{k} = F2c/(sin(Orientation(k))^2);
715     end
716 end
717
718 Failure_Stress_6_Direction = cell(Number_of_plyies,1);

```

```

719 for k = 1:Number_of_plies
720 if Tau_6(k)>0
721 Failure_Stress_6_Direction{k} = F6/(cos(Orientation(k))*sin(Orientation(k)));
722 else
723 Failure_Stress_6_Direction{k} = F6/(cos(Orientation(k))*sin(Orientation(k)));
724 end
725 end
726
727 Max_Stress_Pass_1_Direction = cell(Number_of_plies,1);
728 for k = 1:Number_of_plies
729 if Failure_Stress_1_Direction{k} > 0
730 if Failure_Stress_1_Direction{k} - Sigma_1(k)>0
731 Max_Stress_Pass_1_Direction{k} = 1;
732 else
733 Max_Stress_Pass_1_Direction{k} = 0;
734 end
735 else
736 if Failure_Stress_1_Direction{k} - Sigma_1(k)<0
737 Max_Stress_Pass_1_Direction{k} = 1;
738 else
739 Max_Stress_Pass_1_Direction{k} = 0;
740 end
741 end
742 end
743
744 Max_Stress_Pass_2_Direction = cell(Number_of_plies,1);
745 for k = 1:Number_of_plies
746 if Failure_Stress_2_Direction{k} > 0
747 if Failure_Stress_2_Direction{k} - Sigma_2(k)>0
748 Max_Stress_Pass_2_Direction{k} = 1;
749 else
750 Max_Stress_Pass_2_Direction{k} = 0;
751 end
752 else
753 if Failure_Stress_2_Direction{k} - Sigma_2(k)<0
754 Max_Stress_Pass_2_Direction{k} = 1;
755 else
756 Max_Stress_Pass_2_Direction{k} = 0;
757 end
758 end
759 end
760
761 Max_Stress_Pass_6_Direction = cell(Number_of_plies,1);
762 for k = 1:Number_of_plies
763 if Failure_Stress_6_Direction{k} > 0
764 if Failure_Stress_6_Direction{k} - Tau_6(k)>0
765 Max_Stress_Pass_6_Direction{k} = 1;
766 else
767 Max_Stress_Pass_6_Direction{k} = 0;
768 end
769 else
770 if Failure_Stress_6_Direction{k} - Tau_6(k)<0
771 Max_Stress_Pass_6_Direction{k} = 1;
772 else
773 Max_Stress_Pass_6_Direction{k} = 0;
774 end
775 end
776 end
777
778 if sum(cell2mat(Max_Stress_Pass_1_Direction)) == Number_of_plies &&...

```

```

779     sum(cell2mat(Max_Stress_Pass_2_Direction)) == Number_of_plies &&...
780     sum(cell2mat(Max_Stress_Pass_6_Direction)) == Number_of_plies
781 Max_Stress_Failure_Analysis = 1;
782 else
783 Max_Stress_Failure_Analysis = 0;
784 end
785
786 %% Maximum Strain failure analysis
787 Failure_Strain_1_Direction = cell(Number_of_plies,1);
788 for k = 1:Number_of_plies
789 if Epsilon_1(k)>0
790 Failure_Strain_1_Direction{k} = F1t/E1;
791 else
792 Failure_Strain_1_Direction{k} = -F1c/E1;
793 end
794 end
795
796 Failure_Strain_2_Direction = cell(Number_of_plies,1);
797 for k = 1:Number_of_plies
798 if Epsilon_2(k)>0
799 Failure_Strain_2_Direction{k} = F2t/E2;
800 else
801 Failure_Strain_2_Direction{k} = -F2c/E2;
802 end
803 end
804
805 Failure_Strain_6_Direction = cell(Number_of_plies,1);
806 for k = 1:Number_of_plies
807 Failure_Strain_6_Direction{k} = F6/G12;
808 end
809
810 Max_Strain_Pass_1_Direction = cell(Number_of_plies,1);
811 for k = 1:Number_of_plies
812 if Failure_Strain_1_Direction{k} > 0
813 if Failure_Strain_1_Direction{k} - Epsilon_1(k)>0
814 Max_Strain_Pass_1_Direction{k} = 1;
815 else
816 Max_Strain_Pass_1_Direction{k} = 0;
817 end
818 else
819 if Failure_Strain_1_Direction{k} - Epsilon_1(k)<0
820 Max_Strain_Pass_1_Direction{k} = 1;
821 else
822 Max_Strain_Pass_1_Direction{k} = 0;
823 end
824 end
825 end
826
827 Max_Strain_Pass_2_Direction = cell(Number_of_plies,1);
828 for k = 1:Number_of_plies
829 if Failure_Strain_2_Direction{k} > 0
830 if Failure_Strain_2_Direction{k} - Epsilon_2(k)>0
831 Max_Strain_Pass_2_Direction{k} = 1;
832 else
833 Max_Strain_Pass_2_Direction{k} = 0;
834 end
835 else
836 if Failure_Strain_2_Direction{k} - Epsilon_2(k)<0
837 Max_Strain_Pass_2_Direction{k} = 1;
838 else

```

```

839 Max_Strain_Pass_2_Direction{k} = 0;
840 end
841 end
842 end
843
844 Max_Strain_Pass_6_Direction = cell(Number_of_plies,1);
845 for k = 1:Number_of_plies
846 if Failure_Strain_6_Direction{k} > 0
847 if Failure_Strain_6_Direction{k} - Gamma_6(k)>0
848 Max_Strain_Pass_6_Direction{k} = 1;
849 else
850 Max_Strain_Pass_6_Direction{k} = 0;
851 end
852 else
853 if Failure_Strain_6_Direction{k} - Gamma_6(k)<0
854 Max_Strain_Pass_6_Direction{k} = 1;
855 else
856 Max_Strain_Pass_6_Direction{k} = 0;
857 end
858 end
859 end
860
861 if sum(cell2mat(Max_Strain_Pass_1_Direction)) == Number_of_plies &&...
862     sum(cell2mat(Max_Strain_Pass_2_Direction)) == Number_of_plies &&...
863     sum(cell2mat(Max_Strain_Pass_6_Direction)) == Number_of_plies
864 Max_Strain_Failure_Analysis = 1;
865 else
866 Max_Strain_Failure_Analysis = 0;
867 end
868
869 %% Tsai-Hill failure analysis
870
871 F1_TH = cell(Number_of_plies,1);
872 for k = 1:Number_of_plies
873 if Sigma_1(k)>0
874 F1_TH{k} = F1t;
875 else
876 F1_TH{k} = F1c;
877 end
878 end
879
880 F2_TH = cell(Number_of_plies,1);
881 for k = 1:Number_of_plies
882 if Sigma_1(k)>0
883 F2_TH{k} = F2t;
884 else
885 F2_TH{k} = F2c;
886 end
887 end
888
889 F6_TH = cell(Number_of_plies,1);
890 for k = 1:Number_of_plies
891 F6_TH{k} = F6;
892 end
893
894 A_TH = 1./((cell2mat(F1_TH)') .^2);
895 B_TH = 1./((cell2mat(F2_TH)') .^2);
896 C_TH = -1./((cell2mat(F1_TH)') .^2);
897 D_TH = 1./((cell2mat(F6_TH)') .^2);
898

```

```

899
900 Tsai_Hill_Pass_Fail = cell(Number_of_plies,1);
901 for k = 1:Number_of_plies
902 Tsai_Hill_Pass_Fail{k} = (A_TH(k)*Sigma_1(k)^2)+(B_TH(k)*Sigma_2(k)^2)+...
903 (C_TH(k)*Sigma_1(k)*Sigma_2(k))+...
904 (D_TH(k)*Tau_6(k)^2);
905 end
906
907 if sum(cell2mat(Tsai_Hill_Pass_Fail)) < Number_of_plies
908 Tsai_Hill_Failure_Analysis = 1;
909 else
910 Tsai_Hill_Failure_Analysis = 0;
911 end
912
913 %% FAILURE ANALYSIS CRITERIA SELECTION
914
915 % Tsai_Wu = 1
916 % Maximum_Stress = 2
917 % Maximum_Strain = 3
918 % Tsai_Hill = 4
919
920 Failure_Mode_Analysis_Criteria = 1 ;
921
922 %% Results
923 fprintf('%s\n','')
924
925 if Failure_Mode_Analysis_Criteria == 1
926     if Tension_Test_Pass == One & Compression_Test_Pass == One
927         fprintf('For Tsai-Wu failure criteria tank = Pass\n')
928     else fprintf('For Tsai-Wu failure criteria tank = Fail\n')
929     end
930
931 elseif Failure_Mode_Analysis_Criteria == 2
932     if Max_Stress_Failure_Analysis == 1
933         fprintf('For maximum stress failure criteria tank = Pass\n')
934     else fprintf('For maximum stress failure criteria tank = Fail\n')
935     end
936
937 elseif Failure_Mode_Analysis_Criteria == 3
938     if Max_Strain_Failure_Analysis == 1
939         fprintf('For maximum strain failure criteria tank = Pass\n')
940     else fprintf('For maximum strain failure criteria tank = Fail\n')
941     end
942
943 elseif Failure_Mode_Analysis_Criteria == 4
944     if Tsai_Hill_Failure_Analysis == 1
945         fprintf('For Tsai-Hill failure criteria tank = Pass\n')
946     else fprintf('For Tsai-Hill failure criteria tank = Fail\n')
947     end
948 else fprintf('Please select failure analysis criteria\n')
949 end
950 fprintf('%s\n','')
951 fprintf('Common bulkhead tank height = %0.4f in\n',...
952     Total_Tank_Height_CB)
953 fprintf('%s\n','')
954
955 fprintf('Combined individual tank heights = %0.4f in\n',...
956     Combine_Tank_Height_IT)
957 fprintf('Individual HTP tank height = %0.4f in\n',...
958     Height_HTP_IT)

```



```

959 fprintf('Individual RP-1 tank height                = %0.4f in\n',...
960         Height_RP1_IT)
961 fprintf('%s\n','')
962 %% Weight Calculation
963
964 Outer_Radius = Radius+Laminate_Thickness;
965
966 %Common Bulkhead Calculation
967 Liner_Volume_CB = 1.5*(4/3)*pi()*((Radius^3)-(Inner_Radius^3))+ ...
968                 pi()*Midsection_Height_CB*((Radius^2)-(Inner_Radius^2));
969 Liner_Weight_CB = Liner_Density*Liner_Volume_CB;
970 Composite_Volume = (4/3)*pi()*((Outer_Radius^3)-(Radius^3))+ ...
971                 pi()*Midsection_Height_CB*((Outer_Radius^2)-(Radius^2));
972 Composite_Weight = Composite_Density*Composite_Volume;
973 if Tension_Test_Pass == One & Compression_Test_Pass == One
974 Total_Weight_CB = Liner_Weight_CB+Composite_Weight;
975 else Total_Weight_CB = nan
976 end
977
978 %Individual Tank Calculation
979 Liner_Volume_IT = 2*(4/3)*pi()*((Radius^3)-(Inner_Radius^3))+ ...
980                 pi()*Midsection_Height_IT*((Radius^2)-(Inner_Radius^2));
981 Liner_Weight_IT = Liner_Density*Liner_Volume_IT;
982 Composite_Volume = 2*(4/3)*pi()*((Outer_Radius^3)-(Radius^3))+ ...
983                 pi()*Midsection_Height_IT*((Outer_Radius^2)-(Radius^2));
984
985 Composite_Vol_HTP = 2*(4/3)*pi()*((Outer_Radius^3)-(Radius^3))+ ...
986                 pi()*Midsection_Height_HTP*((Outer_Radius^2)-(Radius^2));
987 Composite_Vol_RP1 = 2*(4/3)*pi()*((Outer_Radius^3)-(Radius^3))+ ...
988                 pi()*Midsection_Height_RP1*((Outer_Radius^2)-(Radius^2));
989
990 Liner_Volume_HTP = (4/3)*pi()*((Radius^3)-(Inner_Radius^3))+ ...
991                 pi()*Midsection_Height_HTP*((Radius^2)-(Inner_Radius^2));
992 Liner_Volume_RP1 = (4/3)*pi()*((Radius^3)-(Inner_Radius^3))+ ...
993                 pi()*Midsection_Height_RP1*((Radius^2)-(Inner_Radius^2));
994
995 Liner_Weight_HTP = Liner_Density*Liner_Volume_HTP;
996 Liner_Weight_RP1 = Liner_Density*Liner_Volume_RP1;
997
998 Composite_Weight = Composite_Density*Composite_Volume;
999 Composite_Weight_HTP = Composite_Density*Composite_Vol_HTP; %1b
1000 Composite_Weight_RP1 = Composite_Density*Composite_Vol_RP1; %1b
1001
1002 Weight_HTP_IT = Composite_Weight_HTP+Liner_Weight_HTP; %kg
1003 Weight_RP1_IT = Composite_Weight_RP1+Liner_Weight_RP1; %kg
1004
1005 if Tension_Test_Pass == One & Compression_Test_Pass == One
1006 Total_Weight_IT = Liner_Weight_IT+Composite_Weight;
1007 else Total_Weight_IT = nan
1008 end
1009
1010 Estimate_Buffering_Factor = 1.5;
1011 Propellant_COPV_Safe_Weight_CB = Total_Weight_CB*Estimate_Buffering_Factor;
1012
1013 fprintf('Propellant tank weight common bulkhead design = %0.4f Lb\n',...
1014         Total_Weight_CB)
1015 fprintf('                                           = %0.4f Kg\n',...
1016         Total_Weight_CB*0.453592)
1017
1018 fprintf('Individual HTP tank weight                = %0.4f Lb\n',...

```

```

1019         Weight_HTP_IT)
1020 fprintf('                                     = %0.4f Kg\n',...
1021         Weight_HTP_IT*0.453592)
1022 fprintf('Individual RP-1 tank weight         = %0.4f Lb\n',...
1023         Weight_RP1_IT)
1024 fprintf('                                     = %0.4f Kg\n',...
1025         Weight_RP1_IT*0.453592)
1026
1027 fprintf('Combined tank weight individual tank design = %0.4f Lb\n',...
1028         Total_Weight_IT)
1029 fprintf('                                     = %0.4f Kg\n',...
1030         Total_Weight_IT*0.453592)
1031
1032 fprintf('%s\n','')
1033
1034
1035 %% Excel Output
1036 if Tension_Test_Pass == One & Compression_Test_Pass == One
1037 if Write_to_Excel == 0
1038 return
1039 end
1040 else
1041     fprintf('ERROR HAS OCCURED. CHECK INPUT VALUES AND LOOK FOR "NaN"')
1042     return
1043 end
1044 %%%%%%%%%%%%%%%%%%%%%%%%%%%%%%%%%%%%%%%%%%%%%%%%%%%%%%%%%%%%%%%%%%%%%%%%%
1045 %% General Rocket Info
1046 xlswrite('Master.xlsx',Aero_Optimum_Radius, 'Rocket_Main', 'C3');
1047 xlswrite('Master.xlsx',Radius, 'Rocket_Main', 'C6');
1048 xlswrite('Master.xlsx',Inner_Radius, 'Rocket_Main', 'C7');
1049 xlswrite('Master.xlsx',HTP_Volume, 'Rocket_Main', 'C10');
1050 xlswrite('Master.xlsx',HTP_Density, 'Rocket_Main', 'C11');
1051 xlswrite('Master.xlsx',HTP_Mass, 'Rocket_Main', 'C12');
1052 xlswrite('Master.xlsx',Midsection_Height_HTP, 'Rocket_Main', 'C13');
1053 xlswrite('Master.xlsx',RP1_Volume, 'Rocket_Main', 'C14');
1054 xlswrite('Master.xlsx',RP1_Density, 'Rocket_Main', 'C15');
1055 xlswrite('Master.xlsx',RP1_Mass, 'Rocket_Main', 'C16');
1056 xlswrite('Master.xlsx',Midsection_Height_RP1, 'Rocket_Main', 'C17');
1057 xlswrite('Master.xlsx',Total_Propellant_Mass, 'Rocket_Main', 'C18');
1058 xlswrite('Master.xlsx',MEOP, 'Rocket_Main', 'C19');
1059
1060 %% Composite Properties
1061
1062 % Reinforcement: Toray T1000G Carbon Fiber
1063 xlswrite('Master.xlsx',Fiber_Density, 'Composite', 'C3');
1064 xlswrite('Master.xlsx',Fiber_Longitudinal_Modulus, 'Composite', 'C4');
1065 xlswrite('Master.xlsx',Fiber_Transverse_Modulus, 'Composite', 'C5');
1066 xlswrite('Master.xlsx',Fiber_Axial_Shear_Modulus, 'Composite', 'C6');
1067 xlswrite('Master.xlsx',Fiber_Transverse_Shear_Modulus, 'Composite', 'C7');
1068 xlswrite('Master.xlsx',Fiber_Poissons_Ratio, 'Composite', 'C8');
1069 xlswrite('Master.xlsx',Fiber_Longitudinal_Tensile_Strength, 'Composite', 'C9');
1070 xlswrite('Master.xlsx',Fiber_Longitudinal_CTE, 'Composite', 'C10');
1071 xlswrite('Master.xlsx',Fiber_Transverse_CTE, 'Composite', 'C11');
1072
1073 % Matrix: 3501-6 Epoxy
1074 xlswrite('Master.xlsx',Matrix_Density, 'Composite', 'C14');
1075 xlswrite('Master.xlsx',Matrix_Youngs_Modulus, 'Composite', 'C15');
1076 xlswrite('Master.xlsx',Matrix_Shear_Modulus, 'Composite', 'C16');
1077 xlswrite('Master.xlsx',Matrix_Poissons_Ratio, 'Composite', 'C17');
1078 xlswrite('Master.xlsx',Matrix_Tensile_Strength, 'Composite', 'C18');

```

```

1079 xlswrite('Master.xlsx',Matrix_Compressive_Strength, 'Composite','C19');
1080 xlswrite('Master.xlsx',Matrix_Shear_Strength, 'Composite','C20');
1081 xlswrite('Master.xlsx',Matrix_CTE, 'Composite','C21');
1082 xlswrite('Master.xlsx',Matrix_Glass_Transition_Temperture, 'Composite','C22');
1083 xlswrite('Master.xlsx',Matrix_Maximum_Use_Temperature, 'Composite','C23');
1084
1085 % Composite Lamina Properties
1086 xlswrite('Master.xlsx',Number_of_plies, 'Composite','C26');
1087 xlswrite('Master.xlsx',Fiber_Volume_Fraction, 'Composite','C27');
1088 xlswrite('Master.xlsx',Lamina_Thickness(1,1), 'Composite','C28');
1089 xlswrite('Master.xlsx',E1, 'Composite','C29');
1090 xlswrite('Master.xlsx',E2, 'Composite','C30');
1091 xlswrite('Master.xlsx',G12, 'Composite','C31');
1092 xlswrite('Master.xlsx',v12, 'Composite','C32');
1093 xlswrite('Master.xlsx',a1, 'Composite','C33');
1094 xlswrite('Master.xlsx',a2, 'Composite','C34');
1095 xlswrite('Master.xlsx',F1t, 'Composite','C35');
1096 xlswrite('Master.xlsx',F1c, 'Composite','C36');
1097 xlswrite('Master.xlsx',F2t, 'Composite','C37');
1098 xlswrite('Master.xlsx',F2c, 'Composite','C38');
1099 xlswrite('Master.xlsx',F6, 'Composite','C39');
1100
1101 % Laminate Structure
1102 xlswrite('Master.xlsx',Orientation, 'Composite','G25');
1103
1104 % Composite Laminate Properties
1105 xlswrite('Master.xlsx',E_x, 'Composite','C42');
1106 xlswrite('Master.xlsx',E_y, 'Composite','C43');
1107 xlswrite('Master.xlsx',G_xy, 'Composite','C44');
1108 xlswrite('Master.xlsx',v_xy, 'Composite','C45');
1109 xlswrite('Master.xlsx',v_yx, 'Composite','C46');
1110 xlswrite('Master.xlsx',n_sx, 'Composite','C47');
1111 xlswrite('Master.xlsx',n_xs, 'Composite','C48');
1112 xlswrite('Master.xlsx',n_sy, 'Composite','C49');
1113 xlswrite('Master.xlsx',n_ys, 'Composite','C50');
1114 xlswrite('Master.xlsx',Composite_Density, 'Composite','C51');
1115 xlswrite('Master.xlsx',avg_ax*10^6, 'Composite','C52');
1116 xlswrite('Master.xlsx',avg_ay*10^6, 'Composite','C53');

```

6.1.3 Probability of Failure Analysis Script - MATLAB

```
1 %Probability of Failure Analysis
2 clear;
3 clc;
4
5 %% Variable Initiation
6 fprintf('Variable Initiation:')
7 fprintf('%s\n','')
8
9 Material = 1 ...
10 %     1; %Carbon Fiber / Epoxy
11 %     2; %Kevlar Fiber / Epoxy
12 %     3; %Glass Fiber / Epoxy
13
14 MEOP = 1000; %Psi
15 Expected_Burst_Strength = 1100; %Psi
16 Percent_ULT = (MEOP/Expected_Burst_Strength)*100;
17 Loading_Time = 1; %Hours
18
19 if Material == 1
20     fprintf('Material:                Carbon Fiber / Epoxy\n')
21     Alpha = 0.20;
22     Beta = (1.4*(10^51))*(10^(-0.515*Percent_ULT));
23 else if Material == 2
24     fprintf('Material:                Kevlar Fiber / Epoxy\n')
25     Alpha = 0.93;
26     Beta = (2.0*(10^18))*(10^(-0.198*Percent_ULT));
27 else if Material == 3
28     fprintf('Material:                Glass Fiber / Epoxy\n')
29     Alpha = 1.00;
30     Beta = (1.4*(10^13))*(10^(-0.158*Percent_ULT));
31 else
32     fprintf('Error: Please Select Material Option\n')
33 end
34 end
35 end
36 fprintf('Maximum Expected Operating Pressure      = %0.2f Psi\n',MEOP)
37 fprintf('Expected Burst Pressure                    = %0.2f Psi\n',...
38     Expected_Burst_Strength)
39 fprintf('Percent loading of ultimate burst strength    = %0.2f \n',...
40     Percent_ULT)
41 fprintf('Weibull shape factor                        = %0.2f \n',Alpha)
42 fprintf('Weibull characteristic life                  = %0.2f \n',Beta)
43
44 Probability_of_Survival = exp(-((Loading_Time/Beta))^Alpha);
45 fprintf('Probability of Survival Current Configuration = %0.2f Psi\n',...
46     Expected_Burst_Strength)
47
48
49 while Probability_of_Survival<0.999
50 Percent_ULT = (MEOP/Expected_Burst_Strength)*100;
51 if Material == 1
52     Alpha = 0.20;
53     Beta = (1.4*(10^51))*(10^(-0.515*Percent_ULT));
54 else if Material == 2
55     Alpha = 0.93;
56     Beta = (2.0*(10^18))*(10^(-0.198*Percent_ULT));
57 else if Material == 3
58     Alpha = 1.00;
```

```

59     Beta = (1.4*(10^13))*(10^(-0.158*Percent_ULT));
60 else
61     fprintf('Error: Please Select Material Option\n')
62 end
63 end
64 end
65 Probability_of_Survival = exp(-((Loading_Time/Beta))^Alpha);
66 Expected_Burst_Strength = Expected_Burst_Strength+1; %Psi
67 end
68 fprintf('%s\n', '-----')
69 fprintf('Required Burst Strength Survival Prob. of 0.999 = %0.2f Psi\n',...
70     Expected_Burst_Strength)

```

6.1.4 Slosh Mitigation Baffle Analysis Script- MATLAB

```

1 %% Propellant Tank Baffle Design
2 clear;
3 clc;
4
5 syms zeta w delta d D R F g rho n N m M H;
6
7 %% Miles Expression
8
9 Miles_expression = (2*pi())*2.83*exp(-4.60*(d/R)*((R^2-(R-w)^2)/R^2)^(3/2)...
10 *(zeta/R)^(1/2))- delta == 0;
11
12 Baffle_depth = vpa(solve(Miles_expression,d),5); %inches
13
14 %% O'Neill's Expression
15 ONeill_expression = (2*pi())*2.16*exp(-4.60*(d/R)*((R^2-(R-w)^2)/R^2)^(3/2)...
16 *(F/(rho*g*R^3))^(1/2))- delta == 0;
17
18 Baffle_depth = vpa(solve(ONeill_expression,d),5); %inches
19
20 %% Bauers Extension
21 clear;
22
23 % Variables
24
25 % N = total number of submerged baffles
26 % M = total number of unsubmerged baffles
27 % B = total number of baffles
28 % D = spacing between baffles
29 % L = fluid level
30 % V = fluid volume
31 % V0 = initial fluid volume
32 % Vf = final fluid volume
33 % VFR = dV/dt
34 % t = time
35
36 % @ t = 0:
37 % tank is full, therefore L=H, B=N, M=0, V0=(pi*R^2)H
38 % @ t = end:
39 % tank is empty, therefore L=0, B=M, N=0, Vf=0
40
41 % Initial conditions:
42
43
44 %Timing
45 Burn_time = 100; %.....sec
46 Time_step = 1; %.....sec
47
48 %Tank Properties
49 R = 7.76; %..... inches
50 Vol_L = 647.5; %.....Liters
51 V = Vol_L* 61.0237; %.....in^3
52 V0 = V; %.....in^3
53 VFR = V/Burn_time; %.....in^3/sec
54 H = (V-(4/3)*pi()*R^3)/(pi()*R^2)+2*R; %..... inches
55 L = V/(pi()*R^2); %..... inches
56 L0 = L; %..... inches
57
58

```

```

59     %Assumptions
60     zeta = 6; %..... inches
61     N = 9; %..... count
62     M = 1; %..... count
63     w = 2; %..... inches
64
65     B = M+N;
66     D = H/(B-1);
67     k = 1;
68
69     dmat = cell(1,Burn_time/Time_step);
70     BE1 = cell(B,Burn_time/Time_step);
71     BE2 = cell(B,Burn_time/Time_step);
72     L_track = cell(1,Burn_time/Time_step);
73     V_track = cell(1,Burn_time/Time_step);
74
75     for t = 0:Time_step:Burn_time
76
77         V = V0 -(t*(VFR));
78         V_track{k} = V;
79
80         L = V/(pi()*R^2);
81         L_track{k} = L;
82
83         if L-(N-1)*D > 0;
84             d = L-(N-1)*D;
85         else;
86             N = N-1;
87             M = M+1;
88             d = D;
89         end
90
91         dmat{k}=d;
92
93     if N >=1
94     for n=1:N
95     % an_bar declairation
96     an1 = (w/R)*(2-(w/R));
97     an2 = (1/2)*(1-(((d/R)+(n-1)*(D/R))/(zeta/R)));
98     an3 = (2/pi())*(((d/R)+(n-1)*(D/R))/(zeta/R));
99     an4 = log(((zeta/R)+sqrt((zeta/R)^2-((d/R)+(n-1)*(D/R))^2)/...
100             ((d/R)+(n-1)*(D/R)));
101     an5 = (1/pi())*(((d/R)+(n-1)*(D/R))/(zeta/R));
102     an6 = sqrt((zeta/R)^2-((d/R)+(n-1)*(D/R))^2);
103     an7 = (1/pi())*asin((((d/R)+(n-1)*(D/R))/(zeta/R)));
104     an8 = (1/2)*(((d/R)+(n-1)*(D/R))/(zeta/R));
105     an9 = (1/2)*((1-(w/R))^2)*(1-(((d/R)+(n-1)*(D/R))/((1-(w/R))*(zeta/R))));
106     an10 = (2/pi())*(((d/R)+(n-1)*(D/R))*(1-(w/R))/(zeta/R));
107     an11 = log(((zeta/R)+sqrt((zeta/R)^2-(((d/R)+(n-1))/(1-(w/R)))*(D/R))^2)/...
108             (((d/R)+(n-1)*(D/R))/(1-(w/R))));
109     an12 = (1/pi())*(((d/R)+(n-1)*(D/R))*(1-(w/R))/((zeta/R)^2));
110     an13 = sqrt(((zeta/R)^2)+(((d/R)+(n-1)*(D/R))^2)/((1-(w/R))^2));
111     an14 = (1/pi())*((1-(w/R))^2)*asin(((d/R)+(n-1)*(D/R))/((1-(w/R))*(zeta/R)));
112     an15 = (1/2)*(1-(w/R))*(((d/R)+(n-1)*(D/R))/((zeta/R)));
113
114     if ((d/R)+(n-1)*(D/R)) >= (zeta/R)
115         an_bar = (w/R)*(2-(w/R));
116
117     elseif ((zeta/R)*(1-(w/R))) <= ((d/R)+(n-1)*(D/R)) <= (zeta/R)
118         an_bar = an1-an2+an3*an4-an5*an6+an7-an8;

```

```

119 else
120 an_bar = an1-an2+an3*an4-an5*an6+an7-an8+an9-an10*an11+an12*...
121                                     an13-an14+an15;
122 end
123
124 BE1{n,k} = exp(-4.6*((d\R)+(n-1)*(D/R)))*an_bar^(3/2);
125 end
126 else
127 n=0;
128 BE1{1,k} = exp(-4.6*((d\R)+(n-1)*(D/R)))*an_bar^(3/2);
129 end
130
131
132 for m = 1:M
133 % am_bar declairation
134 am1 = (1/2)*(1-((m*(D/R)-(d/R))/(zeta/R)));
135 am2 = (2/pi())*((m*(D/R)-(d/R))/(zeta/R));
136 am3 = log(((zeta/R)+sqrt(((zeta/R)^2)-((m*(D/R)-(d/R))^2)))/(m*(D/R)-(d/R)));
137 am4 = (1/pi())*((m*(D/R)-(d/R))/(zeta/R)^2);
138 am5 = sqrt(((zeta/R)^2)-((m*(D/R)-(d/R))^2));
139 am6 = (1/pi())*asin(((m*(D/R)-(d/R))/(zeta/R)));
140 am7 = (1/2)*((m*(D/R)-(d/R))/(zeta/R));
141 am8 = (1/2)*((1-(w/R))^2)*(1-(((m*(D/R)-(d/R))/((1-(w/R))*(zeta/R)))));
142 am9 = (2/pi())*((m*(D/R)-(d/R))*(1-(w/R))/(zeta/R));
143 am10 = log(((zeta/R)+sqrt(((zeta/R)^2)-((m*(D/R)-(d/R))/((1-(w/R))^2)))/...
144             ((m*(D/R)-(d/R))/(1-(w/R))));
145 am11 = (1/pi())*((m*(D/R)-(d/R))*(1-(w/R))/(zeta/R)^2);
146 am12 = sqrt(((zeta/R)^2)-(((m*(D/R)-(d/R))/(1-(w/R)))^2));
147 am13 = (1/pi())*((1-(w/R))^2)*asin(((m*(D/R)-(d/R))/((1-(w/R))*(zeta/R))));
148 am14 = (1/2)*(1-(w/R))*((m*(D/R)-(d/R))/(zeta/R));
149
150
151 if (m*(D/R)-(d/R)) >= (zeta/R)
152     am_bar = 0;
153
154 elseif ((zeta/R)*(1-(w/R))) <= ((D/R)-(d/R)) <= (zeta/R)
155     am_bar = am1-am2*am3+am4*am5-am6+am7;
156
157 else
158     am_bar = am1-am2*am3+am4*am5-am6+am7-am8+am9*am10-am11*am12+...
159                                     am13-am14;
160 end
161
162 BE2{m,k} = exp(-4.6*(m*(D/R)-(d/R)))*am_bar^(3/2);
163 end
164
165
166 k = k+1;
167 end
168
169 empties = cellfun('isempty',BE1);
170 BE1(empties) = {0};
171 BE1 = cellfun(@(M)subsasgn(M,substruct('()',{isnan(M)}),0),BE1,'uniform',0);
172
173 empties = cellfun('isempty',BE2);
174 BE2(empties) = {0};
175 BE2 = cellfun(@(M)subsasgn(M,substruct('()',{isnan(M)}),0),BE2,'uniform',0);
176
177 L_track = cell2mat(L_track);
178 V_track = cell2mat(V_track);

```



```

179
180 % Summation terms
181 BECoeff = 2.83*sqrt((zeta/R));
182 Bauer_Delta = BECoeff.*sum(real(cell2mat(cellfun(@plus, BE1, BE2, 'uni', 0))));
183 Bauer_Delta(Bauer_Delta < 0) = 0;
184 Bauer_Delta(Bauer_Delta > 1) = 0;
185
186 % Plots
187 Baffle = [0:D:H];
188
189 % figure(1)
190 % plot(0:Time_step:Burn_time, Bauer_Delta(1,:))
191 % xlim([0 Burn_time])
192 % title('Damping factor vs burn time in draining tank at constant flow rate')
193 % xlabel('Engine burn time (sec)')
194 % ylabel('Damping factor')
195 % x0=0;
196 % y0=600;
197 % width=1920;
198 % height=400;
199
200
201 plot(L_track(1,:), Bauer_Delta(1,:))
202 xlim([0 L0])
203 set(gca, 'XDir', 'reverse')
204 title('Damping factor vs fluid level in draining tank at constant flow rate')
205 xlabel('Fluid level (in)')
206 ylabel('Damping factor')
207 x0=0;
208 y0=600;
209 width=1920;
210 height=400;
211 set(gcf, 'position', [x0, y0, width, height])
212 h = gobjects(size(Baffle));
213 for i = 1:numel(Baffle)
214     h(i) = xline(Baffle(i), '-. ');
215 end
216
217 % figure (3)
218 % plot(V_track(1,:), Bauer_Delta(1,:))
219 % xlim([0 V0])
220 % set(gca, 'XDir', 'reverse')
221 % title('Damping factor vs fluid volume in draining tank at constant flow rate')
222 % xlabel('Fluid volume (in^3)')
223 % ylabel('Damping factor')
224 % x0=0;
225 % y0=600;
226 % width=1920;
227 % height=400;
228 % set(gcf, 'position', [x0, y0, width, height])
229 % h = gobjects(size(Baffle));
230 % for i = 1:numel(Baffle)
231 %     h(i) = xline(Baffle(i), '-. ');
232 % end
233
234 % figure (4)
235 % dmat = cell2mat(dmat)
236 % plot(0:Time_step:Burn_time, dmat(1,:), '-. ')
237 % xlim([0 Burn_time])
238 % title('Damping factor vs fluid level in draining tank at constant flow rate')

```

```

239 % xlabel('Fluid level (in)')
240 % ylabel('Damping factor')
241 % x0=0;
242 % y0=600;
243 % width=1920;
244 % height=400;
245
246 %% Weight contribution
247
248 Baffle_thickness = 0.1; %inches
249
250 % 6061-T6 Aluminum
251 Density = 0.0975; %lb/in^3
252
253 Baffle_area = pi()*(R^2-(R-w)^2); %in^2
254 Baffle_volume = Baffle_area*Baffle_thickness; %in^3
255 Baffle_weight = Baffle_volume*Density; %lb
256 Total_baffle_weight = B*Baffle_weight; %lb
257 Total_baffle_volume = B*Baffle_volume; %in^3
258 Fluid_raise = Total_baffle_volume/(pi()*R^2); %inches
259
260 fprintf('Total baffle system weight = %0.4f lb\n',Total_baffle_weight)
261 % fprintf('Total baffle system volume = %0.4f in^3\n',Total_baffle_volume)
262 fprintf('Fluid rise due to baffle volume = %0.4f in\n',Fluid_raise)

```

6.1.5 Stacking Center of Mass Script- MATLAB

```

1 %% Center of gravity shift
2 clear;
3 clc;
4
5 % Variables
6 % L = fluid level
7 % V = fluid volume
8 % V0 = initial fluid volume
9 % Vf = final fluid volume
10 % VFR = dV/dt
11 % t = time
12 % R = rocket optimal radius
13 % r = tank inner radius
14 % S = space between tanks
15
16
17
18 % Initial conditions:
19     %Constants
20     Time_step = .01; %.....sec
21     Burn_time = 100; %.....sec
22     R = 8; %.....inches
23     r = 7.8; %.....inches
24     S = 24; %.....inches
25
26     %HTP
27     HTP_Vol_L = 647.5; %.....Liters
28
29     V_HTP = HTP_Vol_L* 61.0237; %.....in^3
30     H_HTP = (V_HTP-(4/3)*pi()*r^3)/(pi()*r^2)+2*R; %.....inches
31     Density_HTP = 0.02926311; %.....lbm/in^3
32     VFR_HTP = V_HTP/Burn_time; %.....in^3/sec
33     L_HTP = V_HTP/(pi()*r^2); %.....inches
34     M_HTP = V_HTP*Density_HTP %.....lbm
35     Tank_mass_HTP = 170.6365; %.....lbm
36
37
38     %RP1
39     RP1_Vol_L = HTP_Vol_L/7 ; %.....Liters
40
41     V_RP1 = RP1_Vol_L* 61.0237; %.....in^3
42     H_RP1 = (V_RP1-(4/3)*pi()*r^3)/(pi()*r^2)+2*R;%.....inches
43     Density_RP1 = 0.0520233; %.....lbm/in^3
44     VFR_RP1 = V_RP1/Burn_time; %.....in^3/sec
45     L_RP1 = V_RP1/(pi()*r^2); %.....inches
46     M_RP1 = V_RP1*Density_RP1; %.....lbm
47     Tank_mass_RP1 = 33.8473; %.....lbm
48
49
50
51
52 k = 1;
53 H_Stack = H_HTP + H_RP1 + S;
54
55 L_HTP_track = cell(1,Burn_time/Time_step);
56 L_RP1_track = cell(1,Burn_time/Time_step);
57 V_HTP_track = cell(1,Burn_time/Time_step);
58 V_RP1_track = cell(1,Burn_time/Time_step);

```

```

59 M_HTP_track = cell(1,Burn_time/Time_step);
60 M_RP1_track = cell(1,Burn_time/Time_step);
61 X_HTP = cell(1,Burn_time/Time_step);
62 X_RP1 = cell(1,Burn_time/Time_step);
63 CM = cell(1,Burn_time/Time_step);
64
65
66 %% Case 1 - RP1 tank on top
67
68 for t = 0:Time_step:Burn_time
69
70     V_HTP_track{k} = V_HTP -(t*(VFR_HTP));
71     V_RP1_track{k} = V_RP1 -(t*(VFR_RP1));
72
73     L_HTP_track{k} = V_HTP_track{k}/(pi()*R^2);
74     L_RP1_track{k} = V_RP1_track{k}/(pi()*R^2);
75
76     M_HTP_track{k} = V_HTP_track{k}*Density_HTP;
77     M_RP1_track{k} = V_RP1_track{k}*Density_RP1;
78
79     X_HTP{k} = L_HTP_track{k}/2;
80     X_RP1{k} = L_RP1_track{k}/2 + H_HTP + S;
81
82     X_HTP_Tank = H_HTP/2;
83     X_RP1_Tank = H_RP1/2 + H_HTP + S;
84
85     CM{k} = (M_HTP_track{k}*X_HTP{k}+ M_RP1_track{k}*X_RP1{k}+...
86             Tank_mass_HTP*X_HTP_Tank + Tank_mass_RP1*X_RP1_Tank)/...
87             (M_HTP_track{k}+M_RP1_track{k}+Tank_mass_HTP+Tank_mass_RP1);
88
89     k = k+1;
90 end
91
92 CM_RP1_top = cell2mat(CM);
93 Total_Volume = cell2mat(cellfun(@plus,V_HTP_track,V_RP1_track,'uni',0));
94 Total_Volume = Total_Volume.*0.0163871; %in^3 to liter
95 plot(Total_Volume,CM_RP1_top,'-.')
96 hold on
97
98 %% Case 2 - HTP tank on top
99 k = 1;
100
101 for t = 0:Time_step:Burn_time
102
103     V_HTP_track{k} = V_HTP -(t*(VFR_HTP));
104     V_RP1_track{k} = V_RP1 -(t*(VFR_RP1));
105
106     L_HTP_track{k} = V_HTP_track{k}/(pi()*R^2);
107     L_RP1_track{k} = V_RP1_track{k}/(pi()*R^2);
108
109     M_HTP_track{k} = V_HTP_track{k}*Density_HTP;
110     M_RP1_track{k} = V_RP1_track{k}*Density_RP1;
111
112     X_HTP{k} = L_HTP_track{k}/2 + H_RP1 + S;
113     X_RP1{k} = L_RP1_track{k}/2;
114
115     X_HTP_Tank = H_HTP/2 + H_RP1 + S;
116     X_RP1_Tank = H_RP1/2;
117
118     CM{k} = (M_HTP_track{k}*X_HTP{k}+ M_RP1_track{k}*X_RP1{k}+...

```

```

119         Tank_mass_HTP*X_HTP_Tank + Tank_mass_RP1*X_RP1_Tank)/...
120         (M_HTP_track{k}+M_RP1_track{k}+Tank_mass_HTP+Tank_mass_RP1);
121
122     k = k+1;
123     end
124
125     CM_HTP_top = cell2mat(CM);
126
127     plot(Total_Volume,CM_HTP_top)
128
129     legend('RP1 = Top','HTP = Top')
130     xlabel('Total propellant volume (liter)')
131     ylabel('Center of Mass (inches from bottom of tank stack)')
132     set(gca, 'XDir','reverse')
133     ylim([70,140])
134     xlim([0,((V_HTP+V_RP1)*0.0163871)])

```



```

59 max_stress_2 = isolate(sig2==F2c,taus);
60 max_stress_3 = isolate(abs(tau6)==F6,taus);
61
62 max_stress=[165/(cos((pi*theta)/180)*sin((pi*theta)/180));...
63             33/(2*cos((pi*theta)/180)*sin((pi*theta)/180));...
64             abs(11/(cos((pi*theta)/180)^2 - sin((pi*theta)/180)^2)]];
65
66 Max_Stress_Solition = min(max_stress,[],'all');
67 Max_stress_track{k} = Max_Stress_Solition;
68
69 %% Maximum Strain Condition
70 ep1 = simplify(epsilon_u_1t - epsilon_1 == 0);
71 ep2 = simplify(epsilon_u_2c - epsilon_2 == 0);
72 g6 = simplify(gamma_u_6 - gamma_6 == 0);
73
74 max_strain_1 = isolate(ep1,taus);
75 max_strain_2 = isolate(ep2,taus);
76 max_strain_3 = isolate(g6,taus);
77
78 max_strain = [27500/(107*sin((pi*theta)/90));...
79              46860/(1447*sin((pi*theta)/90));...
80              abs(11/cos((pi*theta)/90))];
81
82 Max_Strain_Solition = min(max_strain,[],'all');
83 Max_strain_track{k} = Max_Strain_Solition;
84
85 %% Tsai-Hill
86 Tsai_Hill_Criterion =((sig1^2)/(F1t^2))+((sig2^2)/(F2c^2))+...
87                      ((tau6^2)/(F6^2))-((sig1*sig2)/(F1t^2))= 1;
88
89 RHS_Tsai_Hill_Criterion_Solution = isolate(Tsai_Hill_Criterion,taus);
90
91 Tsai_Hill_Criterion_Solution = (9075*((4*cos((pi*theta)/180)^4)/121-...
92                               (464*cos((pi*theta)/180)^2*sin((pi*theta)/180)^2)/9075+...
93                               (4*sin((pi*theta)/180)^4)/121)^(1/2)/(2*(75*cos((pi*theta)/180)^4-...
94                               116*cos((pi*theta)/180)^2*sin((pi*theta)/180)^2+...
95                               75*sin((pi*theta)/180)^4));
96
97
98 Tsai_Hill_track{k} = Tsai_Hill_Criterion_Solution;
99
100 %% Tsai-Wu
101 f1 = (1/F1t)-(1/F1c);
102 f2 = (1/F2t)-(1/F2c);
103 f11 = 1/(F1t*F1c);
104 f22 = 1/(F2t*F2c);
105 f66 = 1/(F6^2);
106 f12 = (-1/2)*sqrt(f11*f22);
107
108 Tsai_Wu_Criterion = f1*sig1+f2*sig2+f11*(sig1^2)+f22*...
109                   (sig2^2)+f66*(tau6^2)+2*f12*sig1*sig2=1;
110
111 Tsai_Wu_RHS = isolate(Tsai_Wu_Criterion,taus);
112
113 Tsai_Wu_Criterion_Solution = (1395035020574284840960*(31125*...
114                               ((3931652815671024788192322571*cos((pi*theta)/180)^2*...
115                               sin((pi*theta)/180)^2)/135146197360353491288064000000+...
116                               (4*cos((pi*theta)/180)^4)/121+(4*sin((pi*theta)/180)^4)/121)^(1/2)+...
117                               5674*cos((pi*theta)/180)*sin((pi*theta)/180))/...
118                               (3*(239231212205920747520000*cos((pi*theta)/180)^4-...

```

```

119     29963128917397358985591*cos((pi*theta)/180)^2*sin((pi*theta)/180)^2+...
120     239231212205920747520000*sin((pi*theta)/180)^4));
121
122
123 Tsai_Wu_track{k} = Tsai_Wu_Criterion_Solution;
124
125 k = k+1;
126 end
127
128 Max_stress_track = cell2mat(Max_stress_track);
129 Max_strain_track = cell2mat(Max_strain_track);
130 Tsai_Hill_track = cell2mat(Tsai_Hill_track);
131 Tsai_Wu_track = cell2mat(Tsai_Wu_track);
132
133 figure(1)
134 hold on
135 plot(0:Theta_step:90,Max_stress_track)
136 plot(0:Theta_step:90,Max_strain_track,'--')
137 plot(0:Theta_step:90,Tsai_Hill_track)
138 plot(0:Theta_step:90,Tsai_Wu_track)
139 legend('Max Stress','Max Strain','Tsai-Hill','Tsai-Wu')
140 xlabel('Orientation Angle (deg)')
141 ylabel('Predicted Shear Strength (ksi)')
142 title('Comparison of predicted shear strength by failure criteria')
143 x0=0;
144 y0=400;
145 width=1920;
146 height=1000;
147 set(gcf,'position',[x0,y0,width,height])
148 hold off
149
150
151 %%\////////////////////////////////// TENSILE STRENGTH ////////////////////////////////////
152 syms theta sig1 sig2 tau6 sigx sigy taus
153 sigy = 0;
154 taus = 0;
155
156 %% By maximum strain theory ...
157 epsilon_u_1t = F1t/E1;
158 epsilon_u_1c = -F1c/E1;
159 epsilon_u_2t = F2t/E2;
160 epsilon_u_2c = -F2c/E2;
161 gamma_u_6 = F6/G12;
162 %% Transformations
163 T = [m^2 n^2 2*m*n; n^2 m^2 -2*m*n;-m*n m*n (m^2-n^2)];
164 sigglobal = [sigx;sigy;taus];
165 siglocal = T*sigglobal;
166 sig1 = siglocal(1);
167 sig2 = siglocal(2);
168 tau6 = siglocal(3);
169 %% Strain relations
170 epsilon_1 = (sig1/E1)-v21*(sig2/E2);
171 epsilon_2 = (sig2/E2)-v12*(sig1/E1);
172 gamma_6 = tau6/G12;
173
174 %% Set Iteration Step Size
175 Theta_step = 1; % degrees
176
177 %% Loop
178 %%

```



```

179 k = 1;
180 Max_stress_track = cell(1,90*Theta_step);
181 Max_strain_track = cell(1,90*Theta_step);
182 Tsai_Hill_track = cell(1,90*Theta_step);
183 Tsai_Wu_track = cell(1,90*Theta_step);
184
185 for theta = 0:Theta_step:90
186     %% Maximum Stress Condition
187     max_stress_1 = isolate(sig1==F1t,sigx);
188     max_stress_2 = isolate(sig2==F2t,sigx);
189     max_stress_3 = isolate(abs(tau6)==F6,sigx);
190
191     max_stress = [abs(330/cos((theta*pi)/180)^2);...
192                 abs(83/(10*sin((theta*pi)/180)^2));...
193                 abs(11/(cos((pi*theta)/180)*sin((pi*theta)/180))];
194
195     Max_Stress_Solition = min(max_stress,[],'all');
196     Max_stress_track{k} = Max_Stress_Solition;
197
198     %% Maximum Strain Condition
199     ep1 = simplify(epsilon_u_1t - epsilon_1 == 0);
200     ep2 = simplify(epsilon_u_2t - epsilon_2 == 0);
201     g6 = simplify(gamma_u_6 - gamma_6 == 0);
202
203     max_strain_1 = isolate(ep1,sigx);
204     max_strain_2 = isolate(ep2,sigx);
205     max_strain_3 = isolate(g6,sigx);
206
207
208     max_strain = [abs(82500/(250*cos((pi*theta)/180)^2 - 71*sin((pi*theta)/180)^2));...
209                 abs(-11786/(27*cos((pi*theta)/180)^2 - 1420*sin((pi*theta)/180)^2));...
210                 abs(-22/sin((pi*theta)/90))];
211
212     Max_Strain_Solition = min(max_strain,[],'all');
213     Max_strain_track{k} = Max_Strain_Solition;
214
215     %% Tsai-Hill
216     Tsai_Hill_Criterion = ((sig1^2)/(F1t^2))+((sig2^2)/(F2t^2))+...
217         ((tau6^2)/(F6^2))-((sig1*sig2)/(F1t^2)) == 1;
218
219     RHS_Tsai_Hill_Criterion_Solution = isolate(Tsai_Hill_Criterion,sigx);
220
221     Tsai_Hill_Criterion_Solution = (375106050*((899*cos((pi*theta)/180)^2*...
222         sin((pi*theta)/180)^2)/27225 + cos((pi*theta)/180)^4/27225 + ...
223         (400*sin((pi*theta)/180)^4)/6889)^(1/2)/(6193211*...
224         cos((pi*theta)/180)^2*sin((pi*theta)/180)^2 + ...
225         6889*cos((pi*theta)/180)^4 + 10890000*sin((pi*theta)/180)^4);
226
227     Tsai_Hill_track{k} = Tsai_Hill_Criterion_Solution;
228
229     %% Tsai-Wu
230     f1 = (1/F1t)-(1/F1c);
231     f2 = (1/F2t)-(1/F2c);
232     f11 = 1/(F1t*F1c);
233     f22 = 1/(F2t*F2c);
234     f66 = 1/(F6^2);
235     f12 = (-1/2)*sqrt(f11*f22);
236
237     Tsai_Wu_Criterion = f1*sig1+f2*sig2+f11*(sig1^2)+f22*...
238         (sig2^2)+f66*(tau6^2)+2*f12*sig1*sig2==1;

```

```

239
240 Tsai_Wu_RHS = isolate(Tsai_Wu_Criterion, sigx);
241
242 Tsai_Wu_Criterion_Solution = (507285462027012669440*(342375*...
243 ((1669507779061630946001571*cos((pi*theta)/180)^2*...
244 sin((pi*theta)/180)^2)/52104558018449538809856000 +...
245 (841*cos((pi*theta)/180)^4)/17015625 +...
246 (170569*sin((pi*theta)/180)^4)/7502121)^(1/2) +...
247 332*cos((pi*theta)/180)^2 - 30875*sin((pi*theta)/180)^2)/...
248 (2797700784390072440833125*cos((pi*theta)/180)^2*...
249 sin((pi*theta)/180)^2 + 4210469334824205156352*...
250 cos((pi*theta)/180)^4 + 126821365506753167360000*...
251 sin((pi*theta)/180)^4);
252
253
254
255 Tsai_Wu_track{k} = Tsai_Wu_Criterion_Solution;
256
257 k = k+1;
258 end
259
260 Max_stress_track = cell2mat(Max_stress_track);
261 Max_strain_track = cell2mat(Max_strain_track);
262 Tsai_Hill_track = cell2mat(Tsai_Hill_track);
263 Tsai_Wu_track = cell2mat(Tsai_Wu_track);
264
265
266 figure(2)
267 hold on
268 plot(0:Theta_step:90,Max_stress_track)
269 plot(0:Theta_step:90,Max_strain_track,'--')
270 plot(0:Theta_step:90,Tsai_Hill_track)
271 plot(0:Theta_step:90,Tsai_Wu_track)
272 legend('Max Stress','Max Strain','Tsai-Hill','Tsai-Wu')
273 xlabel('Orientation Angle (deg)')
274 ylabel('Predicted Tensile Strength (ksi)')
275 title('Comparison of predicted tensile strength by failure criteria')
276 x0=0;
277 y0=400;
278 width=1920;
279 height=1000;
280 set(gcf,'position',[x0,y0,width,height])
281 hold off
282
283
284
285
286 %%%%%%%%%%%%%%%%%%%%%%%%%%%%%%%%%%%%%%%%%%%%%%%%%%%%%%%%%%%%%%%%%%%%%%%%% COMPRESSIVE STRENGTH %%%%%%%%%%%%%%%%%%%%%%%%%%%%%%%%%%%%%%%%%%%%%%%%%%%%%%%%%%%%%%%%%%%%%%%%%

```

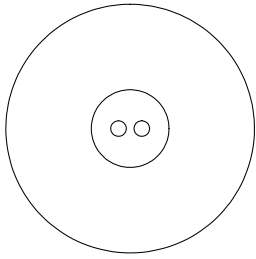
6.2 Appendix B

6.2.1 Drawings

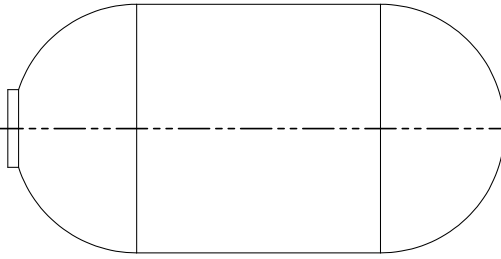
NOTE: ALL IMAGES ARE FROM 11/06/2020 AND SHOULD NOT BE TREATED AS CURRENT. CHECK WITH LRL VP OF STRUCTURES ENGINEERING AND VP OF PROPULSION ENGINEERING FOR NEW COPIES OF DRAWINGS. ALL DRAWINGS ARE FIRST REVISION COPIES AND WILL BE ALTERED BEFORE USE. DRAWINGS MUST ALSO FIRST UNDERGO REVIEW BY A PROFESSIONAL ENGINEER BEFORE USE.

- N2 COPV Design Drawings
- RP1 COPV Design Drawings
- HTP COPV Design Drawings

4

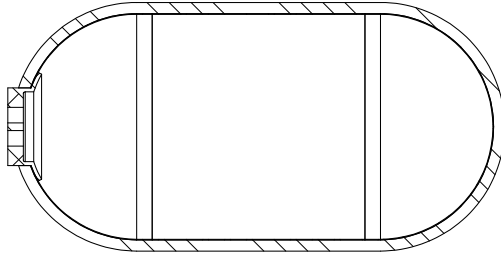


A



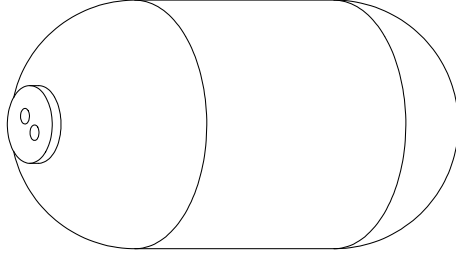
A

3



SECTION A-A
SCALE 1 : 8

2



1

N2 COPV Assembly

B

A

| ITEM NO. | PART NUMBER | DESCRIPTION | QTY. |
|----------|-------------------------|--------------------------------|------|
| 1 | N2 Liner Assembly | Liner Assembly | 1 |
| 2 | N2_Cylinder | Cylinder | 1 |
| 3 | N2_Hemispherical_Closed | Hemispherical Closed Tank Head | 1 |
| 4 | N2_Hemispherical_Open | Hemispherical Open Tank Head | 1 |
| 5 | N2_Bottom | Bottom Polar Boss | 1 |
| 6 | N2 Overwrap | Overwrap | 1 |

3

2

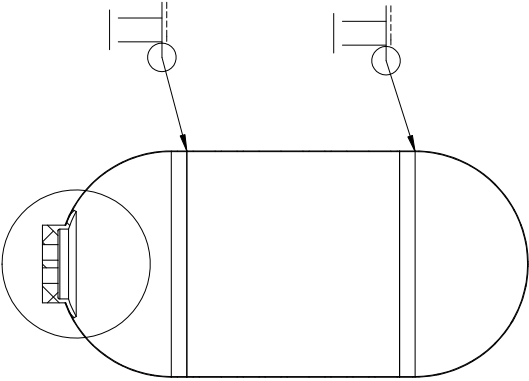
1

4



3

C

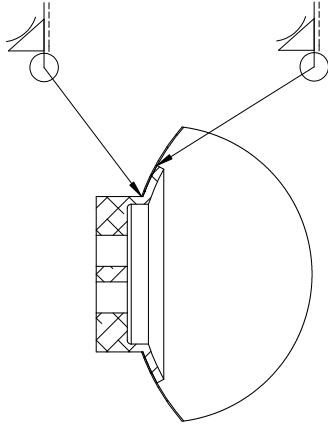


SECTION B-B
SCALE 1 : 8

2

| ITEM NO. | PART NUMBER | DESCRIPTION | QTY. |
|----------|-------------------------|--------------------------------|------|
| 1 | N2_Cylinder | Cylinder | 1 |
| 2 | N2_Hemispherical_Closed | Hemispherical Closed Tank Head | 1 |
| 3 | N2_Hemispherical_Open | Hemispherical Open Tank Head | 1 |
| 4 | N2_Bottom | Bottom Polar Boss | 1 |

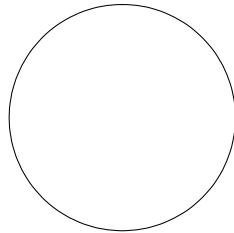
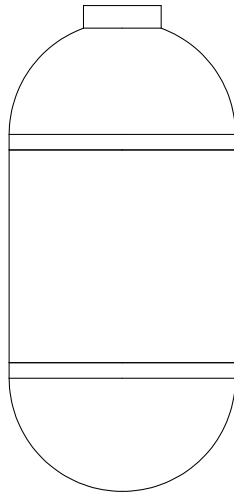
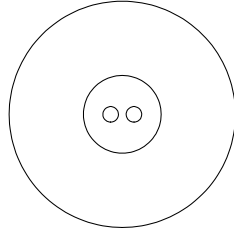
B



DETAIL C

B

A



| UNLESS OTHERWISE SPECIFIED: | DRAWN | CHECKED | NAME | DATE |
|--|--------------------|---------|------------|----------|
| DIMENSIONS ARE IN INCHES | John Slugg | | John Slugg | 11/06/20 |
| TOLERANCES: | | | | |
| ANGULAR: | | | | |
| MACH ±0.5 BEND ±1.0 | | | | |
| TWO PLACE DECIMAL ±.01 | | | | |
| THREE PLACE DECIMAL ±.005 | | | | |
| INTERPRET GEOMETRIC TOLERANCING PER: ASME Y14.5-09 | | | | |
| MATERIAL: | 6061 Aluminum | | | |
| FINISH: | Clean with acetone | | | |
| DO NOT SCALE DRAWING | | | | |

TITLE:

N2 Liner
Assembly

SIZE DWG. NO. REV

B N2 COPV Assembly

SCALE: 1:8 WEIGHT: SHEET 2 OF 7

3

2

1

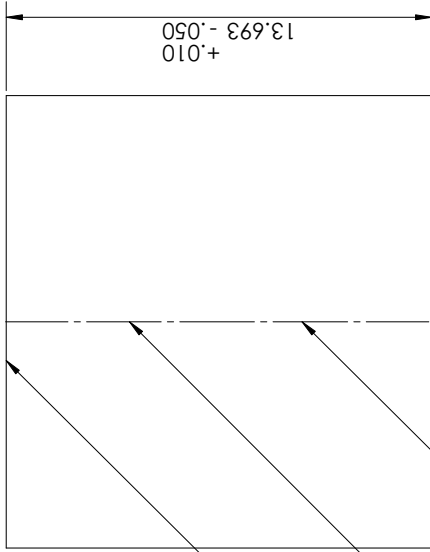
4

3

2

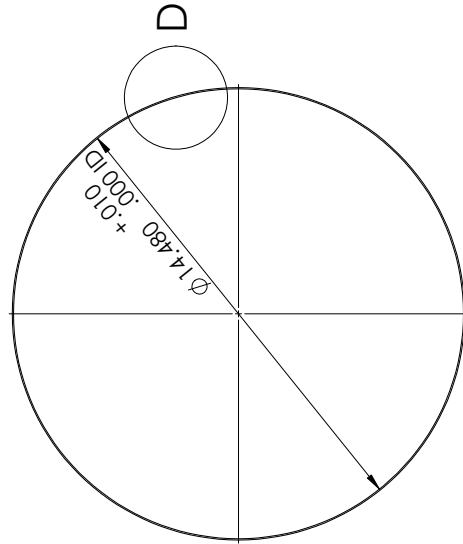
1

/// .01 A

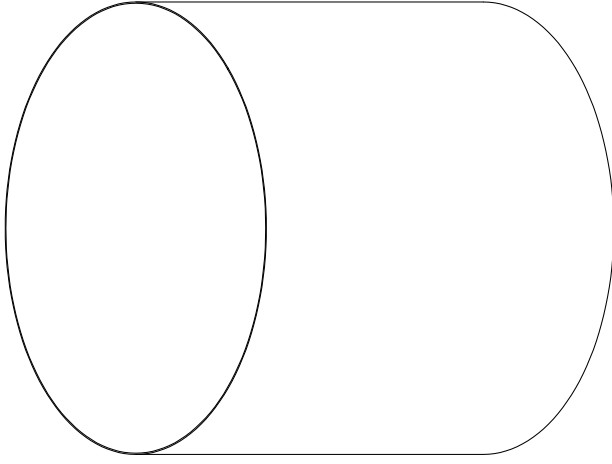


NOTE: LINE REPRESENTS FULL LENGTH WELD SEAM USED TO FORM CYLINDER FROM SHEET

.040 MIN.



DETAIL D
SCALE 1 : 1



NOTE: ALL UNITS IN INCHES UNLESS OTHERWISE STATED

| UNLESS OTHERWISE SPECIFIED: | | NAME | DATE |
|--|------------|---------------------------------|------|
| DRAWN | John Slugg | 11/06/20 | |
| CHECKED | | | |
| FRACTIONAL ± | | | |
| ANGULAR: MACH ± | BEND ± | | |
| TWO PLACE DECIMAL ± | ENG APPR. | | |
| THREE PLACE DECIMAL ± | MFG APPR. | | |
| | Q.A. | | |
| COMMENTS: | | | |
| Cylinder is rolled and welded from sheet material. Baffles and baffle assembly is used as a framework for stability. | | | |
| MATERIAL | | SIZE DWG. NO. | |
| 6061 Aluminum | | B N2 COPV Assembly | |
| FINISH | | REV | |
| Clean with acetone | | 1 | |
| DO NOT SCALE DRAWING | | SCALE: 1:4 WEIGHT: SHEET 3 OF 7 | |

TITLE: N2 - Cylinder

B

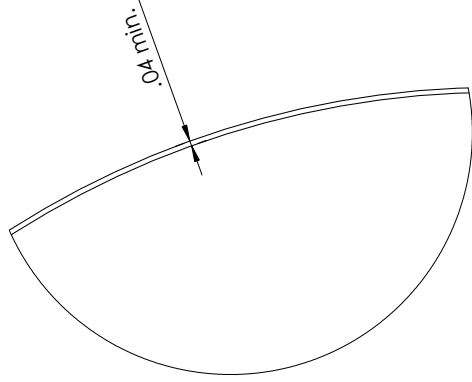
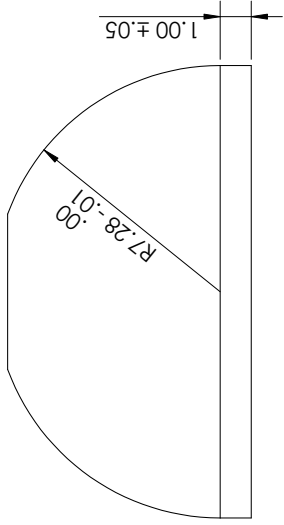
A

4

3

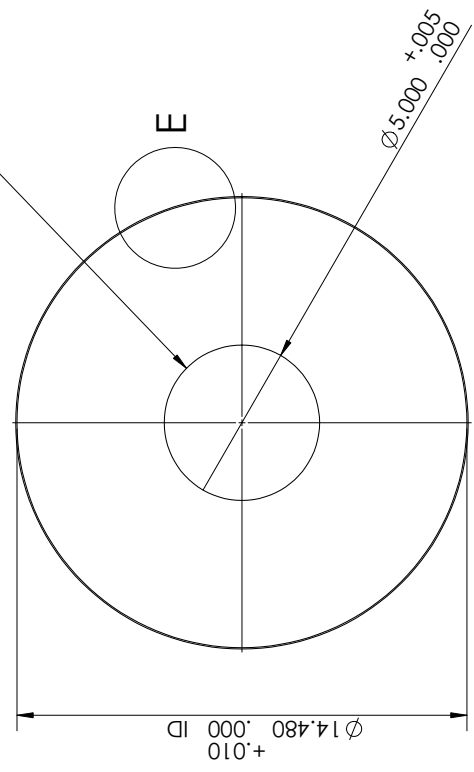
2

1



DETAIL E
SCALE 1 : 1

NOTE: CENTER HOLE CUT FROM FULL HEMISPHERE HEAD



NOTE: ALL UNITS IN INCHES UNLESS OTHERWISE STATED

| UNLESS OTHERWISE SPECIFIED: | | NAME | DATE |
|--|------------------|------------|--------------|
| DIMENSIONS ARE IN INCHES | | John Slugg | 11/06/20 |
| TOLERANCES: | | | |
| ANGULAR: | | | |
| MACH ± 0.5 BEND ± 1.0 | | | |
| TWO PLACE DECIMAL ± 0.1 | | | |
| THREE PLACE DECIMAL ± 0.05 | | | |
| | | | |
| | | | |
| | | | |
| | | | |
| INTERPRET GEOMETRIC TOLERANCING PER: ASME Y14.5-09 | | | |
| MATERIAL: 6061 Aluminum | | | |
| FINISH: Clean with acetone | | | |
| DO NOT SCALE DRAWING | | | |
| TITLE: Hemispherical open tank head | | | |
| SIZE: DWG. NO. B | N2 COPV Assembly | | |
| REV | | | |
| SCALE: 1:4 | WEIGHT: | | |
| | | | SHEET 4 OF 7 |

3

2

1

1

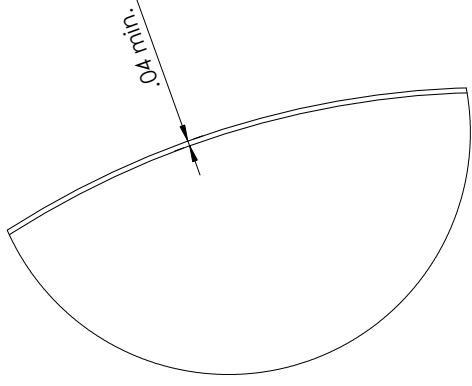
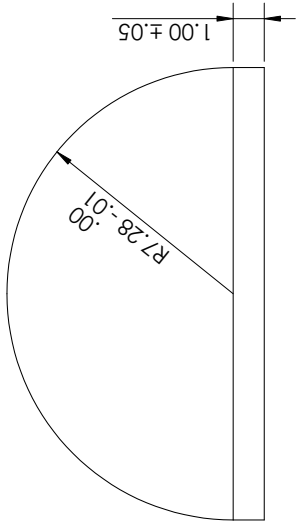
2

3

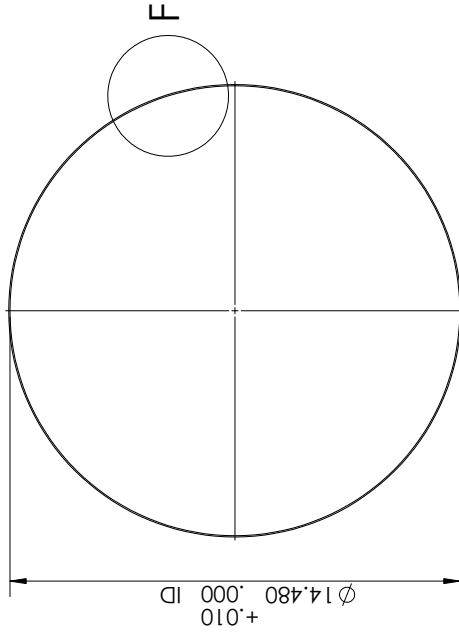
4

B

A



DETAIL F
SCALE 1 : 1



NOTE: ALL UNITS IN INCHES UNLESS OTHERWISE STATED

| UNLESS OTHERWISE SPECIFIED: | | NAME | DATE |
|--|--------------------|------------|----------|
| DIMENSIONS ARE IN INCHES | DRAWN | John Slugg | 11/06/20 |
| TOLERANCES: | CHECKED | | |
| ANGULAR: | | | |
| MACH ±0.5 BEND ±1.0 | BNG APPR. | | |
| TWO PLACE DECIMAL ±.01 | MFG APPR. | | |
| THREE PLACE DECIMAL ±.005 | Q.A. | | |
| INTERPRET GEOMETRIC TOLERANCING PER: ASME Y14.5-09 | COMMENTS: | | |
| MATERIAL | 6061 Aluminum | | |
| FINISH | Clean with acetone | | |
| DO NOT SCALE DRAWING | | | |

| TITLE: | | SIZE | DWG. NO. | REV |
|------------------------------|--|------|------------------|-----|
| Hemispherical open tank head | | B | N2 COPV Assembly | 1 |

| SCALE: | 1:4 | WEIGHT: | SHEET 5 OF 7 |
|--------|-----|---------|--------------|
| | | | |

3

2

1

4

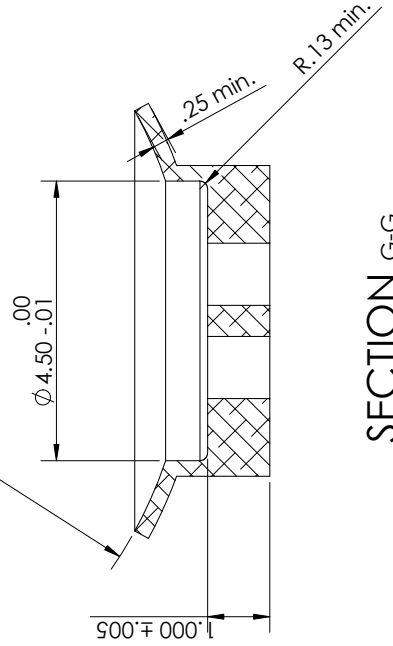
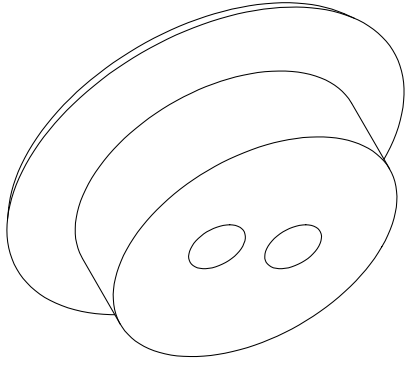
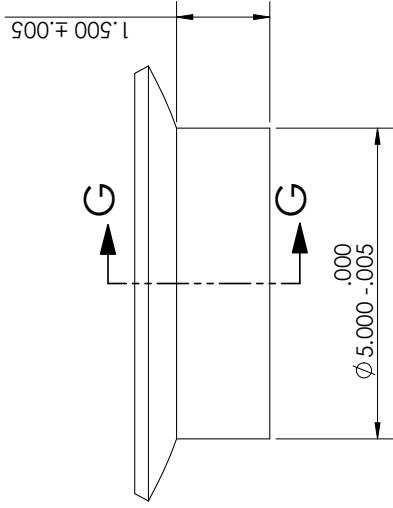
3

2

1

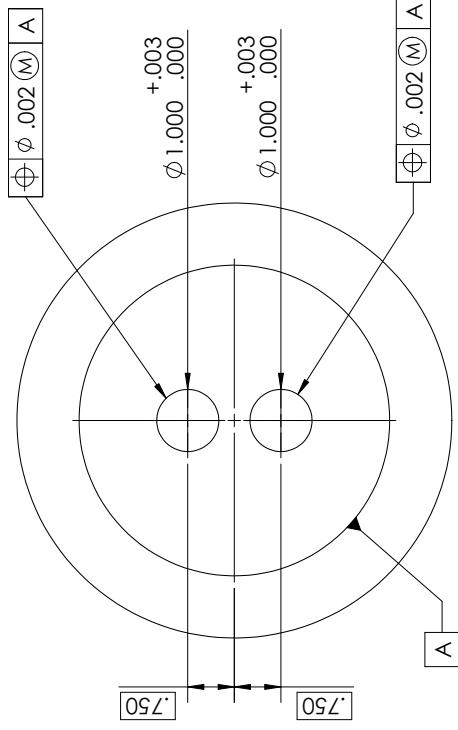
NOTE: POLAR BOSS NEEDS REDESIGN FOR COMPATIBILITY WITH PLUMBING SYSTEM DURING THE PLUMBING DESIGN PROCESS.

NOTE: ALL UNITS IN INCHES UNLESS OTHERWISE STATED



SECTION G-G

SCALE 1 : 2



A

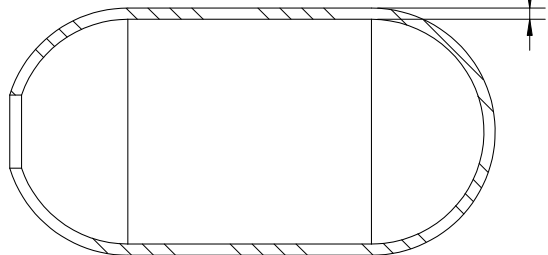
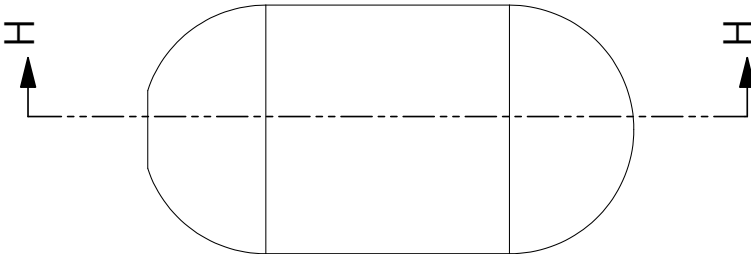
B

A

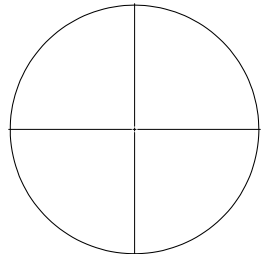
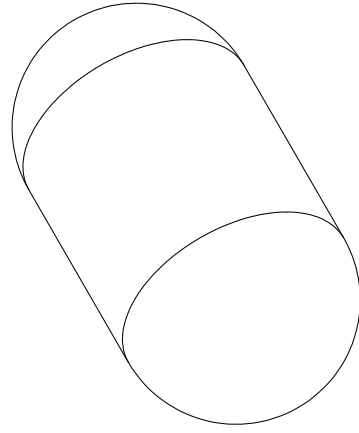
B

| UNLESS OTHERWISE SPECIFIED: | | NAME | DATE |
|--|--------------------|----------------------|----------|
| DIMENSIONS ARE IN INCHES | | John Slugg | 11/06/20 |
| TOLERANCES: | | | |
| ANGULAR: | | | |
| MACH ±0.5 BEND ±1.0 | | | |
| TWO PLACE DECIMAL ±.01 | | | |
| THREE PLACE DECIMAL ±.005 | | | |
| INTERPRET GEOMETRIC TOLERANCING PER: ASME Y14.5-09 | | | |
| MATERIAL: | 6061 Aluminum | | |
| FINISH: | Clean with acetone | | |
| DO NOT SCALE DRAWING | | | |
| TITLE: | | Bottom Polar Boss | |
| SIZE | DWG. NO. | REV | |
| B | N2 COPV Assembly | 1 | |
| SCALE: 1:2 | | WEIGHT: SHEET 6 OF 7 | |

4 3 2 1



SECTION H-H
SCALE 1 : 8

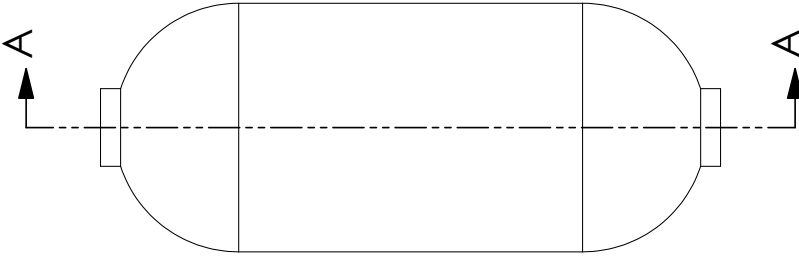


NOTE : BY VIRTUE OF THE FILAMENT WINDING
MANUFACTURING PROCESS ALL DIMENSIONS
FOR THE OVERWRAP WILL BE DEPENDANT ON
FINAL DIMENSIONS OF THE LINER ASSEMBLY

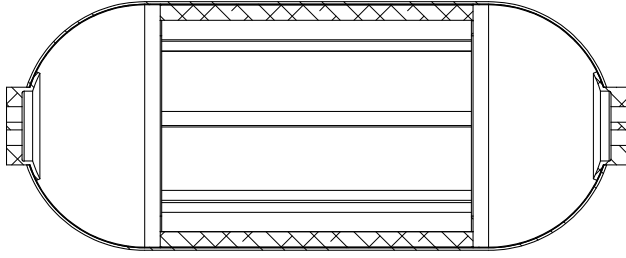
| UNLESS OTHERWISE SPECIFIED: | | NAME | DATE |
|--------------------------------|----------------------|----------------|----------|
| DIMENSIONS ARE IN INCHES | DRAWN | John Slugg | 11/06/20 |
| TOLERANCES: | CHECKED | | |
| ANGULAR: | BNG APPR. | | |
| MACH ±0.5 BEND ±1.0 | MFG APPR. | | |
| TWO PLACE DECIMAL ±.01 | Q.A. | | |
| THREE PLACE DECIMAL ±.005 | COMMENTS: | | |
| INTERPRET GEOMETRIC | MATERIAL | T11000G/3501-6 | |
| TOLERANCING PER: ASME Y14.5-09 | FINISH | Sand and paint | |
| | DO NOT SCALE DRAWING | | |
| SIZE | DWG. NO. | REV | |
| B | N2 COPV Assembly | | |
| SCALE: 1:8 | WEIGHT: | SHEET 7 OF 7 | |

Overwrap

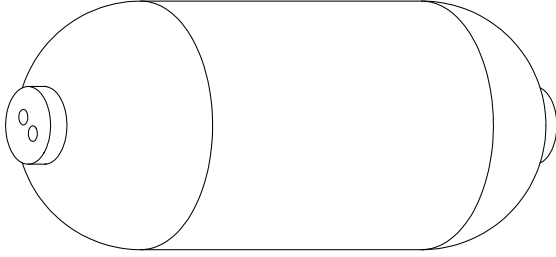
4



3



2



1

RP1 COPV Assembly

B

B

SECTION A-A

SCALE 1 : 8

A

A

| ITEM NO. | PART NUMBER | DESCRIPTION | QTY. |
|----------|---------------------|------------------------------|------|
| 1 | RP1 Liner Assembly | Liner Assembly | 1 |
| 2 | RP1_Cylinder | Cylinder | 1 |
| 3 | Hemispherical_Open | Hemispherical Open Tank Head | 2 |
| 4 | RP1 Baffle Assembly | Baffle Assembly | 1 |
| 5 | Individual_Baffle | Circumferential Baffle | 2 |
| 6 | RP1 | Vertical Angle Aluminum | 8 |
| 7 | RP1_Top | Top Polar Boss | 1 |
| 8 | RP1_Bottom | Bottom Polar Boss | 1 |
| 9 | RP1 Overwrap | Overwrap | 1 |

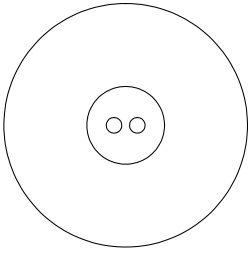
3

SOLIDWORKS Educational Product. For Instructional Use Only.

2

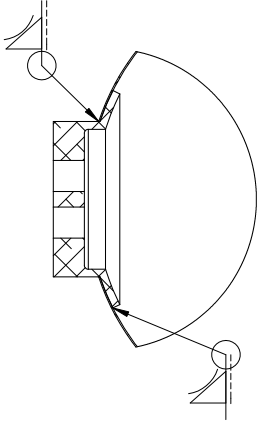
1

4



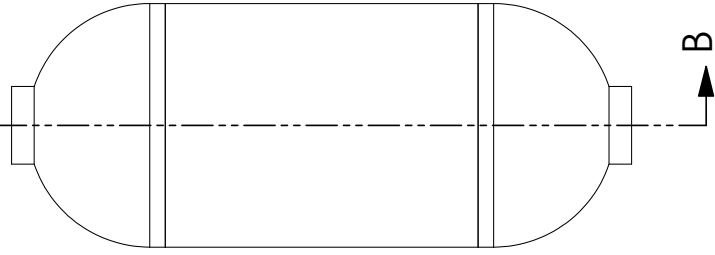
B

3



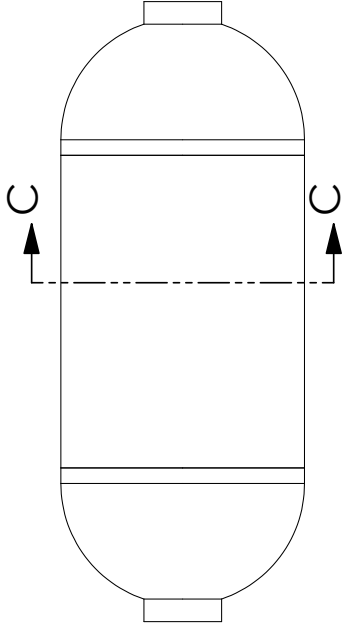
DETAIL D

B



A

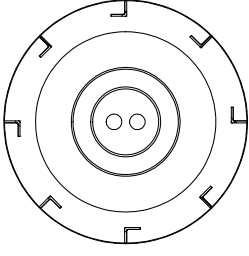
2



SECTION C-C

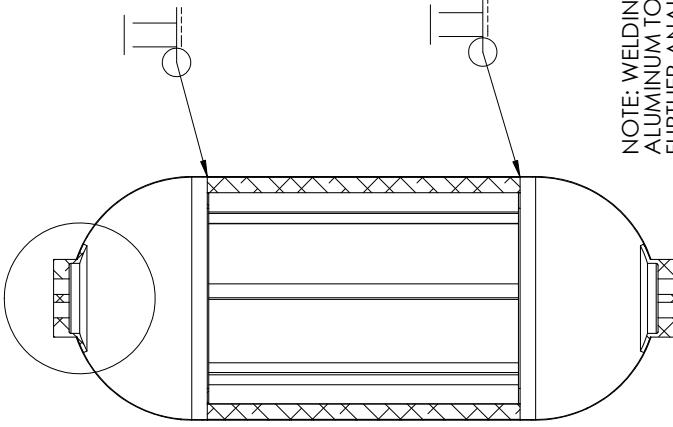
SCALE 1:8

1



B

D



SECTION B-B

SCALE 1:8

3

| ITEM NO. | PART NUMBER | DESCRIPTION | QTY. |
|----------|---------------------|------------------------------|------|
| 1 | RP1_Cylinder | Cylinder | 1 |
| 2 | Hemispherical_Open | Hemispherical Open Tank Head | 2 |
| 3 | RP1 Baffle Assembly | Baffle Assembly | 1 |
| 4 | RP1_Top | Top Polar Boss | 1 |
| 5 | RP1_Bottom | Bottom Polar Boss | 1 |

| UNLESS OTHERWISE SPECIFIED: | | NAME | DATE |
|--|----------------------|--------------------|----------|
| DIMENSIONS ARE IN INCHES | DRAWN | John Slugg | 11/06/20 |
| TOLERANCES: | CHECKED | | |
| ANGULAR: | BNG APPR. | | |
| MACH±0.5 BEND ±1.0 | MFG APPR. | | |
| TWO PLACE DECIMAL ±0.01 | Q.A. | | |
| THREE PLACE DECIMAL ±0.05 | COMMENTS: | | |
| INTERPRET GEOMETRIC TOLERANCING PER: ASME Y14.5-09 | MATERIAL | 6061 Aluminum | |
| | FINISH | Clean with acetone | |
| | DO NOT SCALE DRAWING | | |

NOTE: WELDING OF VERTICAL ANGLE ALUMINUM TO CYLINDER REQUIRES FURTHER ANALYSIS BEFORE SELECTION

TITLE:

RP1 Liner Assembly

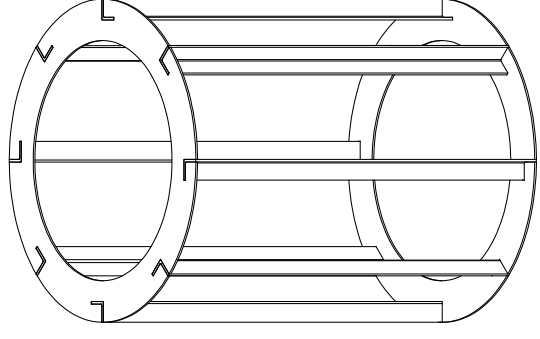
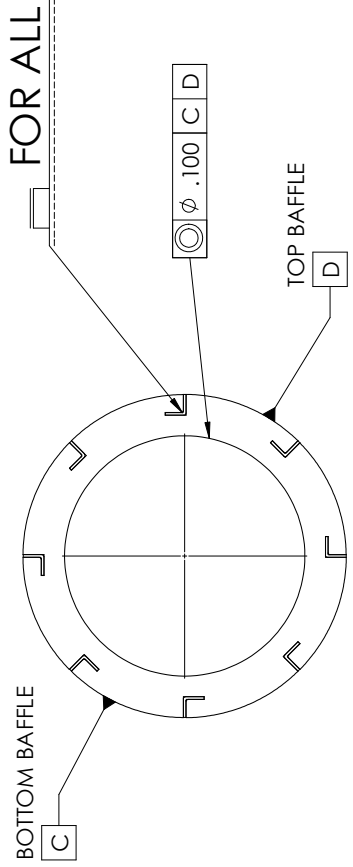
SIZE DWG. NO. REV

B RP1 COPV Assembly

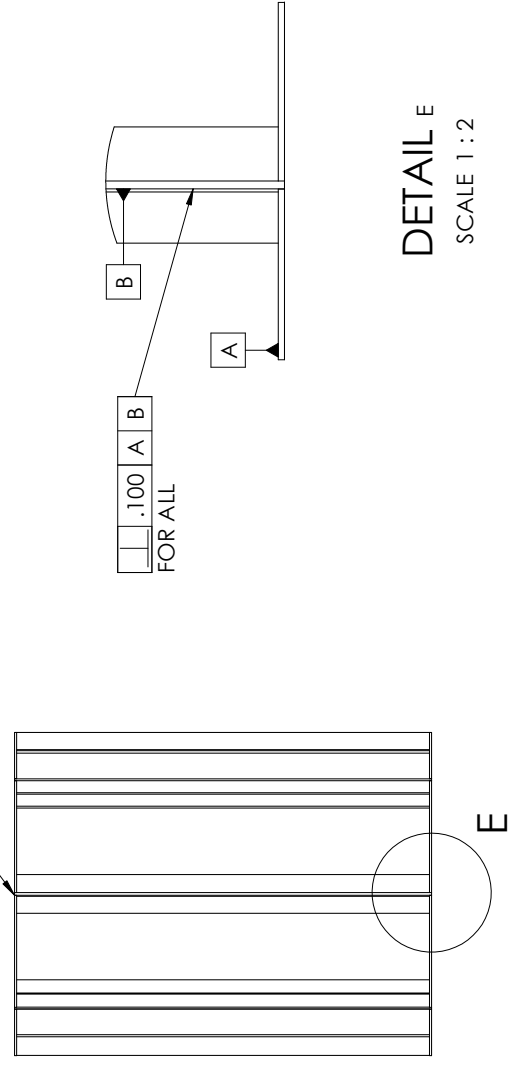
SCALE: 1:8 WEIGHT: SHEET 2 OF 10

4 3 2 1

| ITEM NO. | PART NUMBER | DESCRIPTION | QTY. |
|----------|-------------------|-------------------------|------|
| 1 | Individual_Baffle | Circumferential Baffle | 2 |
| 2 | RP1 | Vertical Angle Aluminum | 8 |



NOTE: EXTERNAL FACES OF CIRCUMFERENTIAL BAFFLES LIE FLUSH WITH ENDS OF VERTICAL ANGLE ALUMINUM



DETAIL E
SCALE 1 : 2

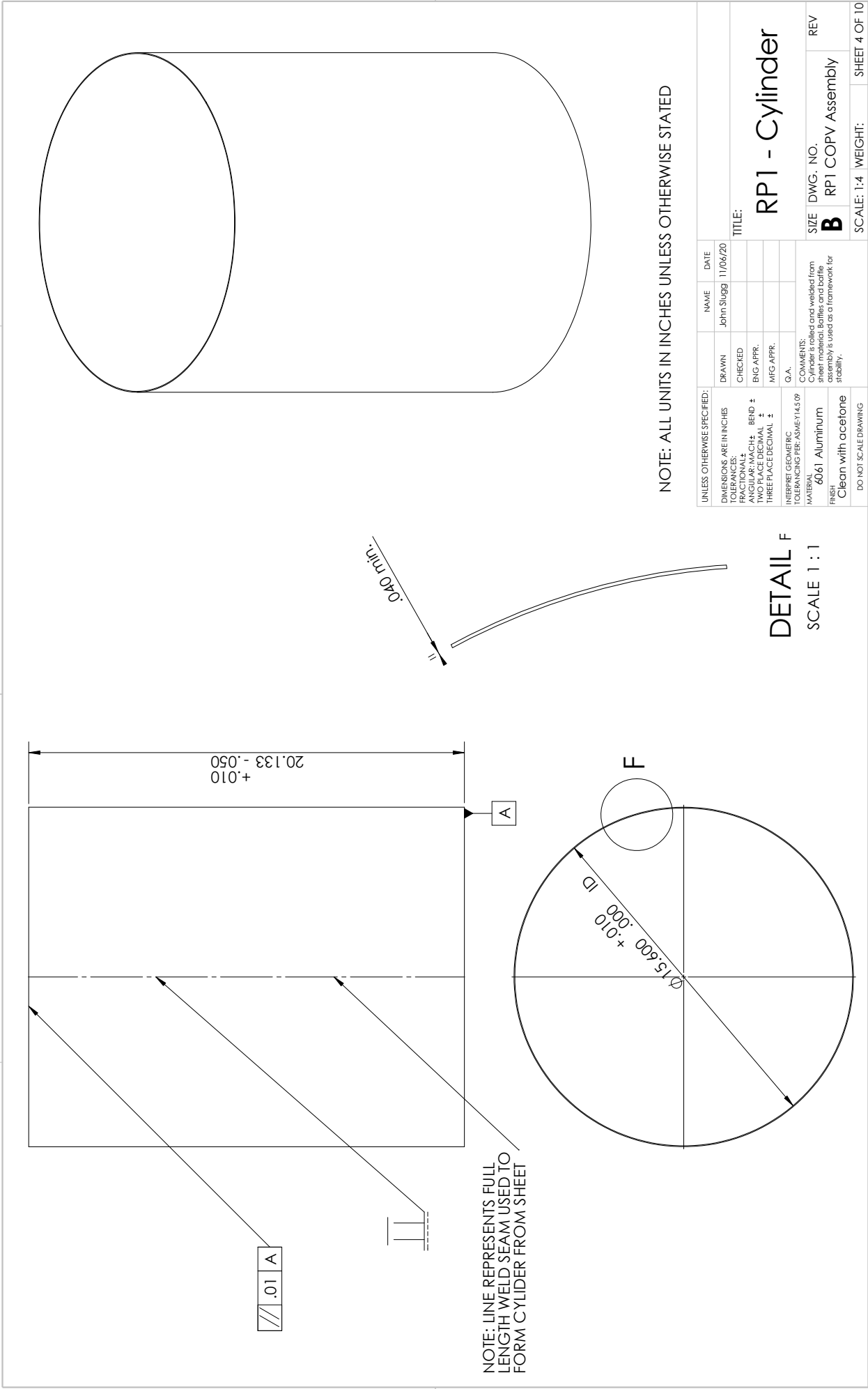
NOTE: ALL UNITS IN INCHES UNLESS OTHERWISE STATED

| UNLESS OTHERWISE SPECIFIED: | DRAWN | NAME | DATE |
|--|------------|------------|----------|
| DIMENSIONS ARE IN INCHES | John Slugg | John Slugg | 11/06/20 |
| TOLERANCES: | CHECKED | | |
| ANGULAR: | BNG APPR. | | |
| MACH ±0.5 BEND ±1.0 | MFG APPR. | | |
| TWO PLACE DECIMAL ±.01 | Q.A. | | |
| THREE PLACE DECIMAL ±.005 | COMMENTS: | | |
| INTERPRET GEOMETRIC TOLERANCING PER: ASME Y14.5-09 | | | |
| MATERIAL: | | | |
| 6061 Aluminum | | | |
| FINISH: | | | |
| Clean with acetone | | | |
| DO NOT SCALE DRAWING | | | |

RP1 Baffle
Assembly

| | | |
|------------|-------------------|---------------|
| SIZE | DWG. NO. | REV |
| B | RP1 COPV Assembly | |
| SCALE: 1:6 | WEIGHT: | SHEET 3 OF 10 |

4 3 2 1



/// .01 A

NOTE: LINE REPRESENTS FULL LENGTH WELD SEAM USED TO FORM CYLINDER FROM SHEET

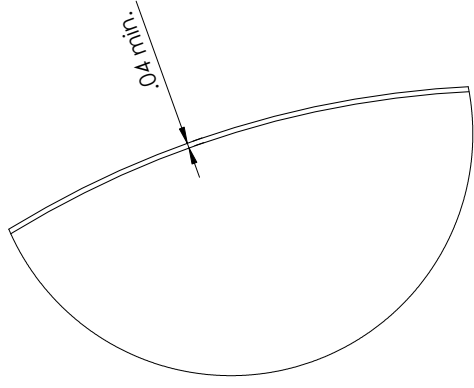
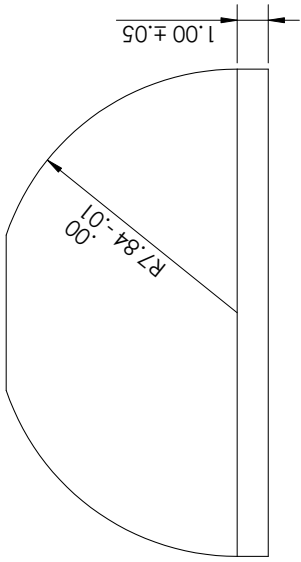
DETAIL F
SCALE 1 : 1

NOTE: ALL UNITS IN INCHES UNLESS OTHERWISE STATED

| UNLESS OTHERWISE SPECIFIED: | | NAME | DATE |
|--|------------|----------|-------------------|
| DRAWN | John Slugg | 11/06/20 | |
| CHECKED | | | |
| FRACTIONAL ± | | | |
| ANGULAR: MACH ± | BEND ± | | |
| TWO PLACE DECIMAL ± | ENG APPR. | | |
| THREE PLACE DECIMAL ± | MFG APPR. | | |
| INTERPRET GEOMETRIC TOLERANCING PER: ASME Y14.5-09 | Q.A. | | |
| COMMENTS: | | | |
| Cylinder is rolled and welded from sheet material. Baffles and baffle assembly is used as a framework for stability. | | | |
| MATERIAL | | SIZE | DWG. NO. |
| 6061 Aluminum | | B | RP1 COPV Assembly |
| FINISH | | REV | |
| Clean with acetone | | 1 | |
| DO NOT SCALE DRAWING | | | SHEET 4 OF 10 |

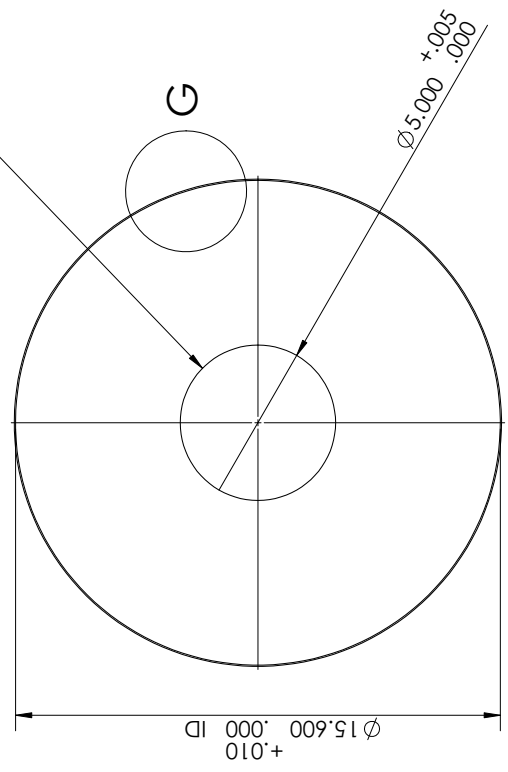
TITLE: RP1 - Cylinder

4 3 2 1



DETAIL G
SCALE 1 : 1

NOTE: CENTER HOLE CUT FROM FULL HEMISPHERE HEAD

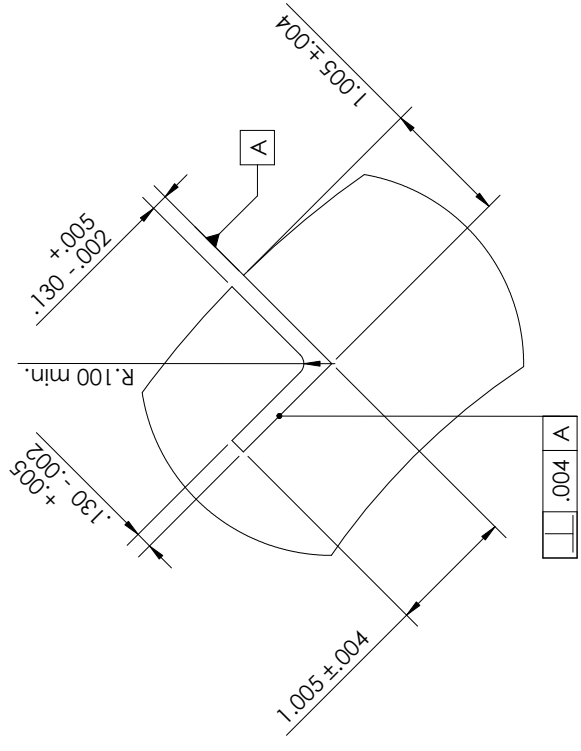
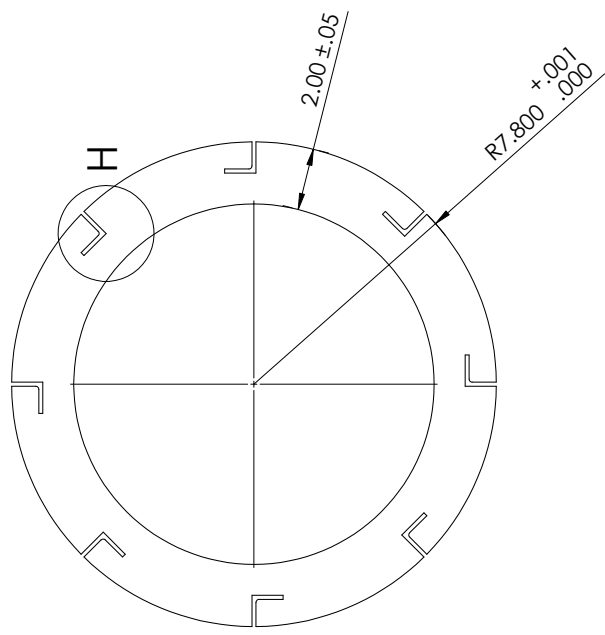
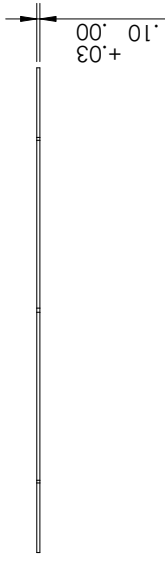


NOTE: ALL UNITS IN INCHES UNLESS OTHERWISE STATED

| UNLESS OTHERWISE SPECIFIED: | | NAME | DATE |
|--|--------------------|----------|------|
| DRAWN | John Slugg | 11/06/20 | |
| CHECKED | | | |
| ANGULAR: | | | |
| MACH±0.5 BEND ±1.0 | | | |
| TWO PLACE DECIMAL ±.01 | | | |
| THREE PLACE DECIMAL ±.005 | | | |
| INTERPRET GEOMETRIC TOLERANCING PER: ASME Y14.5-09 | | | |
| MATERIAL | 6061 Aluminum | | |
| FINISH | Clean with acetone | | |
| DO NOT SCALE DRAWING | | | |

| | | | | |
|------------------------------|--|---------|-------------------|-----|
| TITLE: | | SIZE | DWG. NO. | REV |
| Hemispherical open tank head | | B | RP1 COPV Assembly | |
| SCALE: 1:4 | | WEIGHT: | SHEET 5 OF 10 | |

4 3 2 1



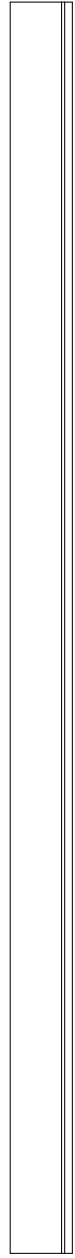
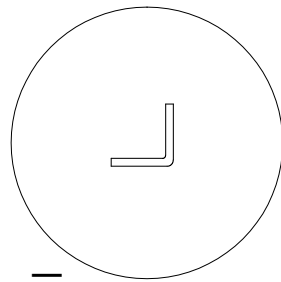
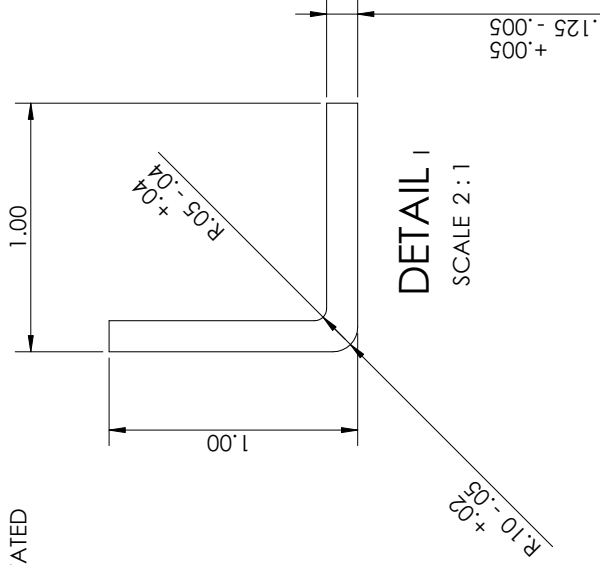
DETAIL H
SCALE 1 : 1

| | | | |
|--|-----------|-----------------------|----------|
| UNLESS OTHERWISE SPECIFIED: | | NAME | DATE |
| DIMENSIONS ARE IN INCHES | | John Slugg | 11/06/20 |
| TOLERANCES: | | | |
| ANGULAR: | | | |
| MACH ± 0.5 BEND ± 1.0 | | | |
| TWO PLACE DECIMAL ± 0.1 | | | |
| THREE PLACE DECIMAL ± 0.05 | | | |
| Q.A. | | | |
| INTERPRET GEOMETRIC TOLERANCING PER: ASME Y14.5-09 | | | |
| MATERIAL: | COMMENTS: | | |
| 6061 Aluminum | | | |
| FINISH: | | | |
| Clean with acetone | | | |
| DO NOT SCALE DRAWING | | | |
| TITLE: | | REV | |
| Circumferential Baffle | | B | |
| SIZE DWG. NO. | | RP1 COPV Assembly | |
| SCALE: 1:4 | | WEIGHT: SHEET 6 OF 10 | |

NOTE: ALL UNITS IN INCHES UNLESS OTHERWISE STATED

4 3 2 1

NOTE: ALL UNITS IN INCHES UNLESS OTHERWISE STATED



| UNLESS OTHERWISE SPECIFIED: | | NAME | DATE |
|--|----------------------|--------------------|---------------|
| DIMENSIONS ARE IN INCHES | DRAWN | John Slugg | 11/06/20 |
| TOLERANCES: | CHECKED | | |
| ANGULAR: | BNG APPR. | | |
| MACH ±0.5 BEND ±1.0 | MFG APPR. | | |
| TWO PLACE DECIMAL ±.01 | Q.A. | | |
| THREE PLACE DECIMAL ±.005 | COMMENTS: | | |
| INTERPRET GEOMETRIC TOLERANCING PER: ASME Y14.5-09 | MATERIAL | 6061 Aluminum | |
| | FINISH | Clean with acetone | |
| | DO NOT SCALE DRAWING | | |
| | SIZE | DWG. NO. | REV |
| | B | RP1 COPV Assembly | |
| | SCALE: 1:16 | WEIGHT: | SHEET 7 OF 10 |

Vertical Angle Aluminum

SOLIDWORKS Educational Product. For Instructional Use Only. 3 2 1

B

A

B

A

4

3

2

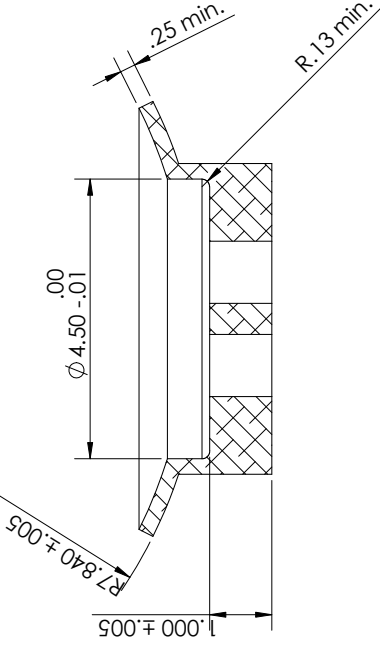
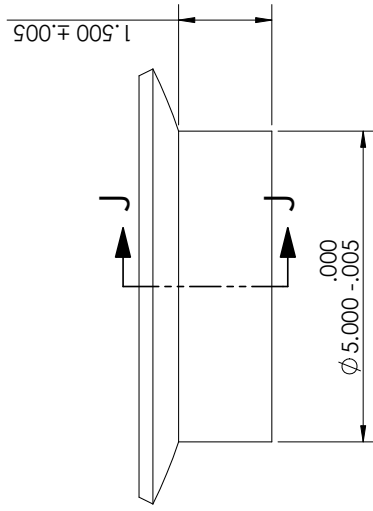
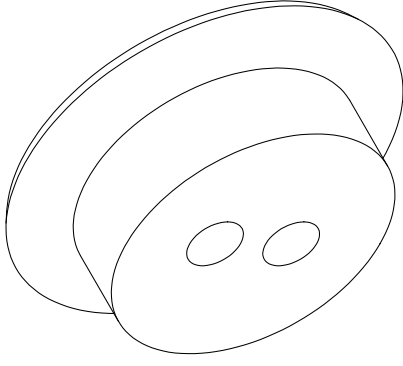
1

NOTE: POLAR BOSS NEEDS REDESIGN FOR COMPATIBILITY WITH PLUMBING SYSTEM DURING THE PLUMBING DESIGN PROCESS.

NOTE: ALL UNITS IN INCHES UNLESS OTHERWISE STATED

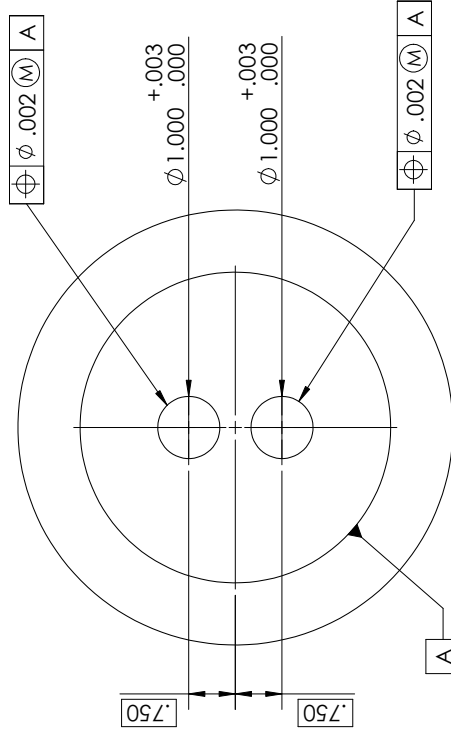
B

B



SECTION J-J

SCALE 1 : 2



A

A

| | | | |
|--|--------------------|------------|----------|
| UNLESS OTHERWISE SPECIFIED: | | NAME | DATE |
| DIMENSIONS ARE IN INCHES | | John Slugg | 11/06/20 |
| TOLERANCES: | | | |
| ANGULAR: | | | |
| MACH ±0.5 BEND ±1.0 | BNG APPR. | | |
| TWO PLACE DECIMAL ±.01 | MFG APPR. | | |
| THREE PLACE DECIMAL ±.005 | Q.A. | | |
| INTERPRET GEOMETRIC TOLERANCING PER: ASME Y14.5-09 | COMMENTS: | | |
| MATERIAL | 6061 Aluminum | | |
| FINISH | Clean with acetone | | |
| DO NOT SCALE DRAWING | | | |

TITLE:

Top Polar Boss

SIZE DWG. NO. REV

B RP1 COPV Assembly

SCALE: 1:2 WEIGHT:

SHEET 8 OF 10

3

2

1

4

3

2

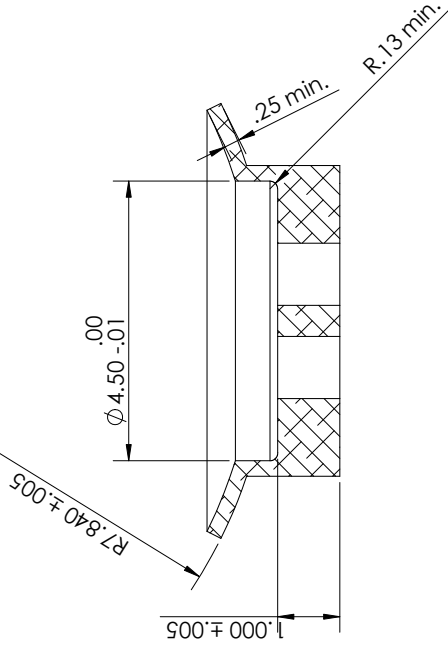
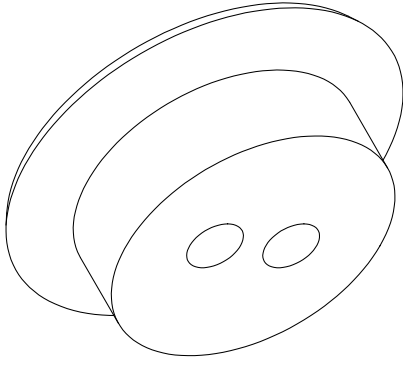
1

NOTE: POLAR BOSS NEEDS REDESIGN FOR COMPATIBILITY WITH PLUMBING SYSTEM DURING THE PLUMBING DESIGN PROCESS.

NOTE: ALL UNITS IN INCHES UNLESS OTHERWISE STATED

B

B

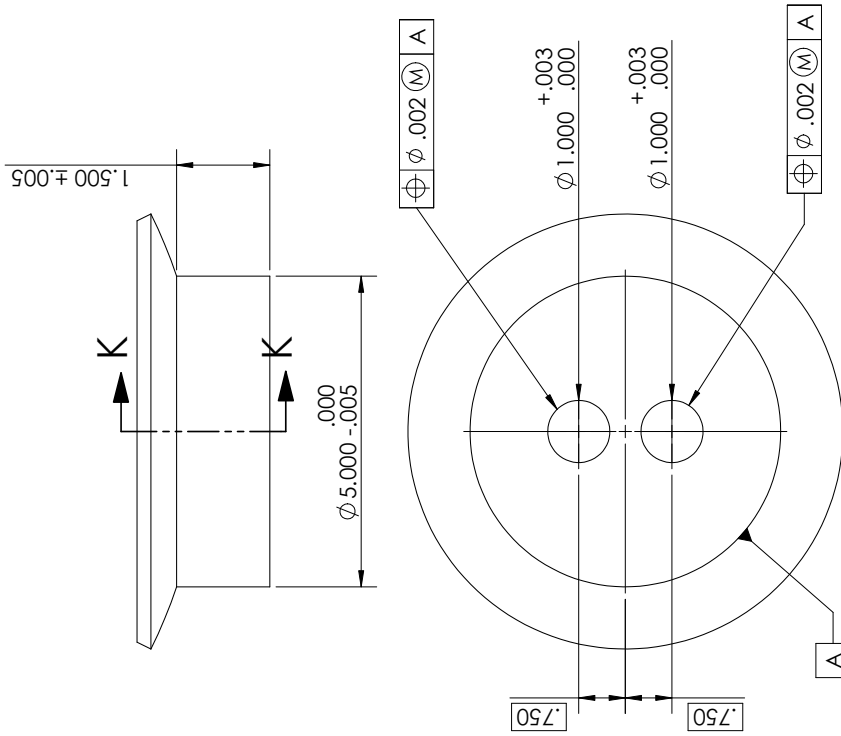


SECTION K-K

SCALE 1:2

A

A



| UNLESS OTHERWISE SPECIFIED: | | NAME | DATE |
|--|--------------------|----------|------|
| DRAWN | John Slugg | 11/06/20 | |
| CHECKED | | | |
| ANGULAR: | | | |
| MACH±0.5 | BEND ±1.0 | | |
| TWO PLACE DECIMAL | ±.01 | | |
| THREE PLACE DECIMAL | ±.005 | | |
| INTERPRET GEOMETRIC TOLERANCING PER: ASME Y14.5-09 | | | |
| MATERIAL | 6061 Aluminum | | |
| FINISH | Clean with acetone | | |
| DO NOT SCALE DRAWING | | | |

TITLE: **Bottom Polar Boss**

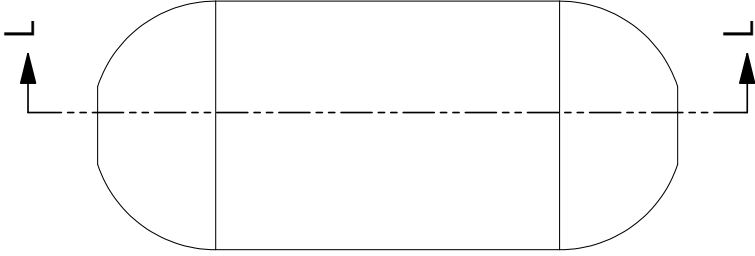
| | | |
|------------|-------------------|---------------|
| SIZE | DWG. NO. | REV |
| B | RP1 COPV Assembly | |
| SCALE: 1:2 | WEIGHT: | SHEET 9 OF 10 |

3

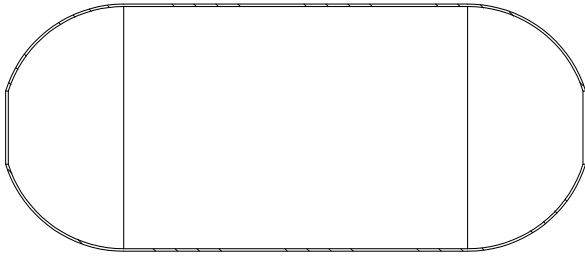
2

1

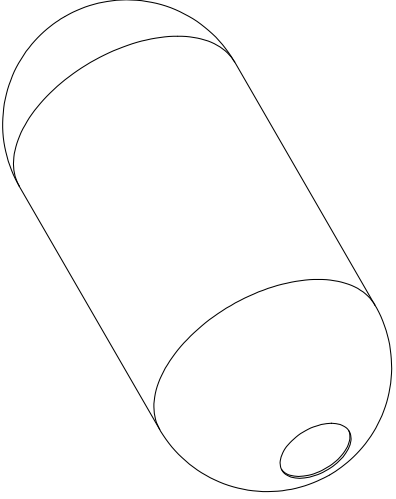
4



3



2



1

B

B

A

A

SECTION L-L

SCALE 1 : 8

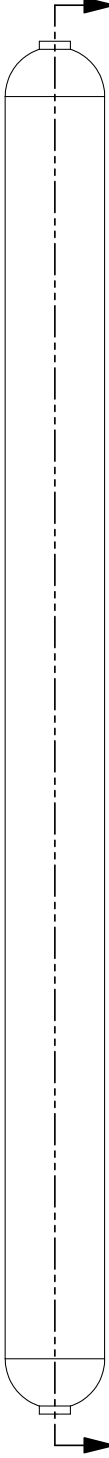
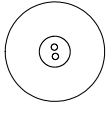
NOTE : BY VIRTUE OF THE FILAMENT WINDING
 MANUFACTURING PROCESS ALL DIMENSIONS
 FOR THE OVERWRAP WILL BE DEPENDANT ON
 FINAL DIMENSIONS OF THE LINER ASSEMBLY

| UNLESS OTHERWISE SPECIFIED: | | NAME | DATE |
|--------------------------------|-------------------|----------------|----------|
| DIMENSIONS ARE IN INCHES | | John Slugg | 11/06/20 |
| TOLERANCES: | | | |
| ANGULAR: | | | |
| MACH ±0.5 BEND ±1.0 | | | |
| TWO PLACE DECIMAL ±.01 | | | |
| THREE PLACE DECIMAL ±.005 | | | |
| INTERPRET GEOMETRIC | | | |
| TOLERANCING PER: ASME Y14.5-09 | | | |
| MATERIAL: | COMMENTS: | | |
| T11000G/3501-6 | | | |
| FINISH: | | | |
| Sand and Paint | | | |
| DO NOT SCALE DRAWING | | | |
| SIZE | DWG. NO. | REV | |
| B | RP1 COPV Assembly | | |
| SCALE: 1:8 | WEIGHT: | SHEET 10 OF 10 | |

Overwrap

4 3 2 1

HTP COPV Assembly

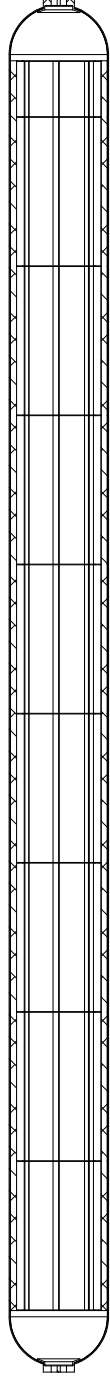


A

A

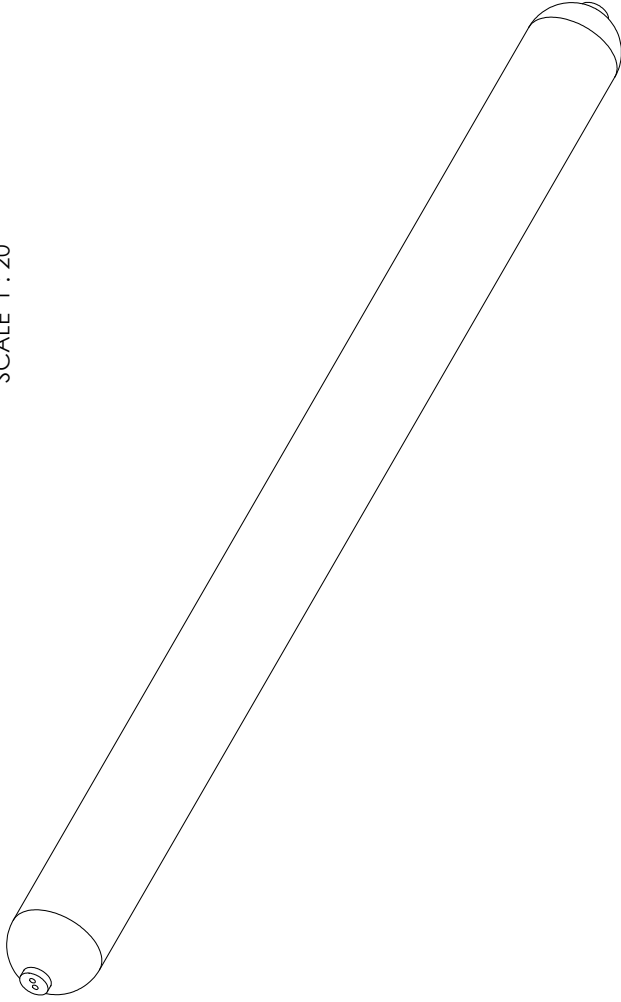
B

B



SECTION A-A

SCALE 1 : 20



A

A

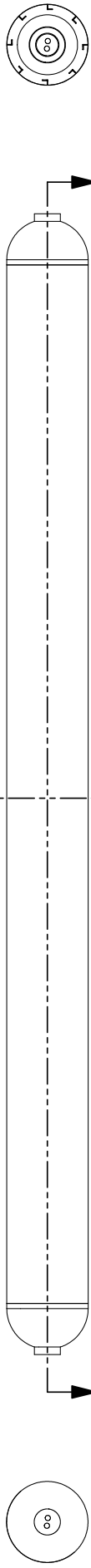
| ITEM NO. | PART NUMBER | DESCRIPTION | QTY. |
|----------|---------------------|------------------------------|------|
| 1 | HTP Liner Assembly | Liner Assembly | 1 |
| 2 | HTP_Cylinder | Cylinder | 1 |
| 3 | Hemispherical_Open | Hemispherical Open Tank Head | 2 |
| 4 | HTP Baffle Assembly | Baffle Assembly | 1 |
| 5 | Individual_Baffle | Circumferential Baffle | 10 |
| 6 | HTP | Vertical Angle Aluminum | 8 |
| 7 | HTP_Top | Top Polar Boss | 1 |
| 8 | HTP_Bottom | Bottom Polar Boss | 1 |
| 9 | HTP Overwrap | Overwrap | 1 |

1

2

3

4 3 2 1



C

C

B

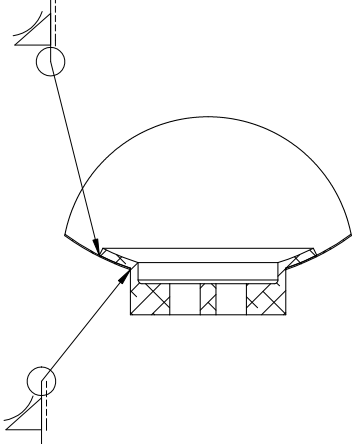
B

SECTION D-D
SCALE 1 : 20



SECTION C-C

SCALE 1 : 20



DETAIL B
SCALE 1 : 4

NOTE: WELDING OF VERTICAL ANGLE ALUMINUM AND
INNER CIRCUMFERENTIAL BAFFLES TO CYLINDER
REQUIRES FURTHER ANALYSIS BEFORE SELECTION

| ITEM NO. | PART NUMBER | DESCRIPTION | QTY. |
|----------|---------------------|------------------------------|------|
| 1 | HTP_Cylinder | Cylinder | 1 |
| 2 | Hemispherical_Open | Hemispherical Open Tank Head | 2 |
| 3 | HTP Baffle Assembly | Baffle Assembly | 1 |
| 4 | HTP_Top | Top Polar Boss | 1 |
| 5 | HTP_Bottom | Bottom Polar Boss | 1 |

| UNLESS OTHERWISE SPECIFIED: | NAME | DATE |
|--|--------------------|----------|
| DIMENSIONS ARE IN INCHES | John Slugg | 11/06/20 |
| TOLERANCES: | | |
| ANGULAR: | | |
| MACH ±0.5 BEND ±1.0 | | |
| TWO PLACE DECIMAL ±0.1 | | |
| THREE PLACE DECIMAL ±0.05 | | |
| MFG APPR. | | |
| Q.A. | | |
| INTERPRET GEOMETRIC TOLERANCING PER: ASME Y14.5-09 | | |
| MATERIAL | 6061 Aluminum | |
| FINISH | Clean with acetone | |
| DO NOT SCALE DRAWING | | |

HTP Liner
Assembly

| | | |
|-------------|-------------------|---------------|
| SIZE | DWG. NO. | REV |
| B | HTP COPV Assembly | |
| SCALE: 1:20 | WEIGHT: | SHEET 2 OF 10 |

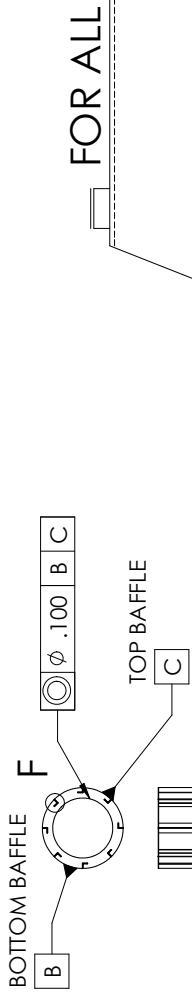
1

2

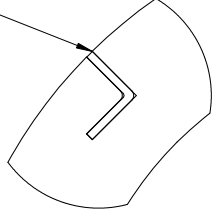
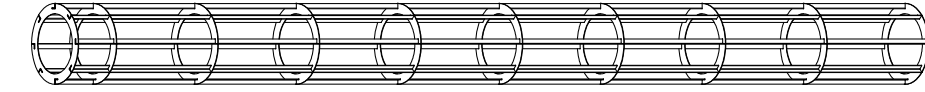
3

4

| ITEM NO. | PART NUMBER | DESCRIPTION | QTY. |
|----------|-------------------|-------------------------|------|
| 1 | Individual_Baffle | Circumferential Baffle | 10 |
| 2 | HTP | Vertical Angle Aluminum | 8 |



FOR ALL



DETAIL E
SCALE 1 : 2

NOTE: ALL UNITS IN INCHES UNLESS OTHERWISE STATED

| UNLESS OTHERWISE SPECIFIED: | | NAME | DATE |
|--------------------------------|--------------------|------------|----------|
| DIMENSIONS ARE IN INCHES | | John Slugg | 11/06/20 |
| TOLERANCES: | | | |
| ANGULAR: | | | |
| MACH ±0.5 | BEND ±1.0 | | |
| TWO PLACE DECIMAL | ±.01 | | |
| THREE PLACE DECIMAL | ±.005 | | |
| INTERPRET GEOMETRIC | Q.A. | | |
| TOLERANCING PER: ASME Y14.5-09 | COMMENTS: | | |
| MATERIAL: | 6061 Aluminum | | |
| FINISH: | Clean with acetone | | |
| DO NOT SCALE DRAWING | | | |

| | | |
|-------------|-------------------|---------------------|
| TITLE: | | HTP Baffle Assembly |
| SIZE | DWG. NO. | REV |
| B | HTP COPV Assembly | |
| SCALE: 1:24 | WEIGHT: | SHEET 3 OF 10 |

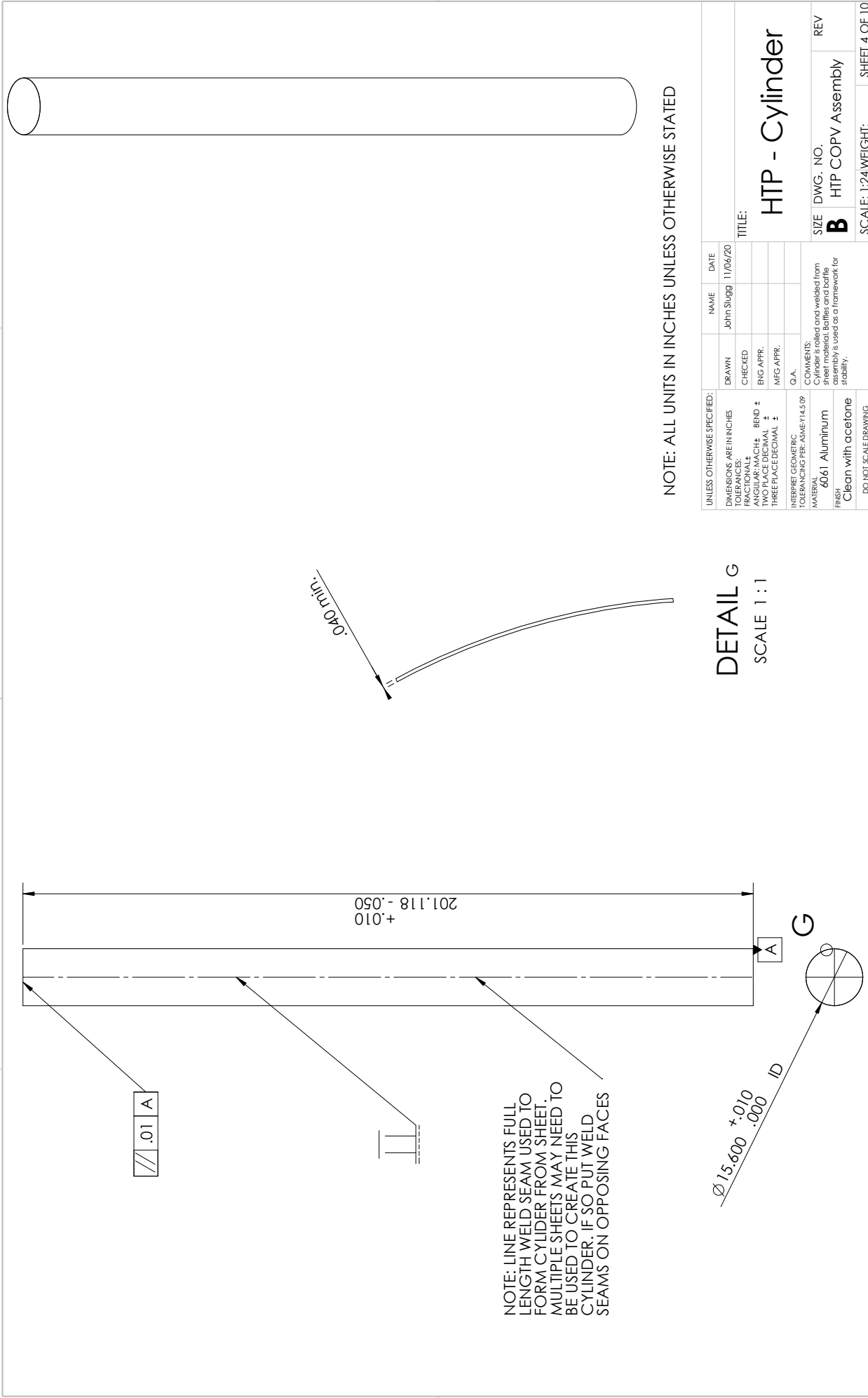
1

2

3

4

4 3 2 1



NOTE: LINE REPRESENTS FULL LENGTH WELD SEAM USED TO FORM CYLINDER FROM SHEET. MULTIPLE SHEETS MAY NEED TO BE USED TO CREATE THIS CYLINDER. IF SO PUT WELD SEAMS ON OPPOSING FACES

DETAIL G
SCALE 1 : 1

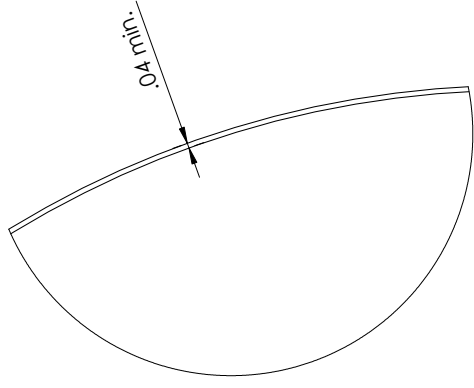
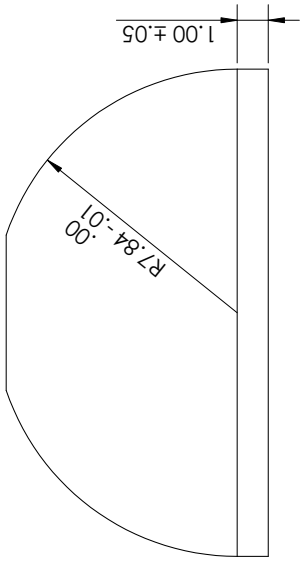
NOTE: ALL UNITS IN INCHES UNLESS OTHERWISE STATED

| UNLESS OTHERWISE SPECIFIED: | | NAME | DATE |
|--|------------|----------|------|
| DRAWN | John Slugg | 11/06/20 | |
| CHECKED | | | |
| ANGULAR: MACH ± | BEND ± | | |
| TWO PLACE DECIMAL ± | ENG APPR. | | |
| THREE PLACE DECIMAL ± | MFG APPR. | | |
| | Q.A. | | |
| COMMENTS: | | | |
| INTERPRET GEOMETRIC TOLERANCING PER: ASME Y14.5-09 | | | |
| MATERIAL: 6061 Aluminum | | | |
| FINISH: Clean with acetone | | | |
| DO NOT SCALE DRAWING | | | |

| | | |
|----------------|-------------------|-----|
| SIZE | DWG. NO. | REV |
| B | HTP COPV Assembly | |
| TITLE: | | |
| HTP - Cylinder | | |

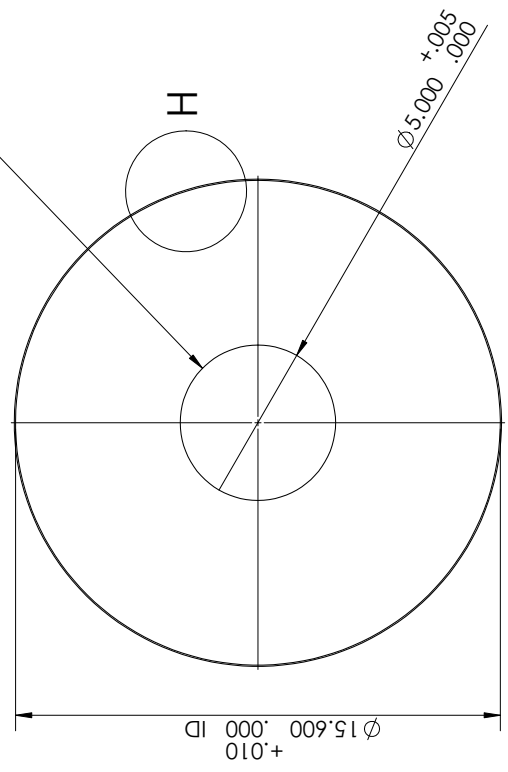
| | | |
|-------------|---------|---------------|
| SCALE: 1:24 | WEIGHT: | SHEET 4 OF 10 |
|-------------|---------|---------------|

4 3 2 1



DETAIL H
SCALE 1 : 1

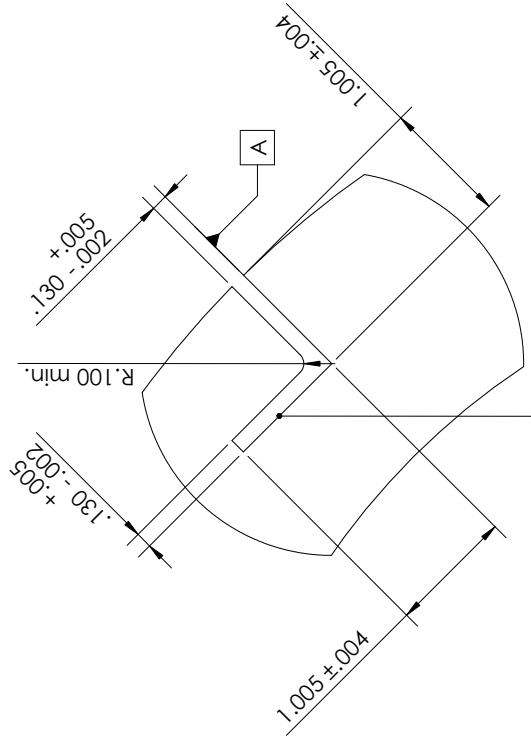
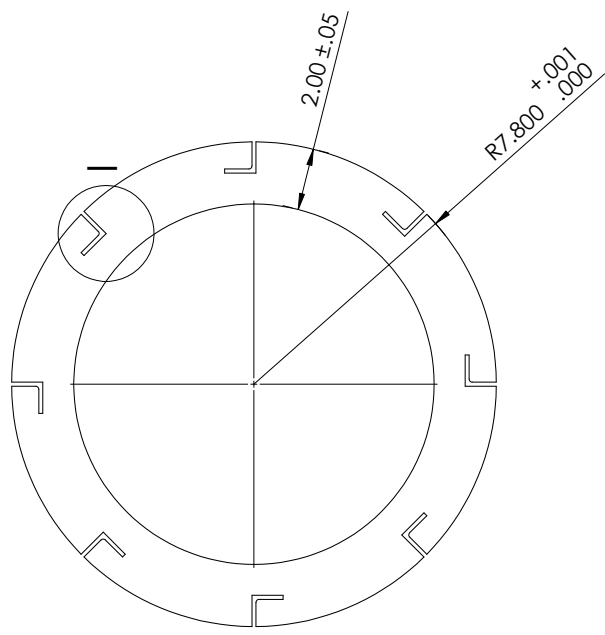
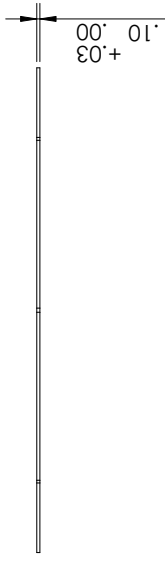
NOTE: CENTER HOLE CUT FROM FULL HEMISPHERE HEAD



NOTE: ALL UNITS IN INCHES UNLESS OTHERWISE STATED

| UNLESS OTHERWISE SPECIFIED: | | NAME | DATE |
|--------------------------------|-------------------|------------------------------|---------------|
| DIMENSIONS ARE IN INCHES | | John Slugg | 11/06/20 |
| TOLERANCES: | | | |
| ANGULAR: | | | |
| MACH±0.5 BEND ±1.0 | | | |
| TWO PLACE DECIMAL ±.01 | | | |
| THREE PLACE DECIMAL ±.005 | | | |
| | | | |
| INTERPRET GEOMETRIC | | | |
| TOLERANCING PER: ASME Y14.5-09 | | | |
| MATERIAL: | | | |
| 6061 Aluminum | | | |
| FINISH: | | | |
| Clean with acetone | | | |
| DO NOT SCALE DRAWING | | | |
| TITLE: | | Hemispherical open tank head | |
| SIZE | DWG. NO. | REV | |
| B | HTP COPV Assembly | | |
| SCALE: 1:4 | | WEIGHT: | SHEET 5 OF 10 |

4 3 2 1



.004 A

DETAIL I
SCALE 1 : 1

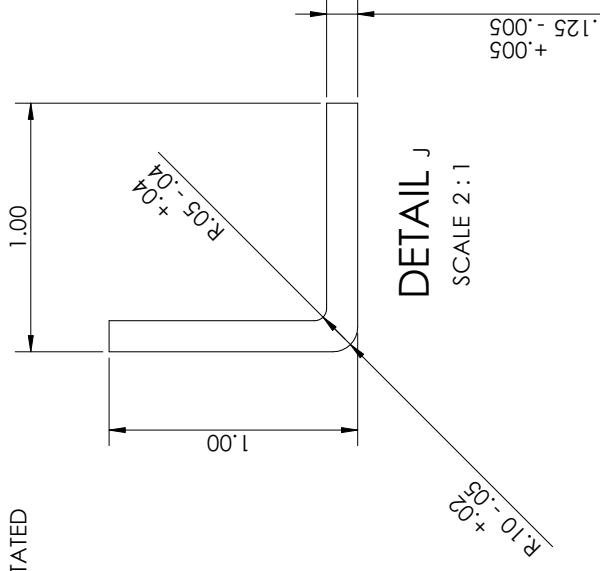
| | | | |
|--------------------------------|--------------------|---------------------|-----------------------|
| UNLESS OTHERWISE SPECIFIED: | | NAME | DATE |
| DIMENSIONS ARE IN INCHES | | John Slugg | 11/06/20 |
| TOLERANCES: | | | |
| ANGULAR: | | | |
| MACH ±0.5 BEND ±1.0 | | | |
| TWO PLACE DECIMAL ±0.1 | | | |
| THREE PLACE DECIMAL ±0.05 | | | |
| INTERPRET GEOMETRIC | | | |
| TOLERANCING PER: ASME Y14.5-09 | | | |
| MATERIAL: | 6061 Aluminum | COMMENTS: | |
| FINISH: | Clean with acetone | SIZE DWG. NO. | REV |
| DO NOT SCALE DRAWING | | B HTP COPV Assembly | 1 |
| | | SCALE: 1:4 | WEIGHT: SHEET 6 OF 10 |

Circumferential Baffle

NOTE: ALL UNITS IN INCHES UNLESS OTHERWISE STATED

4 3 2 1

NOTE: ALL UNITS IN INCHES UNLESS OTHERWISE STATED



201.12

J (L)

| UNLESS OTHERWISE SPECIFIED: | | NAME | DATE |
|--|--------------------|-------------------------|---------------|
| DIMENSIONS ARE IN INCHES | | John Slugg | 11/06/20 |
| TOLERANCES: | | | |
| ANGULAR: | | | |
| MACH ±0.5 BEND ±1.0 | | | |
| TWO PLACE DECIMAL ±.01 | | | |
| THREE PLACE DECIMAL ±.005 | | | |
| Q.A. | | | |
| INTERPRET GEOMETRIC TOLERANCING PER: ASME Y14.5-09 | | | |
| MATERIAL: | 6061 Aluminum | | |
| FINISH: | Clean with acetone | | |
| DO NOT SCALE DRAWING | | | |
| TITLE: | | Vertical Angle Aluminum | |
| SIZE | DWG. NO. | REV | |
| B | HTP COPV Assembly | | |
| SCALE: 1:16 | | WEIGHT: | SHEET 7 OF 10 |

SOLIDWORKS Educational Product. For Instructional Use Only. 3 2 1

B

A

B

A

4

3

2

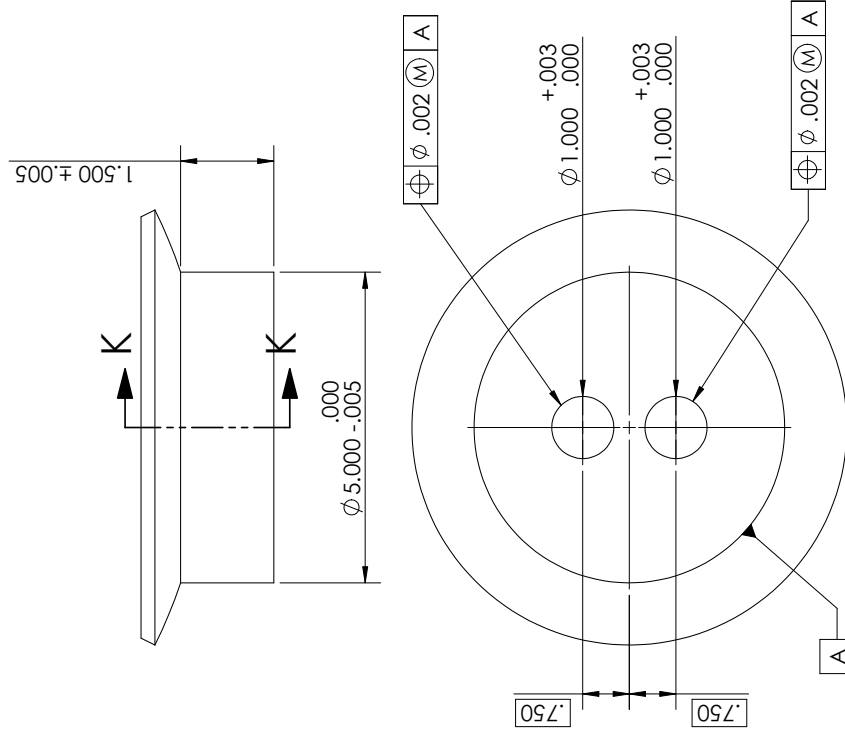
1

NOTE: POLAR BOSS NEEDS REDESIGN FOR COMPATIBILITY WITH PLUMBING SYSTEM DURING THE PLUMBING DESIGN PROCESS.

NOTE: ALL UNITS IN INCHES UNLESS OTHERWISE STATED

B

B



SECTION K-K

SCALE 1 : 2

A

A

| UNLESS OTHERWISE SPECIFIED: | | NAME | DATE |
|--|----------------------------|------------|----------|
| DIMENSIONS ARE IN INCHES | DRAWN | John Slugg | 11/06/20 |
| TOLERANCES: | CHECKED | | |
| ANGULAR: MACH ±0.5 BEND ±1.0 | BNG APPR. | | |
| TWO PLACE DECIMAL ±.01 | MFG APPR. | | |
| THREE PLACE DECIMAL ±.005 | Q.A. | | |
| INTERPRET GEOMETRIC TOLERANCING PER: ASME Y14.5-09 | COMMENTS: | | |
| MATERIAL: 6061 Aluminum | FINISH: Clean with acetone | | |
| DO NOT SCALE DRAWING | | | |

TITLE: **Top Polar Boss**

SIZE DWG. NO. **B** HTP COPV Assembly REV

SCALE: 1:2 WEIGHT: SHEET 8 OF 10

3

2

1

4

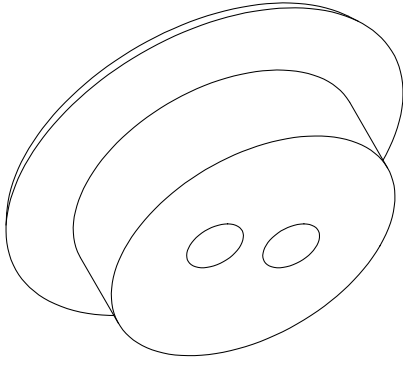
3

2

1

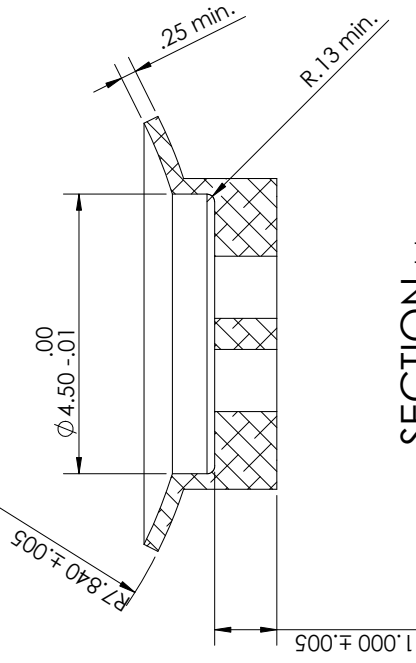
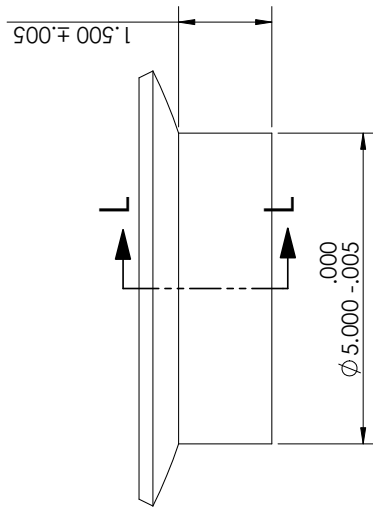
NOTE: POLAR BOSS NEEDS REDESIGN FOR COMPATIBILITY WITH PLUMBING SYSTEM DURING THE PLUMBING DESIGN PROCESS.

NOTE: ALL UNITS IN INCHES UNLESS OTHERWISE STATED

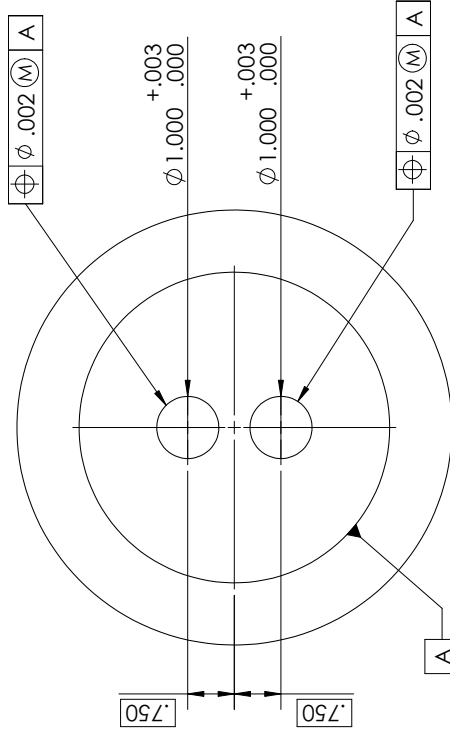


B

A



SECTION L-L
SCALE 1 : 2



| UNLESS OTHERWISE SPECIFIED: | | NAME | DATE |
|--|--------------------|----------|------|
| DRAWN | John Slugg | 11/06/20 | |
| CHECKED | | | |
| ANGULAR: | | | |
| MACH±0.5 BEND ±1.0 | BNG APPR. | | |
| TWO PLACE DECIMAL ±.01 | MFG APPR. | | |
| THREE PLACE DECIMAL ±.005 | Q.A. | | |
| INTERPRET GEOMETRIC TOLERANCING PER: ASME Y14.5-09 | COMMENTS: | | |
| MATERIAL | 6061 Aluminum | | |
| FINISH | Clean with acetone | | |
| DO NOT SCALE DRAWING | | | |

TITLE: **Bottom Polar Boss**

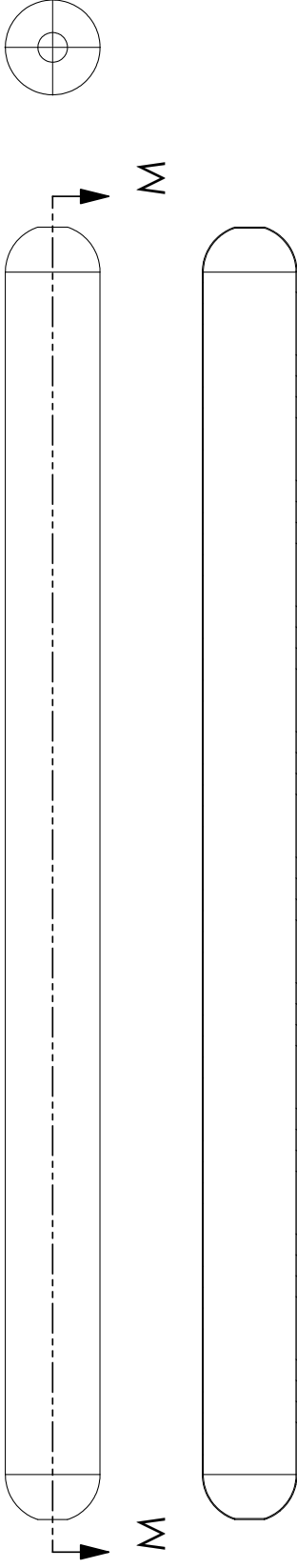
SIZE DWG. NO. REV
B HTP COPV Assembly
 SCALE: 1:2 WEIGHT: SHEET 9 OF 10

3

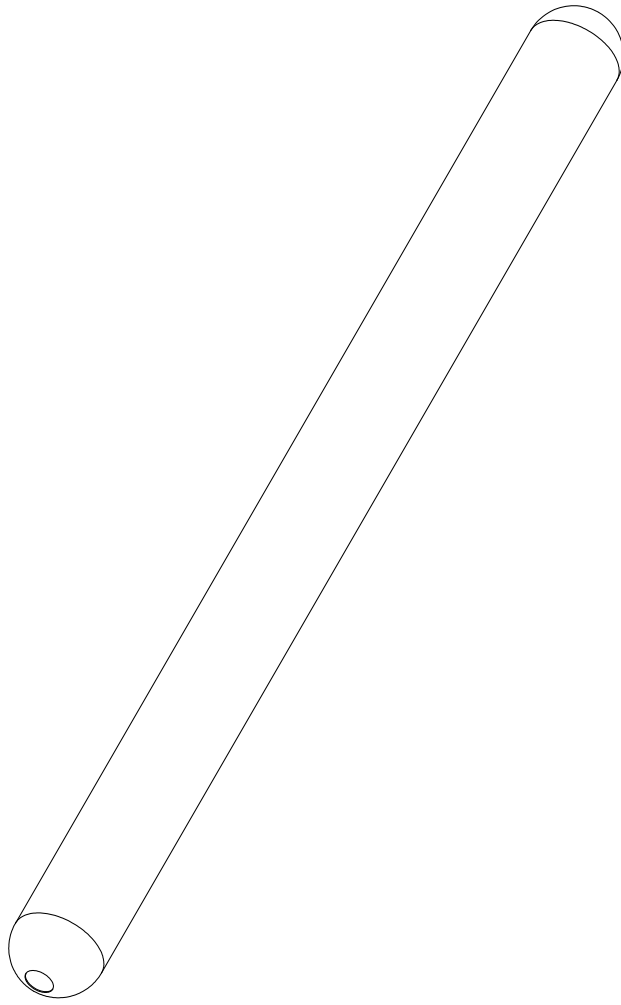
2

1

4 3 2 1




SECTION M-M
SCALE 1 : 20



NOTE : BY VIRTUE OF THE FILAMENT WINDING
MANUFACTURING PROCESS ALL DIMENSIONS
FOR THE OVERWRAP WILL BE DEPENDANT ON
FINAL DIMENSIONS OF THE LINER ASSEMBLY

| | | | |
|--------------------------------|-------------------|----------------|----------------|
| UNLESS OTHERWISE SPECIFIED: | | NAME | DATE |
| DIMENSIONS ARE IN INCHES | | John Slugg | 11/06/20 |
| TOLERANCES: | | CHECKED | |
| ANGULAR: | BEND ±1.0 | ENG APPR. | |
| TWO PLACE DECIMAL | ±.01 | MFG APPR. | |
| THREE PLACE DECIMAL | ±.005 | Q.A. | |
| INTERPRET GEOMETRIC | | COMMENTS: | |
| TOLERANCING PER: ASME Y14.5-09 | | MATERIAL: | T1000G/3501-6 |
| FINISH | | Sand and Paint | |
| DO NOT SCALE DRAWING | | | |
| TITLE: | | Overwrap | |
| SIZE | DWG. NO. | REV | |
| B | HTP COPV Assembly | | |
| SCALE: 1:20 | | WEIGHT: | SHEET 10 OF 10 |

6.2.2 Fiber data sheet



Toray Composite Materials America, Inc.

T1000G

INTERMEDIATE MODULUS CARBON FIBER

Legacy intermediate modulus fiber with excellent processability in traditional manufacturing methods (filament winding). Manufactured in Japan.

PRODUCT DESIGNATION

| T1000G | C | 12,000 | 4 | 0 | D |
|------------|--------|----------------|-------------|-------------------|---------------|
| Fiber Type | Twist* | Filament Count | Sizing Type | Surface Treatment | Sizing Amount |

*C: Never Twisted

FIBER PROPERTIES

| PROPERTY | ENGLISH | METRIC | METHOD |
|-------------------|----------|------------------------|------------|
| Tensile Strength | 924 ksi | 6,370 MPa | TY-030B-01 |
| Tensile Modulus | 43.0 Msi | 294 GPa | TY-030B-01 |
| Strain at Failure | | 2.2% | TY-030B-01 |
| Density | | 1.80 g/cm ³ | TY-030B-02 |
| Filament Diameter | | 5 μm | |
| Yield | 12K | 485 g/1000m | TY-030B-03 |

RESIN SYSTEM COMPATIBILITY

| SIZING TYPE & AMOUNT | RESIN SYSTEM COMPATIBILITY | METHOD |
|----------------------|----------------------------|------------|
| 40D (0.7%) | Epoxy | TY-030B-05 |

FUNCTIONAL PROPERTIES

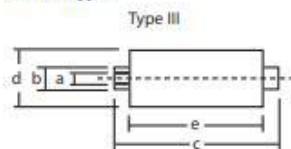
| PROPERTY | VALUE |
|------------------------------|-------------------------------|
| CTE | -0.6 α · 10 ⁻⁶ /°C |
| Specific Heat | 0.752 J/g · °C |
| Thermal Conductivity | 0.105 J/cm · s · °C |
| Electric Resistivity | 1.4 × 10 ¹² Ω · cm |
| Chemical Composition: Carbon | >95% |
| Na + K | <50 ppm |

PACKAGING

The table below summarizes the tow sizes, twists, sizing types, and packaging available for standard material. Other bobbin sizes may be available on a limited basis.

| TOW SIZES | BOBBIN NET WEIGHT (kg) | BOBBIN TYPE | BOBBIN SIZE (mm) | | | | | SPOOL PER CASE | CASE NET WEIGHT (kg) |
|-----------|------------------------|-------------|------------------|------|-----|-----|-----|----------------|----------------------|
| | | | a | b | c | d | e | | |
| 12K | 2.0 | III | 76.5 | 82.5 | 280 | 140 | 252 | 12 | 24 |

Bobbin Type:





T1000G
T1000G Rev.0: Updated January 17, 2018



www.toraycma.com
253-846-1777

6.2.3 Link to project file downloads

<https://www.johnslugg.com/copv-design>

6.2.4 Parametric model update sequence

1. Begin by opening COPV analysis scripts Propellant_COPVs.m and Propellant_COPVs.m shown in appendices 6.1.1 and 6.1.2.
2. Make any necessary revisions to the design within the scripts and at the top of the scripts set variable “Write_to_Excel” equal to 1.
3. Ensure that the the master spreadsheet “Master.xlsx” is closed, then run the scripts.
4. After the scripts have compiled open “Master.xlsx” and review the changes. Note: Before elongating the propellant COPV laminate sequence by more than 5 plies, you must first “insert” additional columns within the master sheet at the end of the propellant laminate sequence to avoid overwriting other unrelated informaiton within the spreadsheet. You must also update the Excel input commands at the bottom of the Propellant_COPVs.m matlab script. Future updates may alleviate this issue.
5. After the Master spreadsheet has been confirmed to be updated correctly open all SolidWorks Parts:
 - (a) Angle_Alum
 - (b) Cylinders
 - (c) Individual_Baffle
 - (d) Overwraps
 - (e) Polar_Bosses
 - (f) Tank_Head
 - (g) Tubing
6. The design tables within these files must be updated. To open the design table such that it can be updated, do the following:
 - (a) At the top of the design tree, there are tiles, one of which will be white and the rest will be gray.
 - (b) Click on the “Configuration” tile which is denoted with two boxes connected to a vertical line. If you do not see this tile, use the two arrows to navigate through the tiles using the opposing arrows until you have found it.
 - (c) Once in the Configurations tab, open the items revealing the “Tables” folder. Open the Tables folder revealing the parts design table.
 - (d) Right click the design table and select “Edit Table in New Window”. This will open excel. A windows alert may open; just click enable.

- (e) Once Excel has been opened, click the “Data” tab, then click “Refresh All”.
 - (f) Ensure you are in the “Lined_to_SolidWorks” sheet, click save, and then close the spreadsheet.
7. After the design changes are updates, the parts should reflect to match the changes. There are some items that can only be edited within the design table and do not automatically update with the changes in the Matlab analysis scripts. To check other configurations, double click the translucent configurations in the Configurations tile.
 8. Once the part has been updated, save and close the part. Perform this sequence on each of the seven parts and the update sequence has been completed. All assemblies should now have been automatically updated accordingly.